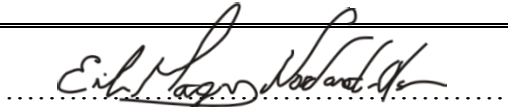




Universitetet
i Stavanger

Faculty of Science and Technology

MASTER'S THESIS

| | |
|---|---|
| Study program/Specialization: Petroleum Geosciences Engineering | Spring semester, 2015 Open |
| Writer: Erik Magnus Nordaunet-Olsen |  (Writer's signature) |
| Faculty supervisor: Alejandro Escalona, University of Stavanger External supervisor(s): Tore Skar, Suncor Energy Norge A/S Laila E. Pedersen, Suncor Energy Norge A/S | |
| Thesis title: Controls on upper Paleozoic Carbonate Build-up Development in the South Central Norwegian Barents Sea | |
| Credits (ECTS): 30 | |
| Keywords: <i>Carbonate build-ups</i> <i>Bjarmeland Platform</i> <i>Finnmark Platform</i> <i>Seismic geomorphology</i> <i>Reticulated ridges</i> | Pages: 154 + Enclosure: 12 + Front page: 9 + CD Stavanger, 12 th June, 2015 |

**Controls on upper Paleozoic Carbonate Build-up
Development in the South Central Norwegian Barents
Sea**

By

Erik Magnus Nordaunet-Olsen

Thesis

Presented to the Faculty of Science and Technology
University of Stavanger

**University of Stavanger
June 2015**

Acknowledgements

First and foremost I want to thank and acknowledge my thesis advisor Tore Skar. I really appreciate the time, ideas and effort that have been given to make my thesis experience productive and fulfilling. Tore Skar has been instrumental in guiding this study, and I was really privileged to have him as supervisor. This thesis would never been possible without his commitment and encouragement. I would also like to convey my deepest sense of gratitude to my university supervisor, Professor Alejandro Escalona, who has given me the opportunity to conduct my research within the specific field and for his numerous valuable comments during this study. I would like to express my gratitude to co-supervisor Laila E. Pedersen for her guidance and great contribution of knowledge and experience, valuable comments and encouragement from the start until the end of the project. Gratitude also goes to Wim Leknes, Andrew Thurlow and Mark Rowan for their very valuable comments and for sharing their knowledge. I am forever grateful for your help.

This thesis has been carried out at Suncor Energy Norge A/S, since January 2015. A number of people deserve thanks for their support, help and discussions. It is therefore my greatest pleasure to thank all of my friends and colleagues in the Suncor Energy Norge. The steep learning curve and all the knowledge you guys have shared over that last couple of years is something that I truly appreciate.

I wish to thank my fellow classmates and friends at the Petroleum Geoscience Engineering class of 2015 for sharing numerous coffees, lunches, and laugh at all times. Thanks guys and good luck too all of you in your future careers.

I would like to acknowledge my family for their encouragement and love. For my parents who has supported me in all my pursuits. Finally, Cathrine B. Johansen without you, supporting and believing in me, this would have been so much harder to achieve.

Erik Magnus Nordaunet-Olsen
University of Stavanger
12th June, 2015

Abstract

This study focusses on aspects related to carbonate build-ups in an upper Paleozoic succession in the south central Norwegian Barents Sea. Seismic and well data are used to map and characterize the protozoan and heterozoan carbonate build-ups in order to assess the factors that control their distribution within the Gipsdalen- and Bjarmeland Groups. The main objectives are (1) to describe, compare, and contrast geomorphological characteristics of the carbonate succession on the Bjarmeland and Finnmark Platforms, (2) to determine the controlling factors on the distribution of the carbonate build-up development, and lastly (3) examine the impact of evaporites on the distribution and development of the carbonate build-ups.

The upper section of the Gipsdalen Group consists of protozoan carbonates and evaporites with occasional carbonate build-ups that were deposited in an arid-warm marine environment in a global icehouse period. The Bjarmeland Group consists of heterozoan carbonates with build-ups deposited in post-glacial environment. Previous studies have suggested that faults play a role in the distribution of carbonate build-ups in the Norwegian Barents Sea.

The two areas on the Finnmark Platform (north and south) have been used in order to compare against two areas on Bjarmeland Platform (east and west). The carbonate build-up sequence observed on the eastern Bjarmeland Platform is comparable with the build-up sequence on the northern Finnmark Platform. The two areas share similarities as both are located on footwall uplifts. The geomorphology of these carbonate units are characterized as large build-up complexes. In contrast, the geomorphology of the western Bjarmeland Platform and the southern Finnmark Platform differs significantly. These units consist of polygonal build-up morphologies of reticulated arrangement with cellular structures of various scales; this depositional pattern is similar in architecture to modern patch and pinnacle reef systems observed in Holocene carbonate systems (e.g. Abrolhos Islands in Western Australia). The similarities defining these elements are that carbonate build-ups stack vertically above the layered evaporite sequence of the Gipsdalen Group. The layered evaporite sequences are observed on both platforms where salt pillows are a main characteristic. The carbonate build-ups deposit vertically above thin units of evaporites, opposed to laterally absent where the salt pillows are present, suggesting that salt has been displaced by the weight of the growing build-up. The result supports antecedent topography as a dominant component affecting the carbonate build-up succession in the eastern Bjarmeland Platform and the northern Finnmark Platform. Furthermore, the build-up development in the two areas on western Bjarmeland Platform, and southern Finnmark Platform, has been controlled by physical conditions influenced by a combination of biotic self-organization, fossil reef growth and karst-induced structures caused by dissolution of the underlying carbonate strata. The current geomorphology of the carbonate build-up succession has been enhanced due to remobilization of the mobile evaporite unit as a result of differential loading by the carbonate build-ups.

Table of Contents

| | |
|--|-----|
| 1. Introduction..... | 1 |
| 1.1 Previous Studies | 2 |
| 1.2 Objectives..... | 4 |
| 1.3 Carbonate Background – Controlling factors..... | 5 |
| 1.3.1 Carbonate and Evaporite Deposition..... | 5 |
| 1.3.2 The Controlling Factors..... | 5 |
| 2. Regional Geological Settings..... | 10 |
| 2.1 Late Devonian – Mississippian | 13 |
| 2.2 Pennsylvanian – Early Permian..... | 15 |
| 2.3 Early Permian – Middle Permian | 16 |
| 2.4 Late Permian | 17 |
| 3. Database and Methodology..... | 18 |
| 3.1 Well Data..... | 18 |
| 3.2 Seismic Data..... | 20 |
| 3.3 Seismic Well-tie | 22 |
| 3.3.1 Seismic Wavelet | 22 |
| 3.3.2 Seismic Well-tie | 23 |
| 3.4 Seismic Interpretation and Visualization Methods | 26 |
| 3.4.1 Seismic Interpretation..... | 26 |
| 3.4.2 Seismic Stratigraphic Framework | 27 |
| 3.4.3 Seismic Attributes..... | 32 |
| 5. Results..... | 37 |
| 5.1 Bjarmeland Platform | 37 |
| 5.1.1 Seismic Area A (BG0804)..... | 37 |
| 5.1.2 Seismic Area B (NH0608)..... | 57 |
| 5.2 Finnmark Platform | 77 |
| 5.2.1 Seismic Area C (SH9102) | 77 |
| 5.2.2 Seismic Area D (ST9802)..... | 96 |
| 5.3 Summary | 119 |
| 5.3.1 Bjarmeland Platform..... | 119 |

| | |
|--|-----|
| 5.3.2 Finnmark Platform..... | 122 |
| 6. Discussion..... | 125 |
| 6.1 Bathymetric Control on Carbonate Development..... | 125 |
| 6.1.1 Structural Control..... | 125 |
| 6.1.2 Antecedent Karst Topography..... | 126 |
| 6.2 Hydrodynamic Control..... | 135 |
| 6.2.1 Wave Movement Control..... | 135 |
| 6.2.2 Spur and Groove..... | 137 |
| 6.2.3 Biotic Self-organization..... | 139 |
| 6.3 Evaporite as Controlling Factor on Carbonate Build-up Development..... | 141 |
| 7. Conclusions..... | 145 |
| 8. References..... | 148 |
| | |
| Appendices..... | 155 |
| Appendix 1 - Well descriptions..... | 155 |
| Appendix 1.1 - Well 7124/3-1..... | 155 |
| Appendix 1.2 - Well 7226/11-1..... | 156 |
| Appendix 1.3 - Well 7229/11-1..... | 158 |
| Appendix 1.4 - Well 7128/4-1..... | 159 |
| Appendix 1.5 - Well 7128/6-1..... | 161 |
| Appendix 2 - Seismic interpretation and attribute methods..... | 163 |
| Appendix 2.1 - Seismic well-tie background..... | 163 |
| Appendix 2.2 - Vertical and horizontal resolutions..... | 164 |
| Appendix 2.3 - Seismic attribute background..... | 166 |

List of Figures

| | |
|---|----|
| Figure 1 - Regional map of the Norwegian Barents Sea with structural elements highlighted. | 2 |
| Figure 2 - Controls on marine organic carbonate accumulation in a platform setting..... | 6 |
| Figure 3 - Deposition of Holocene carbonates marked with latitude. | 7 |
| Figure 4 - Rate of $\text{Ca}_2(\text{CO}_3)$ production per unit area versus depth in clear marine water..... | 8 |
| Figure 5 - Regional map of the greater Barents Sea area presented with structural elements..... | 10 |
| Figure 6 - The upper Paleozoic lithostratigraphic column of SC Barents Sea region | 12 |
| Figure 7 - Paleogeographic orientation of the south central Barents Sea. A) Paleogeographic map of Early Mississippian; B) Pennsylvanian; C) Early Permian; D) Late Permian | 14 |
| Figure 8 - Regional structural elements map presented with the data coverage..... | 18 |
| Figure 9 - Seismic Wavelet applied in order to create a seismic well-tie..... | 22 |
| Figure 10 - The Power Spectrum of the seismic wavelet used in the seismic well-tie process... .. | 22 |
| Figure 11 - Seismic well tie from well 7128/4-1 on the Finnmark Platform..... | 23 |
| Figure 12 - Seismic well-tie from well 7229/11-1 on Finnmark Platform | 24 |
| Figure 13 - Seismic sections with corresponding reflectors and seismic well-tie.. .. | 25 |
| Figure 14 - The upper Paleozoic lithostratigraphy of the south central Norwegian Barents Sea, with comparisons of different seismic sequences from previous authors and this thesis..... | 27 |
| Figure 15 - Well section with defined seismic sequences. | 30 |
| Figure 16 - Seismic section and Geoseismic section with seismic correlated seismic sequences from Bjarmeland- to Finnmark Platform through the thinnest part of the Nordkapp basin | 31 |
| Figure 17 - The spectral decomposition workflow. | 33 |
| Figure 18 - Diagram of the seismic frequency spectrum in the seismic surveys..... | 36 |
| Figure 19 - Regional structural elements map marked with the outline of Area A. | 37 |
| Figure 20 - Seismic sections of Area A. A) Seismic Inline 2473; B) Geoseismic Inline 2473; C) Seismic Xline 3417; D) Geoseismic Xline 3417 | 39 |
| Figure 21 - The zoomed seismic x-line A) Close-up zoom of the seismic x-line 3417. B) Geoseismic x-line 3417..... | 40 |
| Figure 22 - Time surface map of top Pre-SS horizon.. .. | 41 |
| Figure 23 - A) Time surface map of top SS 1; B) Isochron map of SS 1 | 44 |
| Figure 24 - A) Time surface map of top SS 2; B) Isochron map of SS 2 | 47 |
| Figure 25 - Seismic attribute maps of SS 2. A) RMS Amplitude; B) Variance map. T; C) Red-green-blue (RGB) color blended spectral decomposition map..... | 48 |
| Figure 26 - A) Time surface map of top SS 3; B) Isochron map of SS 3. | 52 |
| Figure 27 - Attribute maps of SS 3. A) RMS Amplitude map; B) Variance map; C) Frequency RGB blended map..... | 53 |
| Figure 28 - A) Time surface map of top SS 4; B) Isochron map of SS 4..... | 56 |
| Figure 29 - Regional structural elements map with the outline of Area B. | 57 |
| Figure 30 - Seismic sections of Area B A) Seismic inline 2978; B) Geoseismic inline 2978..... | 59 |
| Figure 31 - seismic section of Area B. A) Seismic x-line 1831, B) Geoseismic x-line 1831..... | 60 |
| Figure 32 - Time surface map of top Pre-SS. | 61 |

| | |
|--|-----|
| Figure 33 - A) Time surface map of top SS 1; B) Isochron map of SS 1. | 63 |
| Figure 34 - A) Time surface map of top SS 2; B) Isochron map of SS 2. | 66 |
| Figure 35 - Seismic attribute maps of SS 2. A) RMS Amplitude map; B) Variance map; C) RGB Color blend map..... | 67 |
| Figure 36 - A) Time surface map of top SS 3; B) Isochron map SS 3 | 70 |
| Figure 37 - Seismic attribute maps of SS 3. A) RMS Amplitude map; B) Variance map; C) RGB Color blend map..... | 71 |
| Figure 38 - A) Time surface map of top SS 4; B) Time thickness map of SS 4. The thickness map shows a uniform thick succession within SS 4. | 73 |
| Figure 39 - A) Time surface map of top SS 5; B) Isochron map of SS 5. | 75 |
| Figure 40 - Regional structural elements map indicating the outline of Area C. | 77 |
| Figure 41 - Seismic sections of Area C. 17A: Seismic Inline 477, 17B: Geoseismic Inline 477. | 79 |
| Figure 42 - Seismic sections of Area C. A) Seismic x-line 627; B) Geoseismic x-line 627. | 80 |
| Figure 43 - Time surface map of top Pre-SS | 81 |
| Figure 44 - A) Time surface map of top SS 1; B) Isochron map of SS 1. | 84 |
| Figure 45 - A) Time surface map of top SS 2; B) Isochron map of SS 2. | 87 |
| Figure 46 - Seismic attribute maps of SS 2. A) RMS Amplitude map; B) Variance map..... | 88 |
| Figure 47 - A) Time surface map of top SS 3; B) Isochron map of SS 3. | 91 |
| Figure 48 - Seismic attribute maps of SS 3. A) RMS Amplitude map; B) Variance map..... | 92 |
| Figure 49 - A) Time surface map of top SS 4; B) Isochron map of SS 4. | 95 |
| Figure 50 - Regional map of SC Norwegian Barents Sea shown with outline of Area D. | 96 |
| Figure 51 - Seismic sections of Area D on southeastern Finnmark Platform. A) Seismic Inline 1796; B) Geoseismic Inline 1796. | 98 |
| Figure 52 – Close-up zoom of Area D. A) Seismic Inline 1796, B) Geoseismic Inline 1796. .. | 99 |
| Figure 53 - Seismic section of Area D on southeastern Finnmark Platform. A) Seismic x-line 7151, B) Geoseismic section of x-line 7151..... | 100 |
| Figure 54 - Time surface map of top Pre-SS. | 101 |
| Figure 55 - A) Time surface map of top SS 1; B) Isochron of SS 1 | 104 |
| Figure 56 – Conceptual calculation of the slope angle of the Finnmark Platform. | 105 |
| Figure 57 - A) Time surface map of top SS 2; B) Isochron map of SS 2. | 107 |
| Figure 58 - Seismic attribute maps of SS 2. A) RMS Amplitude map; B) RGB blended map. | 108 |
| Figure 59 - A) Time surface map of top SS 3; B) Isochron of SS 3..... | 111 |
| Figure 60 - Seismic attribute maps of SS 3. A) Variance map; B) RGB Color blend map..... | 112 |
| Figure 61 - A) Time surface map of top SS 4; B) Isochron map of SS 4. | 115 |
| Figure 62 - A) Time surface map of top SS 5; B) Isochron map of SS 5. | 118 |
| Figure 63 – Conceptual geomodel of carbonate systems growing on footwall uplifted highs. . | 125 |
| Figure 64 - Comparison of surface maps of SS 3 from Area A and Area C, presented with structural features..... | 128 |
| Figure 65 - Comparison of modern and ancient sinkhole and doughnut structures. A) The great blue hole, Belize; B) Doughnut structure in Area C shown on the surface map of top SS 3. | 129 |

| | |
|---|-----|
| Figure 66 - Analogue compilation of Holocene reefs with attached patch and pinnacle reef architectures. A) Kanton Island, Kiribati; B) Abrolhos Island, Western Australia; C) Mataiva, French Polynesia; D) Isla Pérez, Mexico..... | 130 |
| Figure 67 - Geological model of carbonate build-ups developing the seismic geomorphology based on the topography of antecedent karstified surface. A) Seismic section of Area D; B) Geoseismic section of Area D illustrating the karstified protozoan carbonate surface; C) Highstand sea-level model of the build-up development; D) Lowstand sea-level development of the carbonate build-up; E) 2D map view of a build-up mound; F) 3D geological model of the carbonate build-up network developed in the lagoon environment..... | 132 |
| Figure 68 - Comparison of the geomorphological characteristics of reticulated carbonate systems from analogues versus the top SS 4 surface from Area A. A) Kanton Island, Kiribati; B) Abrolhos Island, Western Australia; C) Seismic Area A | 134 |
| Figure 69 – The windward and leeward directions on the Bjarmeland Platform areas. A) Area A; B) Area B | 136 |
| Figure 70 - Spurs and grooves at Sombrero Key Reef in the Florida Keys..... | 137 |
| Figure 71 - Example of the possible spur and groove system on the Bjarmeland Platform. | 138 |
| Figure 72 – A) Autocatalysis in activator-inhibitor system; B) Impact of autocatalysis on the scale dependent feedback in ecological systems; C) Feedback curve of long- and short-distance facilitation | 139 |
| Figure 73 - Comparison of maze pattern networks of trees, and shrubs versus reticulated carbonate build-up systems. A) Tree networks in Western Siberia; B) Reticulated reefs in Mataiva Island, C) Reticulated carbonate build-ups, Bjarmeland Platform. | 140 |
| Figure 74 - The thickness variations of evaporite and carbonates. A) The isochron map of SS 2 in Area B; B) Isochron map of SS 3 in Area B..... | 142 |
| Figure 75 - Development of salt weld and salt pillow structures caused by differential loading effects..... | 143 |
| Figure 76 - Differences in stress contraction and extension affecting the differential loading of the mobile evaporite unit | 143 |
| Figure 77 - The RMS Amplitude map of SS 2 show the different salt tectonic structures..... | 144 |
| Figure 78 – Regional depositional models of the south central Barents Sea. A) Model of SS 2; B) Model of SS 3. | 146 |

Appendix Figures

| | |
|---|-----|
| Appendix 1.1: Figure 79 - Well data of the Upper Paleozoic succession in well 7124/3-1. | 155 |
| Appendix 1.2: Figure 80 - Well data of the Upper Paleozoic succession in well 7226/11-1. ... | 156 |
| Appendix 1.3: Figure 81 - Well data of the Upper Paleozoic succession in well 7229/11-1. ... | 158 |
| Appendix 1.4: Figure 82 - Well data of the Upper Paleozoic succession in well 7128/4-1. | 159 |
| Appendix 1.5: Figure 83 - Well data of the Upper Paleozoic succession in well 7128/6-1. | 161 |
| Appendix 2.1: Figure 84 - Synthetic seismogram theory | 163 |

List of Tables

| | |
|---|-----|
| Table 1 – Summary table of well data used in the thesis. | 19 |
| Table 2 - P-wave velocities at the group well tops extracted from the sonic logs. | 19 |
| Table 3 - 3D Seismic coverage on Finnmark- and Bjarmeland Platforms..... | 20 |
| Table 4 - 2D Seismic data coverage on Finnmark- and Bjarmeland Platforms..... | 20 |
| Table 5 - Seismic survey information table. | 21 |
| Table 6 - Results of the wavelength, vertical- and horizontal resolution of the seismic areas. ... | 26 |
| Table 7 - Seismic horizons with responses in seismic section and acoustic impedance..... | 28 |
| Table 8 - Seismic frequency comparison of source data versus the spectrally enhanced data. ... | 35 |
| Table 9 - Seismic facies summary table for the Bjarmeland Platform region. | 121 |
| Table 10 - Seismic facies summary table for the Finnmark Platform region. | 124 |

Appendix Tables

| | |
|---|-----|
| Appendix 2.2: Table 11 - Acoustic velocities for the Bjarmeland Group | 165 |
| Appendix 2.2: Table 12 - wavelength, vertical and horizontal resolution of the seismic areas | 165 |

1. Introduction

The Barents Sea area is located offshore North Norway and has become a focus of hydrocarbon exploration since the early 1980s. Exploration started with the discovery of the Snøhvit field in 1984, and continued with several major discoveries during the 2000s and 2010s (e.g. Goliat, Johan Castberg and Wisting). The recent discoveries in the upper Paleozoic carbonate succession (i.e. Gotha and Alta) have shed new light and attention on the carbonate succession in the Norwegian Barents Sea.

The carbonate succession in the Barents Sea consists of Mississippian – Early Permian warm-water carbonates of the Gipsdalen Group and Early Permian – Late Permian cold water carbonates of the Bjarmeland and Tempelfjorden Groups. Carbonate build-ups are a common feature within the Gipsdalen and Bjarmeland Groups, on both the Finnmark Platform and Loppa High (e.g. Stemmerik et al. 1999; Elvebakk et al, 2002; Samuelsberg et al. 2003). The carbonate succession identified on the platforms and highs in the Norwegian Barents Sea are also identified elsewhere in the arctic region by subsurface data and in field outcrop analogs, e.g. Timan-Pechora basin, Svalbard, Sverdrup Land and Northeast Greenland.

The differences in carbonate depositional environments, and processes affecting the morphology are elaborated and exemplified by the results obtained from the different datasets adapted in this study. The thesis describes the local variability and the semi-regional extent of the Pennsylvanian to Early Permian carbonate successions within the Gipsdalen and Bjarmeland Groups. The study provides a new seismic stratigraphic framework, which build on previous established framework of Samuelsberg et al. (2003) and Colpaert et al. (2006). The study focus on the carbonate morphology and the controlling factors of the upper Paleozoic carbonate succession, located on the Bjarmeland and Finnmark Platforms, located in the south-central Norwegian Barents Sea (Figure 1). The upper Paleozoic carbonates on the Bjarmeland Platform are considered to be a hitherto undescribed succession. The succession on the Finnmark Platform has been relatively extensive studied over the last 20 years (e.g. Bugge et al. 1995; Samuelsberg et al. 2003; Colpaert et al. 2006; Rafaelsen et al. 2008). Seismic and well data are used to construct the seismic stratigraphic framework and interpret key surfaces representative for the carbonate succession. 3D Seismic interpretation is applied to characterize the respective sequences within the carbonate succession, and to further assess the factors controlling their development, distribution and geomorphology.

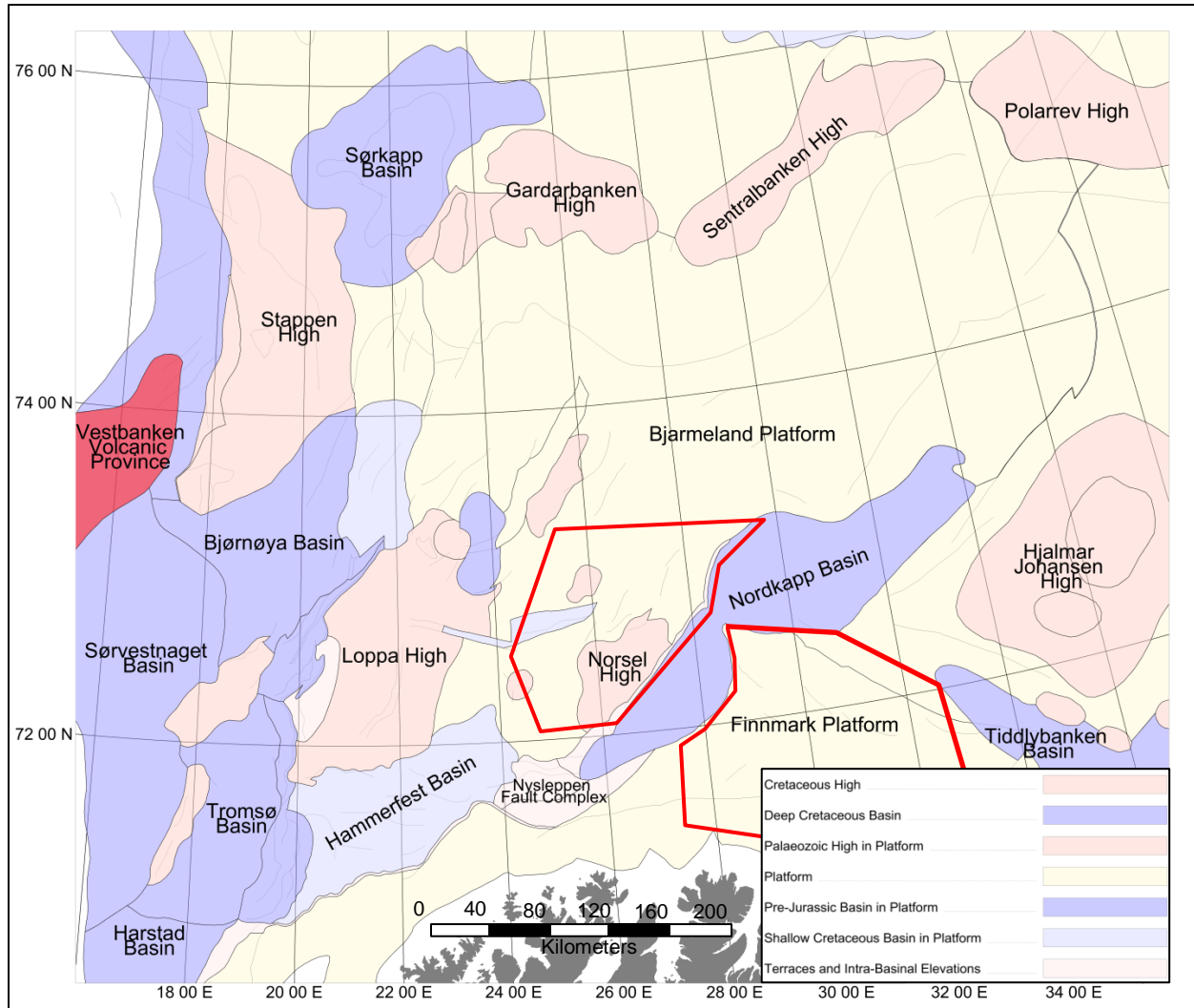


Figure 1 - Regional map of the Norwegian Barents Sea with structural elements highlighted. The two areas of interest for this study are indicated by the two red polygons.

1.1 Previous Studies

Over the last 30 years several studies have been published on the Paleozoic carbonates of the Barents Sea, Timan-Pechora basin, Sverdrup land, Svalbard and northeast Greenland. Previous research focus on the carbonate succession in the Barents Sea region has had an extensive focus on the carbonate sedimentology and reservoir properties, and, in parts, on karstification processes. The studies conducted on the upper Paleozoic succession in the Norwegian Barents Sea, have on the other hand, primarily focused on the Loppa High and Finnmark Platform.

The research conducted on the carbonate succession on the Finnmark Platform and Loppa High, have shed light on the structural component in regards to the carbonate succession. Yet this has not been extensively covered. The succession on the Finnmark Platform is considered as the most detailed studied carbonate sequence in the Norwegian Barents Sea. During the late 1980s

and 90s, extensive research were focused on the upper Paleozoic carbonate succession, this resulted in extensive coring and sedimentological analysis of the carbonate succession.

The seismic interpretative approach for researching the carbonate succession in the Norwegian Barents Sea carried out over previous years, has concentrated their effort on the Loppa High and Finnmark Platform. Samuelsen et al. (2003), Colpaert et al. (2006), and Rafaelsen et al. (2008) conducted 3D seismic analysis of the carbonate succession on the Finnmark Platform, which focused on mapping and investigation of the carbonate evolution. Research of the upper Paleozoic section, has shown lack of attention in regards the controlling factors on the deposition, geomorphology and distribution of the carbonate succession. Studies on the carbonates on Loppa High has focused on paleo-karst systems, reservoir potential, and presence of carbonate build-ups on the structural high (Stemmerik et al. 1999; Elvebakk et al. 2002; Carrillat et al. 2005; Ahlborn et al. 2014).

The relationship between carbonates and evaporate systems is relatively undescribed in the Barents Sea region. The research conducted by Ahlborn et al. (2014), investigate the Early Permian interbedded evaporate and carbonate sequence on the north flank of the Loppa high. Ahlborn et al. (2014) argue for the resemblance with the sequence on the Loppa High, and the Gipshuken Formation on Svalbard. The study focuses on the aspect of the karstification processes affecting the transgressive carbonate sequence on the Loppa High. The carbonate and evaporites relationship of the Carboniferous to Permian successions are analyzed on outcrop data in Sverdrup Land, Canada by Beauchamp et al. (1994); Concluding that the carbonate build-ups grew on major structural highs, and that there is a considerable sea-level control on the distribution of carbonates and evaporites.

Elvebakk et al. (2002) shed light on the structural controls affecting the carbonate build-up systems from isolated build-ups into linked mosaic systems, and interpreted these systems as fault controlled. Development of reticulated patched and pinnacle reefs has been recognized in Holocene systems, and was initially described by Hoffmeister and Ladd (1945), concluding on solution structures as governing factor on growth shape of reticulated reef systems. Later studies, e.g. Purkis et al. (2010) and Purdy and Bertram (1983) have strongly argued for, and adapted the interpretation for karst-induced structures as controls on growth-shape. Schlager and Purkis (2014) discuss that comprehensive evidences for karst-induced control remains as circumstantial, and thus propose biotic self-organization as contributing factor for the development of reticulated reef systems.

The controlling factors on the carbonate succession in the Barents Sea are considered to be hitherto undescribed. Stemmerik et al. (1989) studied the controls on the Pennsylvanian carbonates on outcrop analogues in the Amdrup Land, North Greenland. Concluding that localization and morphology were dominant factors for the distribution of the carbonate build-up

successions. The most recent study on the controlling factors is the study by Colpaert et al. (2006) argues that faults contribute to the distribution of the carbonate build-ups.

1.2 Objectives

The aim of the study is to investigate the upper Paleozoic carbonate succession on the Bjarmeland and Finnmark Platforms. The thesis sought to clarify and develop an understanding of the depositional processes, and the physical controlling factors affecting the carbonate geomorphology of the Pennsylvanian to Middle Permian carbonate build-up succession. The four research objectives are:

- Determine, compare, and contrast geomorphological characteristics of the carbonate succession on the Bjarmeland and Finnmark Platforms.
- Quantify and describe the differences and similarities of the carbonate geomorphology in the units on the Bjarmeland and Finnmark Platforms.
- Determine the physical controlling factors on the distribution of the carbonate build-up development.
- Examine the impact of evaporite deposits on the distribution of the carbonate build-up development.

1.3 Carbonate Background – Controlling factors

1.3.1 Carbonate and Evaporite Deposition

The carbonate factory is defined as the generally shallow seafloor located within the photic zone. Carbonate sediments consist of particles that are born in this zone. The variability of particles made in the carbonate factory is born in a variety of grain sizes, precipitated directly from seawater or as crystalized skeletons (Kendall and Jones, 1992). The sedimentary grains generally for reefs, mounds or as widespread sub tidal deposits. The carbonate factory and carbonate accumulation is a direct relation to the eustatic sea level changes, where carbonates rely on a certain number of factors for growth, with the highest rate of accumulation located within the photic zone. Consequently, sea-level highstand results in shut-down of the carbonate factory, and sea level lowstand results in sub aerial exposure of the platform (Kendall and Jones, 1992).

The evaporite factory opposed to the carbonate factory relies on sea-level lowstand in order to precipitate evaporites from the saline water. The largest accumulations of evaporites are located in shallow marine conditions. Nonetheless, the evaporite factory can take place in terrestrial clastic and carbonate sedimentary settings. The variety in depositional environments varies from continental lakes, coastal salinas, and sabkha deposits, to shallow- and deep basinal environments i.e. during sea level lowstand (Kendall and Jones, 1992).

1.3.2 The Controlling Factors

The carbonate forming process is complex and relies on a number of factors in order to grow (Figure 2). Because carbonates are organic material, and deposit in-situ, they develop predictable pattern in their growth behavior. Consequently, understanding of the processes controlling the carbonate growth is essential for understanding carbonate distribution, growth pattern and morphology.

1.3.2.1 Physical Factors

Temperature and climate are two of the most important physical conditions for carbonate development. Carbonates are classified into two different groups: heterozoan- and protozoan carbonate associations (James, 1997). Protozoan carbonates are primarily controlled by light and sea-level temperature and often referred to as warm-water carbonates. Heterozoan carbonates are light independent carbonates (e.g. bryozoans, barnacles and crinoids) and are referred as cold-water carbonates are primarily light dependent. The large-scale production of carbonate is confined to areas where warm tropical to semitropical waters are present, i.e. generally latitudes ranging from Tropic of Capricorn to Tropic of Cancer ($\sim -24^\circ$ to $+24^\circ$). The Holocene distribution of the largest carbonate production areas, strongly reflect the importance of temperature and climate (Figure 3).

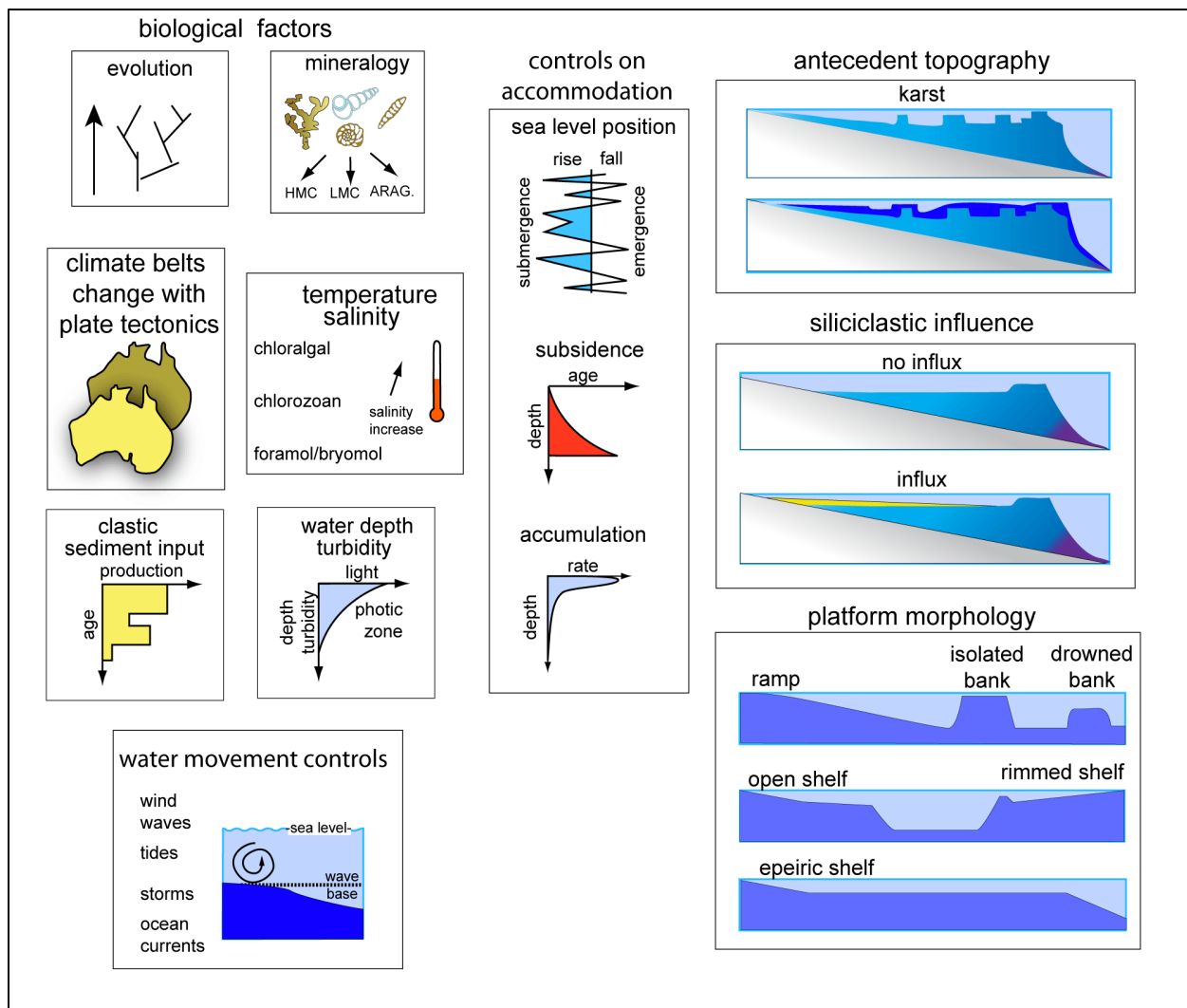


Figure 2 - Controls on marine organic carbonate accumulation in a platform setting (Modified from Kendall and Tucker, 2010; after Jones and Desrochers, 1992).

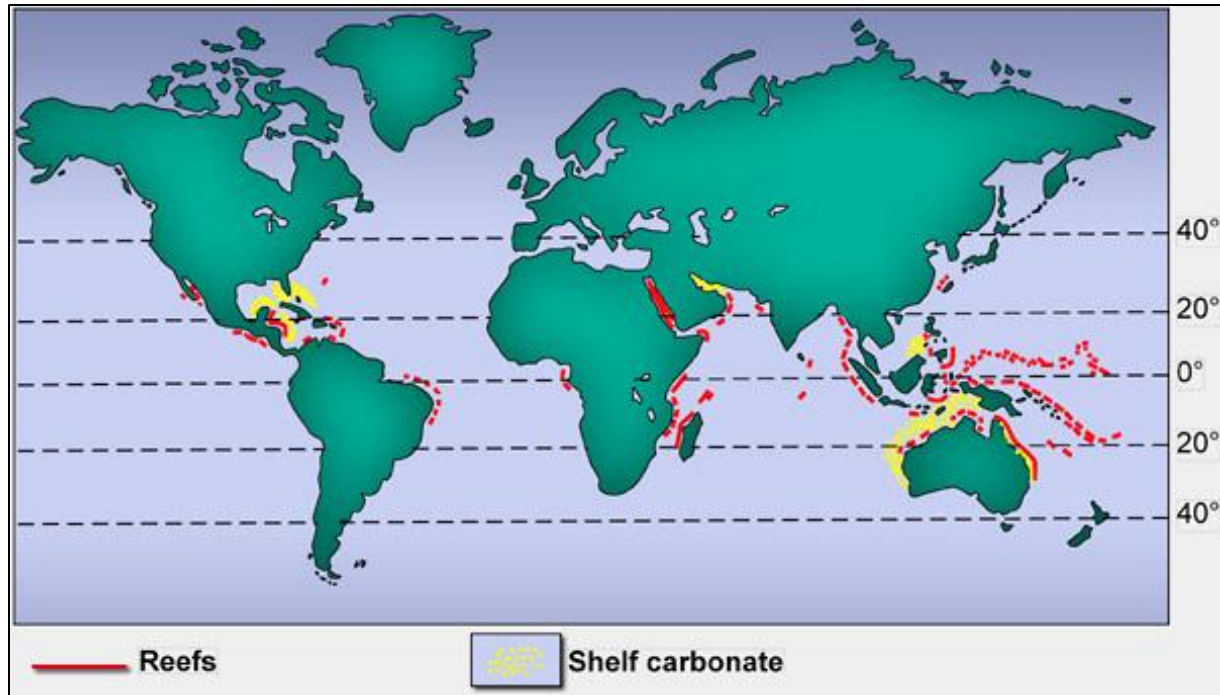


Figure 3 - Deposition of Holocene carbonates marked with latitude (Loucks et al., 2003).

The basis of photosynthesis is light, i.e. organic growth onshore as well as offshore relies on nutrients and energy from the sun (Schlager, 2005). The majority of marine organisms (e.g. algae and corals) are a part of the photosynthesis. Consequently water clarity is an important component to maintain the growth and production of these organisms (James and Kendall, 1992). The decrease in light penetration is an exponential function of water depth; this means that the photosynthesis is sensitive to the water depth. This means that the antecedent topography during deposition of the carbonate sequence is an important factor for controlling areas of carbonate production (Figure 2). The light penetration equation through sea-level in clear-water is presented below:

$$S_z = S_0 * e^{-kz} \quad (\text{Eq. 1.3})$$

S_0 and S_z are solar irradiance at sea level and depth z . The attenuation coefficient, k , depends on the turbidity currents of the water and is high in areas with high production of plankton or suspended sediment load. Evidently, the attenuation coefficient, k , is low in areas with clear waters (Figure 4; Bice, 1991; Schlager, 2005).

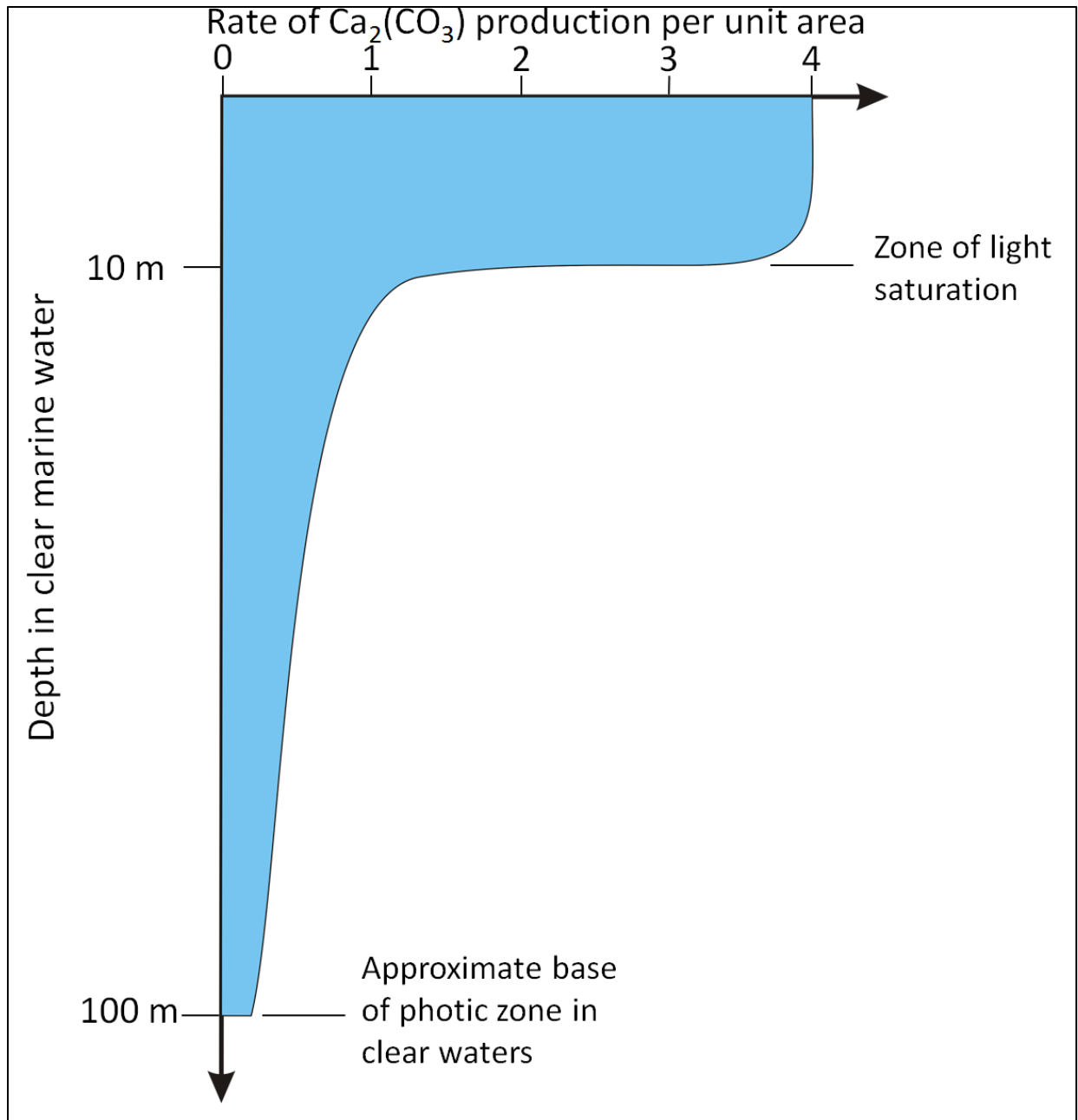


Figure 4 - Rate of $\text{Ca}_2(\text{CO}_3)$ production per unit area versus depth in clear marine water (after Schlager, 2005).

1.3.2.2 Biological factors

The biological factors controlling the deposition of carbonate sediments consists of a certain number of parameters (Figure 2). Three most significant factors are growth rate, growth form, and skeletal mineralogy (James and Kendall, 1992). The organism growth rate is dependent upon inherent biological parameters and the optimal conditions for the growth environment. The carbonate sedimentary growth form (e.g. corals, bryozoans, phylloid algae, among others) is dependent upon physical properties such as light or physical energy levels in order to change

their growth form. Corals and bryozoans are examples of carbonate growing in a shallow-marine condition with high levels of water movement; the growth forms of these carbonate sediments are generally robust and compact. However, opposed to the shallow-marine high energy carbonates, the organisms born in deep-marine environments do not rely on the same conditions as in the shallow-marine environments. Consequently, the growth form of these organisms varies and their general shape is identified as being more delicate and platy (Loucks et al., 2003). As a result of the growth form affecting the carbonate sediments, the skeletal mineralogy developed by the different organisms will differ dependent on growth form and rate and therefor results in develop different mineralogy (Loucks et al., 2003).

1.3.2.3 Chemical factors

The chemical factors controlling the carbonate organism consists primarily of nutrition, salinity, and carbonate saturation in the water. Organic materials have different tolerances for absolute salinity and influxes of salinity in their living environment. Consequently, too high or low salinity levels will result in shut down of the carbonate factory. Carbonates are living organisms, and require nutrients to live, grow and essentially reproduce (James and Kendall, 1992; Loucks et al., 2003).

The marine environments where carbonate sediments are generated are generally saturated by calcite, high Mg-calcite, and aragonite. These minerals are the main building bricks, and mineral saturation allows cementation for creating carbonate particles (Flügel, 2004). The shallow-marine environment is normally saturated with respect to these minerals, however, in deep-marine environments, the water can be undersaturated. Consequently, as a result of undersaturation, grains transported to deep-marine environments will be dissolved (Loucks et al., 2003).

2. Regional Geological Settings

The Barents Sea is located on the northern hemisphere covering an area that extends from the island of Novaya Zemlya in the east to the continental slope of the Norwegian-Greenland Sea to the west, bounded by Svalbard and Franz Josef land in the north and Norway and Russia in the south (Figure 5).

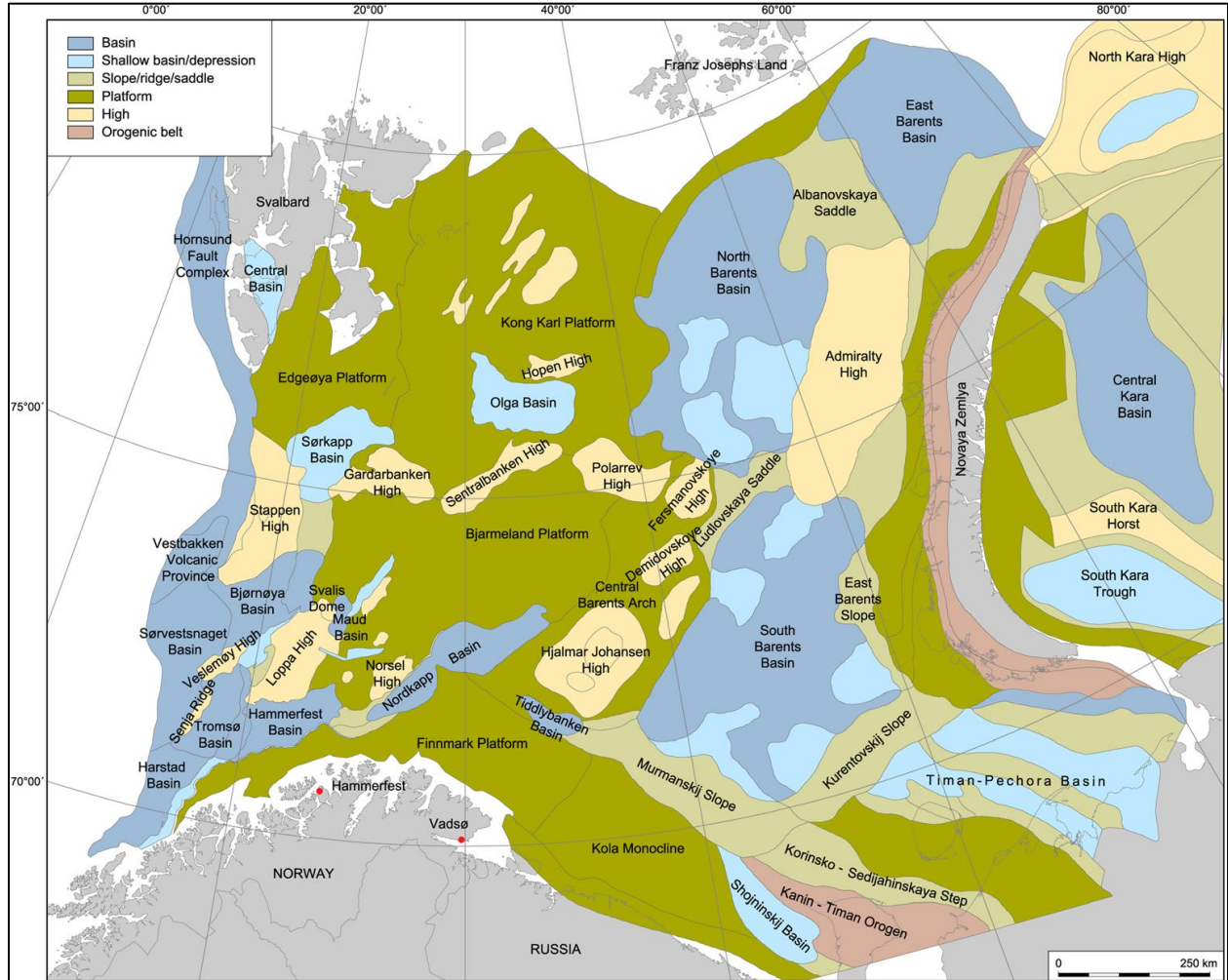


Figure 5 - Regional map of the greater Barents Sea area presented with structural elements (Henriksen et al., 2011).

The Norwegian Barents Sea has been repeatedly influenced by major tectonic phases, climatic changes and glaciations during a series of occasions in the geological past (Frakes et al. 1992). These changes have impacted the platform margins and structural settings from the Pre-Cambrian to Cenozoic.

The Barents Sea region is subdivided into a large number of basins and structural highs (Figure 5). South Central Norwegian Barents Sea region comprises of the Bjarmeland Platform, Nordkapp Basin, Finnmark Platform, Tiddlybanken Basin and Hjalmar Johansen High (Figure 5). The Barents Sea region comprises of two dominant structural trends developed as a result of

two major collisional events. These two collisions dominate the structural fabric in the region (Dodson, 2014), which governs the orientation of the extensional events that occurred in the Late Devonian, Late Paleozoic and Late Jurassic (Henriksen et al., 2011). The first structural trend was development in the Caledonian Orogeny in the Ordovician – Early Devonian (Rey et al., 1997). The Caledonides were created as a result of the closing of Iapetus Sea during the collision of the Laurentia and Baltica plates (Rey et al., 1997; Dodson, 2014). The second structural trend was developed during the Late Permian and the creation of the Uralian Orogeny. The Urals were developed during the collision of the Lauratian-Baltica and Western Siberian plates (Puchkov, 2009).

The two structural trends dominating the Barents Sea governs the development of the structural elements in the south central Barents Sea region. The Nordkapp Basin is defined by its overall SW-NE trend orientation is controlled by the structural lineament developed by the Caledonian Orogeny and the Tiddybanken Basin confined by its NW-SE orientation is controlled by the structural lineament developed during the Uralian Orogeny (Dodson, 2014). These two basins are confined by the Bjarmeland Platform to the north, Finnmark Platform to the southeast, and the Hjalmar Johansen High in the northeast part of the Norwegian Barents Sea (Figure 5). The Finnmark Platform is bounded to the south by the exposed Caledonides of the Norwegian mainland and to the north by the Nordkapp Basin. The eastern boundary is defined by the Kola Monocline, whereas the Troms-Finnmark Fault Complex defines the western limit (Rønnevik et al., 1982; Gabrielsen et al., 1990). The Bjarmeland Platform is located on a stable platform situated between the Hammerfest Basin and Nordkapp Basin to the south and southeast, by the Gardarbakken High and Sentralbanken Highs (Gabrielsen et al., 1990).

The upper Paleozoic succession in the Norwegian Barents Sea shelf consists of a Mississippian siliciclastics sequence followed by carbonate sequence ranging from Carboniferous to Late Permian in age (Bugge et al. 1995; Stemmerik et al., 1995). The carbonate succession consists of deposits of warm-water (protozoan) and cold-water (heterozoan) carbonate deposits. The deposition of the carbonate succession occurred from the Pennsylvanian – Late Permian. The succession comprises of dolomite-dominated protozoan carbonates in the lower sequence deposited during the Pennsylvanian – Lower Permian in the Gipsdalen Group (Figure 6). Heterozoan limestone and bryozoan build-ups in the Bjarmeland Group deposited during the Lower to Middle Permian (Figure 6). The upper carbonate sequence is defined as the Tempelfjorden Group, and consists of deep-marine silica-rich limestone, chert, and spiculites (Figure 6; Larssen et al., 2005; Larssen et al., 2002).

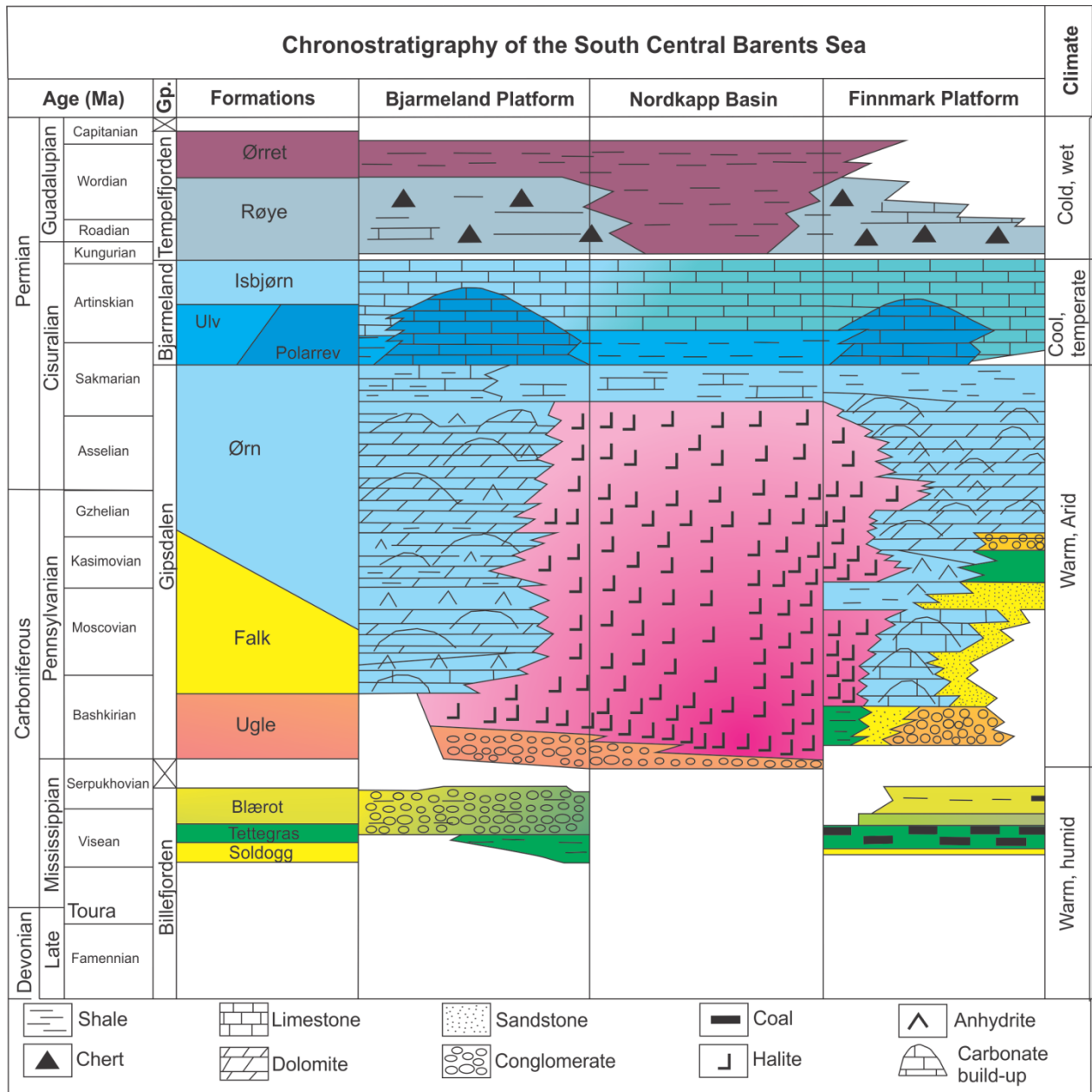


Figure 6 – The upper Paleozoic lithostratigraphic column of Bjarmeland Platform, Nordkapp Basin and Finnmark Platform (Modified from Larssen et al., 2005).

2.1 Late Devonian – Mississippian

During the Upper Devonian – Mississippian times, the southeastern Norwegian Barents Sea was situated at a paleolatitude approximately 15°N, resulting in a warm and humid climatic environment (Figure 7A; Stemmerik et al., 1999; Beauchamp, 1994). The Norwegian Barents Sea experienced regional extensional related tectonic events resulting in the development of large graben systems, e.g. Nordkapp Basin, during the Late Devonian - Early Carboniferous (Henriksen et al., 2011).

The Mississippian sequence of the Barents Sea and Svalbard region is termed the Billefjorden Group (Figure 6). The deposition of the Mississippian, Billefjorden Gp. occurred on alluvial plain-, graben and half-graben settings. The depositional sequence of the Upper Devonian – Lower Carboniferous units is described as a syn-tectonic sedimentary succession (Rønnevik et al. 1982). Deposition of the Billefjorden Gp. is defined as a transition in depositional environment from continental fluvial facies to marginal marine facies (Larssen et al., 2002).

The Billefjorden Gp. is subdivided into three different formations (Fm.), Soldogg Fm., Tettegras Fm. and Blærerot Fm. (Figure 6). The Soldogg Fm. is identified as an alluvial facies consisting of sandstone and conglomeratic sandstone with some laminae of shale, silt and coal (Larssen et al., 2002). The occurrence of the formation is confined to grabens and half-graben settings, and progressively onlap structural highs (Rønnevik et al. 1982). The deposition of the Tettegras Fm. is confined to half-graben settings and is identified as not being present along the crest of structural highs (Larssen et al. 2002). The depositional environment is interpreted as an extensive flood plain or a delta plain setting; based on the distinctive rhythmic sequences of fining upward cycles topped with coal (Ehrenberg et al. 1998a). The Blærerot Fm. was deposited as the latest stage of the Billefjorden Group. The lower section of the Blærerot Fm. consists of a thin unit of limestone deposits, and thus marks the first period of marine flooding of the Norwegian Barents Sea shelf (Larssen et al. 2002). The deposition of the carbonate unit was followed by deposition of dark shale, interpreted as having a lower shoreface origin (Bugge et al., 1995). The upper part of the Blærerot Fm. is identified as sandstone that possesses the distinctive appearance of upper shoreface sandstone (Bugge et al., 1995; Larssen et al., 2002).

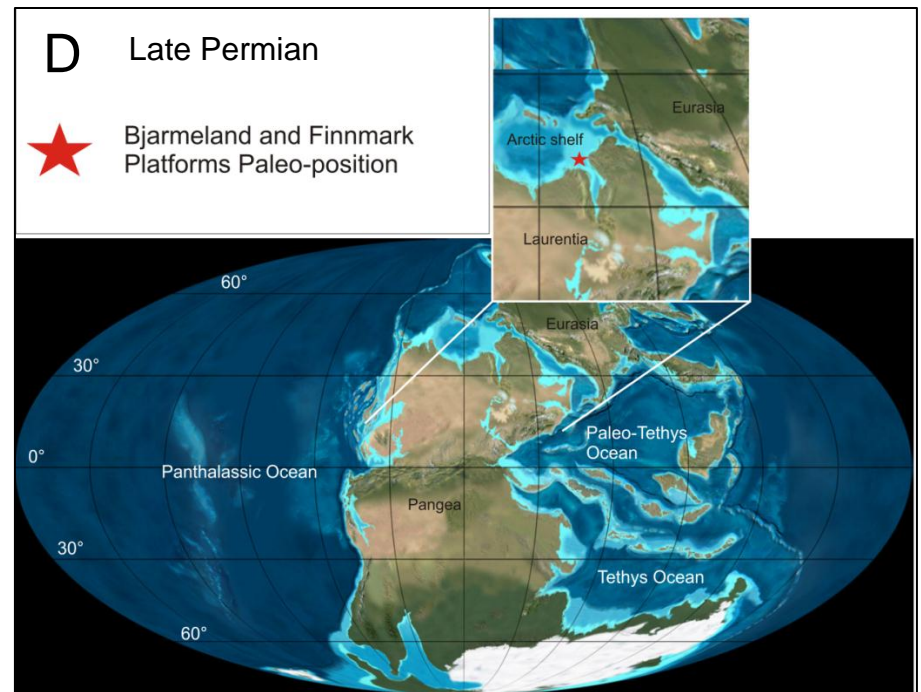
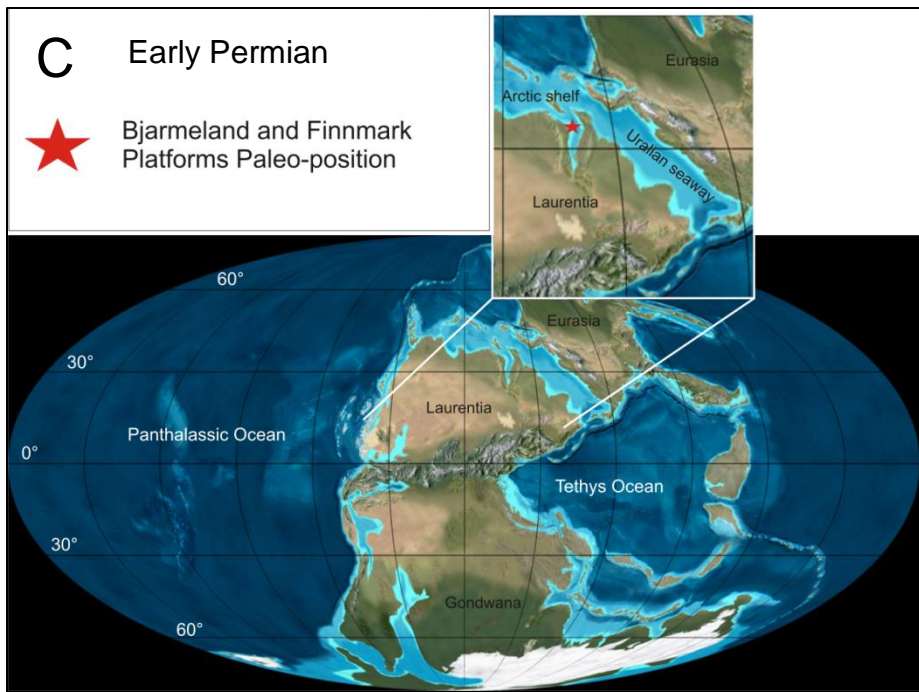
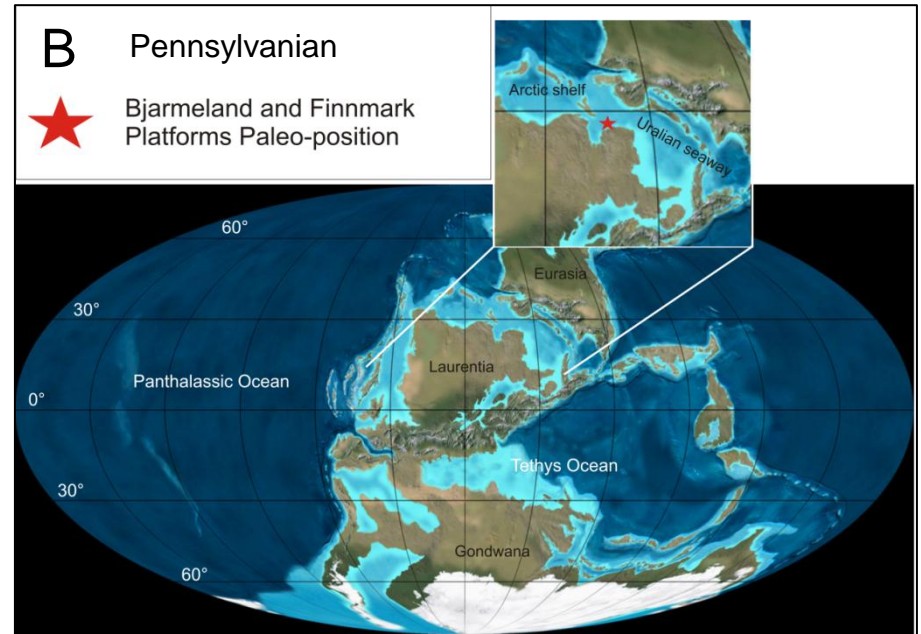
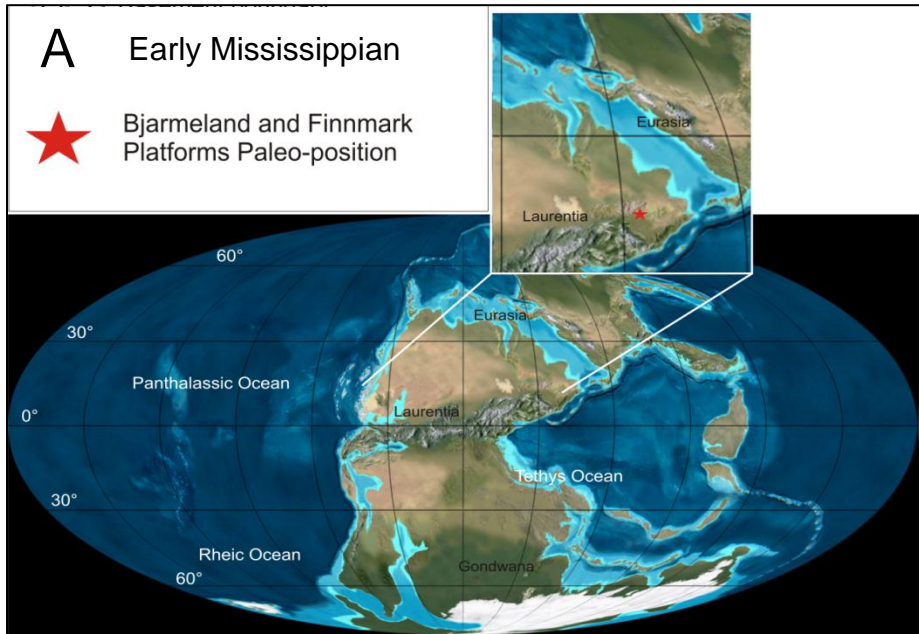


Figure 7 - Paleogeographic orientation of the south central Barents Sea. A) Paleogeographic map of Early Mississippian (Blakey, 2011; Stemmerik et al., 14 1999); **B)** Paleogeographic map of Pennsylvanian (Blakey, 2011; Stemmerik et al., 1999); **C)** Paleogeographic map of Early Permian (Blakey, 2011; Stemmerik et al., 1999); **D)** Paleogeographic map of Late Permian (Blakey, 2011; Stemmerik et al., 1999).

2.2 Pennsylvanian – Early Permian

Pennsylvanian to Early Permian in the Barents Sea region were situated at a paleo-latitude of ~25°N and the climatic setting were warm and arid (Figure 7B; Stemmerik et al., 1999). The Gipsdalen Gp. is widely recognized in the onshore on Svalbard, and in the subsurface of the Norwegian Barents Sea. The Gipsdalen Gp. consists of three highly diachronous sedimentary successions. The tectonic setting of during this period is identified by an active tectonic period in the Bashkirian, and followed by a period of tectonic quiescence in the middle and late Pennsylvanian (Stemmerik et al., 1999; Elvebakk et al., 2002).

The sedimentary strata of the Gipsdalen Gp. are composed of cyclic sedimentary sequences of meter- to tens of meter in thickness, as a result of the high frequency (100 Ky) and amplitude (> 50 m) glacio-eustatic sea-level fluctuations during the Pennsylvanian – Early Permian (Di Lucia et al., 2014, Stemmerik et al. 2008). The meter-thick rhythmic sequences can be correlated over greater distances in the Barents Sea region. The deposition of the heterozoan carbonates occurred in an ‘icehouse world’, with the rhythmic sedimentation as a result of the major glaciation covering the southern hemisphere in the Godwanaland.

The Ugle Fm. is identified as the lower part of the Gipsdalen Gp. is characterized by syn-tectonic alluvial sediments interbedded with shallow marine siliciclastics. The alluvial sediments are deposited during of the Middle Bashkirian rifting event. The sedimentary succession is isolated by fault-controlled basins (Larssen et al., 2002; Larssen et al., 2005). The following sequence, identified as the Falk Fm., was subjected to regional subsidence which resulted in deposition of heterolithic carbonate and siliciclastic sediments. The Gipsdalen Gp. was terminated by a depositional systems consisting of carbonate facies dominated by rhythmic sequences of carbonate facies deposited in the platform settings and evaporite deposition, this succession is defined as the Ørn Fm. (Larssen et al. 2002).

The alluvial sedimentary succession of the lower Gipsdalen Gp. is termed Ugle Fm. The deposition of the formation is confined to half-grabens created during the mid-Bashkirian rifting. The lateral extent of the formation is widespread, but locally developed in half-graben systems. The Ugle Fm. is present on Svalbard and in the subsurface Barents Sea (Larssen et al. 2002). The Falk Fm. is identified as heterolithic unit consisting of siliciclastics and carbonate units (Figure 6). The rhythmic interlayering of siliciclastic and carbonate units is a result of high sea-level fluctuations during this period (Stemmerik et al. 1998). The Falk Fm. was deposited during a period of an overall transgression in sea-level. The Ørn Fm. consists of carbonate facies that is dominated by rhythmic sequences of limestone and dolomite, and evaporites (Figure 6). The Ørn Fm. consists of carbonates that were formed during periods of transgressed sea-level, and followed by carbonate karstification and evaporite deposition in periods of regressed sea-level (Stemmerik et al., 1999). The carbonate biota in the Gipsdalen Gp. is made up of a protozoan carbonate environment. The carbonate environment consists of build-ups composed of Palaeoaplysina-phyllloid algae deposited on the shelf and structural highs, followed by

foraminifera dominated limestone deposits in deeper-marine settings. During sea-level lowstands, there was a progradation of the tidal flat and the platform carbonate units situated on structural highs was subjected to karstification as a result of sub-aerially exposure (Stemmerik et al., 1999; Elvebakk et al., 2002). During sea-level lowstand, precipitation of hypersaline water occurred in the basins and in restricted sub-basins on the platform (Rafaelsen et al. 2008).

2.3 Early Permian – Middle Permian

The Early to Middle Permian succession in the Norwegian Barents Sea is defined as the Bjarmeland Group (Figure 6). The group is subdivided into three different formations stretching from Kungurian to Gzhelian age. The three formations are termed Ulv, Polarrev and Isbjørn Fms. (Larssen et al. 2002). The three formations are well distributed in the Barents Sea region and there is a lateral interfingering between these three formations (Rafaelsen et al., 2008).

During the Early to Middle Permian, there was an abrupt change in paleolatitude affecting the present day Barents Sea area drifting northward to a paleolatitude approximately situated at 30-40°N (Figure 7C; Stemmerik et al., 1999; Beauchamp, 1994). The climatic conditions during this period consisted of cool and sub-tropical conditions. These climatic conditions differ largely from the arid-warm system during the Pennsylvanian-Early Permian and the deposition of Gipsdalen Gp. (Stemmerik and Worsley, 2005).

The climatic change impacted the carbonate fauna in the Bjarmeland Gp., which differ from the fauna in the Gipsdalen Gp. The Bjarmeland Gp. consists of a heterozoan biota dominated by bryozoan build-ups and bioclastic grainstones, while the Gipsdalen Gp. consists of protozoan carbonates including of Palaeoaplysina-phyllloid algae and foraminiferal limestone (Larssen et al., 2002). There is an overall rise in relative sea level throughout the deposition of the Bjarmeland Gp. which is evident in the different formations. The formations are considerably diachronous and show lateral differences between the three formations (Larssen et al., 2002; Larssen et al., 2005). The carbonate biota varies from outer-shelf bryozoan build-ups in the Polarrev Fm., inner-shelf carbonates in the Isbjørn Fm., and to micrite and fine-grained siliciclastic deposits in the Ulv Fm. (Larssen et al., 2002).

2.4 Late Permian

The Late Permian stratigraphy is termed the Tempelfjorden Gp. The group consists of the Røye and Ørret Formations (Figure 6). During the Late Permian, the Barents Sea region drifted towards a paleolatitude of approximately 45°N (Figure 7D; Stemmerik et al., 1999). During the Late Permian there was a drastic change in depositional environment, from a shallow-marine carbonate system in the Gipsdalen and Bjarmeland Groups., to a shelf and basin dominated setting (Larssen et al., 2002). The change in paleo-latitude and the closing of the Uralian seaway in the eastern Barents Sea resulted in severe impact on the climatic environment, which transitioned from temperate to colder and wet conditions (Stemmerik et al. 1999; Larssen et al., 2002). The Uralian seaway was the primary source for influxes of warm sea-water from the Paleo-Tethys Ocean (Figure 7). The dramatic change in the sea-temperature impacted the carbonate system and resulted in a change in the fauna. The fauna changed from a calcite rich carbonate system to a silica-rich system caused by the increased rate of silica in the ocean (Ehrenberg et al., 1998a; Stemmerik et al. 1999).

The Røye Fm. consists of calcareous and silica-rich facies (Ehrenberg et al., 1998a). The silica-rich environment resulted in deposition of dark and light spiculites, spiculitic chert, and fine-grained calcareous siliciclastics including marl, claystone and shale in the deep basinal settings (Larssen et al., 2002). The Ørret Fm. is identified as fine-grained siliciclastics deposited in deep-marine environments. The wet climatic environment during the Late Permian resulted in increased erosion rate and transportation of sand and mud into the marine environment (Ehrenberg et al., 1998a).

Gradual sea-level fluctuation prevailed throughout the Late Permian affecting the depositional facies of the Tempelfjorden Gp. (Larssen et al., 2002). However, the cyclic sedimentation seen in the Pennsylvanian to Middle Permian is less frequent in the Tempelfjorden Group. The glacial icecap covering the southern hemisphere on Gondwanaland is at an end during the Late Permian (Figure 7D). In periods of transgressed sea-level a higher abundance of fine grained siliciclastic was deposited on the platforms. Furthermore, as a result of the high content of silica in the sea-water, colonies of silica sponges were deposited and eventually resulting in spiculite build-ups (Larssen et al., 2002). Periods of sea-level lowstand, deposition of carbonate micrite occurred in shallow marine environment in the near coastal setting. The carbonate biota during this period included deposits of bryozoans, crinoids and brachiopods (Elvebakk et al., 2002).

3. Database and Methodology

3.1 Well Data

18 wildcat wells have penetrated the upper Paleozoic succession in the Norwegian sector of the Barents Sea with the main, regional focus situated on the Loppa High and Finnmark Platform. For the purpose of the identifying the upper Paleozoic succession, and define seismic sequences correlating on both the Bjarmeland and Finnmark Platforms, only five wells has been applied (Table 1). The well data consists of datasheets providing, check shot and/or VSP data, well logs. The well tops applied to seismic well correlation and interpretation were stratigraphic well tops created from seismic sequences. The well tops that are developed based on seismic well-tie, and regional seismic reflectors representative for the upper Paleozoic succession throughout the Bjarmeland and Finnmark Platforms.

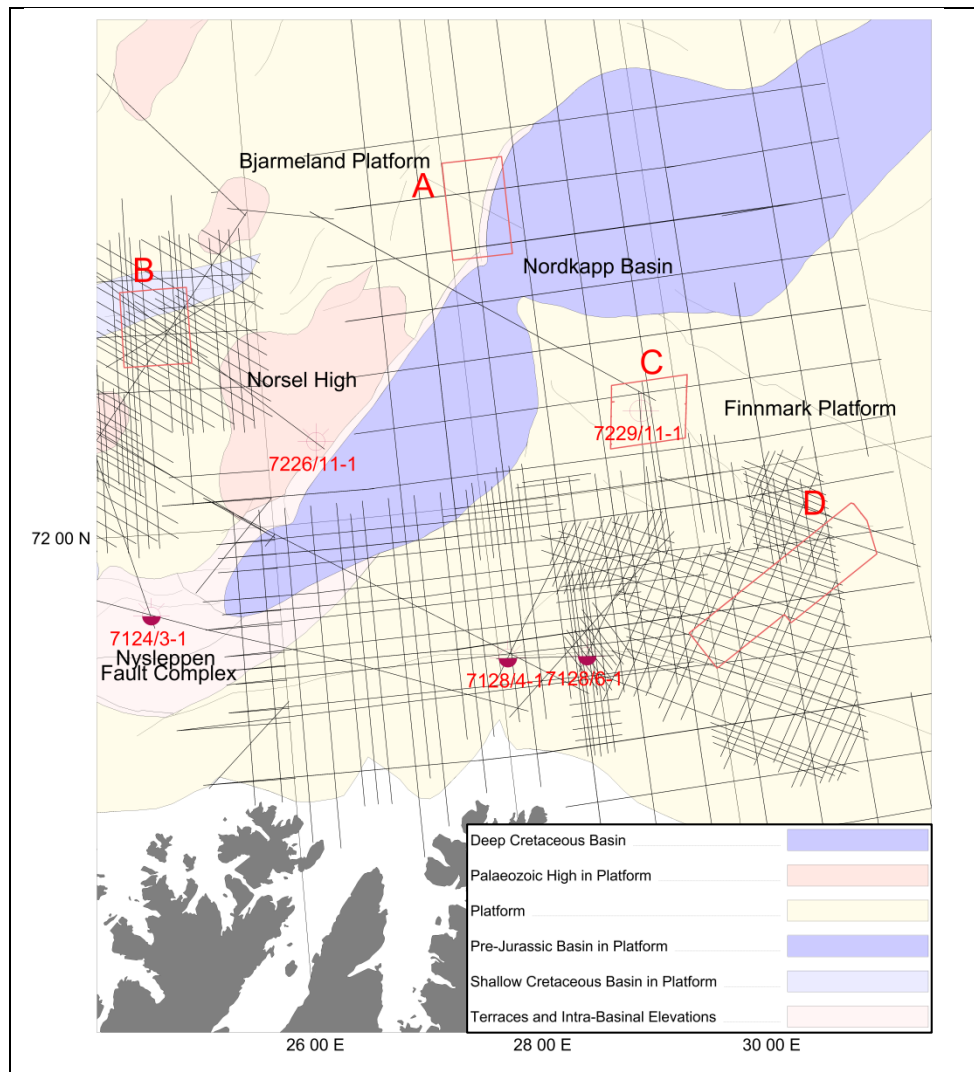


Figure 8 - Regional structural elements map presented with the data coverage (Well data, 3D seismic- and 2D seismic data).

| Well data information | | | | |
|-------------------------|-----------|------|-------------------------------|-------------------------|
| Structural elements | Well | Year | Total measured depth (MD) [m] | Oldest penetrated rocks |
| Nysleppen Fault Complex | 7124/3-1 | 1987 | 4730.0 | Late Carboniferous |
| Norsel High | 7226/11-1 | 1988 | 5200.0 | Pre-Devonian |
| Finnmark Platform | 7229/11-1 | 1993 | 4630.0 | Late Carboniferous |
| | 7128/6-1 | 1991 | 2543.0 | Pre-Devonian |
| | 7128/4-1 | 1994 | 2530.0 | Pre-Devonian |

Table 1 – Summary table of well data used in the thesis.

The acoustic P-wave velocities have been adapted from the sonic logs calibrated with the check shot survey (Table 2).

| Group well tops | Acoustic velocities | | | | | | | | | |
|--------------------------|---------------------|----------------|--------------|----------------|--------------|----------------|--------------|----------------|--------------|----------------|
| | 7124/3-1 | | 7226/11-1 | | 7229/11-1 | | 7128/4-1 | | 7128/6-1 | |
| | Depth [mTVD] | Velocity [m/s] | Depth [mTVD] | Velocity [m/s] | Depth [mTVD] | Velocity [m/s] | Depth [mTVD] | Velocity [m/s] | Depth [mTVD] | Velocity [m/s] |
| <i>Top Tempelfjorden</i> | 3450 | 4433 | 3852 | 5031 | 3853 | 4233 | 1544 | 3358 | 1597 | 3048 |
| <i>Top Bjarmeland</i> | 3927 | 6417 | 4079 | 5965 | 3945 | 5088 | 1679 | 5124 | 1720 | 4748 |
| <i>Top Gipsdalen</i> | 4244 | 6181 | 4308 | 6199 | 4256 | 6252 | 1794 | 5670 | 1809 | 5862 |

Table 2 - Table displaying the P-wave velocities at the group well tops extracted from the sonic logs.

3.2 Seismic Data

The seismic data consists of four 3D-seismic cubes (labeled from A to D) and eleven 2D seismic surveys (Table 3; Table 4). Two 3D and six 2D seismic surveys are located on the Finnmark Platform and two 3D and five 2D seismic surveys are located on the Bjarmeland Platform. Only one well penetrates the succession within 3D seismic surveys (Figure 8). The extensive amount of 2D seismic data is therefore applied to tie between the wells and the 3D seismic cubes.

| 3D Seismic data coverage | | |
|---------------------------------|--------------------------|----------------------------|
| Location | Finnmark Platform | Bjarmeland Platform |
| 3D Seismic survey | A: BG 0804 | C: SH 9102 |
| | B: NH 0608 | D: ST 9802 |

Table 3 - 3D Seismic coverage on Finnmark- and Bjarmeland Platforms.

| 2D Seismic data coverage | | |
|---------------------------------|--------------------------|----------------------------|
| Location | Finnmark Platform | Bjarmeland Platform |
| 2D Seismic survey | AN88-9Q6-1 | MN87-4 |
| | BSS01 | NPD-NOLO-85 |
| | FEC89 | SG8737 |
| | FEC90 | SG8837 |
| | NPD-FOE186 | ST8611 |
| | NPD-FOE286 | |

Table 4 - 2D Seismic data coverage on Finnmark- and Bjarmeland Platforms.

Seismic data covering Area A was acquired in 2008 (Table 5). The area is located on the northeastern margin of the Bjarmeland Platform, along the flank of the Nordkapp Basin (Figure 8). Area B is located on the western margin of the Bjarmeland Platform, crosscutting into the Swaen Graben to the north, and was gathered in 2006 (Figure 8). The seismic area C is located on the northern part of the Finnmark Platform, and the seismic data was sampled in 1991 (Figure 8). The Area D is located on the south eastern part of the Finnmark Platform and was acquired in 1998 (Figure 8; Table 5).

The orientation, length of bins, polarity, datum and frequency content of the seismic survey are listed in the table below (Table 5). The frequency content differs between the different cubes, whereas the dominant frequencies range from 17.25 to 27.00 Hz (Table 5). The mean frequencies range from 22.88 to 32.30 Hz. The highest mean and dominant frequency content is associated with Area B, and the area that consists of the lowest frequency content is Area C (Table 5).

| Seismic survey information table | | | | | | | |
|---|------------------------------------|------------------------------------|------------------------------------|------------------------------------|------------------------------------|------------------------------------|------------------------------------|
| A) BG 0804 | | B) NH 0608 | | C) SH 9102 | | D) ST 9802 | |
| <i>Geodetic datum</i> | ED 50 | <i>Geodetic datum</i> | ED 50 | <i>Geodetic datum</i> | ED 50 | <i>Geodetic datum</i> | ED 50 |
| <i>Projection</i> | UTM 35 | <i>Projection</i> | UTM 35 | <i>Projection</i> | UTM 34 | <i>Projection</i> | UTM 36 |
| <i>Sample interval</i> | 4 | <i>Sample interval</i> | 4 | <i>Sample interval</i> | 4 | <i>Sample interval</i> | 4 |
| <i>Number of inlines</i> | 792 | <i>Number of inlines</i> | 1719 | <i>Number of inlines</i> | 829 | <i>Number of inlines</i> | 2195 |
| <i>Number of X-lines</i> | 2579 | <i>Number of X-lines</i> | 2016 | <i>Number of X-lines</i> | 1143 | <i>Number of X-lines</i> | 5535 |
| <i>Inline interval</i> | 25.12 | <i>Inline interval</i> | 12.54 | <i>Inline interval</i> | 25.14 | <i>Inline interval</i> | 12.59 |
| <i>X-line interval</i> | 12.56 | <i>X-line interval</i> | 12.54 | <i>X-line interval</i> | 25.15 | <i>X-line interval</i> | 12.58 |
| <i>Inline direction from north</i> | - 17.96 ° | <i>Inline direction from north</i> | - 15.18 ° | <i>Inline direction from north</i> | 70.24 ° | <i>Inline direction from north</i> | 39.66 ° |
| <i>Polarity</i> | Zero phase – Normal Polarity (SEG) | <i>Polarity</i> | Zero phase – Normal Polarity (SEG) | <i>Polarity</i> | Zero phase – Normal Polarity (SEG) | <i>Polarity</i> | Zero phase – Normal Polarity (SEG) |
| Seismic survey | | | | | | | |
| Mean Frequency | | Dominant Frequency | | Bandwidth | | | |
| <i>A) BG 0804</i> | | 27.78 Hz | | 25.00 Hz | | 22.25 Hz | |
| <i>B) NH 0608</i> | | 32.30 Hz | | 27.00 Hz | | 28.75 Hz | |
| <i>C) SH 9102</i> | | 24.06 Hz | | 17.25 Hz | | 19.75 Hz | |
| <i>D) ST 9802</i> | | 22.88 Hz | | 21.25 Hz | | 28.25 Hz | |

Table 5 - Seismic survey information table.

3.3 Seismic Well-tie

3.3.1 Seismic Wavelet

The method that has been applied to construct the wavelet for the well-tie process is a multi-wavelet procedure. The multi-wavelet has been used for conducting the seismic well-tie, for all the wells. The multi-wavelet is constructed by using a statistical average calculated based on extracted wavelets, derived from all the five wells. The input data for the multi-wavelet calculation were the five extracted wavelets, which were obtained from the well penetrating the upper Paleozoic succession (Appendix 1). For all the wells, the extracted wavelet has been extracted from the similar interval, which is the Permian-Triassic Unconformity. The multi-wavelet is calculated to have a wavelength of 128 ms, and sample interval of 2 ms (Figure 9). The wavelet is zero phased and has not been modified in regards to phase manipulation, time shifting, or Hanning filtering. The power spectrum reveals that the highest seismic frequencies are located around 25-30 Hz (Figure 10). The wavelet has a normal polarity, in the seismic this means that increase in acoustic impedance results in a red peak, in SEG polarity convention.

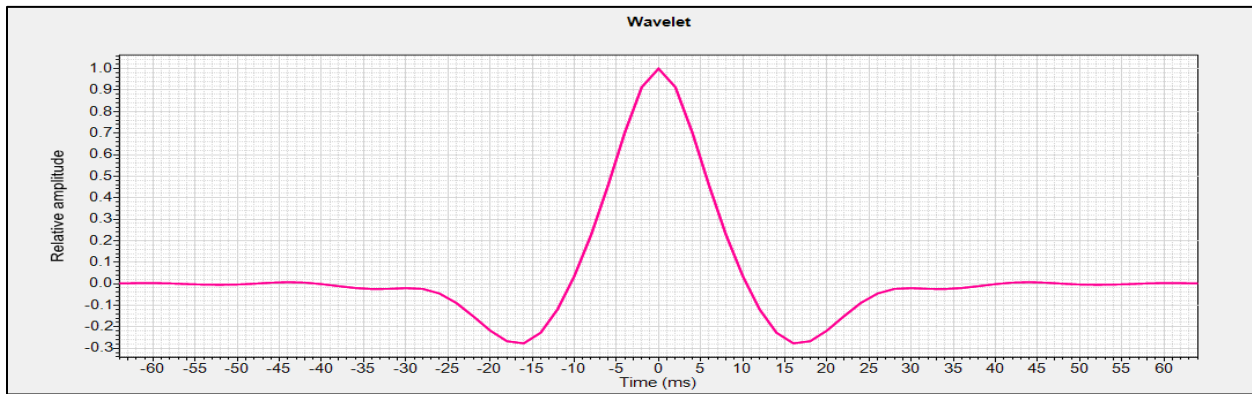


Figure 9 - Seismic Wavelet applied in order to create a seismic well-tie.

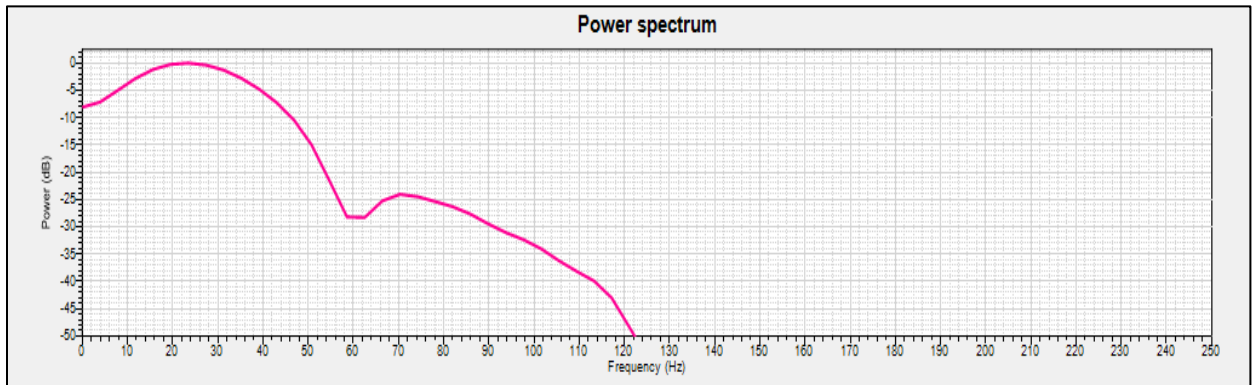


Figure 10 - The Power Spectrum of the seismic wavelet used in the seismic well-tie process.

3.3.2 Seismic Well-tie

The synthetic seismogram has been calculated by using the sonic and density log to compute the acoustic impedance and the multi-wavelet to develop the forward modelling (Appendix 2.1). The sonic log has been calibrated with the time-depth table adapted from the check shot and VSP survey. For well 7128/4-1 the synthetic seismogram has obtained a maximum cross correlation with the seismic data of 56.1 % at -4 ms lag time. This correlation has been obtained across a time lag correlation window is set to 600 ms (Figure 11). The seismic section that has been used to tie the well is CN92-209 on the Finnmark Platform. The seismic line is strike through both wells 7128/6-1 and 7128/4-1, and considered as the best suitable seismic line, for generating the seismic well-tie for the area (Figure 13A).

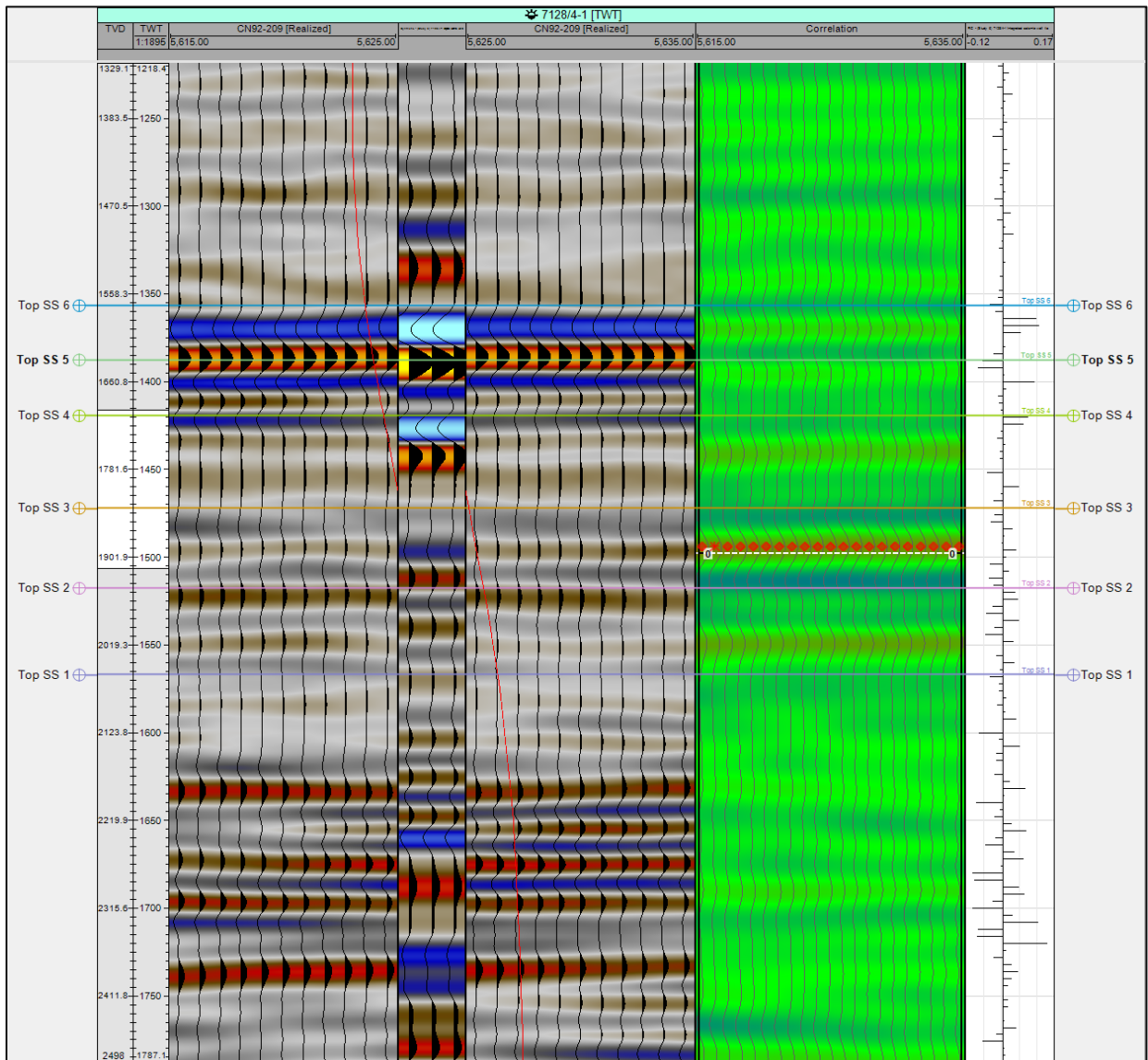


Figure 11 - Seismic well tie from well 7128/4-1 on the Finnmark Platform

The results derived for well 7229/11-1 resulted in maximum cross correlation of 68.5% at 0 ms lag time. This value has been extracted across a time lag correlation window is set to 520 ms (Figure 12). The regional confidence in the seismic well-tie covering the upper Paleozoic successions in the areas from Bjarmeland to Finnmark Platforms (Figure 13B). The low seismic resolution and lack of continuous reflectivity across the Nordkapp Basin, marked with a questionmark in Figure 13B. This causes some degree of uncertainty in the well-tie on the Bjarmeland Platform. Nonetheless, the reflectivity pattern identified as presenting the identical reflectivities as those seen on the Finnmark Platform. Despite the uncertainties by crossing the Nordkapp Basin, this enhance the confidence in the seismic well-tie across the basin (Figure 13B).

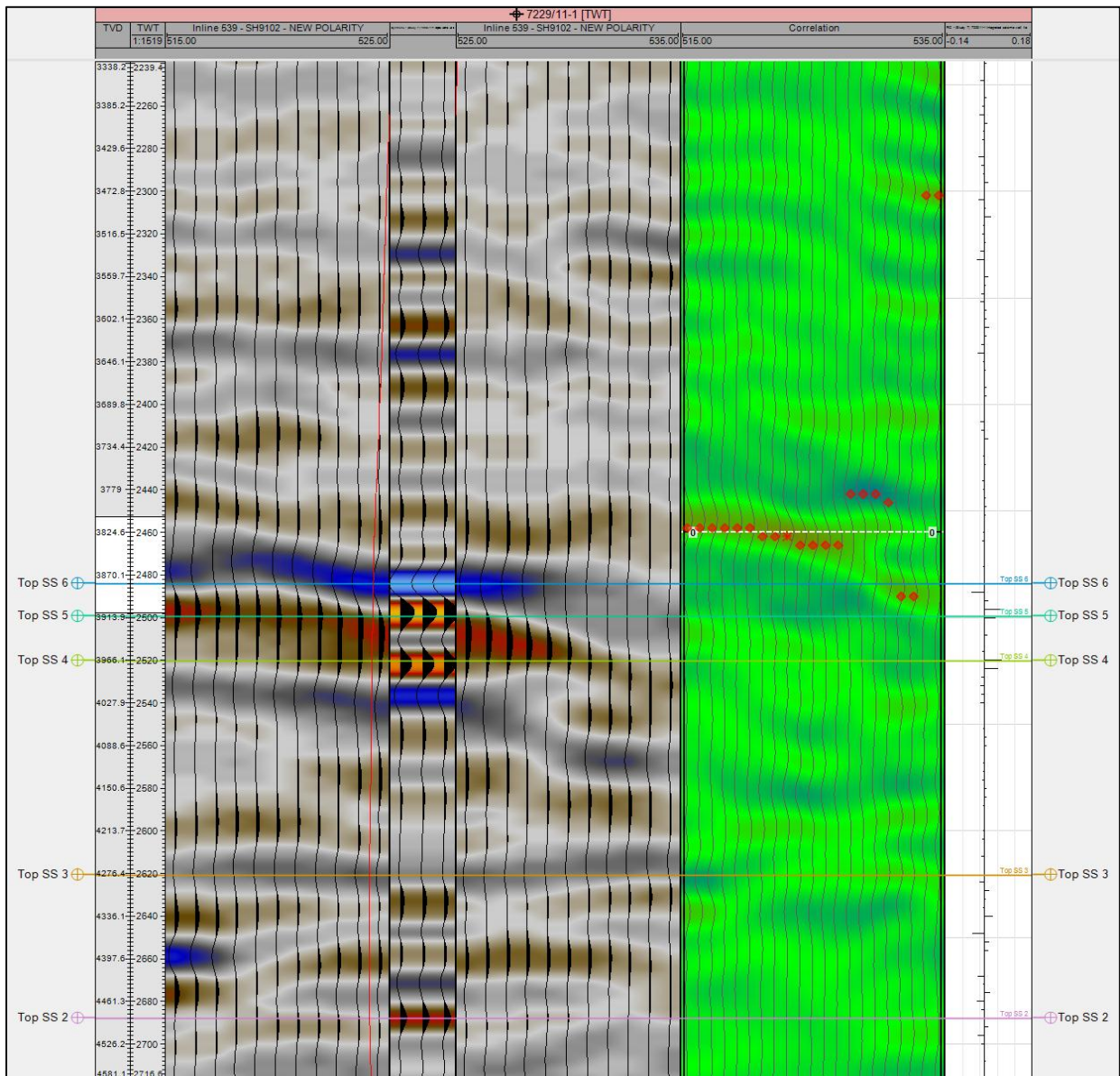


Figure 12 - Seismic well-tie from well 7229/11-1 on Finnmark Platform

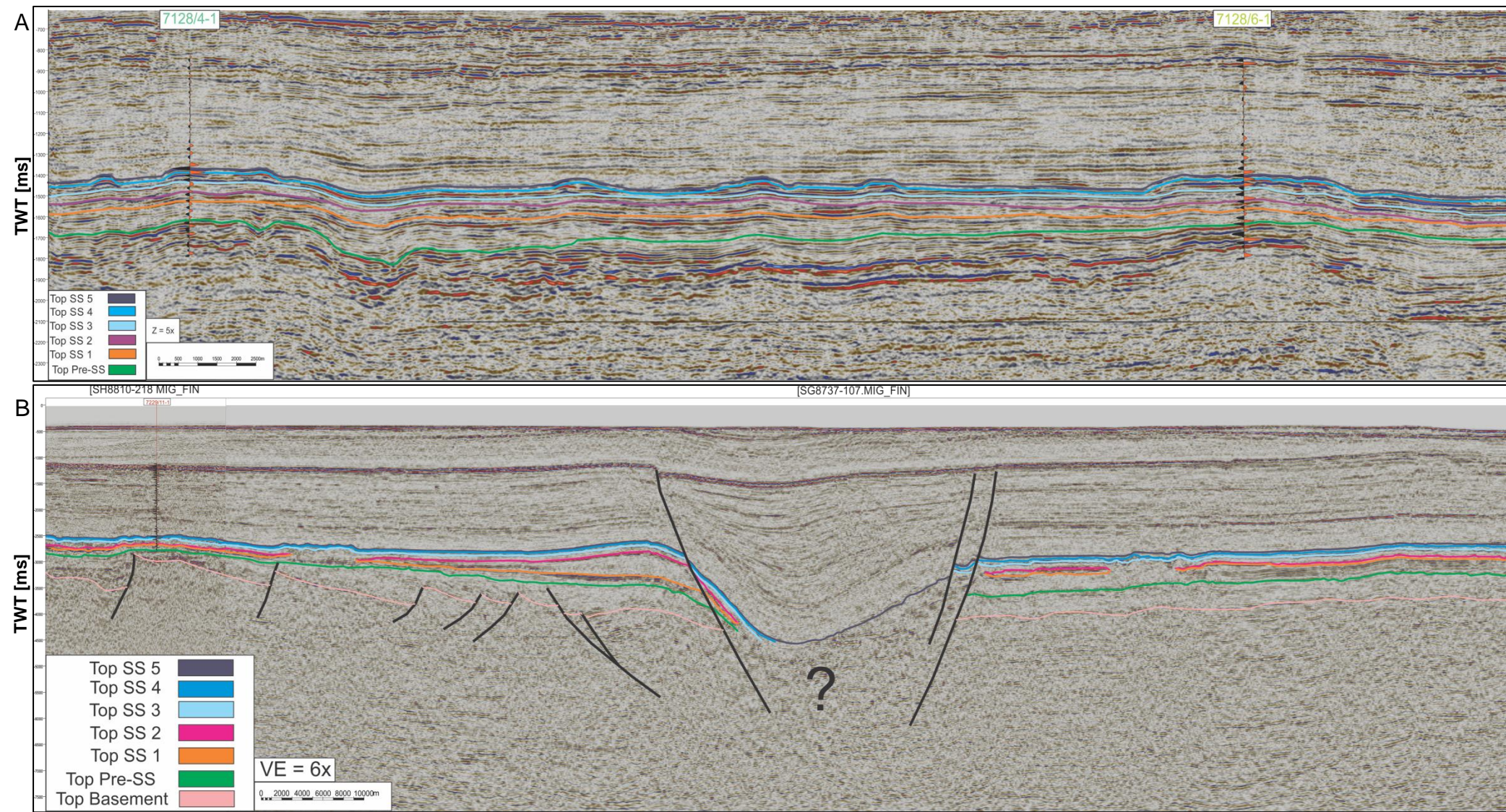


Figure 13 - Seismic sections with corresponding reflectors and seismic well-tie. A) 2D seismic line striking through well 7128/4-1 and 7128/6-1 on Finnmark Platform. B) Composite line striking through 2D seismic line SH8810-218 and 2D seismic line SG8737-107 displayed with the synthetic seismogram from well 7229/11.

3.4 Seismic Interpretation and Visualization Methods

3.4.1 Seismic Interpretation

The seismic interpretation is based on seismic stratigraphic framework developed for the upper Paleozoic succession in the area. The seismic horizons define the boundaries of each seismic sequence. The seismic sequences are divided into different seismic facies units. The seismic facies classification is created to define the seismic parameter variations caused by geological changes within the seismic sequences (Vail, 1987). The interpretation of the seismic data has been conducted using Petrel 2014© by Schlumberger. Seismic attributes have been generated by using the attribute toolbox in Petrel 2013 and the RBG spectral decomposition is generated in GeoTeric© by ffA.

Seismic resolution has been calculated to illustrate the variability of the horizontal- and vertical resolutions in the different 3D seismic areas. There is relatively low variability in the seismic resolution between the four different seismic areas. Except the lower resolution in Area C that deviate from the three other areas (Table 6). Calculation of the vertical- and horizontal resolutions is uncertain, which is related to the average velocities derived from well data (Appendix 2.2). The calculated results of the vertical- and horizontal resolutions, is shown to be relatively similar. Hence, the uncertainty caused by the average velocities is considered as negligible and insignificant for the data quality, essential for conducting this study (Table 6; Appendix 2.2).

| | A) BG0804 | B) NH0608 | C) SH9102 | D) ST9802 |
|------------------------------|------------------|------------------|------------------|------------------|
| Wavelength | 232.9 m | 215 m | 295 m | 232 m |
| Vertical Resolution | 58.8 m | 59.92 m | 73.7 m | 50.1 m |
| Horizontal Resolution | 58.2 m | 53.75 m | 73.6 m | 73.6 m |

Table 6 - Calculated results of the wavelength, vertical- and horizontal resolution of the four seismic areas.

3.4.2 Seismic Stratigraphic Framework

3.4.2.1 Seismic Sequences

The carbonate sequence is divided into three groups: Gipsdalen-, Bjarmeland-, and Tempelfjorden Groups. Several studies have defined the upper Paleozoic succession into seismic sequences, e.g. Sayago et al. (2014), Colpaert et al. (2007); Samuelsberg et al. (2003) and Bugge et al. (1994). However, these studies were conducted on the Loppa High and Finnmark Platform respectively and thus, does not incorporate the regional extent including the Bjarmeland Platform (Figure 14). In this study, five seismic sequences have been defined in the four 3D seismic areas, and correlated with 2D lines (Table 7; Figure 15; Figure 14). The nomenclature established as seismic sequences are identified as seismic reflections, which abide by synchronous geological time lines within the assigned seismic wavelet. A regional seismic line crossing the Nordkapp Basin from NW – SE presents the interpreted seismic sequences (Figure 16). A well correlation section that includes wells from the Nysleppen Fault Complex, Bjarmeland Platform and Finnmark Platform is shown in Figure 19. The well section illustrates an overall thinning of the upper Paleozoic succession, going from the Bjarmeland Platform towards the Finnmark Platform (Figure 15).

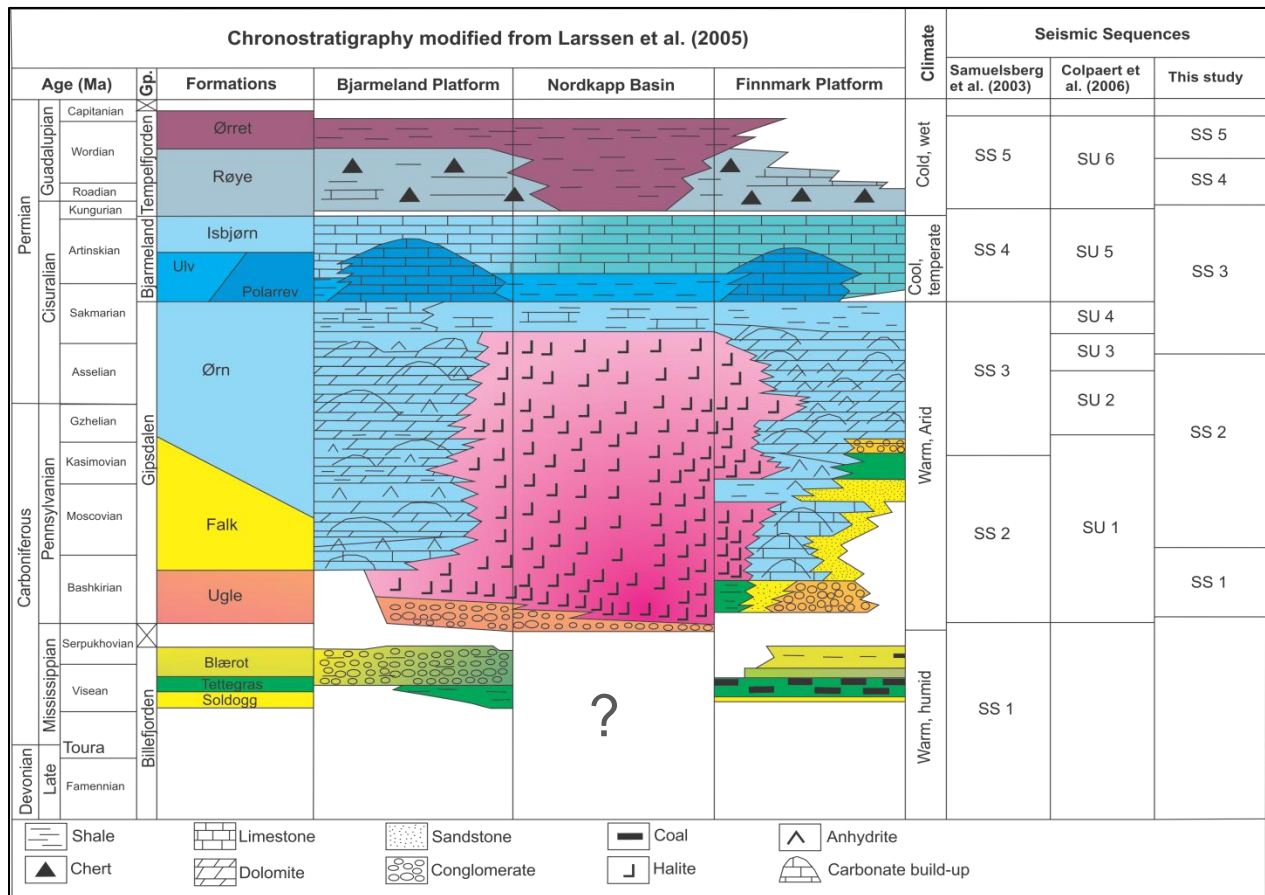


Figure 14 – The upper Paleozoic lithostratigraphy of the south central Norwegian Barents Sea (Larssen et al. 2005). The comparisons of different seismic sequences are taken from previous authors (Samuelsberg et al., 2003; Colpaert et al., 2006) and this thesis.

| Horizon | Acoustic Impedance | Seismic response (peak / through) |
|---------------------------|---------------------------|--|
| Top Seismic Sequence 5 | Decrease | Trough (Blue) |
| Top Seismic Sequence 4 | Increase | Peak (Red) |
| Top Seismic Sequence 3 | Increase | Peak (Red) |
| Top Seismic Sequence 2 | Decrease | Trough (Blue) |
| Top Seismic Sequence 1 | Increase | Peak (Red) |
| Top Pre-Seismic Sequences | Decrease | Trough (Blue) |

Table 7 - Table presenting the seismic horizons with their response in acoustic impedance and in the seismic section.

Pre-Seismic Sequences (Pre-SS)

Well character: The Pre-SS unit observed from well data consists of basement and the Billefjorden Gp. Basement has been penetrated by two the 7226/11-1 and 7128/4-1 (Appendix 1.2; Appendix 1.4). The basement consists of Pre-Devonian low-grade metasedimentary rocks characterized as schist with amphibolite rich facies. The Billefjorden Group comprises of siliciclastic rocks of Mississippian age. The Billefjorden Gp. can be subdivided into a lower and upper section (Figure 15). The lower section is sand rich with occasional interlayering of silt and shale, interpreted as a fluvial deposition. The upper section is dominated by a silt and shale prone succession (Figure 15). The depositional environment is interpreted as meandering river and floodplain deposits (Appendix 1).

Seismic character: The Pre-SS is synchronous to the Top Billefjorden Gp., and characterized by a decrease in acoustic impedance (Table 7). The decrease is caused the lithological change from a carbonate-rich succession, into a fluvial siliciclastic succession. Consequently result in a blue reflector in the synthetic seismogram (Figure 15; Appendix 1).

Seismic Sequence 1 (SS 1)

Well character: SS 1 is identified in the well data as the lower part of the Gipsdalen Group. The sequence can be sub-divided into a lower and upper section (Figure 15). The lower part is spatially confined to parts of the Finnmark Platform and Svalbard (Stemmerik et al., 1999). The lower part consists of alluvial sediments with conglomeratic and sandstone-rich facies, defined as the Ugle Formation. The upper part consists of carbonate and dolomite-rich facies with some interlayering of shale-rich beds. Internally, this succession shows a cyclic pattern that is interpreted to be caused by glacio-eustatic sea-level fluctuations that occurred at this time (Ehrenberg et al., 1998a).

Seismic character: Top SS 1 is defined as an increase in acoustic impedance, and corresponds to the lower part Gipsdalen Group (Table 7). The seismic sequence is confined by the top Pre-SS surface as its base, and the top SS 1 (Figure 15; Appendix 1).

Seismic Sequence 2 (SS 2)

Well character: SS 2 represents the middle part of the Gipsdalen Gp. equivalent to the carbonate, dolomite and evaporitic facies within Ørn Formation. Well penetration within this

sequence (e.g. 7229/11-1) has recorded independent evaporite deposits, and carbonates interbedded with evaporite-rich facies (Figure 15; Appendix 1.3).

Seismic character: Top SS 2 is identified as a decrease in acoustic impedance (Table 7). The decrease in acoustic impedance is caused as a contrast between the anhydrite rich evaporite sequence and the overlying carbonate units (Figure 15; Appendix 1). The base of the sequence is bounded by the top of SS 1 (Figure 15).

Seismic Sequence 3 (SS 3)

Well character: SS 3 comprises of the upper part of the Gipsdalen Gp. equivalent to the Ørn Fm. and the Bjarmeland Group. The well results of the Ørn Fm. identify a sequence that primarily consists of protozoan carbonates and occasional carbonate build-ups (Appendix 1). The carbonate facies sequence within the Bjarmeland Gp. is characterized by a heterozoan succession dominated by platform carbonates and bryozoan build-ups (Appendix 1).

Seismic character: Top SS 3 corresponds to the top Bjarmeland Gp. and identified as an increase in acoustic impedance (Table 7). The seismic sequence is confined within the top of the SS 2, and the Top SS 3 (Figure 15).

Seismic Sequence 4 (SS 4)

Well character: SS 4 represents the lower part of the Tempelfjorden Gp. defined as the Røye Fm. (Larssen et al., 2002; Larssen et al., 2005). The succession comprises of calcareous spiculite and spiculitic limestone. The development of calcareous spiculite mounds is spatially confined to the southeastern margin of the Finnmark Platform, and spiculitic limestone facies is regional extensive throughout the Barents Sea region (Figure 15; Appendix 1.4; Appendix 1.3; Ehrenberg et al., 1998a). The sequence represents a period of overall transgressive sea-level in the Barents Sea region with deposits of open marine carbonates (Appendix 1).

Seismic character: Top SS 4 is characterized as an increase in acoustic impedances and therefore results in a red peak in the seismic section (Table 7). The base of the sequence is bounded by the top SS 3 surface (Figure 15).

Seismic Sequence 5 (SS 5)

Well character: SS 5 is identified in the well data as the upper part of the Tempelfjorden Gp. equivalent to the Ørret Fm. The sequence comprises of deposits of fine-grained open marine siliciclastic sediments (Figure 15; Appendix 1). The shale-rich succession is regionally extensive throughout the Barents Sea region. The top of this sequence is equivalent to the Permian-Triassic unconformity marking the end of the Tempelfjorden Gp. period (Appendix 1).

Seismic character: Top SS 5 corresponds to a decrease in acoustic impedance and corresponds to a blue seismic through (Table 7; Figure 15). The base of sequence corresponds to the top SS 4 surface.

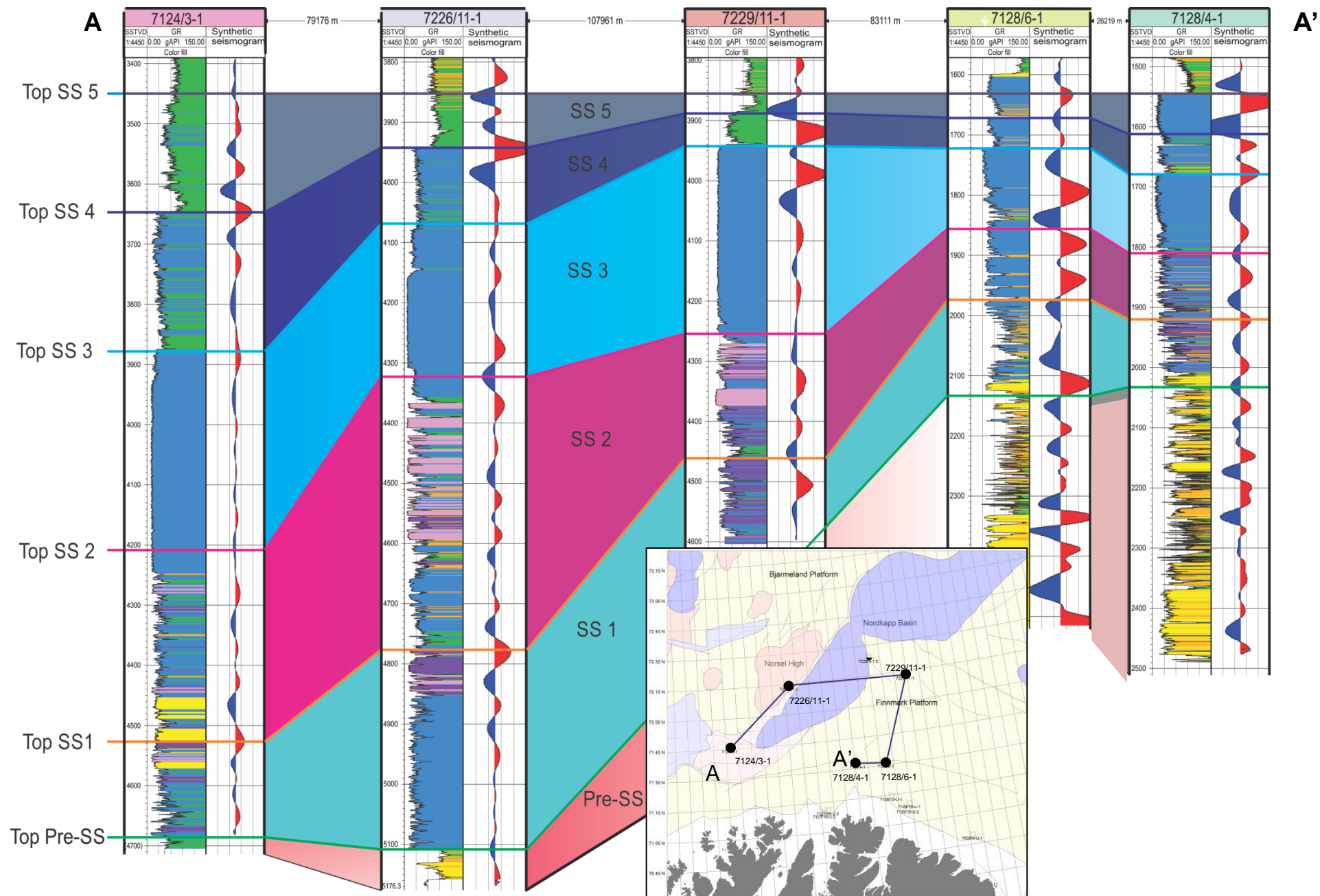


Figure 15 - Well section from the Nysleppen Fault Complex, Norsel High and Finnmark Platform. The well section is defined with the seismic sequences identified for this thesis.

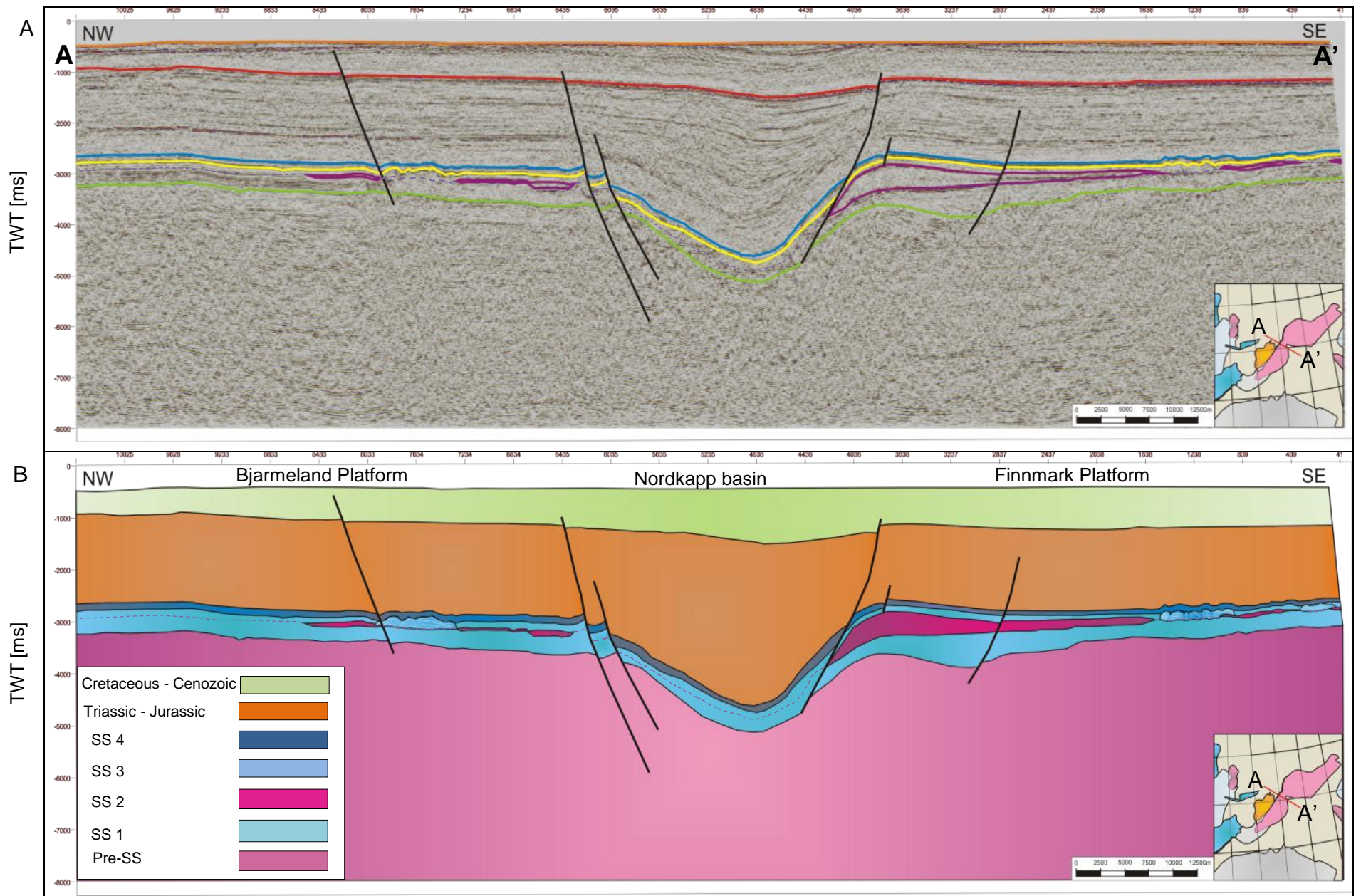


Figure 16 - Seismic section and Geoseismic section with seismic correlated seismic sequences from Bjarmeland- to Finnmark Platform through the thinnest part of the Nordkapp Basin.

3.4.3 Seismic Attributes

Seismic attributes have been generated in this study to enhance the seismic image of the carbonate build-ups succession and to visualize the seismic geomorphology. The attributes that has been applied in this study are RMS Amplitude, variance and color-blended spectral decomposition. The variance attribute operates relatively similar to the RMS amplitude attribute whereas both of the attributes measure variations. The variance attribute measure variations laterally, in contrast to the RMS that measure the vertical variations.

3.4.3.1 RMS Amplitude

The root-mean-square (RMS) Amplitude attribute is derived by calculating the square root of the sum of the squared amplitude, and then divided by the number of samples that have been used. The maps generated from the attribute identify geological features that have been isolated from the background noise and presented in amplitude response. The mathematical formula for calculating the RMS Amplitude is given:

$$amp_{rms, n} = \sqrt{\frac{\sum_{i=1}^n amp_i^2}{k}} \quad (\text{Equ. 3.1})$$

Where amp_{rms} is the RMS amplitude, amp is the amplitude, and k is the number of samples.

3.4.3.2 Variance (Edge method)

The variance attribute represents the variability in trace to-trace for a particular sample interval and developed as a tool to enhance the visibility of the discontinuity trends in the seismic volume. The attribute is a volume attribute that produces lateral changes in acoustic impedance that is interpretable. The attribute is created to visualize the areas with similar traces produce low variance coefficients, and discontinuities then have high variance coefficients.

3.4.3.3 Spectral Decomposition

The spectral decomposition is applied as an attribute to enhance the visualization of the seismic geomorphology within the areas based on the frequency spectrum and contrast within the seismic volumes. In order to apply the spectral decomposition as a seismic attribute on the different horizons, the frequency content within the seismic area are required to be increased in the lower and upper power spectrum. The power spectrum of the seismic volume is increased by multiplying the size of the increase to the respective frequency signal for each of the seismic volumes (Appendix 9.2.2). The equations applied to spectrally enhance the seismic volume and a red-blue-green color blend is created by associating different set of colors to the frequency intervals (Figure 17). The general workflow for developing a RGB spectrally enhanced color blend is presented in Figure 17 below.

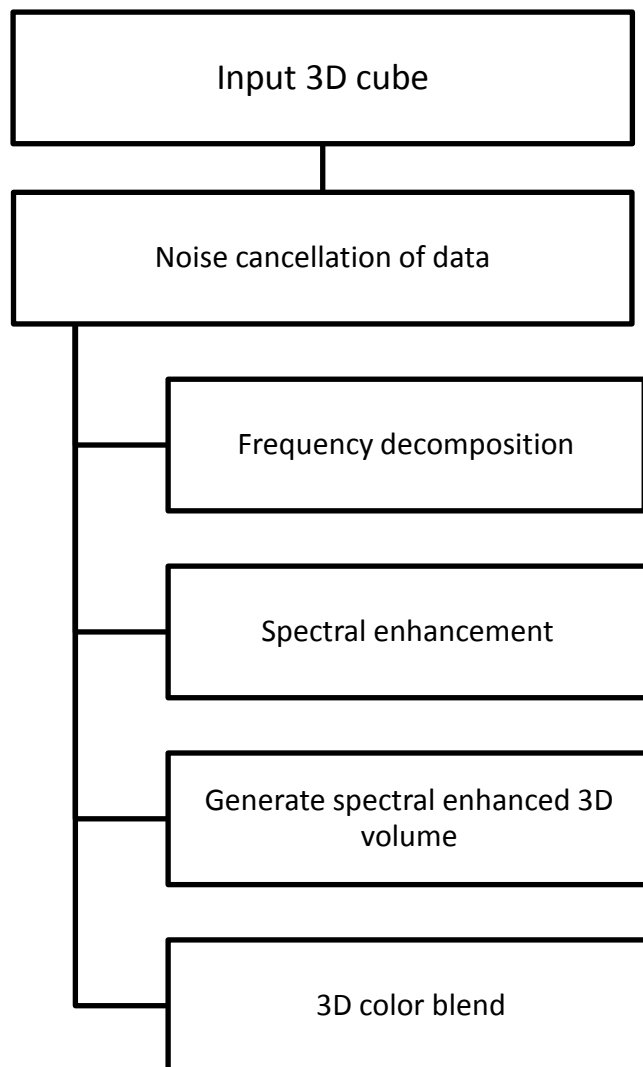


Figure 17 – The workflow that have been applied to generate a spectral decomposed volume.

The input parameters for the spectral enhancement were generated from the frequency decomposition and based on time-slices. The specifications set to frequency decompose the seismic volumes was uniform in the four areas. The decomposition method was set to be constant bandwidth, with a minimum frequency of 10 Hz and maximum frequency of 60 Hz, and 14 bins were applied to the respective seismic cubes.

The dominant frequency content in the different areas varies. In Seismic Area A it is visible that the dominant frequencies is 25 Hz (Table 8; Figure 18A). The mean frequency after spectral enhancement has decreased compared with the original seismic data. The mean frequencies have decreased from 27.27 Hz in the original seismic data to 26.87 Hz in the spectrally enhanced data (Table 11). This is because the frequencies were enhanced in the low frequency spectrum and in the high frequency spectrum (Figure 18A). The frequency spectrum generated from Area A has increased the frequency spectrum below 10 Hz and from 35 – 60 Hz after spectral enhancement (Figure 18A).

The dominant frequency of the original seismic data is significantly higher than in the spectrally enhanced data for seismic cube B (Table 8). The mean frequency in the seismic data is increased in the spectrally enhanced data compared to the original seismic data; after the spectral enhancement the mean frequency has been raised to 34.16 Hz (Table 8). The mean frequency is increased as a result of spectral enhancement of the high frequencies ranging from 35 – 60 Hz (Figure 18B).

The frequency content is enhanced in the higher frequencies giving a dominant frequency in the spectrally enhanced data of 25.00 Hz opposed to 17.25 Hz in the original data (Table 8; Figure 18C). The mean frequency in the spectrally enhanced data compared to the original data is considered as minor, with a 0.47 Hz increase in the spectrally enhanced data (Table 8).

The frequency spectrum in Area D is increased significantly in the spectrally enhanced data. The dominant frequency in the enhanced data is increased to 30.75 Hz compared to 21.25 Hz in the original data. The mean frequency in the seismic spectrum is rather unchanged and is increased in the spectrally enhanced data from 28.88 Hz to 29.19 Hz (Table 8; Figure 18D).

| Seismic survey | Seismic data | Based on time-slice | Mean frequency | Dominant Frequency | Bandwidth |
|-----------------------|---------------------------------|----------------------------|-----------------------|---------------------------|------------------|
| BG 0804 | Noise cancelled source data | - 3224 ms | 27.78 Hz | 25.00 Hz | 22.25 Hz |
| | Spectrally Enhanced Output data | | 26.87 Hz | 21.00 Hz | 24.00 Hz |
| NH 0608 | Noise cancelled source data | - 3232 ms | 32,30 Hz | 27,00 Hz | 28,75 Hz |
| | Spectrally Enhanced Output data | | 34,16 Hz | 21,00 Hz | 42,25 Hz |
| SH 9102 | Noise cancelled source data | - 2696 ms | 24.06 Hz | 17.25 Hz | 19.75 Hz |
| | Spectrally Enhanced Output data | | 24.53 Hz | 25.00 Hz | 23.75 Hz |
| ST 9802 | Noise cancelled source data | - 2712 ms | 28.88 Hz | 21.25 Hz | 28.25 Hz |
| | Spectrally Enhanced Output data | | 28.19 Hz | 30.75 Hz | 25.50 Hz |

Table 8 - Seismic frequency comparison table from Source data versus the spectrally enhanced data.

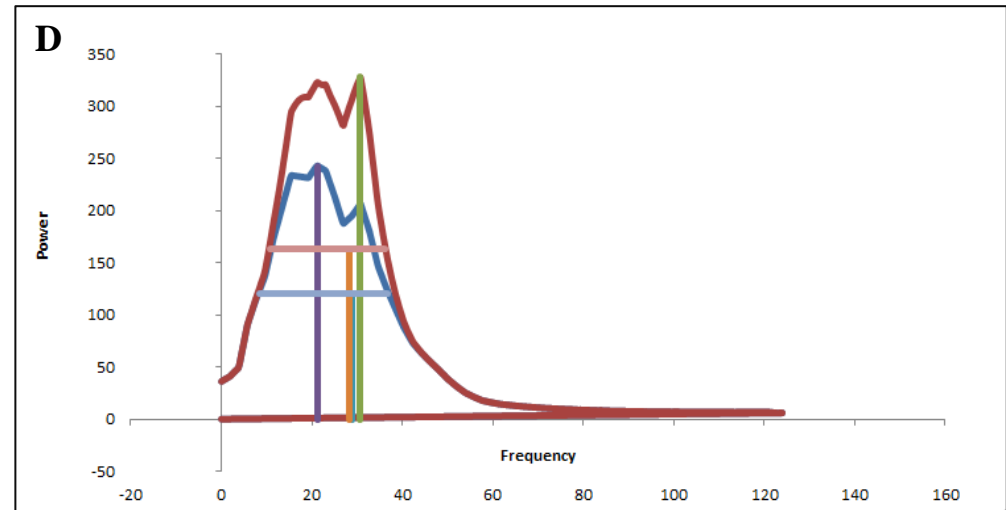
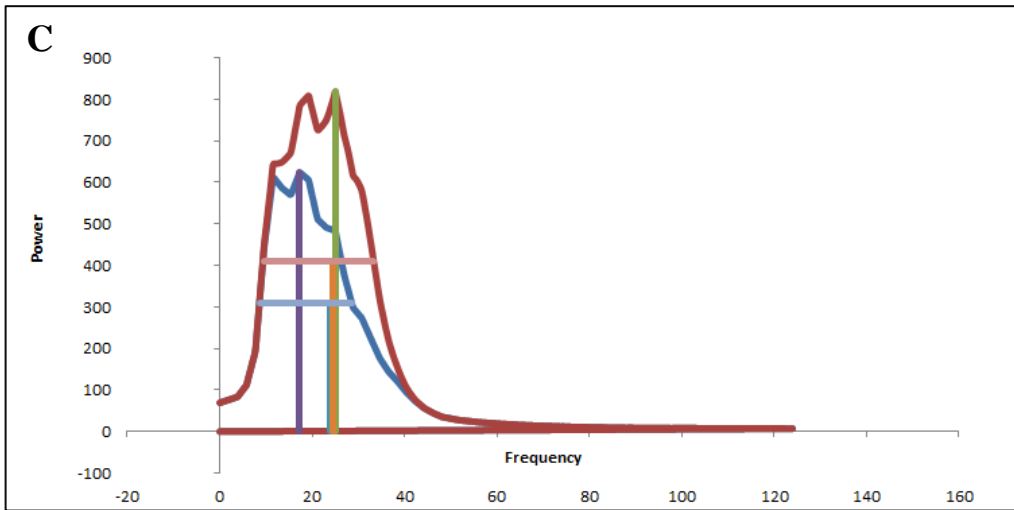
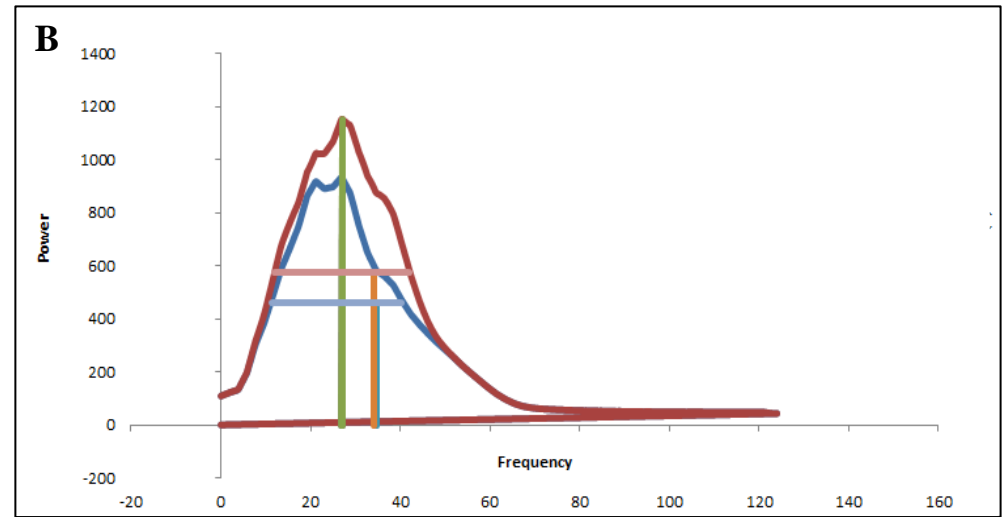
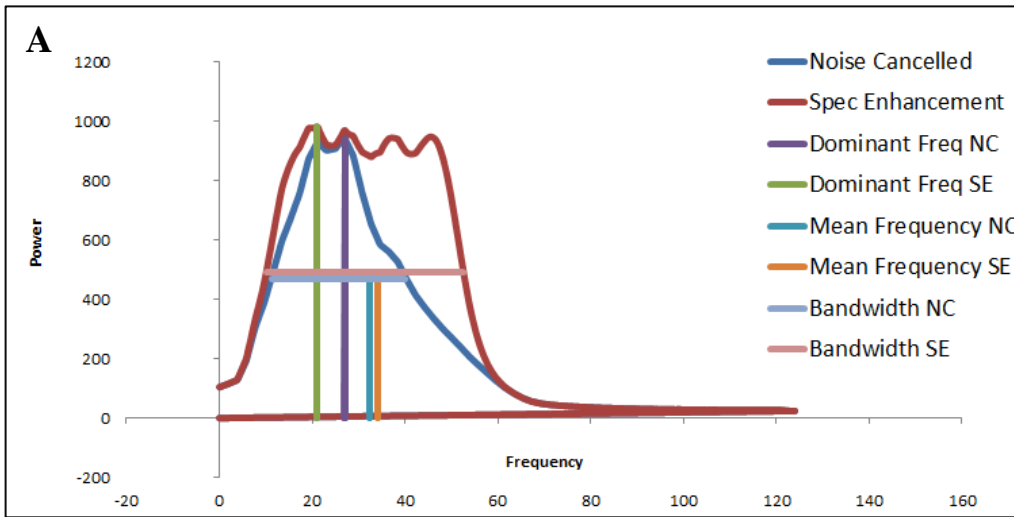


Figure 18 - Diagram of the seismic frequency spectrum in the seismic surveys. A) Seismic Cube A; B) Seismic Cube B; C) Seismic Cube C; D) Seismic Cube D.

5. Results

5.1 Bjarmeland Platform

5.1.1 Seismic Area A (BG0804)

Seismic Area A is located on the eastern part of the Bjarmeland Platform adjacent to the Nordkapp Basin (Figure 19). The area is located approximately 80 km northeast from the closest well penetrating the upper Paleozoic succession. Two seismic lines are used to illustrate the characteristics of the different seismic sequences. Figure 20A shows an approximately 19 km long N-S orientated inline. Figure 20B shows 11 km long x-line striking in a W-E orientation. In the eastern part of the survey a major normal fault is observed crosscutting the Carboniferous to Cretaceous section. The fault strikes in a NE-SW direction and defines the border to the Nordkapp Basin. The fault throw is relatively uniform at the Permian and Lower Cretaceous level suggests a post-Lower Cretaceous origin of the fault (Figure 20B).

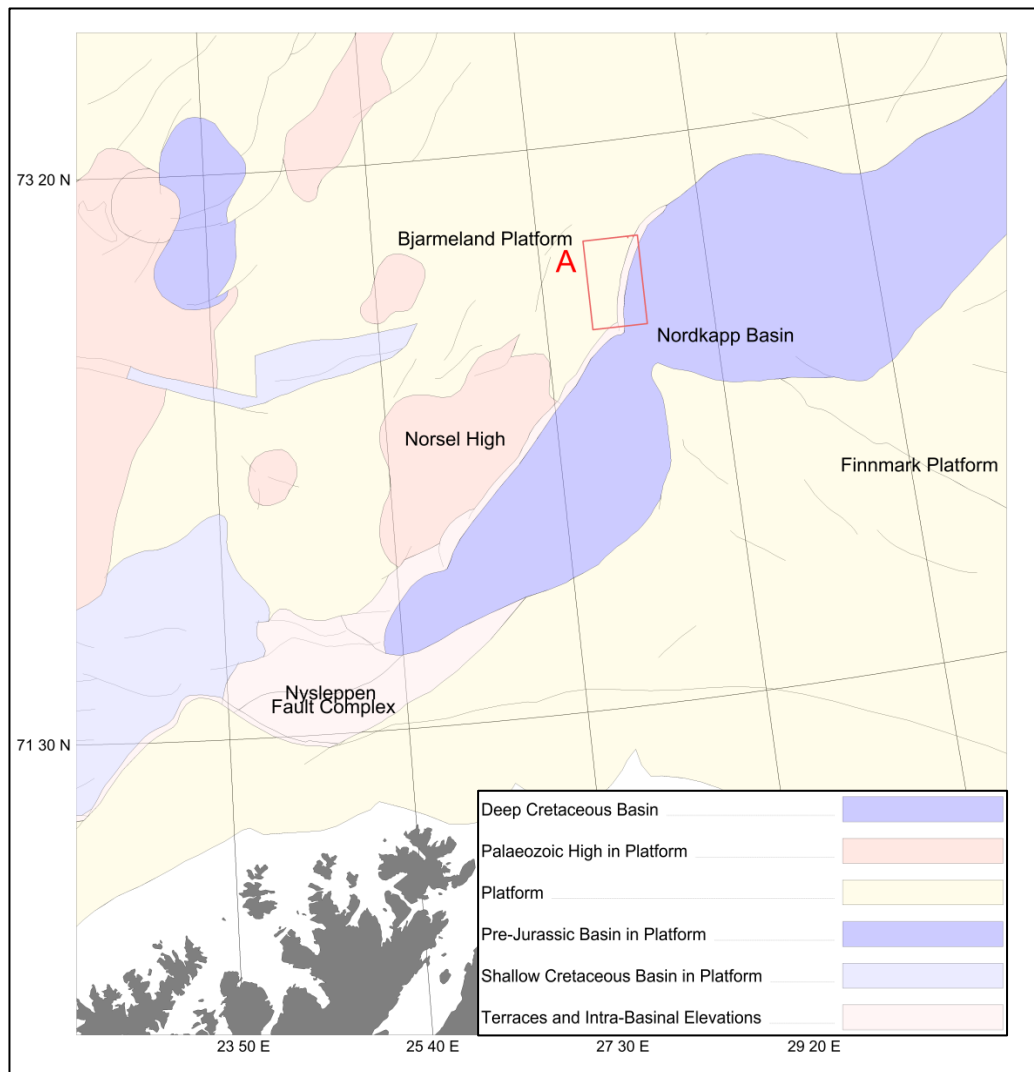


Figure 19 - Regional structural elements map marked with the outline of Area A.

5.1.1.1 Pre-Seismic Sequences

Description Pre-Seismic Sequences

The top of the succession is characterized by a decrease in acoustic impedance, and can be identified as a blue trough in the seismic section (Figure 20; Figure 21). The top of Pre-SS represent the base of the defined seismic sequences within the study area. The overall characteristic of the succession defined as, parallel to sub-parallel reflections with discontinuous to semi-continuous reflection continuity. The succession is divided into two different parts, based on the differences in reflection character.

The lower part (SF 1) is defined by a chaotic and discontinuous reflectivity pattern. The lateral and vertical bounding relationships between the reflectors are limited in the lower unit of Pre-SS caused by the discontinuous reflection pattern and numerous areas embedded with diffraction hyperbolas.

The top of the upper part (SF 2) is defined as a relatively uniform, showing some undulations affecting the reflector geometry. Internally, SF 2 is characterized by reflections that appear as affected by the overlying stratigraphy. This has resulted in differences in energy reflected from the succession. Figure 20 show the differences in reflection energy, where the reflections are more subtle beneath the mound-shaped feature, compared to the lateral reflections.

The surface map derived from the interpreted horizon shows that there are several structural highs and lows throughout the area (Figure 22). In the seismic data it can be seen a dip change on the top reflector, a rapid eastward thickness increase in the overlying SS 1 unit and an abrupt shut-off of amplitudes (Figure 20C; Figure 21). This is interpreted as reflecting a fault situated at this location, although the lateral extent of this fault is poorly expressed on the time surface map (Figure 22).

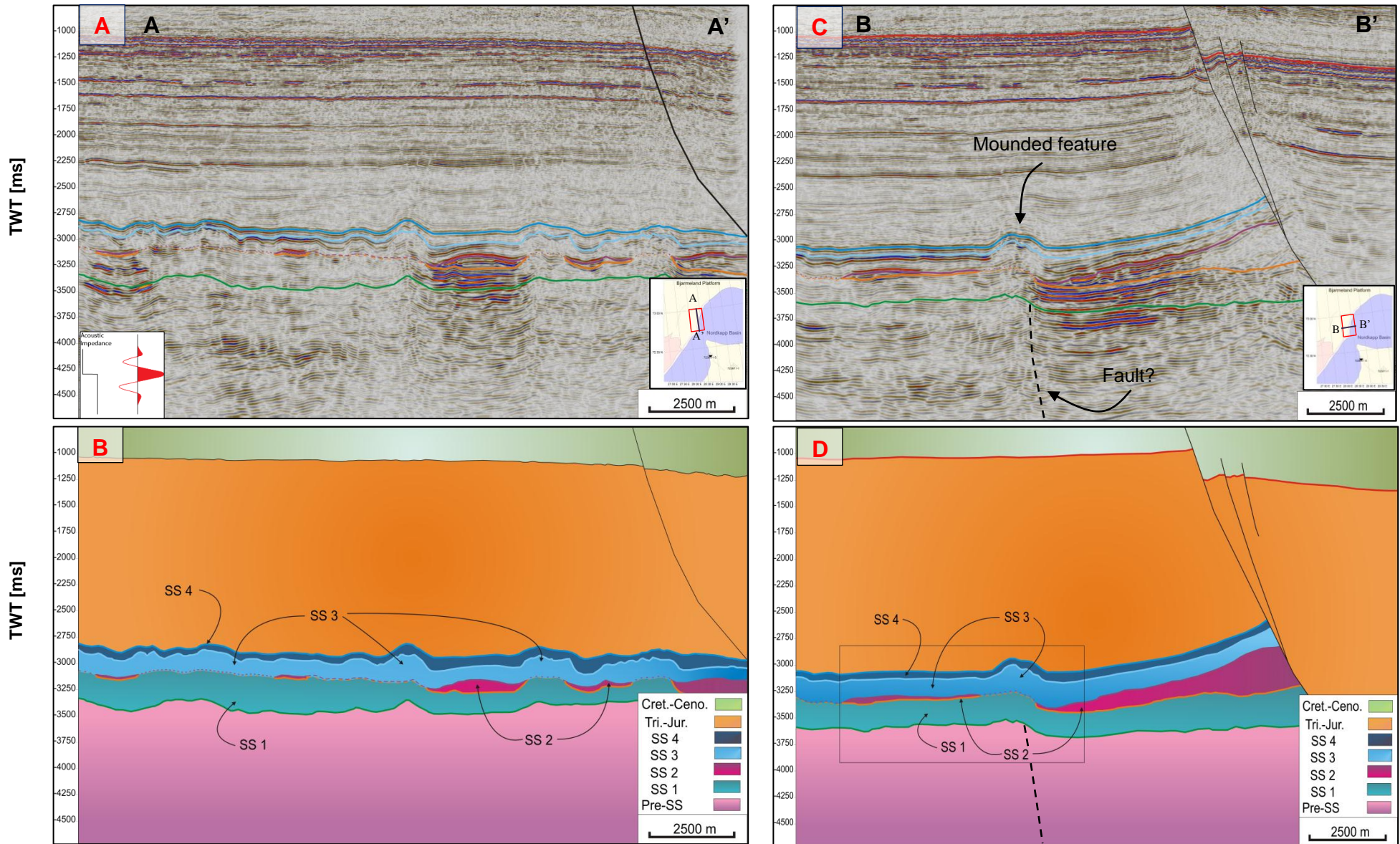


Figure 20 - Seismic sections of Area A on Eastern Bjarmeland Platform. The eastern part of the area is bounded by the major graben bounding fault of the Nordkapp Basin, which dips towards the NE. A) Seismic Inline 2473; B) Geoseismic Inline 2473; C) Seismic Xline 3417; D) Geoseismic Xline 3417. The square in Figure 21D is presenting outline of the zoomed section that is presented in Figure 22.

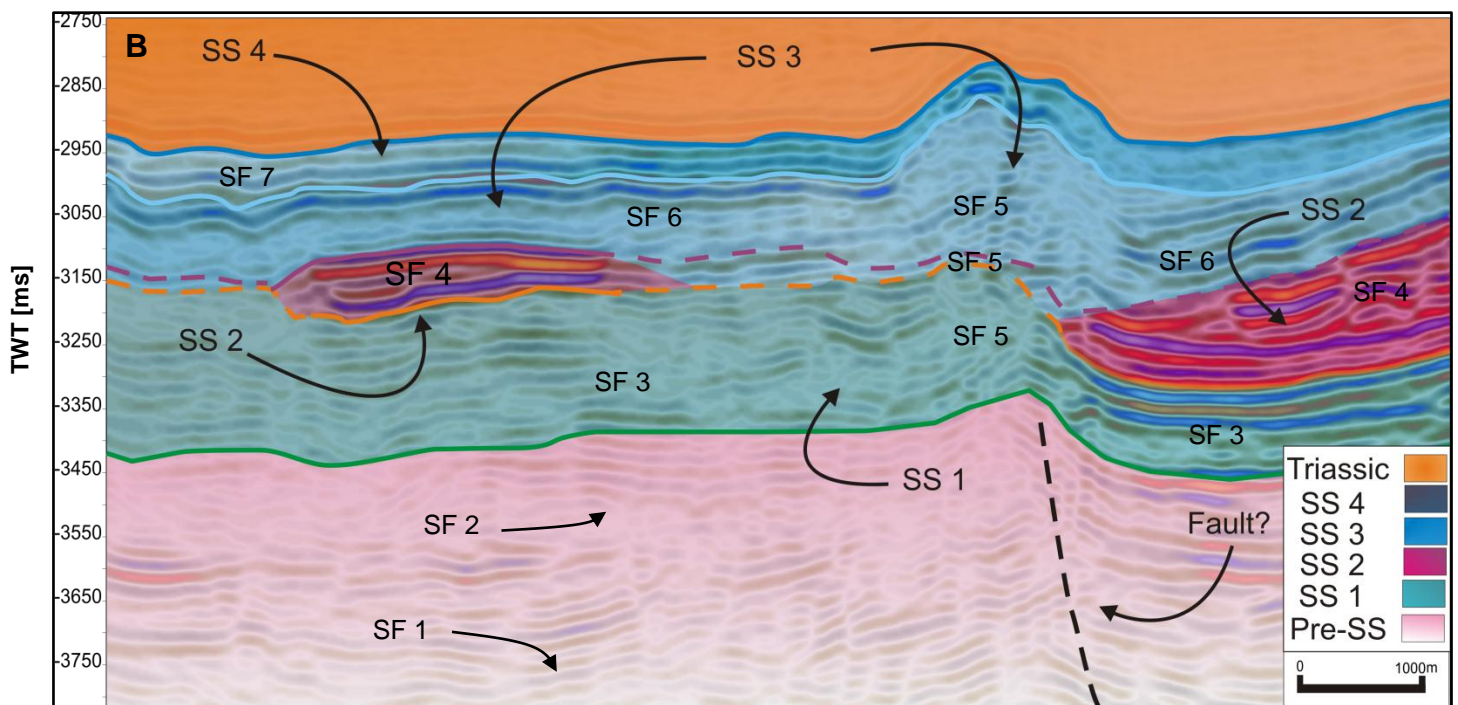
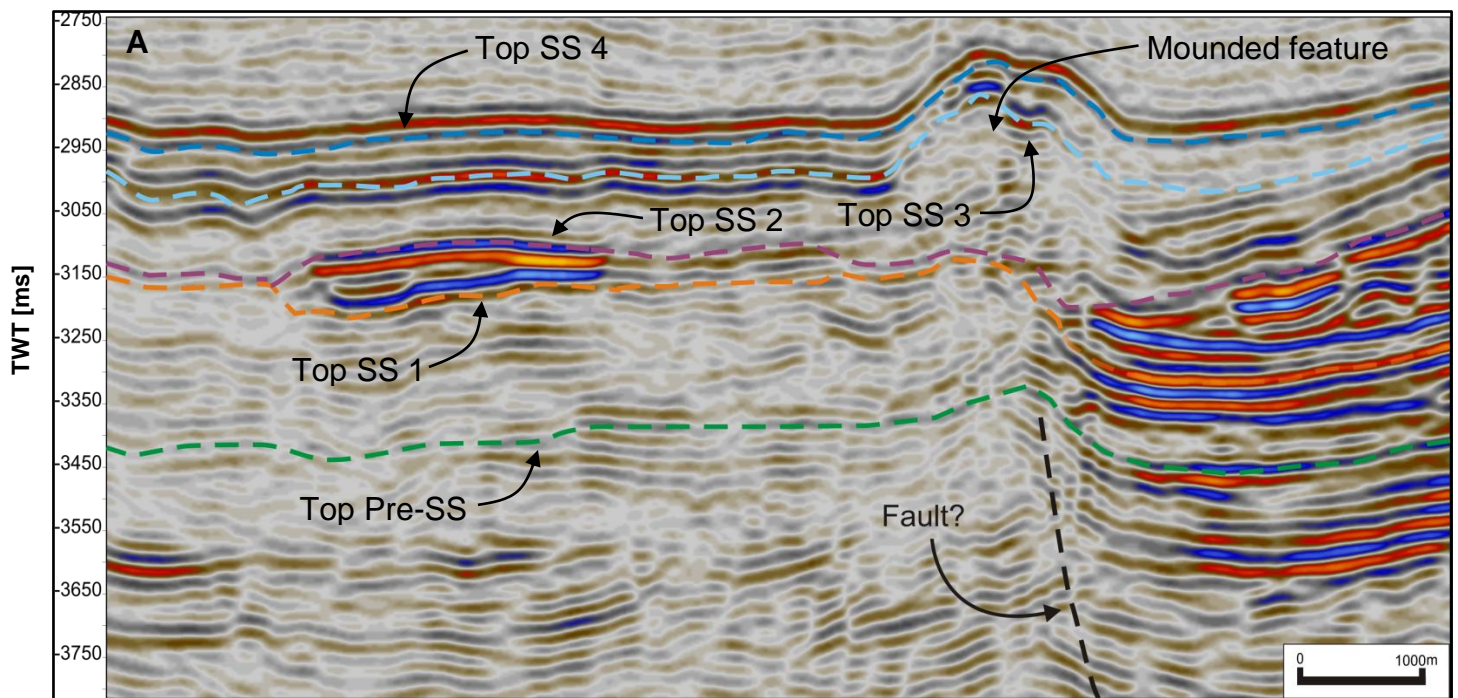


Figure 21 - The seismic x-line is taken from the Area A, marked as a rectangle in Figure 20D. A) Close-up of the seismic x-line 3417. B) Geoseismic x-line 3417 of the area annotated with seismic sequences and possible fault.

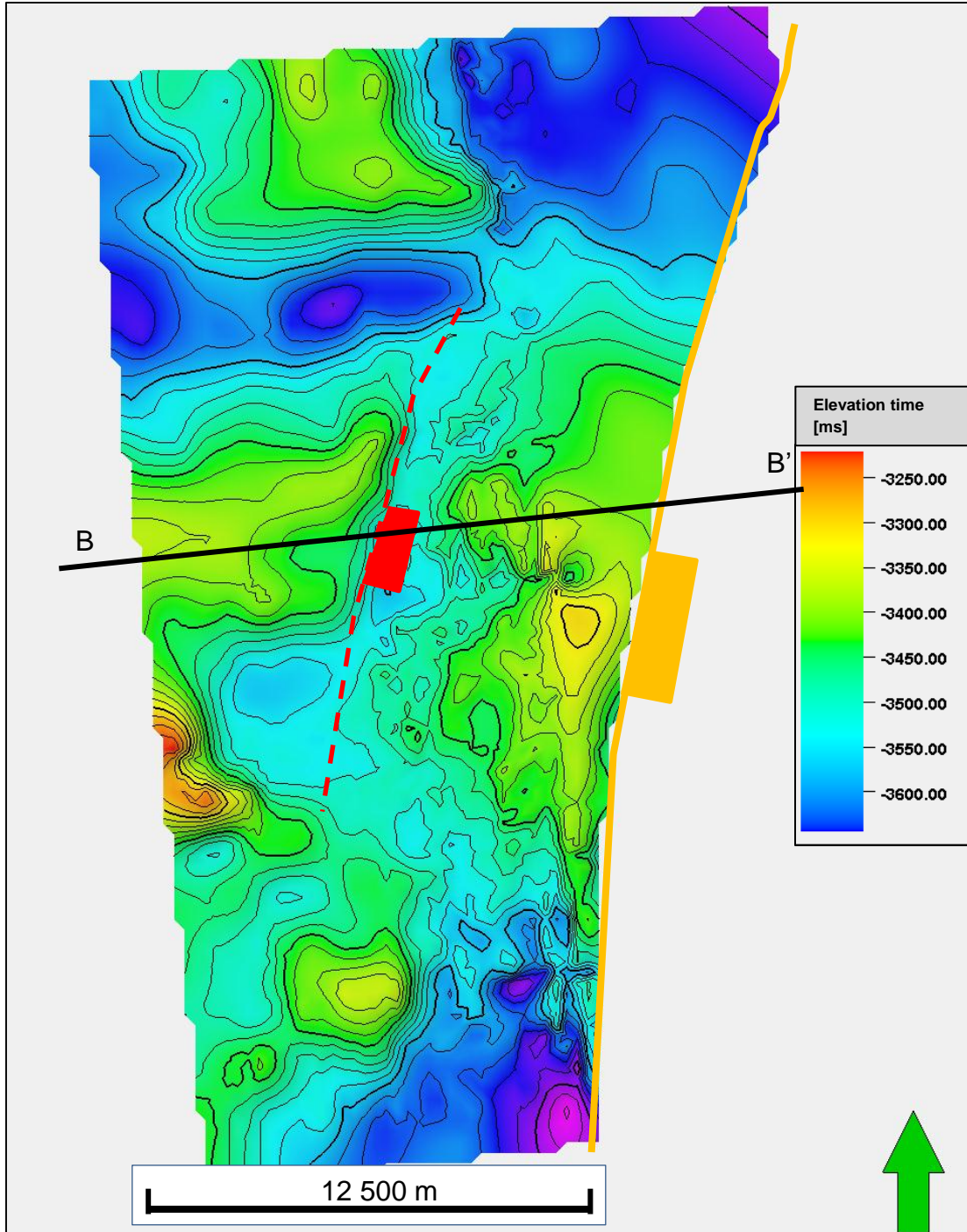


Figure 22 - Structural map of top Pre-SS horizon. The black line represents the orientation of the seismic x-line in Figure 20D. The dotted red line is showing the orientation of the proposed underlying fault that creates the topography. The orange line is identifying the orientation of the major graben bounding fault.

Interpretation Pre-Seismic Sequences

The succession is interpreted to consist of two different units. SF 1 is interpreted as the Pre-Devonian basement rocks (Appendix 1.2), and SF 2 is interpreted as the Mississippian aged, Billefjorden Group (Figure 20). The Billefjorden Gp. is interpreted as deposited unconformable on the metamorphic pre-Devonian basement (Appendix 1.2).

The stronger amplitudes and semi-continuous reflectors seen in the upper part of the succession are interpreted as representing the fluvial dominated Billefjorden Group (Figure 21). The succession is interpreted as being influenced by tectonic events and thus, resulting in normal faulting of the succession. The structural elements developed during the faulting events within the succession are interpreted as creating the topography affecting the unit (Figure 22). The low seismic resolution beneath the overlying mounded succession is interpreted as being caused by the higher velocities in the overlying stratigraphy, compared to the velocities within the upper part of the Pre-SS succession. However, laterally where the overlying mounded features are absent the seismic reflection signal is generally stronger.

5.1.1.2 Seismic Sequence 1

Description Seismic Sequence 1

The top of SS 1 is identified as an increase in acoustic impedance and gives a red peak in the seismic section (Table 7). The top and base of SS 1 are laterally continuous and define the seismic sequence, which extends throughout the seismic volume (Figure 20; Figure 21).

Laterally, SS 1 comprise of two different seismic facies. The first facies (SF 5) is characterized by seismic reflectors that appear as discontinuous and chaotic. SF 5 is laterally confined within areas below the mound shaped feature that are well defined at top SS 4 level (Figure 20; Figure 21). The reflection amplitude and frequency content is considered as low within this seismic facies.

The second seismic facies (SF 3) consists of reflectors that are considered as parallel and, in places, semi-continuous (Figure 20; Figure 21). There is considerable amplitude variations within SF 3, which is exemplified by the eastern versus the western side of the area, comprise of SF 5. This result in different reflectivity pattern within the mound shaped feature, compared to the adjacent seismic facies. This suggests a lithological influence on the seismic response within the sequence (Figure 21).

The areal distribution of the two different seismic facies units is shown in the structural map (Figure 23A). SF 3 occurs mainly in an undulating belt located proximal to the Nordkapp Basin, whereas SF 5 (in white color) is mainly distributed west of this belt. SF 3 is also located spatially distributed more distally from the Nordkapp Basin and thus, occurs as detached patches (Figure 23A).

Figure 23B shows an isochron map of SS 1 that only includes the thickness variations within the SF 3. SF 5 could not be mapped throughout the area, and is therefore shown by the polygon marking the outline of the unit. The thicknesses within SF 3 vary from 100 to 275 ms. and show a thickening of the sequence towards the east. The detached patches of the second facies illustrate an approximately identical thickness of 275 ms.

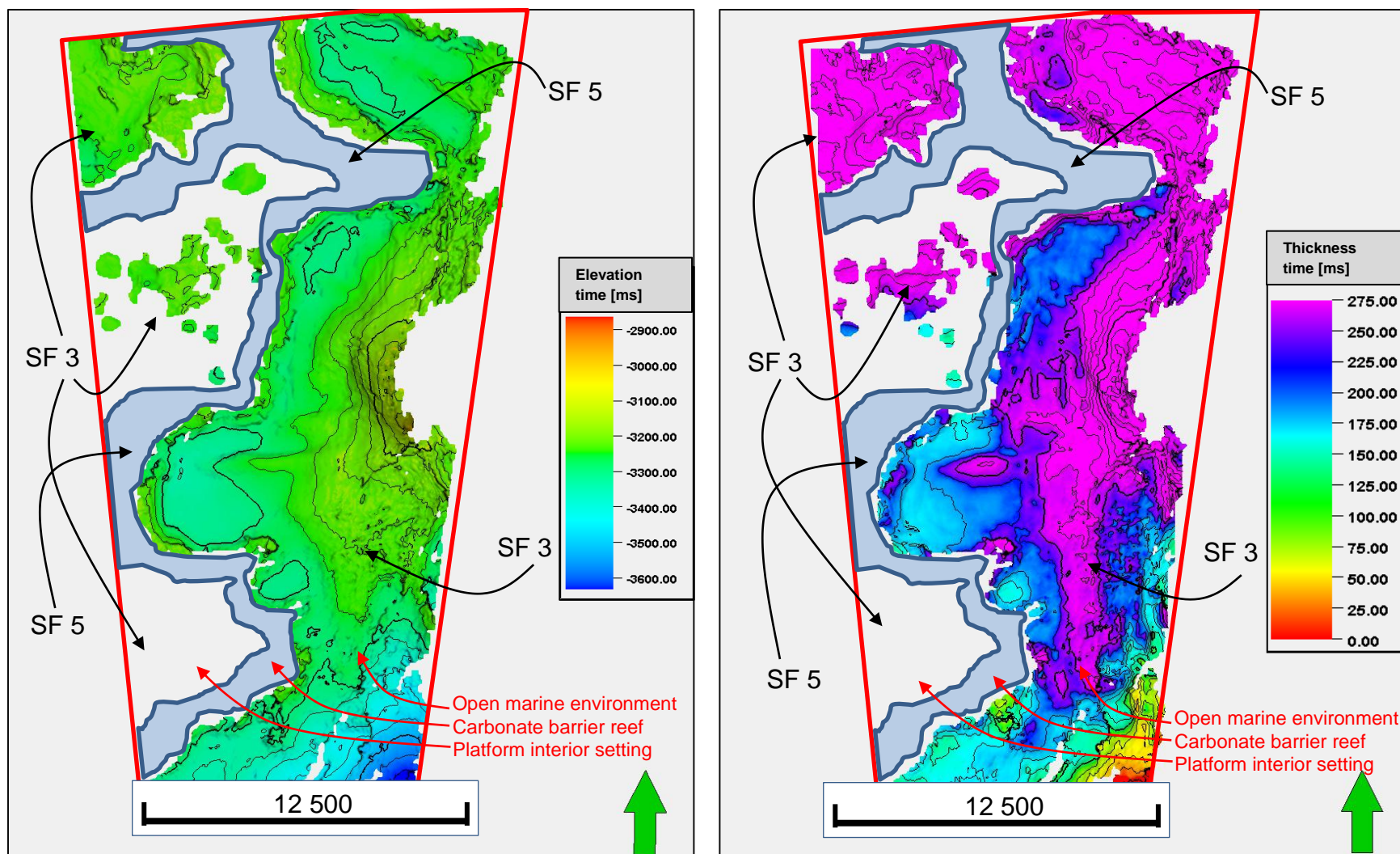


Figure 23 – A) Structural map of top SS 1. The surface map is shows the topographic variations within SF 3, and the lateral extent of the two different seismic facies units (the blue polygon marking the outline of SF 5); B) Time isochron map is derived between top SS 1 and top Pre-SS. The isochron map presents the thickness variations within SF 3. The annotation of SF 3 and SF 5 refer to the first and second seismic facies units described in the sequence.

Interpretation Seismic Sequence 1

The SS 1 is interpreted to represent the lower part of the Gipsdalen Gp., and the sequence is interpreted to consist of two different sedimentary facies, defined by the seismic facies characters identified within the SS 1 (Figure 20; Figure 22). The first facies (SF 3) is considered as the homogenous parallel and semi-continuous reflections, which is interpreted as muddy-limestone facies. The sedimentary facies is interpreted as deposited in a platform interior environment, in the western part of the area, and deposited as open marine environment on the eastern part (Figure 23).

The second facies (SF 5) unit identified by chaotic and discontinuous reflections, is interpreted as the lower part of a carbonate build-up complex. The carbonate build-up system is interpreted as developed on the pale-topography created by fault affecting the Pre-SS succession (Figure 21). SF 5 is interpreted as the earliest stages of a barrier reef complex (Figure 23A). The build-up developed on the platform margin of the Bjarmeland Platform adjacent to the Nordkapp Basin. The barrier complex is developed at this position to shelter the platform interior environment on the Bjarmeland Platform, from the high-energy open marine conditions within the Nordkapp Basin. The sedimentary facies within the mounded feature is interpreted as a protozoan carbonate succession that includes Palaeoaplysina-phyllloid algae build-ups (Appendix 1).

The time thickness map shows a gradual thickening of the sequence towards the east, from the thinnest succession close to the area, which consist of SF 5 and a thickening of the SF 3 towards east (Figure 23B). The thickening of the succession is interpreted as present the direction of the major depocenter interpreted as located within the Nordkapp Basin.

5.1.1.3 Seismic Sequence 2

Description Seismic Sequence 2

The top of SS 2 is defined as a reflector with decrease in acoustic impedance and thus, gives a blue trough in the seismic section (Figure 20; Figure 21). The lateral extent of the SS 2 varies throughout the area, and consists of two different seismic facies units.

The first seismic facies (SF 4) consists of contoured and semi-parallel reflections with high amplitudes defining its top and base. Internally, the reflections are considered to have low resolution and with the magnitude of the seismic amplitudes and frequencies are low. Despite the low resolutions internally in the sequence, there are, in parts, areas within SS 2 that shows internal reflectors (Figure 20C). The geometries of SF 4 vary considerably in thickness. The thickness variations of the sequence are especially visible Figure 20D. The wedge shaped structures thickens significantly towards the normal fault, in the west (Figure 20D). The second seismic facies (SF 5) identified as a chaotic and discontinuous reflectivity, and laterally confined to the areas where the overlying stratigraphy have created mound shaped structures (Figure 21).

The structural map presents a large structural high located in the eastern of the area (Figure 24A). The structural high is associated with the location of the wedge shaped structure observed in the seismic section (Figure 24A; Figure 21B). Internally, the reflectors in SS 2 show a geometry that varies throughout the area. Figure 25 presents the three different attribute map of the SS 2, presenting significant resemblance with the locations of SF 4 (Figure 25; Figure 21). The geometries are considered as relatively flat in the areas shown as anomalies having high RMS amplitudes values, and contoured geometry, in the areas with low RMS amplitude values (Figure 24A; Figure 25A).

The surface and attribute maps identify the outline of a ridge shaped structure trending in a generalized NE-SW direction. The facies within the ridge shaped structure is identified as the mounded facies, defined as SF 5. The RMS map show the areas where SF 5 is identified to have low amplitude variations (Figure 25A). The variance map presents the ridge shaped structure as a high variance zone, compared with the SF 4 illustrated as low variance (Figure 25B). RGB blended spectral decomposed map show the outline SF 5 as low frequency, and SF 4 as high frequency zones (Figure 25C).

The isochron map shows the lateral extent of SF 4, due to the difficulty of mapping continuity of SS 5. (Figure 24B; Figure 24A). SS 5 is therefore excluded from the map, and therefore showing a clipped succession where SS 5 is located (Figure 24B). The isochron map indicate thickening of the succession towards the east, which coincide with the wedge-shaped structure identified in the seismic section (Figure 24B; Figure 20B). The map presents a gradual thickening of SF 4 from the non-depositional parts located along the margins of the clipped sections, towards the east (Figure 24B).

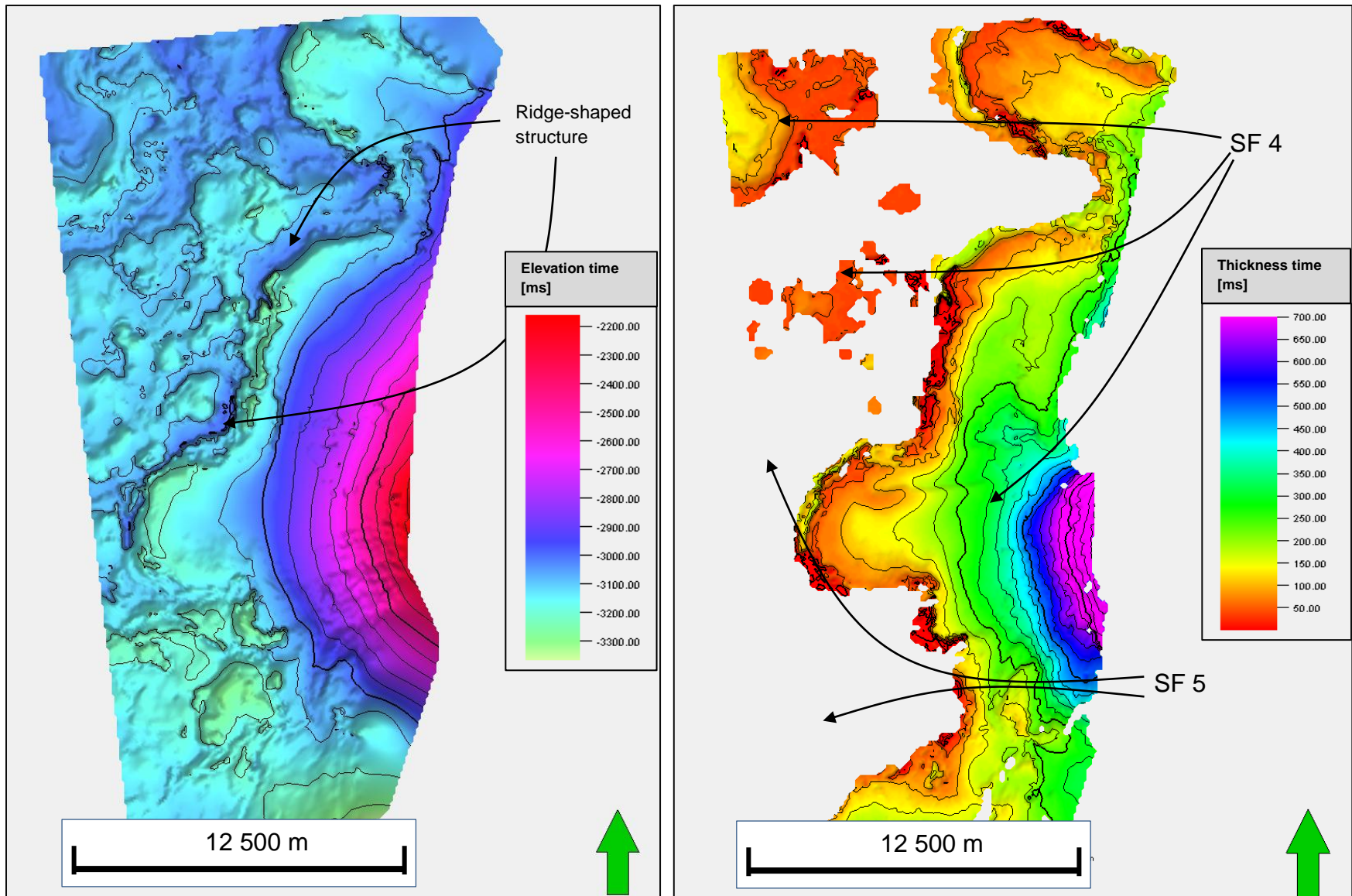


Figure 24 – A) Structural map of top SS 2. B) Time thickness map of top SS 2 to top SS 1. The isochron map shows the thickness variations within SF 4.

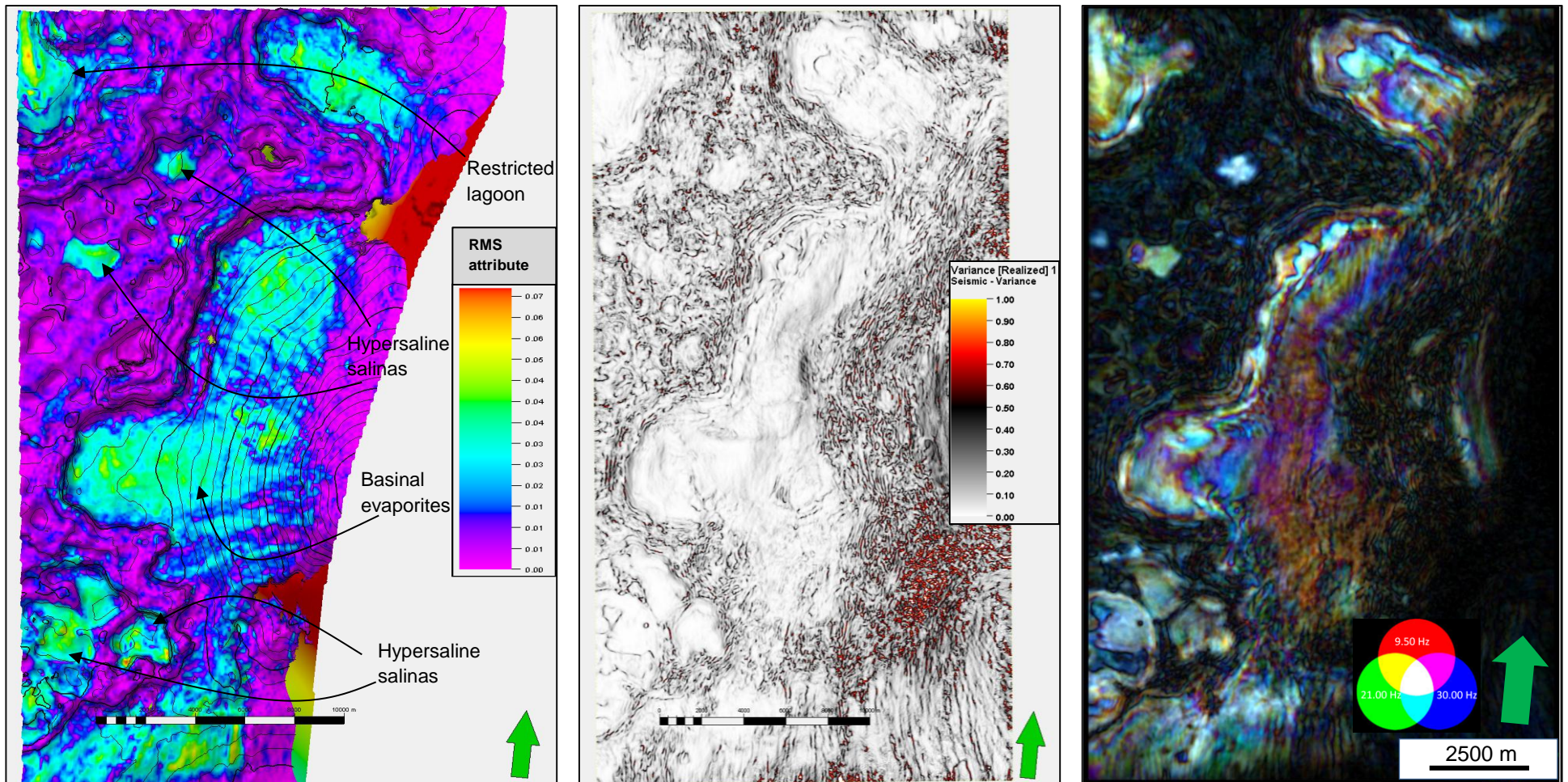


Figure 25 - Seismic attributes derived for SS 2. A) RMS Amplitude map derived from top SS 2 and top SS 1. The amplitude anomalies are showing areas with high amplitudes, and following the areas with no amplitudes coincide with areas without amplitudes.; B) Variance map. The map is taken from time-slice $Z = -3200$ ms.; C) Red-green-blue (RGB) color blended spectral decomposition cube (Red = 9.50 Hz, Green = 21.00 Hz, Blue = 30.00 Hz). The map is taken from time-slice $Z = -3200$ ms.

Interpretation Seismic Sequence 2

SS 2 consist of two different seismic facies units (Figure 20; Figure 21). The first seismic facies (SF 4) is interpreted as an evaporitic unit, and the second seismic facies (SF 5) is interpreted as a carbonate-dominated unit.

The SF 4 is interpreted as a succession of autochthonous evaporite deposits. This interpretation is also supported by the observations from the well data from the Gipsdalen Gp. and from observing the geometry of the SS 2 unit (Appendix 1; Figure 20). The seismic character of the SF 4 is identified as with some intra-laminated reflections, especially within the wedge shaped structure to the eastern flank of the seismic area (Figure 20). These reflections suggest that the wedge shaped structure consists of interbedded sequences of evaporites, clastic sediments and carbonates; also known as layered evaporite sequences (Figure 20). Figure 20 show that the internal reflectivity within the wedge shaped structure contains lower resolutions beneath the fault. The reflections within the wedge shaped structure are identified to have considerably lower resolution beneath the fault (Figure 20). The lower resolution within the wedge shaped structure is interpreted caused due to the location within the fault shadow zone, rather than changes in sedimentary facies. The layered evaporite sequence is therefore interpreted as continuous throughout the wedge-shaped structure (Figure 20B).

The surface and attribute maps of SS 2 illustrates the outline of the evaporitic succession. The evaporitic succession is interpreted as being deposited in the fore reef and reef flat zones. The SF 4 units are interpreted as presenting areas with high amplitudes, low variance and the high frequencies in the three different amplitude maps (Figure 25A; Figure 25B; Figure 25C). The small-round high amplitude and frequency anomalies within the areas subjected to zero amplitude and frequencies is interpreted as salinas confined within the lagoonal environment during sea-level lowstand (Figure 25A; Figure 25C). The areas with significantly higher abundance of amplitude anomalies are interpreted as evaporites deposited in the fore reef zone and basin (Figure 25A; Figure 25C). SF 5 interpreted as a carbonate barrier reef complex is associated with the areas subjected to low amplitudes frequencies in the attribute maps (Figure 25A; Figure 25C). The isochron map of the unit show areas of non-deposition of evaporite confined where the carbonate build-up complex. The isochron map presents a gradual thickening of the evaporitic sequence towards the east, and a relatively thin succession, less than 50 ms. of SF 4, confined within the platform interior (Figure 24B).

The differences in geometries observed from the seismic section, is interpreted as presenting the upper Paleozoic succession as a pre-kinematic sequence within the respective area. Hence, the evaporite successions were mobilized during the lower to middle Triassic. Supporting evidence of syn-kinematic deposition is the overall thinning of the intra-Triassic section on the footwall side of major normal fault, opposed to a distinct thickening of the intra-Triassic succession on the hanging wall side (Figure 20B). This means that the mobilization of evaporites did not affect the deposition of the upper Paleozoic succession the respective seismic area (Figure 20; Figure

21). The thickness variations within SS 2 unit are interpreted to be related to the later staged mobilization of evaporite succession. The salt remobilization created a salt roller structure along the fault boundary. These structures are interpreted as created by evacuated salt from the Nordkapp Basin during the active tectonic period in the Triassic. The number of detached pockets of SF 4, which is confined within the SF 5 succession, is interpreted as salinas developed during eustatic sea-level lowstand (Figure 20; Figure 21; Figure 25A).

5.1.1.4 Seismic Sequence 3

Description Seismic Sequence 3

The top of SS 3 is characterized by an increase in acoustic impedance and therefore displayed as a red peak in the seismic section (Table 7). SS 3 is laterally extensive throughout the area (Figure 20).

The seismic characteristics of SS 3 vary significantly between two different seismic facies that are identified. The first seismic facies (SF 5) is identified as a mound shaped structure (Figure 22). SF 5 considered as is chaotic reflections, with discontinuous to semi-continuous continuity. Internally, the amplitude and frequencies of the reflectors are considered as low amplitudes and frequencies. The bounding relationship of SF 5 is restricted to the mounded shape structures and thus, laterally where the structure is absent there is an abrupt change in seismic character (Figure 20A; Figure 20B). The distinct shut-off of SF 5 is transition into a different seismic facies. The second seismic facies (SF 6) is classified as a uniform thick succession, with parallel and continuous reflection configuration (Figure 20; Figure 21). The amplitude and frequency in this facies system is considered as low to medium (Figure 20). The geometry of the SS 3 is relatively uniform when it is superposed on SF 4, compared to the thick succession of SF 5 within the mounded feature (Figure 21).

The top SS 3 surface map shows the differences in the morphology of SS 3 (Figure 26A). These differences are related to the distribution of the different seismic facies (Figure 26A). The higher elevated structural complex is identified as the SF 5 in the seismic section, and the SF 6 is identified in the western and eastern part of the area, where the higher elevated complex is absent. The surface map presents a network of attached ridge shaped features that is located to the west of the topographic high ridge. These highs consist of thin ridge-shaped features, which enclose cell-shaped lows (Figure 26A). The isochron map of SS 3 identifies the thickness variation in the sequence (Figure 26B). The map shows the distinct thickness trend in thick and thin units. The areas where the SF 4 unit defined in SS 2 is located, results in thin succession of SS 3, and in contrary where SF 4 is thin or absent, the SS 3 results as a thick succession (Figure 26B).

The different attribute maps of the unit supports the observations of the differences in the seismic facies within the sequence. The strongest RMS amplitudes are located within the northern area on a higher elevated structure (Figure 27A), despite the differences in RMS amplitudes in the

area. The RMS amplitude map shows no distinct trend in the distribution of the amplitude map, apart from the outline of the mound-shaped complex (Figure 27A). The variance map identifies the eastern part of the area to consist of high variance, and the western and central parts as areas with low variance (Figure 27B). The differences in variance are indicated on Figure 27B with blue and red arrows; blue arrow indicates areas of high variance, while the red arrow shows examples of low variance. The RGB color blended map from the area visualizes the morphology of the reticulated ridges, located in the western part of the area (Figure 27C). The reticulated features are shown to as blue colored in Figure 27C, opposed to the circular and sub-circular structures illustrated as green colored (Figure 27C). The large build-up feature is visible as a low frequency and black color, has a lateral thickness of approximately 100 m (Figure 27C).

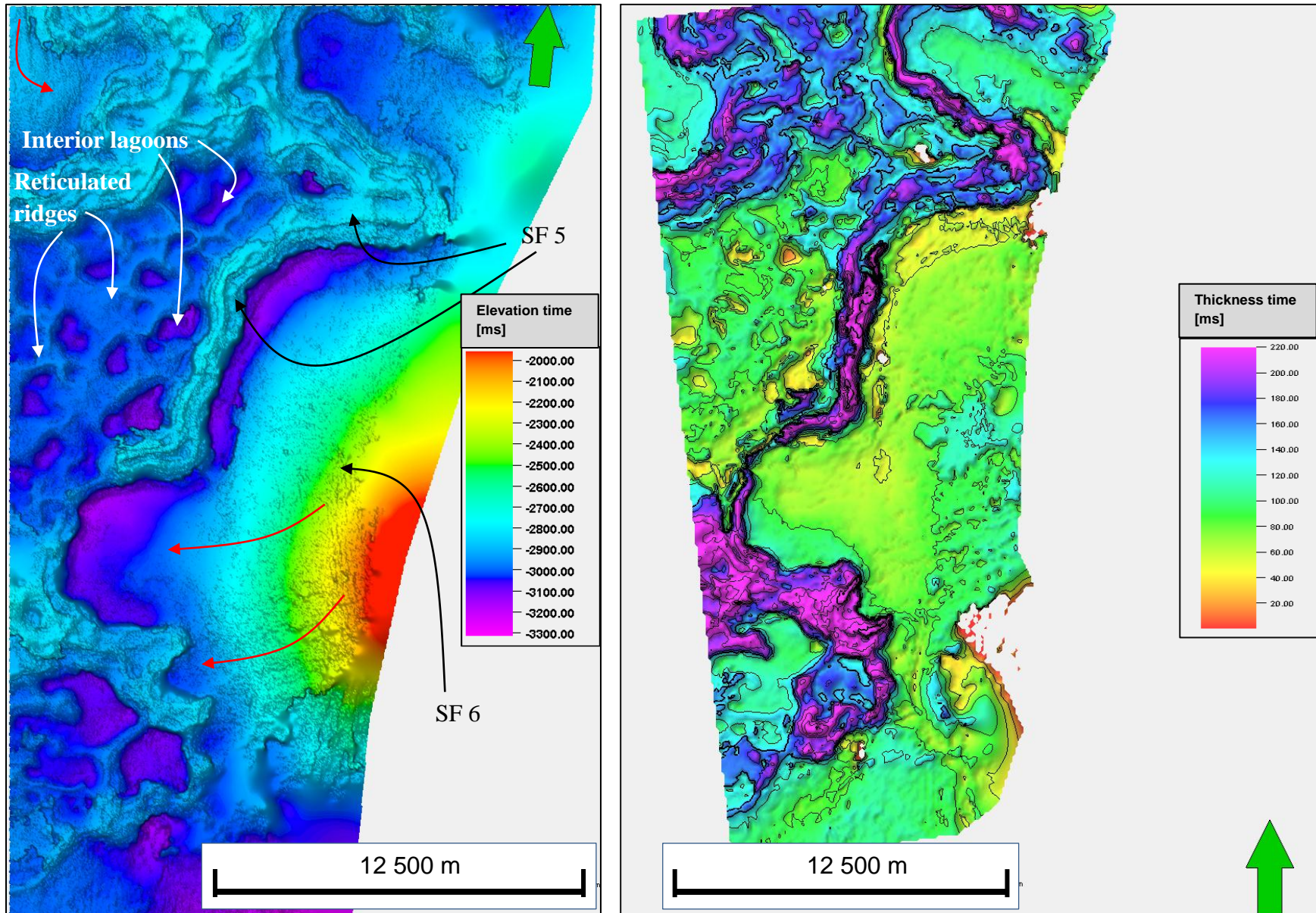


Figure 26 - A) Surface map of top SS 3 illustrated with arrows indicating areas of different seismic facies and morphological features (Red arrow shows examples of horseshoe structures); B) Isochron map of SS 3.

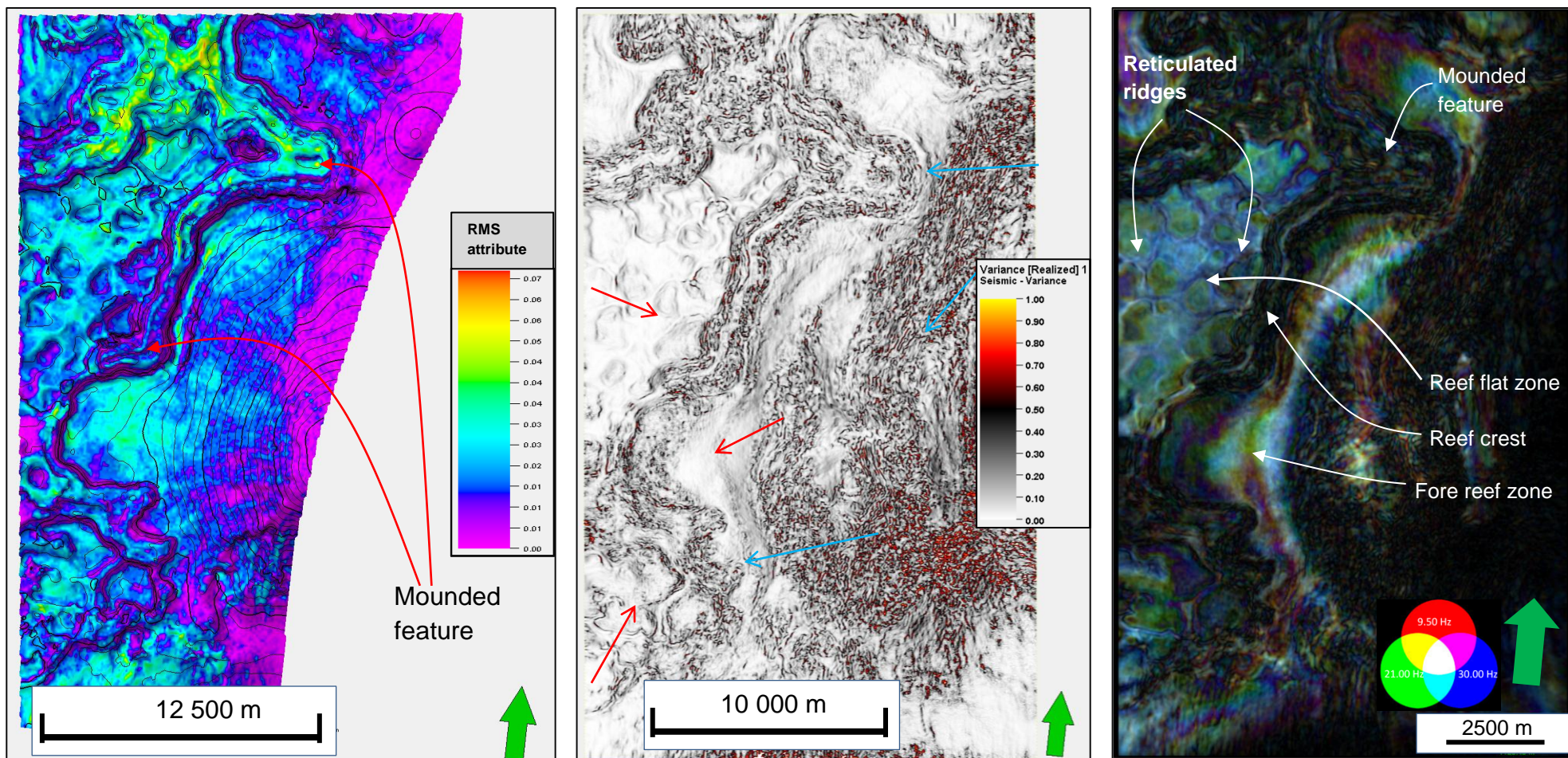


Figure 27 - Attribute maps of SS 3. A) RMS Amplitude map derived between top SS 3 and top SS 2; B) Variance map calculated from time slice $z = -3000\text{ms}$.; C) Frequency RGB blended map from time slice $z = -3000\text{ms}$ (Red = 9.50 Hz, Green = 21.00 Hz, Blue = 30.00 Hz).

Interpretation Seismic Sequence 3

The SS 3 is interpreted as comprising of two different seismic facies units. The first facies (SF 5) is identified by its mounded shape and with a reflection configuration considered as chaotic and contoured (Figure 21). The mound-shaped structure defined as SF 5 is interpreted as representing a carbonate build-up complex. The second seismic facies (SF 6) is defined by its parallel layered and semi-continuous reflections (Figure 20). SF 6 is interpreted as muddy-limestone facies deposited in a lagoonal environment. The geometry of the morphological features in the structural map is interpreted as horseshoe structures. The structures observed in the area show a resemblance with the structural features described as horseshoe structures, by Chidsey et al. (1996) in phylloid algae build-ups in the Paradox Formation, Utah.

The geomorphology of the top SS 3 succession show a surface interpreted as a carbonate depositional environment consisting of fore reef zone, reef crest and reef flat zone (e.g. Figure 27C). The mound shaped structure defined as SF 5 in the seismic section is interpreted as a carbonate barrier reef complex (Figure 21; Figure 27C). The areas dominated by SF 6 confined to the fore reef zone and the reef flat zone (Figure 27C). The barrier reef is interpreted as a barrier, which shelter the western section, from the eastern part, where the Nordkapp Basin is located (Figure 26A). The Nordkapp Basin is interpreted as the regional basin and thus, the carbonate build-up complex on the margin of the basin was developed as a barrier reef on the platform-margin of the Bjarmeland Platform. The average thickness of the carbonate build-up complex is approximately 220 – 240 ms., the thickness within in the lagoonal environments is approximately 50 – 90 ms., and the thickness of the fore-reef zone is relatively uniform with thickness of approximately 100 ms. (Figure 26B). The reef flat zone consists of a reticulated system of carbonate build-ups. These systems link-up and encircle lower elevated cell-shaped features. The reticulated build-up system is interpreted as networks of pinnacle reefs, and the cell-shaped shapes are interpreted as interior lagoons. The different structural shapes are identified with arrows in the map. The horseshoe feature is presented with a red arrow (Figure 27A).

The attribute maps are applied to enhance the visualization of the different depositional facies settings confined within the sequence. The high variance and low frequency zones are interpreted as presenting the two different seismic facies units (Figure 27B). The RGB blended map is presenting a distinct geomorphology with reticulated ridges located in the reef flat zone (Figure 27C). The reticulated shaped structures located in the area interpreted as platform interior setting are interpreted as interconnected pinnacle reefs. Pinnacle reefs develop similar to Patch reefs where they both reach mean sea-level, however, their rise from substrate differs whereas patch reefs reach <20 meter depth, the pinnacle reefs has >20 meter relief (Blanchon, 2011) These reticulated pinnacle reef systems encircle interior lagoons that consist of a facies dominated by muddy limestone. The origin of the geomorphic zonation of the interconnected pinnacle reef complexes are interpreted as systems that is primarily governed by development on the topographic highs around the karst-induced structures (Figure 28C; Figure 28B).

5.1.1.5 Seismic Sequence 4

Description Seismic Sequence 4

The top of SS 4 is marked as an increase in acoustic impedance which gives a seismic response of a red peak (Table 7). SS 4 is identified throughout the entire seismic area. The sequence consists of one seismic facies (SF 7).

SF 7 is identified as parallel reflections with continuous reflection continuity (Figure 20; Figure 21). Internally, SS 4 is identified as consisting of small variations in seismic character. The top of SS 4 presents similar the morphology as identified and described in top SS 3 (Figure 28A; Figure 26A). SS 4 is defined as a uniform thickness succession (Figure 28B; Figure 20). The exceptions in uniform thickness throughout the area are restricted to the margins along the mound shaped structures (Figure 28B). The thickness in these areas is significantly thicker than the lateral surroundings and has an approximate thickness of 200 ms (Figure 28B).

Interpretation Seismic Sequence 4

SS 4 is interpreted to consist of one facies unit (SF 7). The depositional environment is interpreted as pelagic deposition, in an open and deep-marine environment. The sedimentary unit within SS 4 is interpreted as fine-grained siliciclastic sediments and cherty facies. Supporting evidence for this interpretation, are the relative subtle variations in thickness throughout the SS 4 (Figure 28B; Figure 20; Figure 21), and well data observations (e.g. Appendix 1.2; Appendix 1.3; Appendix 1.4).

The depositional environment being of pelagic origin is also supported by the morphology of SS 4, where the sequence is interpreted as deposited concordant on the underlying SS 3. The surface of SS 4 is interpreted as showing the similar morphology as SS 3. SS 4 is interpreted as presenting imprints the underlying topographic signature of the SS 3 (Figure 28A; Figure 26A). The generally uniform thickness of the SS 4 succession observed on seismic sections and the isochron map, support the interpretation of sediments deposited concordant on SS 3, and therefore imprints the surface morphology SS 3 (Figure 20; Figure 28B). Deposition of SS 4 were not affected by growth of carbonate build-ups or by tectonic influence, resulted in deposition of parallel layered and homogenous sediments (Figure 22).

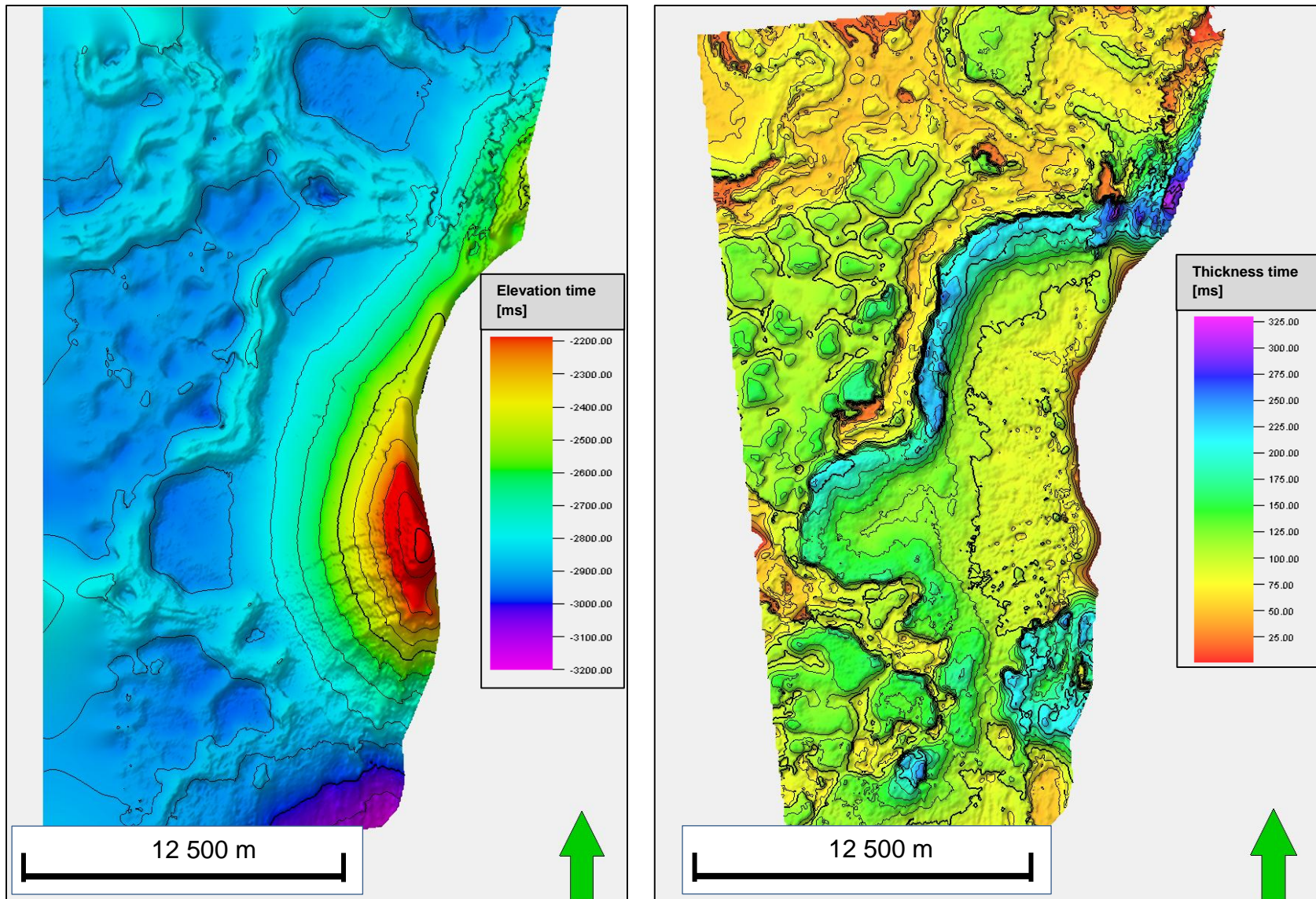


Figure 28 - A) Surface map of top SS 4; B) Time thickness map of derived between top SS 4 and top SS 3.

5.1.2 Seismic Area B (NH0608)

Seismic Area B is located on the western part of the Bjarmeland Platform approximately 200 km northwest of the Nordkapp Basin, 30 km east of Loppa High, and the northern section of the area is located within the Swaen Graben (Figure 29). The section of the area that is located within the Swaen Graben consists of the northward dipping normal fault striking in an east-west direction. Used to illustrate the different seismic sequences in the area, two seismic lines have been chosen, an approximately 20 km long inline striking N-S, and a 17 km long x-line (Figure 30; Figure 31). The northward dipping normal fault has a displacement of approximately 250 ms., the fault crosscuts the entire upper Paleozoic succession and the Late Jurassic succession, this suggest that the event occurred in the Late Jurassic (Figure 30; Figure 31).

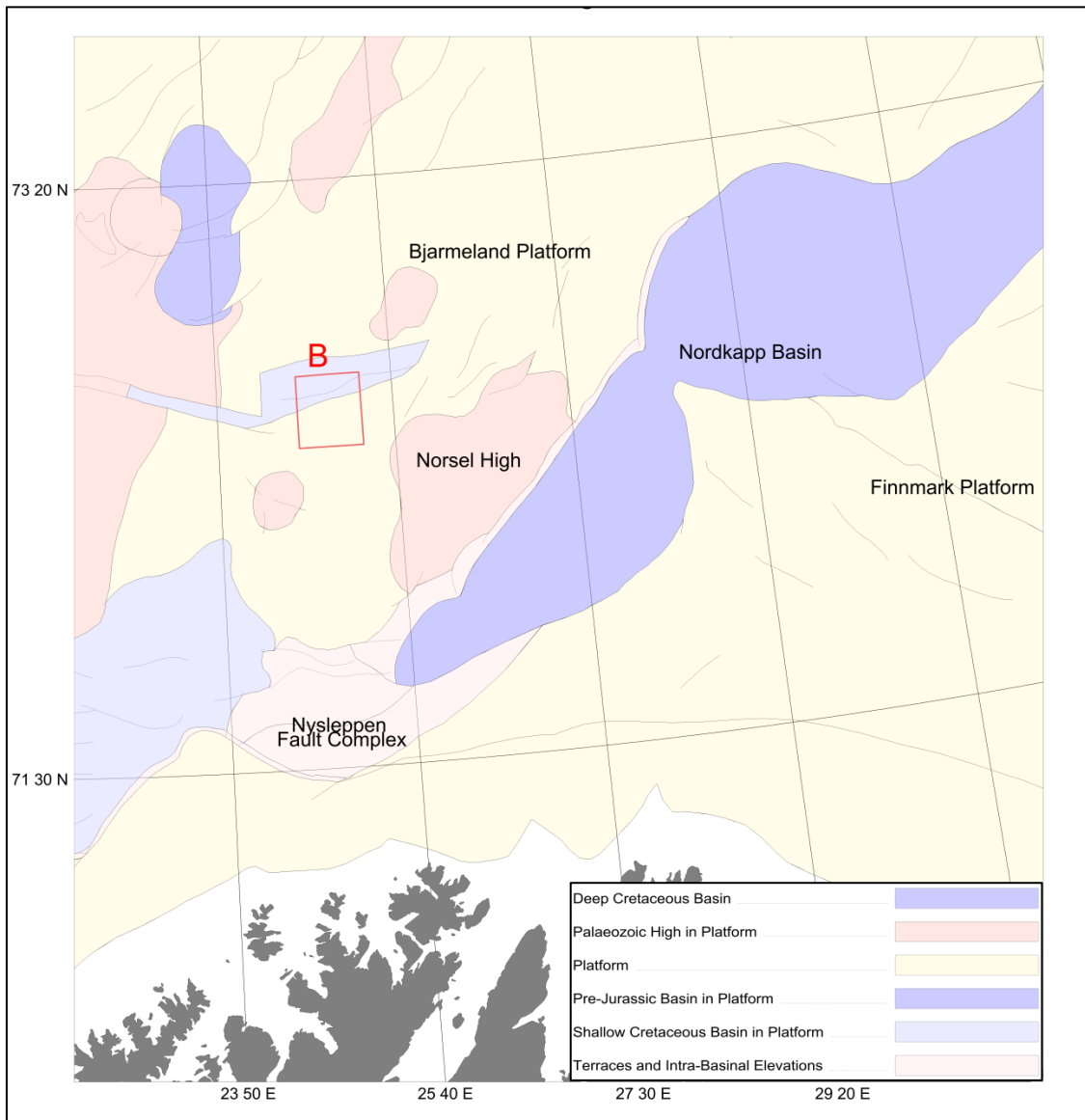


Figure 29 - Regional structural elements map of the SC Norwegian Barents Sea highlighted with the outline of Seismic Area B.

5.1.2.1 Pre-Seismic Sequences

Description Pre-Seismic Sequences

The top of Pre-SS is identified as a decrease in acoustic impedance and is therefore displayed as a blue trough in the seismic section (Figure 15; Figure 30A). The lateral extent of the top reflector unit in Pre-SS is traceable and identified throughout the entire seismic cube. The reflection configuration, continuity, amplitude and frequencies vary within the Pre-SS unit. The section can be divided into two parts based on differences in seismic character. The lower part (SF 1) comprises of reflectors with low frequency and amplitudes (Figure 30; Figure 31). The reflections are considered as discontinuous and chaotic.

The upper part (SF 2) is approximately 400 ms. thick, and consists of frequencies and amplitudes ranging from low to high (Figure 30; Figure 31). The reflection geometry of the upper part is relatively horizontal consisting of parallel and semi-continuous reflectors (Figure 30; Figure 31). The top of the Pre-SS unit show indications of undulations affecting the geometry of the seismic horizon. The surface map of the top Pre-SS presents a surface morphology, which consist of numerous circular features encircled by reticulated ridge shaped highs (Figure 32).

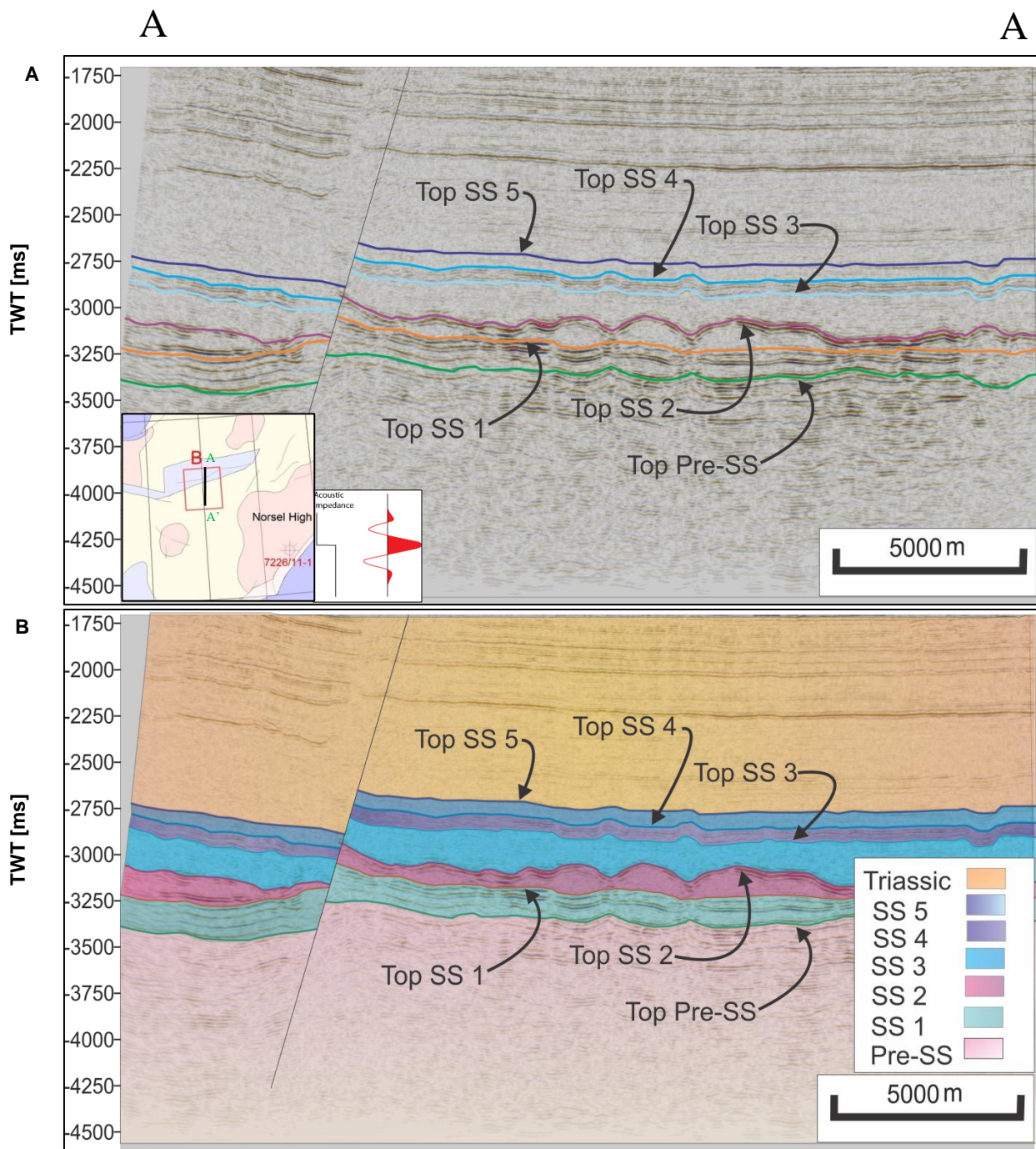


Figure 30 – North-South striking seismic sections of Area B located on the Bjarmeland Platform. A) Seismic in-line 2978; B) Geoseismic in-line 2978.

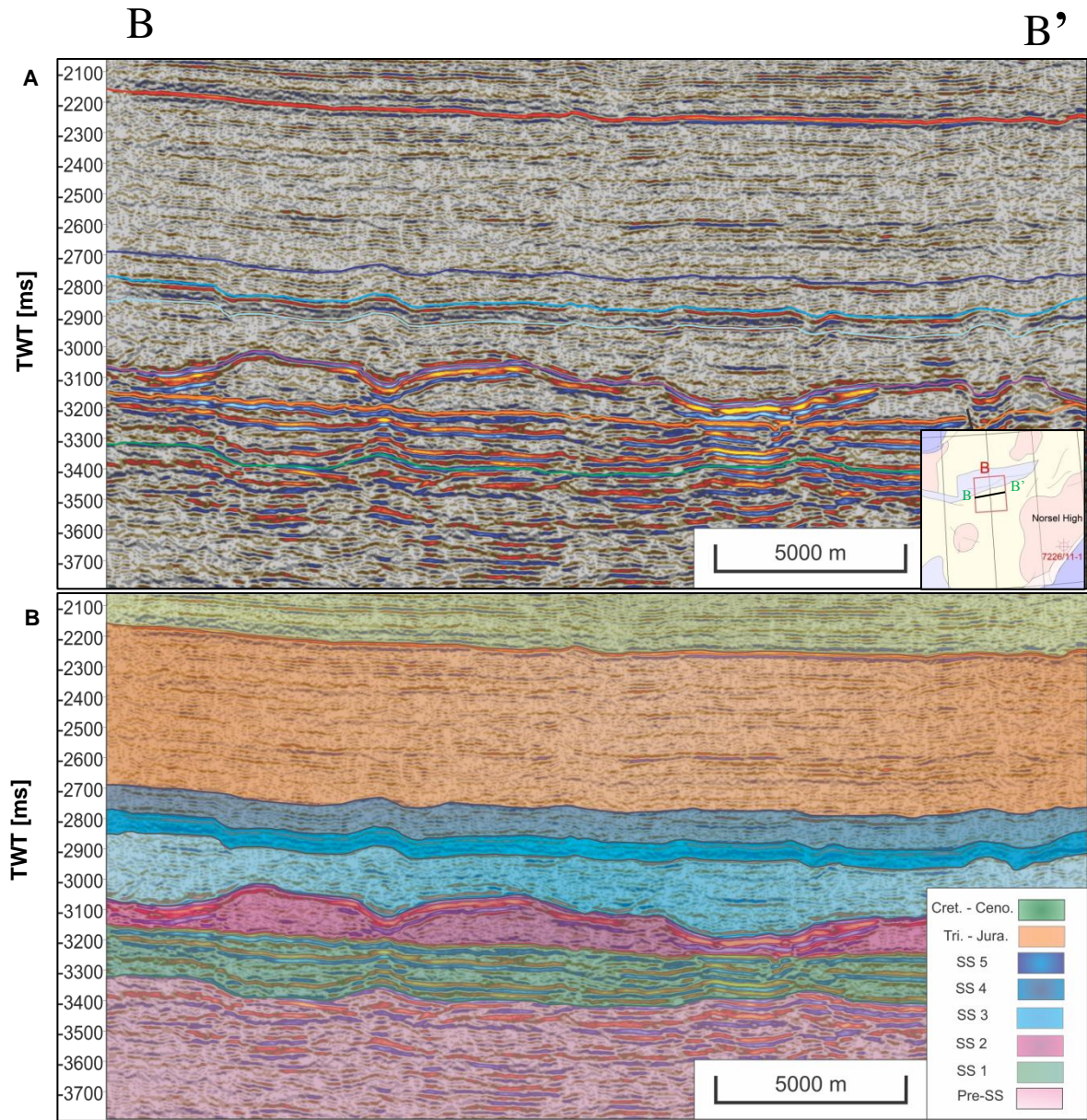


Figure 31 – West-east striking seismic section of Area B. A) Seismic x-line 1831, B) Geoseismic x-line 1831.

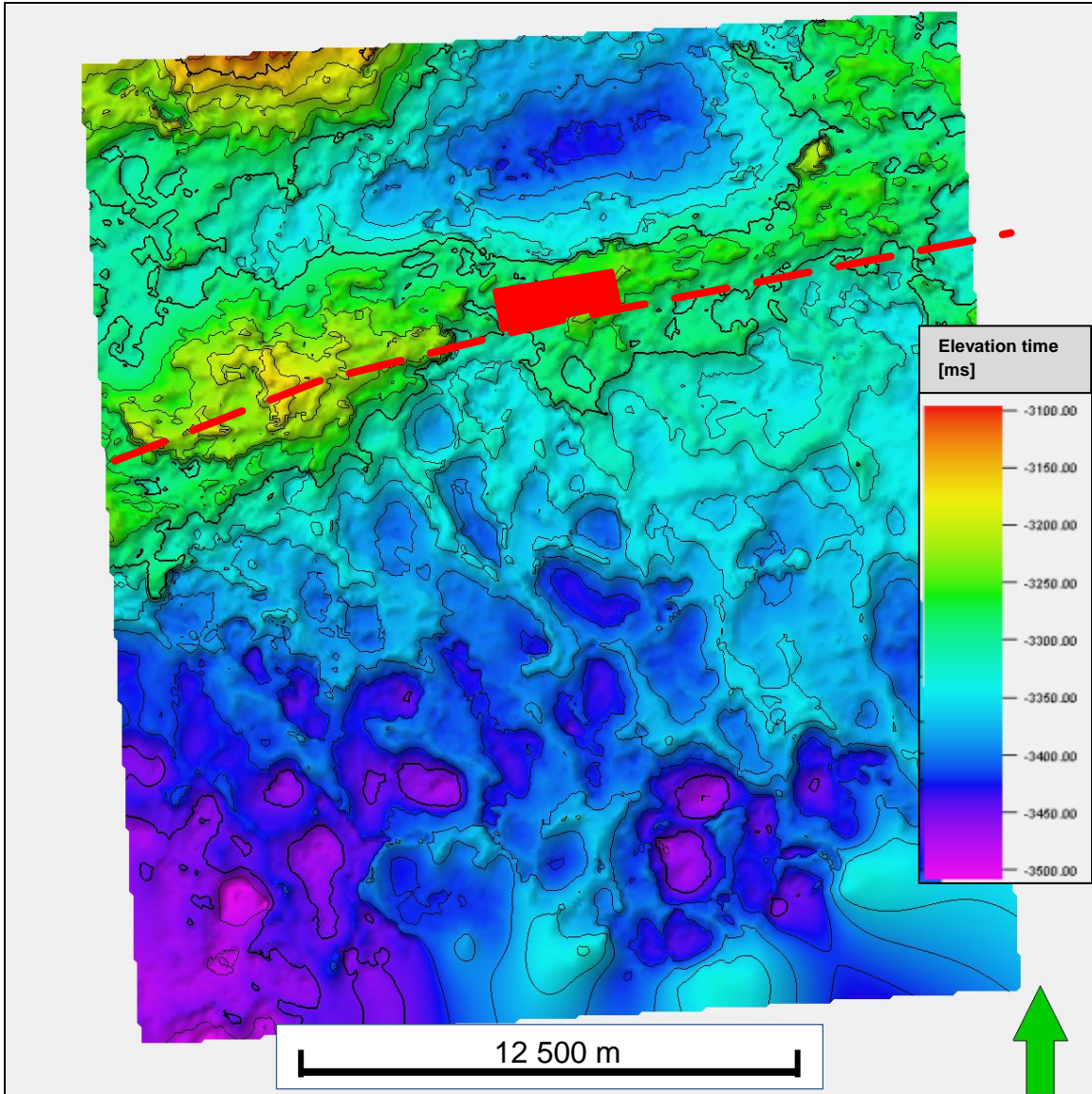


Figure 32 - Time structural map of top Pre-SS. The red line is marking the orientation of the major normal fault that crosscuts the Paleozoic – Mesozoic succession, which is the northward dipping boundary fault of the Swaen Graben.

Interpretation Pre-Seismic Sequences

The Pre-SS succession is interpreted as consisting of two different seismic facies units. The lower part (SF 1), identified by low frequencies and amplitudes is interpreted as the basement rocks in the area (Figure 30; Figure 31). The basement rock has been identified in well 7229/11-1, as pre-Devonian basement with sedimentological character composed of dark colored schist (Appendix 1.2; Ehrenberg et al., 1998a).

The upper part (SF 2) is deposited unconformable on the pre-Devonian basement, and interpreted as the Billefjorden Group (Appendix 1.2).

SF 2 consist of parallel layered and semi-continuous reflections, is interpreted as a fluvial dominated facies composed of heterolithic sediments (Figure 30; Figure 31). The deposition of the upper section is interpreted as deposited in low-relief setting, during a period of tectonic quiescence. This resulted in parallel depositional layers, showing no effect of tectonic influence.

The morphological features shown as circular cell-shaped structures, encircled by reticulated ridge-shaped features, are interpreted as imprints of the overlying stratigraphic succession. This interpretation is supports that the undulations observed on the seismic section in the top Pre-SS horizon, which is cause small pull-up effects created by higher velocities in the overlying strata (Figure 32).

5.1.2.2 Seismic Sequence 1

Description Seismic Sequence 1

The top of the SS 1 horizon is identified as an increase in acoustic impedance giving a seismic response as a blue trough (Table 7). The lateral extent of the top and base of the SS 1 is identified throughout the seismic area (Figure 30; Figure 31). The seismic facies within SS 1 (SF 3) is characterized as a homogenous unit consisting of laminated parallel reflections with continuous to semi-continuous continuity. There are some undulations along the base of the sequence, expressed as small synformal and antiformal structures (Figure 30; Figure 31).

The surface map shows an overall dip of the surface to the southwest (Figure 33A). The map shows a surface with minor local topographic highs and lows, but in general the surface has a rather planar expression (Figure 33A). The sequence has a generally uniform thickness, with an average thickness of 175 ms. (Figure 33B). The map indicates numerous circular features appearing as thickness related anomalies, which deviates from the overall uniform thickness of SS 1.

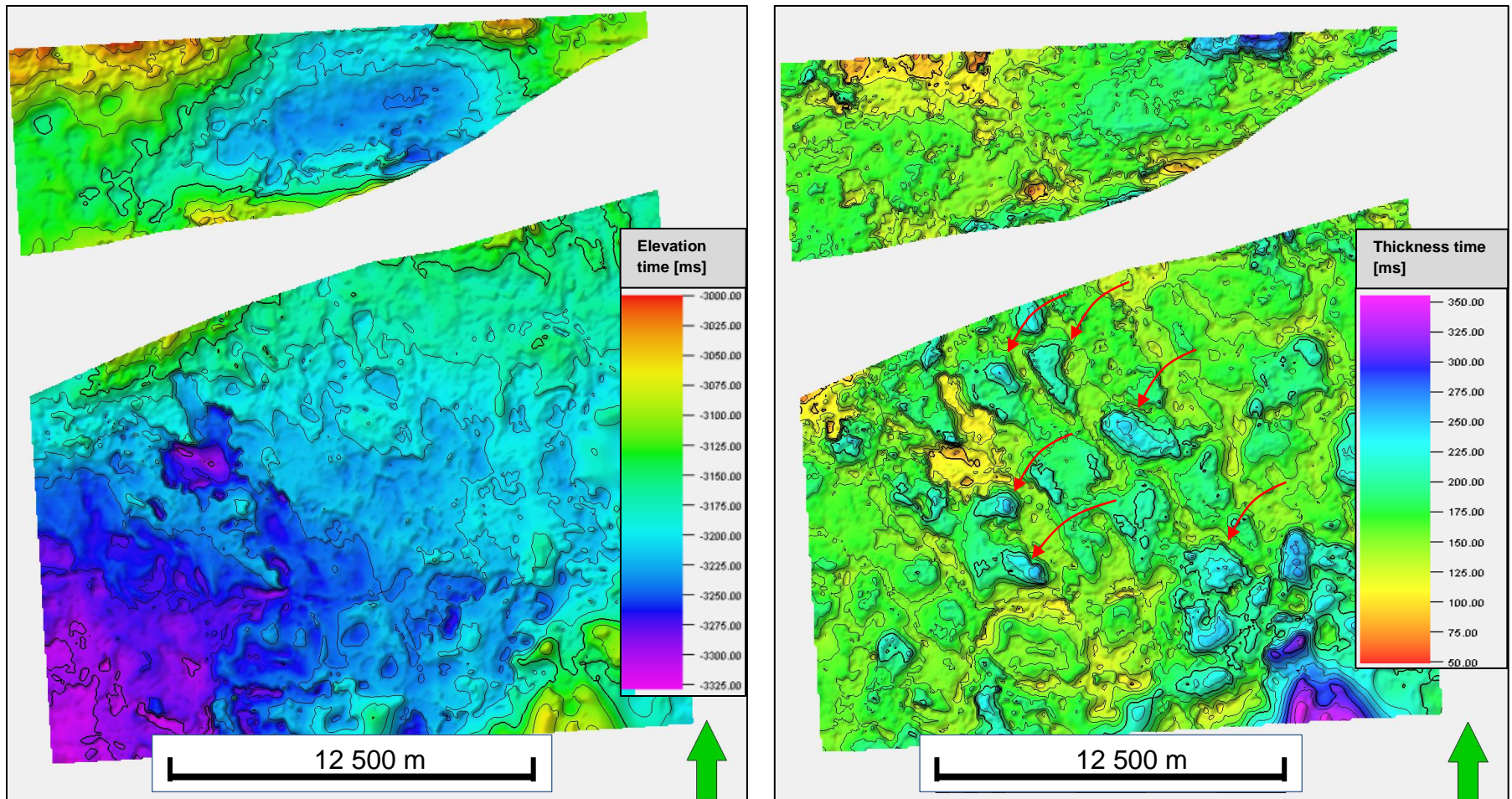


Figure 33 - A) Time surface map of top SS 1; B) Isochron map of SS 1. The circular and elliptically shaped thickness anomalies are marked with red arrows.

Interpretation Seismic Sequence 1

The SS 1 is considered as deposited in an environment affected by relatively little tectonic influence, therefore resulted in deposition laminated parallel reflections (Figure 31). The depositional environment is interpreted as platform interior setting, with sedimentary facies of muddy-limestone. The synformal structures located laterally adjacent to the small antiformal structures is interpreted as being a result of pull-down effect as a result of the overlying younger strata, the antiformal structure laterally is interpreted as pull-up effect caused by the overlying strata (Figure 31). These features coincide with the features identified as pull-up features in the Pre-SS surface (Figure 33A; Figure 31).

The circular and elliptical features observed on the surface map of top SS 1 horizon, are interpreted as imprints of the overlying stratigraphy (Figure 33A). This is also supported by the similar position of the circular features observed on the Pre-SS surface, which are situated beneath the SS 1 at the exact similar position (Figure 33B). The circular features are also indicated on the isochron map as thickness anomalies that deviate from the overall uniform thickness in SS 1 (Figure 33B). These thickness anomalies and are interpreted as identifying the impact of pull-up effects from the seismic signals in the seismic section (Figure 33B). The uniform thickness shown in Figure 33B is interpreted as visualizing the low relief setting during deposition of SS 1.

5.1.2.3 Seismic Sequence 2

Description Seismic Sequence 2

The top of SS 2 is defined as a decrease in acoustic impedance and effectively, a blue trough in the seismic section (Table 7). SS 2 is defined to consist of one distinct seismic facies (SF 4), which is laterally continuous throughout the area.

SS 2 is confined within top and base reflectors, classified as high amplitudes. Internally, the reflectivity pattern within the sequence is identified as low resolution, with discontinuous and chaotic reflectors (Figure 30; Figure 31). The geometry and thickness within of the sequence varies significantly through the seismic volume (Figure 30; Figure 31). The geometric shape of SS 2 is identified by pillow-shaped structures, with lateral and vertical variations. SS 2 shows distinctive variations in thickness on the footwall and hangingwall side of the fault (Figure 30; Figure 31). In the footwall side, the sequence has a generally constant thickness of approximately 100 ms., opposed to the hangingwall side where SS 2 has a thickness of approximately 20 ms. Nonetheless, the thickness of the sequence increases northward on the hangingwall block, to similar thickness as on the footwall side of the fault (Figure 31).

Figure 34A show the current geomorphology of the top of SS 2. The morphology of the area indicates a prominent relationship between highs and lows (Figure 34A). The surface map presents a number of structural highs that is encircled by networks of structural lows. The primary shapes of the structural highs are elongated with a NW-SE strike direction. The

orientations of the elongated structural highs are directed perpendicular to the strike direction of the margin of the Nordkapp Basin (Figure 34A). The orientation and shape of the structural lows are oriented similar as the trend of the structural highs. The geometry of the structural lows consists of valley shaped features. The isochron map shows the thickness variations within the SS 2 (Figure 34B). From the time thickness map shows that there are significant thickness variations throughout the area, and especially in the footwall side of the large fault. The general geometry observed from the isochron map of the area presents a pattern that consists of thick units that have a circular and elliptical shape with an average thickness of 175-200 ms. (Figure 34B). The thick elliptically shaped features are surrounded by thin reticulated units that which has an average thickness of 25 ms. (Figure 34B).

The seismic attribute maps area calculated from the seismic volume to illustrate the seismic geomorphology of the sequence. The RMS map identify that the highest amplitude anomalies are shown to be in the structurally low valleys, and the areas with low amplitude are located in the circular and sub-circular structural highs. The RMS amplitude is calculated as the vertical variability in amplitude between the top SS 2 and top SS 1 surfaces (Figure 35A). The variance map is created to identify the lateral variability in the SS 2 unit. The variance map is presenting a map showing low variability in the structurally low valley shaped features, and effectively high variability the circular and sub-circular structural high features (Figure 35B). The RGB blended map presents a geomorphology consisting of reticulated ridges which comprise of high frequency. These features differ from the low frequency structures which are located within the sub-circular structural highs (Figure 35C).

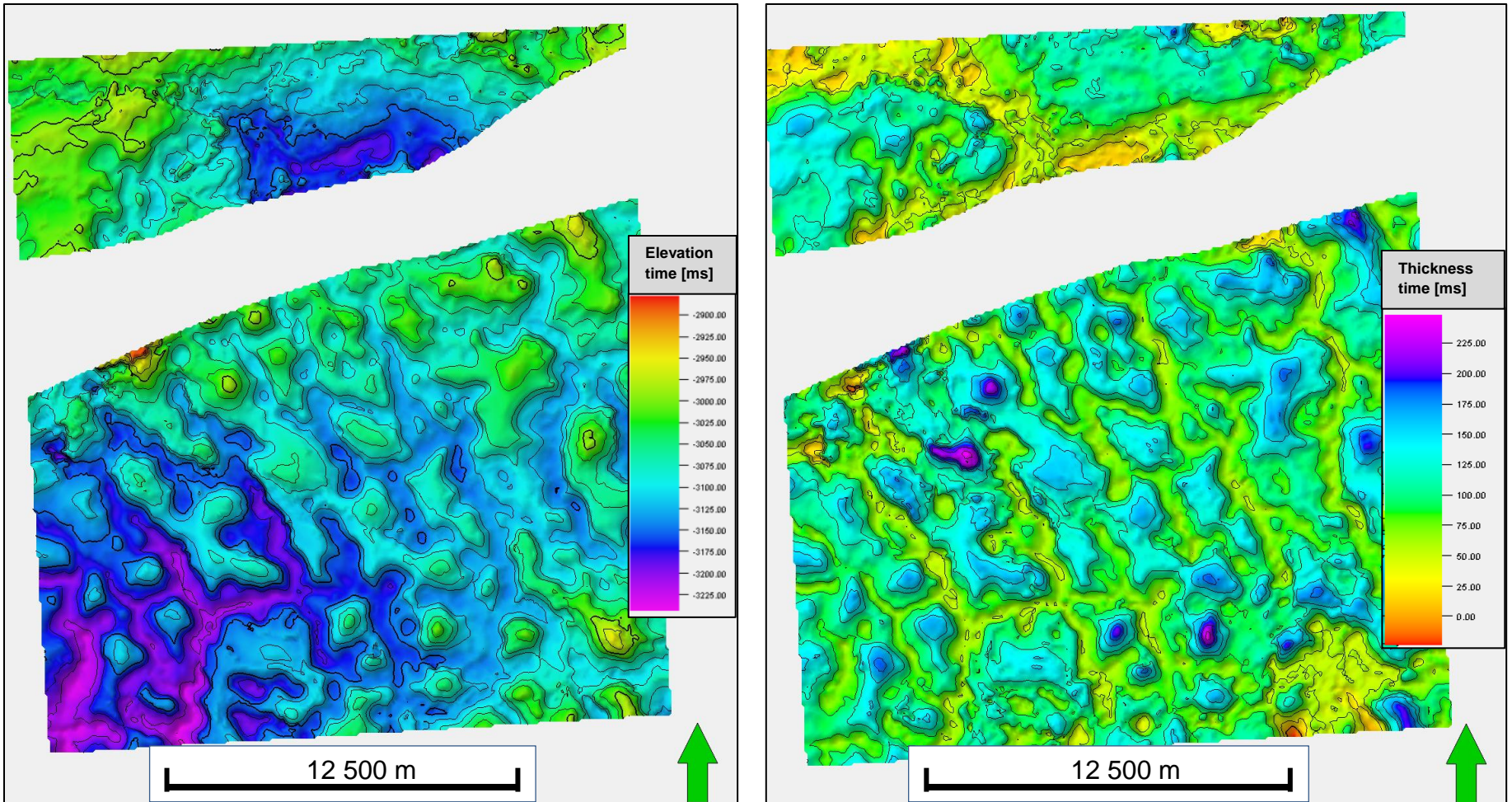


Figure 34 - A) Time surface map of top SS 2; B) Time thickness map of SS 2. The isochron map presents the relationship between the thick and thin successions described and observed in the seismic section.

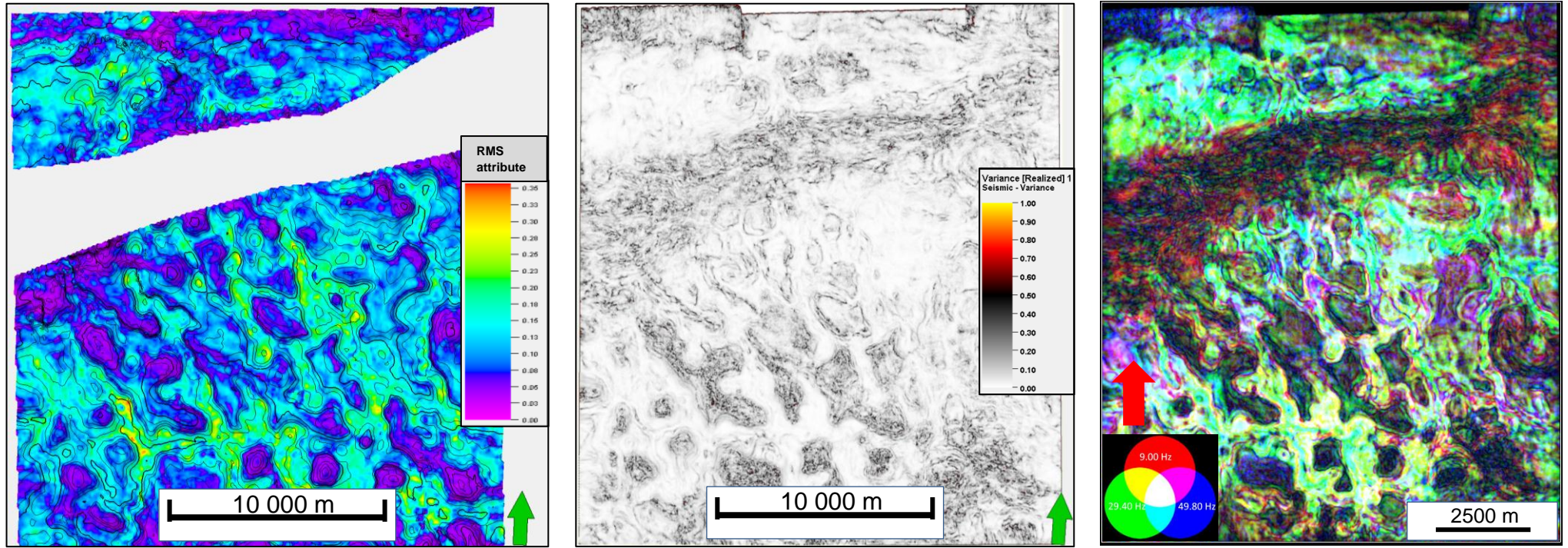


Figure 35 - Seismic attribute maps of SS 2. A) RMS Amplitude map calculated between top SS 2 and top SS 1; B) Variance map of time-slice $z = -3190$ ms. representing near top SS 2; C) RGB Color blend of time-slice $z = -3190$ ms. (Red color = 9.00 Hz, Green color = 29.40 Hz, Blue color = 49.80 Hz).

Interpretation Seismic Sequence 2

SS 2 is interpreted to consist of autochthonous mobile layered evaporites. The interpretation of a mobile evaporite unit is based on the disorderly geometry of SS 2, i.e. the thickening and thinning geometries (Figure 30; Figure 31). The evaporite sequence is interpreted as remobilized into the pillow-shaped structures, caused by differential loading by the overburden sediments. This causes development of thickening and thinning structures. Effectively, thick successions of SS 2 are located vertically below thin deposits overlying sediments. Opposed to the lateral structures where thin succession of SS 3 are located below thicker successions of the overlying stratigraphy (Figure 30; Figure 31). The lateral variations in the effective vertical stress from the overburden sediments results in deformation of the autochthonous evaporite layer.

The surface map is interpreted to visualize the present day topography of the top of the evaporite sequence (Figure 34A). The current morphology of the SS 2 is created as a result triggered by sedimentary differential loading, caused by the superposed strata. The lateral variation of thickness and density in the overburden succession activates the process of sedimentary differential loading; this result in different stress fields in the overburden sedimentary succession (Lou et al., 2012). The evaporitic sequence is affected by the thickest sedimentary sequence of the overlying strata, which sink into the underlying salt succession of SS 2, and causes expulsion of the salt laterally (Ge et al., 1997). Thus, result in development of salt pillow structures developed by the expelled salt. This result in salt weld structures created in the areas subjected to salt evacuation.

The relationships between the high and low RMS amplitudes are interpreted as being a result of the evacuation of mobile evaporites affected by the salt remobilization (Figure 35A). The areas that consist of low RMS amplitudes and cell-shaped structures are interpreted as created due to the salt mobilizing. The evaporite succession evacuated laterally, developing pillow shaped structures, seen on the seismic section and the surface map (Figure 30; Figure 34A). The mobile evaporite unit is considered as homogenous and therefore causing low resolution within the salt pillow structures. Consequently, this results in low amplitude within the salt pillow structures.

5.1.2.4 Seismic Sequence 3

Description Seismic Sequence 3

The top of SS 3 by an increase in acoustic impedance, which results in read peak in the seismic sections (Table 7). The top of SS 3 is laterally continuous and extends throughout the entire seismic area.

The SS 3 is defined as comprising of two different seismic facies units. The first seismic facies within SS 3 (SF 5) consists of heterogeneous reflections considered as chaotic with a discontinuous to semi-continuous continuity. The frequency content within the seismic signal is considered as low, but the magnitude of the amplitude varies from low to medium (Figure 30; Figure 31). The second seismic facies (SF 6) is defined by parallel, and in parts, semi-continuous reflections (Figure 30; Figure 31). The lateral distribution of the two different seismic facies units are related to the geometric relationship within the SS 3, which is identified by geometry with non-uniform thickness (Figure 30; Figure 31). The first seismic facies units area located vertically above the thin SS 2, which results in development of mound shaped features, which differs from the deposits of the second seismic facies unit located superposed on the thick pillow-shaped structures within the SS 2 succession (Figure 31).

The time structural map of the top SS 3 unit is displaying the geomorphology of the SS 3 unit. The surface map is identifying the reticulated and polygonal features of SS 4 that surround depressed circular cells. The distribution of the reticulated features is highest on the footwall side of the Swaen Graben fault (Figure 36A). The number of depressed cells increases from NE-SW, however, the size of the cells decrease in the similar direction (Figure 36A).

The isochron map shows the thickness variations within the SS 3 (Figure 36A). The thickness map reveals a similar trend as observed in Figure 36B. The isochron map identifies opposite thicknesses, as of those observed as thick units within SS 2 (Figure 36B; Figure 34B). The map shows the thick sections deposited as mounded features that stack vertically above the thin parts of SS 2 (Figure 36B).

The RMS Amplitude map displays high amplitudes confined into two areas on the footwall. The areas constraining the high amplitude locations are two narrow low amplitude zones oriented NW-SE (Figure 37A). The variance map presents the locations subjected to high and low vertical variance in the seismic area. The map illustrate that the high variance areas are primarily located in the areas of the reticulated mound-shaped features (Figure 37B). The areas consisting of little internal variance are the areas with sub-circular NW-SE orientated features. The RGB blended time-slice is present the mounded reticulated features consisting of low frequencies and as a consequence, presents the parallel continuous reflection configuration seen in the seismic section as areas with higher frequencies (Figure 37C; Figure 31A).

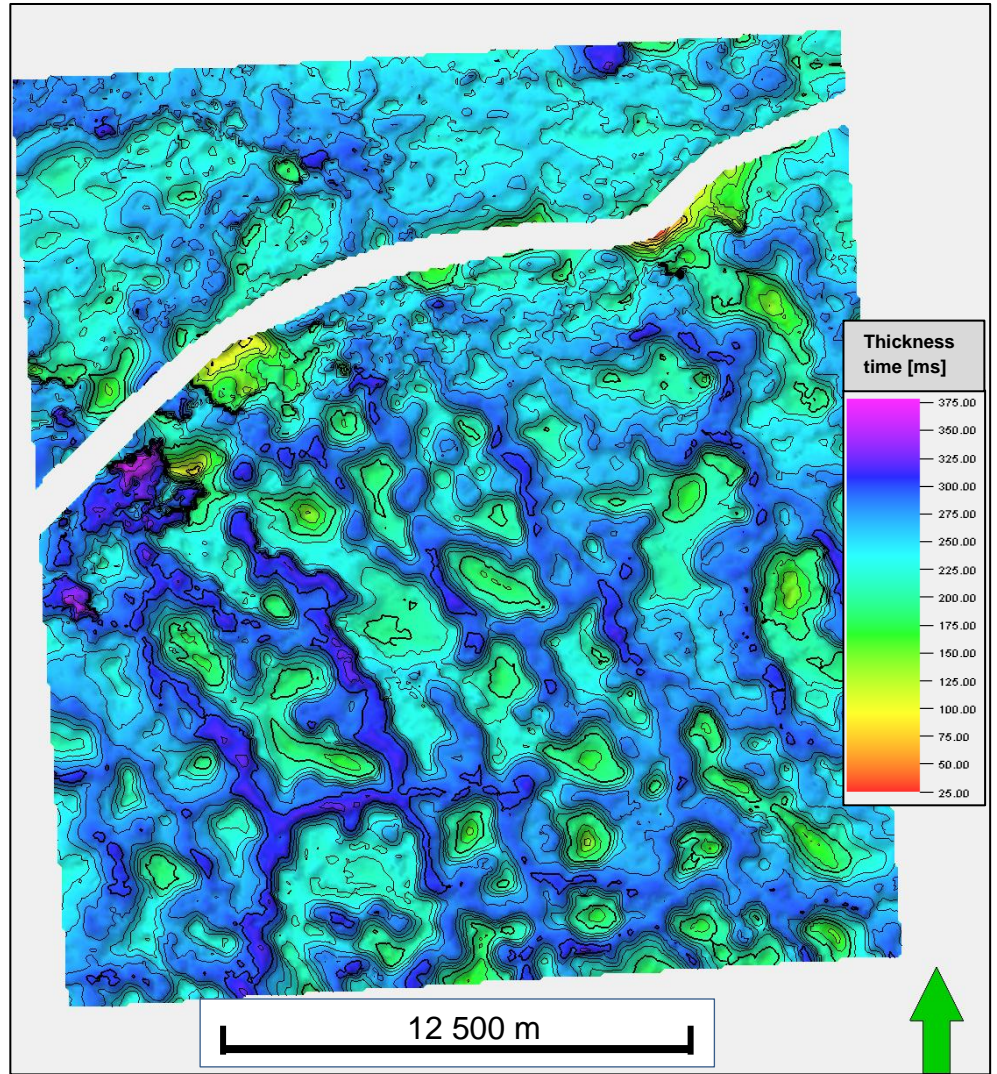
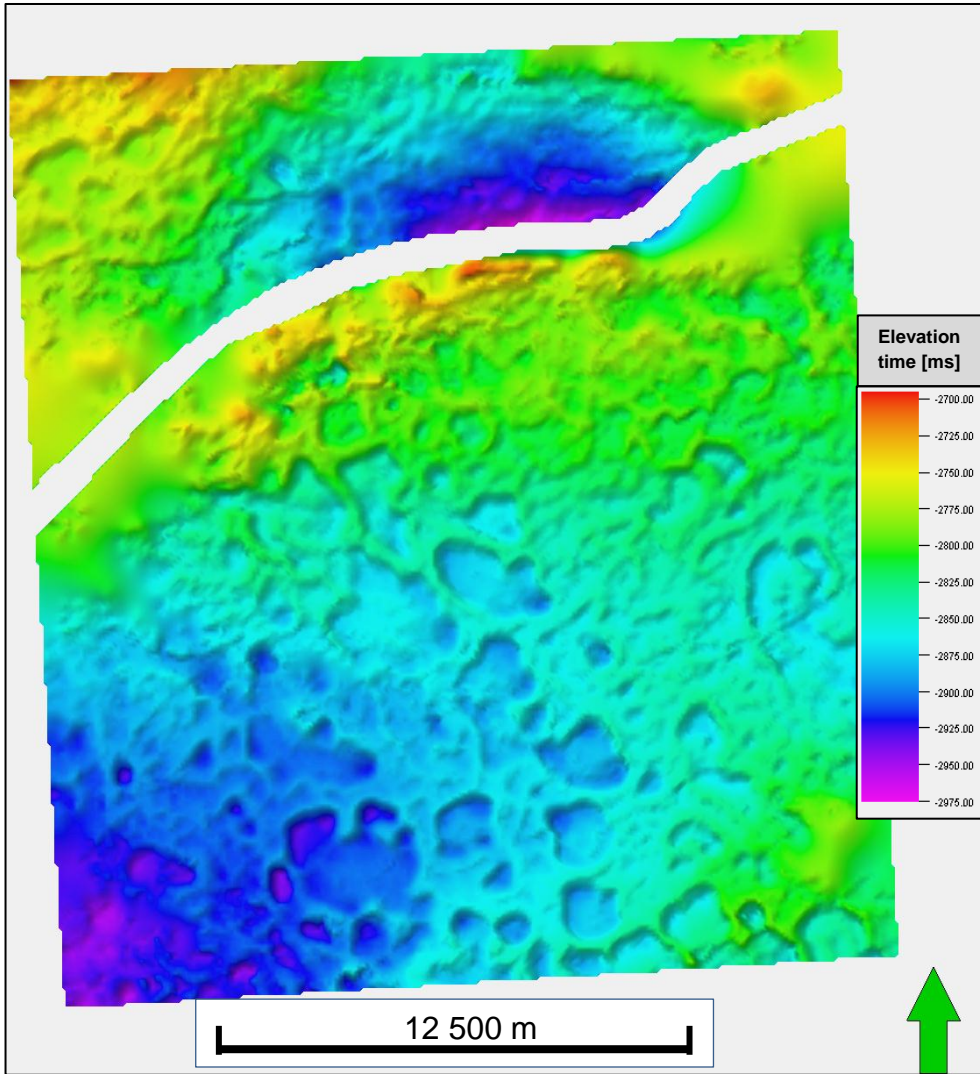


Figure 36 - A) Time surface map of top SS 3; B) Time thickness map of SS 3. The isochron map is present the reticulated ridges as thick features, and the elliptical-shaped features as thins.

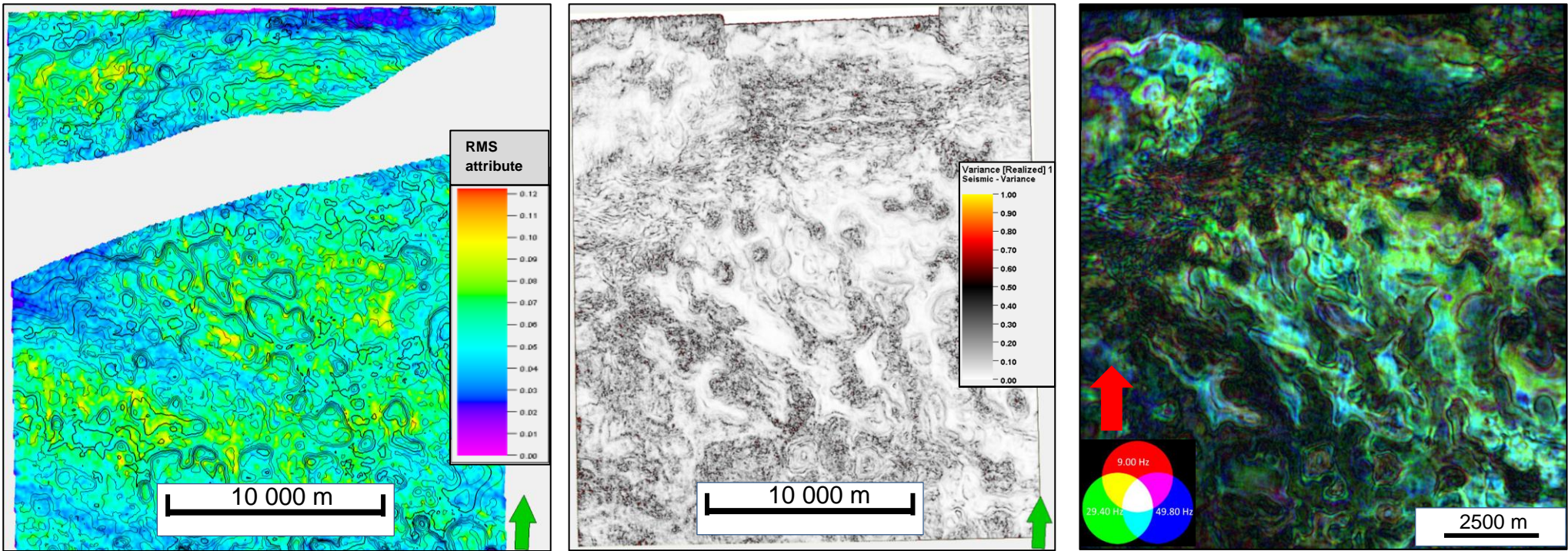


Figure 37 - Seismic attribute maps of SS 3. A) RMS Amplitude map calculated between top SS 3 and top SS 2. ;B) Variance map of time-slice $z = -3080$ ms. representing near top SS 3; C) RGB Color blend of time-slice $z = -3080$ ms. (Red color = 9.00 Hz, Green color = 29.40 Hz, Blue color = 49.80 Hz)

Interpretation Seismic Sequence 3

SF 5 is interpreted as reticulated carbonate build-ups that encircle depressed cell-shaped features (Figure 36A). The reticulated build-ups are located directly above the thin units of SS 2. SF 6 is confined within the depressed features. The depressed features are located above the thicker units of SS 2. SF 6 is interpreted to consist of muddy-limestone (Figure 36A).

The remobilization of the underlying SS 2 resulted in alternation of the morphology SS 3. Figure 36 show the impact of the salt remobilization. The interpretation of SS 3 suggests that the evaporites succession of SS 2 was remobilized by differential loading effects during deposition of SS 3. Effectively, the carbonate build-up succession kept on growing on the antecedent topography of previous mound shapes, which resulted in thick succession comprised of carbonate build-up facies deposited vertically above the thinner successions of SS 2 (Figure 30; Figure 31).

The reticulated features representing the carbonate build-ups are visualized in the variance map (Figure 37B). The low variance zones are interpreted as the interior lagoonal setting, which comprises of SF 6 (Figure 37B). The depositional settings in the interior lagoons are considered as quiet and low energy, which result in low variance in the map (Figure 37B). The area is interpreted as part of a platform interior setting, prograding towards the south. The elliptically-shaped features are oriented perpendicular to the margin of the Nordkapp Basin. These features have the characteristic geometry as spur and groove systems, which grow perpendicular to the platform margin.

5.1.2.5 Seismic Sequence 4

Description Seismic Sequence 4

Top SS 4 is defined by an increase in acoustic impedance and consequently, a red peak in the seismic section (Table 7). The top of SS 4 is identifiable throughout the entire seismic volume (Figure 30; Figure 31).

The internal reflectivity in SS 4 is identified as one seismic facies (SF 7). The reflection configuration within the sequence is considered as parallel, and generally, continuous to semi-continuous reflectors (Figure 30; Figure 31). The seismic reflection geometry visible in SS 4 is considered as uniform on both the hangingwall and footwall side of the fault.

The structural map of the top SS 4 horizon presents a surface with little to no morphological expressions and thus, the map presents a relatively flat topography (Figure 38A). Figure 38A show a general direction of dip for the surface, towards the south. The isochron map created to identify the thickness variations within the SS 4 (Figure 38B). The map shows an overall uniform thickness, which is approximately 75 ms. thick within the sequence (Figure 38B).

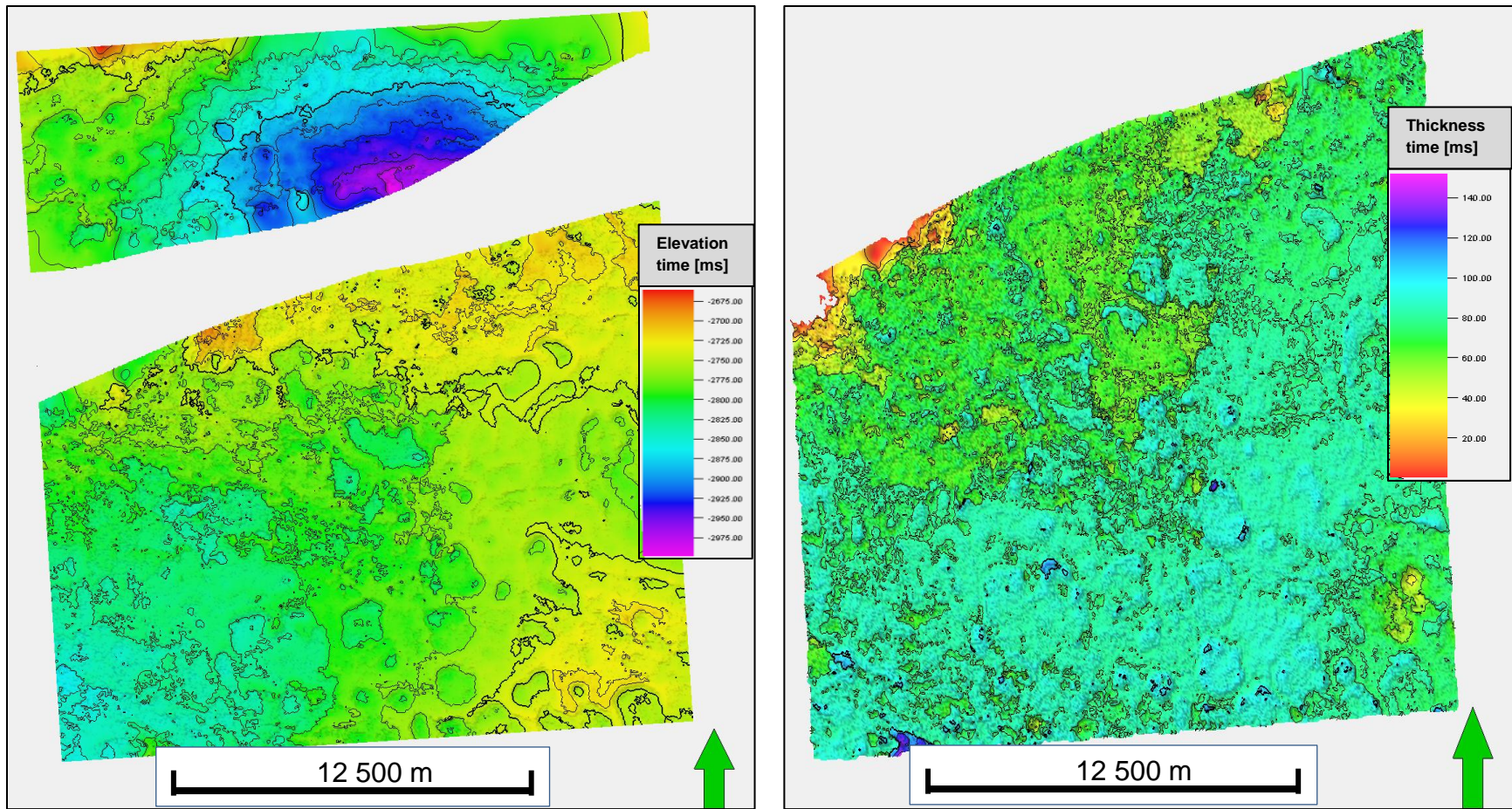


Figure 38 - A) Time surface map of top SS 4; B) Time thickness map of SS 4. The thickness map shows a uniform thick succession within SS 4.

Interpretation Seismic Sequence 4

The SS 4 is interpreted as a unit consisting of one distinct facies that is considered as a homogenous lithology. Internally, SS 4 were identified in the seismic section as a homogenous unit draping the underlying topography. The deposition of SS 4 is interpreted as pelagic or hemipelagic carbonate sediments in an open marine environment. Two main supporting evidences support this interpretation are, firstly, the well data results from the Norsel High that penetrates an approximately 130 meter succession of facies equivalent to SS 4 in well 7226/11-1 (Appendix 1.2). Secondly, the uniform thick unit of SS 4 has constant thickness throughout the area, with parallel and continuous reflections. The unit is deposited in concordance and therefore drapes the underlying topography of SS 3 (Figure 30; Figure 31).

The SS 4 structural map is defined as a succession which is distributed with homogenous topography. Hence, the deposition of the sequence has not been affected by any structural component synchronous as deposition occurred (Figure 38A). Figure 38B indicate uniform thickness of SS 4, this is seen as evidence that the remobilization of the SS 2 occurred prior to the deposition of SS 4. SS 4 is therefore supporting the interpretation of the depositional setting as pelagic or hemipelagic (Figure 38B).

5.1.2.5 Seismic Sequence 5

Description Seismic Sequence 5

The top of SS 5 is presented as a decrease in acoustic impedance and effectively, results in a blue trough (Table 7). The sequence is identified by one distinct seismic facies (SF 8). The reflections within SS 5 are identified as parallel and laterally continuity and, in parts, semi-continuous. The seismic signal varies in magnitude from low to medium amplitudes and low frequencies (Figure 30; Figure 31).

The surface map of the sequence presents a seismic morphology that is considered as relatively flat (Figure 39A). The surface is gently dipping to the southwest towards the Nordkapp Basin (Figure 39A). The SS 5 is considered as a uniform thick sequence of approximately 30 ms. associated with some thickness anomalies presented with a thickness of 70 ms. (Figure 39B).

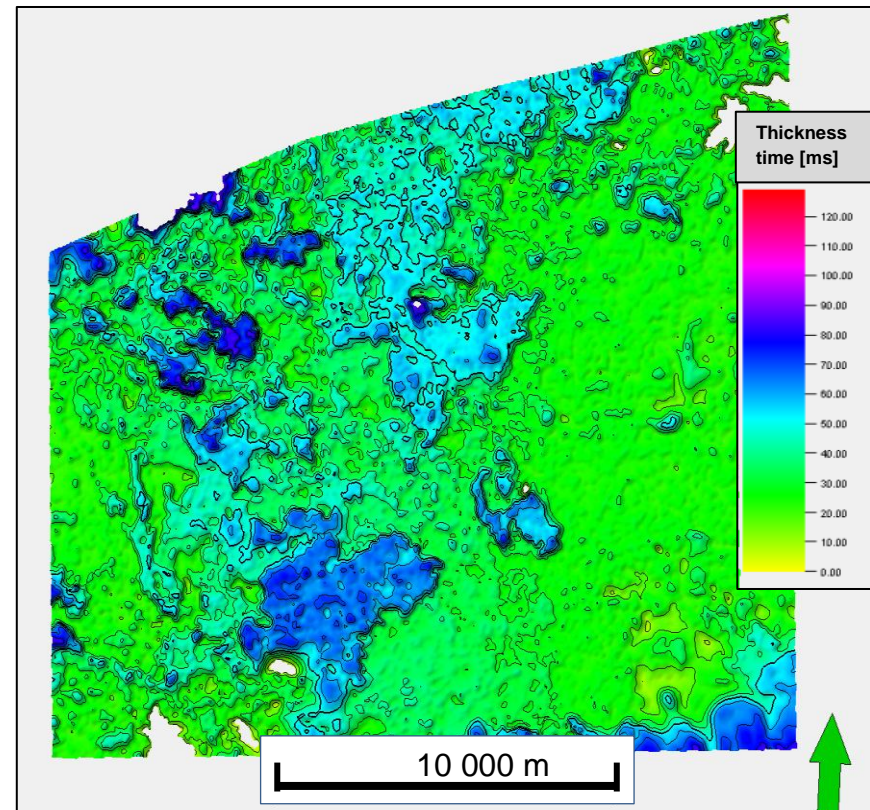
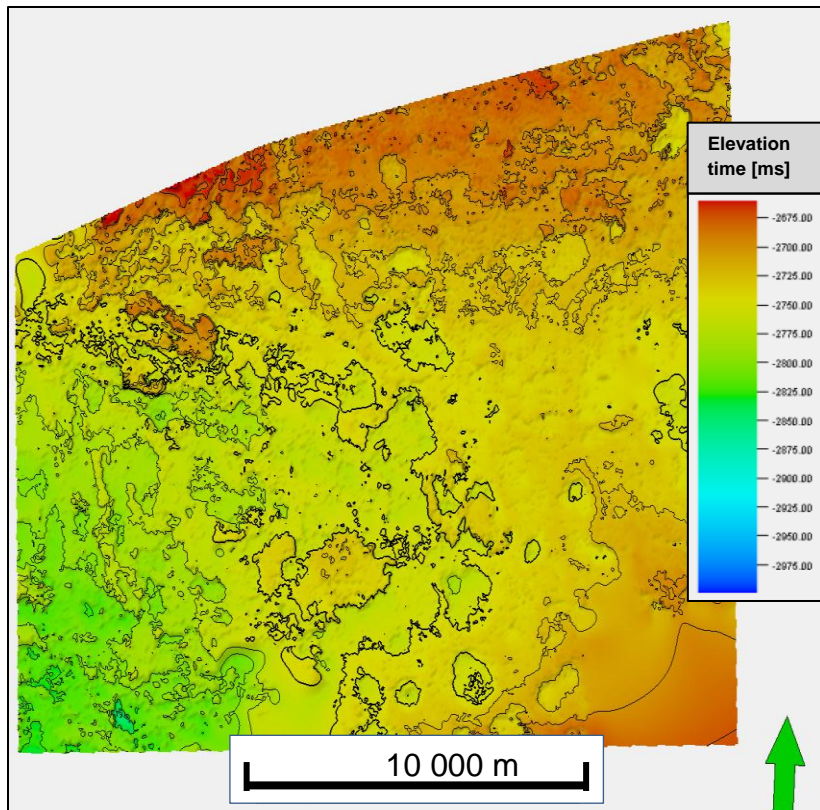


Figure 39 - A) Time surface map of top SS 5; B) Time thickness map of SS 5.

Interpretation Seismic Sequence 5

SS 5 is interpreted as a sequence consisting of a homogenous lithology that is deposited uniformly throughout the area. The lithology of within sequence is interpreted siliciclastic sediments with shale-rich facies. The gentle topographic signature in SS 5 is interpreted as pelagic deposition the siliciclastic sediments. The sedimentary layer is draping the underlying topography of the SS 4 succession, hence, resulting in a uniformly thick succession of average 30 ms. thick throughout the entire seismic area (Figure 39B).

The lithological interpretation of the sequence is also supported by the well data observations from well 7229/11-1, which penetrates the identical succession on the Finnmark Platform. The well data results confirm the presence of shale-rich facies within the upper Paleozoic succession (Appendix 1.2). The topography created on Top SS 5 reflector is caused by the underlying stratigraphic units.

5.2 Finnmark Platform

5.2.1 Seismic Area C (SH9102)

The Seismic Area C is located on the northeastern section of the Finnmark Platform approximately 50 km southeast of the Nordkapp Basin (Figure 40). The area of interest is situated on the Finnmark Platform. To illustrate the seismic signature of the seismic sequences, two lines has been used, the first seismic line is an inline orientated W-E and the length is approximately 25 km., and the second line is an x-line oriented N-S and the length of the line is 21 km (Figure 41; Figure 42).

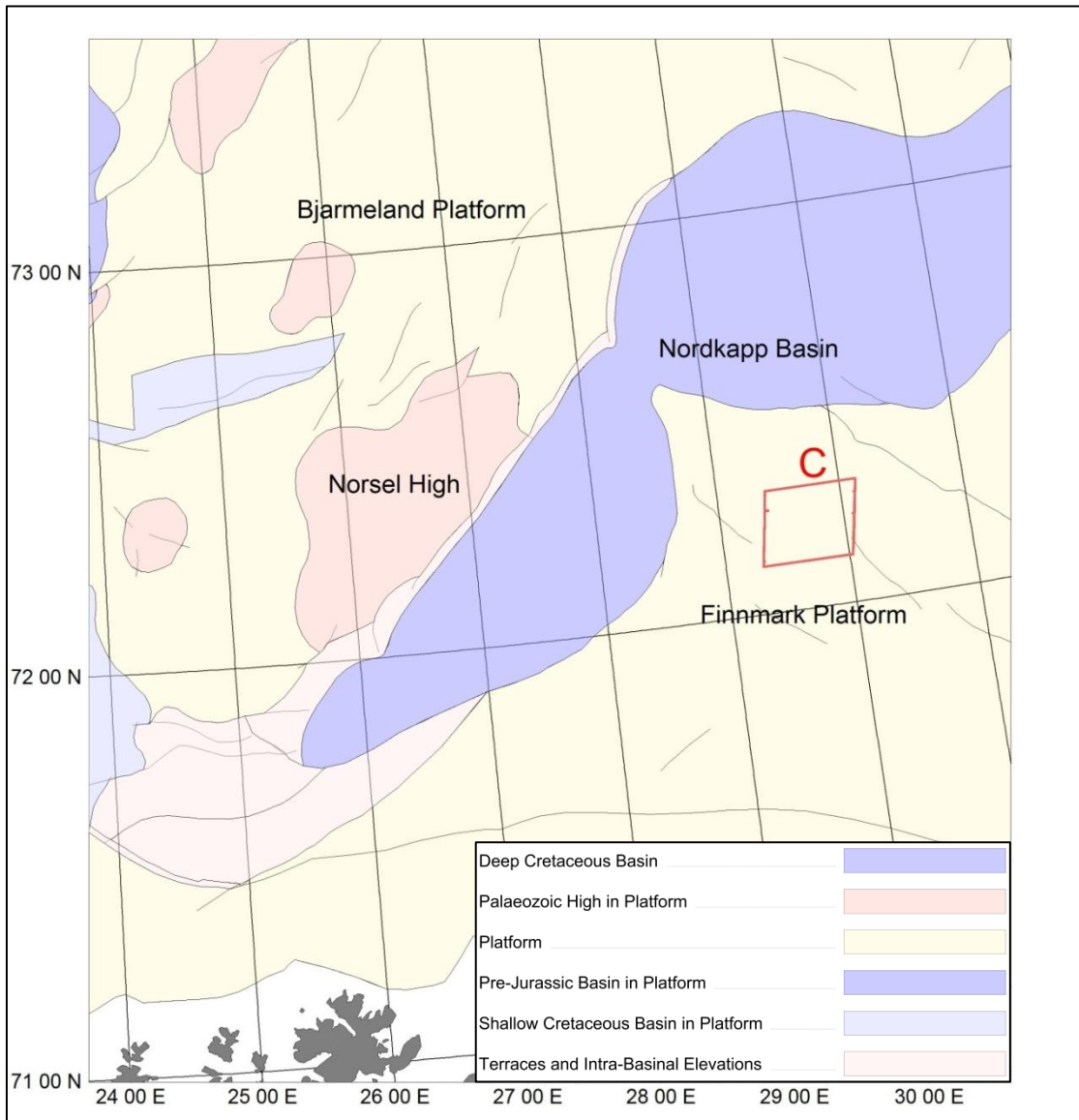


Figure 40 - Regional structural elements map of the SC Norwegian Barents Sea highlighted with the outline of Seismic Area C.

5.2.1.1 Pre-Seismic Sequences

Description Pre-Seismic Sequences

The top of the Pre-SS succession is identified as a decrease in acoustic impedance represented by a blue trough (Table 7).

Reflection characteristic and geometry sub-divided the Pre-SS into three distinct parts (Figure 41A). The lower part (SF 1) is characterized by chaotic and discontinuous reflectors with low amplitudes and frequencies. The middle part is identified by sub-parallel and semi-continuous reflectors. The middle part (SF 2) and has the characteristic geometry of a syn-tectonic succession (Figure 41; Figure 42). The upper part is defined by a reflection configuration of sub-parallel and semi-continuous reflectors, with low amplitudes and frequencies (Figure 41; Figure 42).

The time surface map of top Pre-SS horizon is illustrating by Figure 43. A structural high is observed in the center of the area. This structural high is subjected to multiple series of faulting (Figure 43A). The Pre-SS succession is affected by faulting event (FF 1) identified in Figure 41. The orientation of FF1 is striking NE-SW, and the dip direction is directed towards the SE (Figure 43). These faults are shown in Figure 43, as red lines indicating the dip direction of the faulting event. The second faulting event (FF 2) defined in Figure 42 crosscuts the top Pre-SS 2. This event is presented on the structural map as a fault polygon (Figure 43).

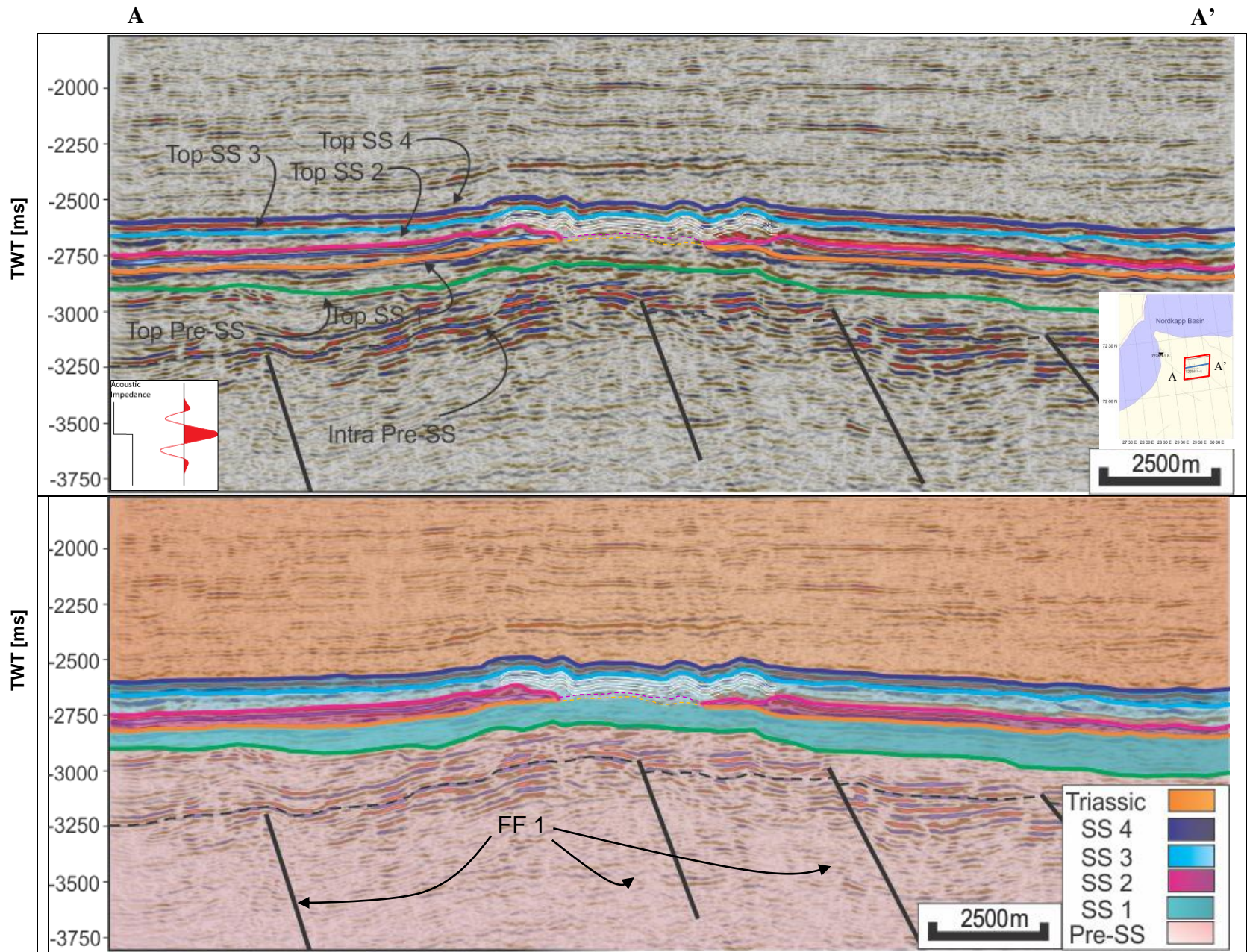


Figure 41 - Seismic sections of Area C on northern Finnmark Platform. 17A: Seismic Inline 477, 17B: Geoseismic Inline 477.

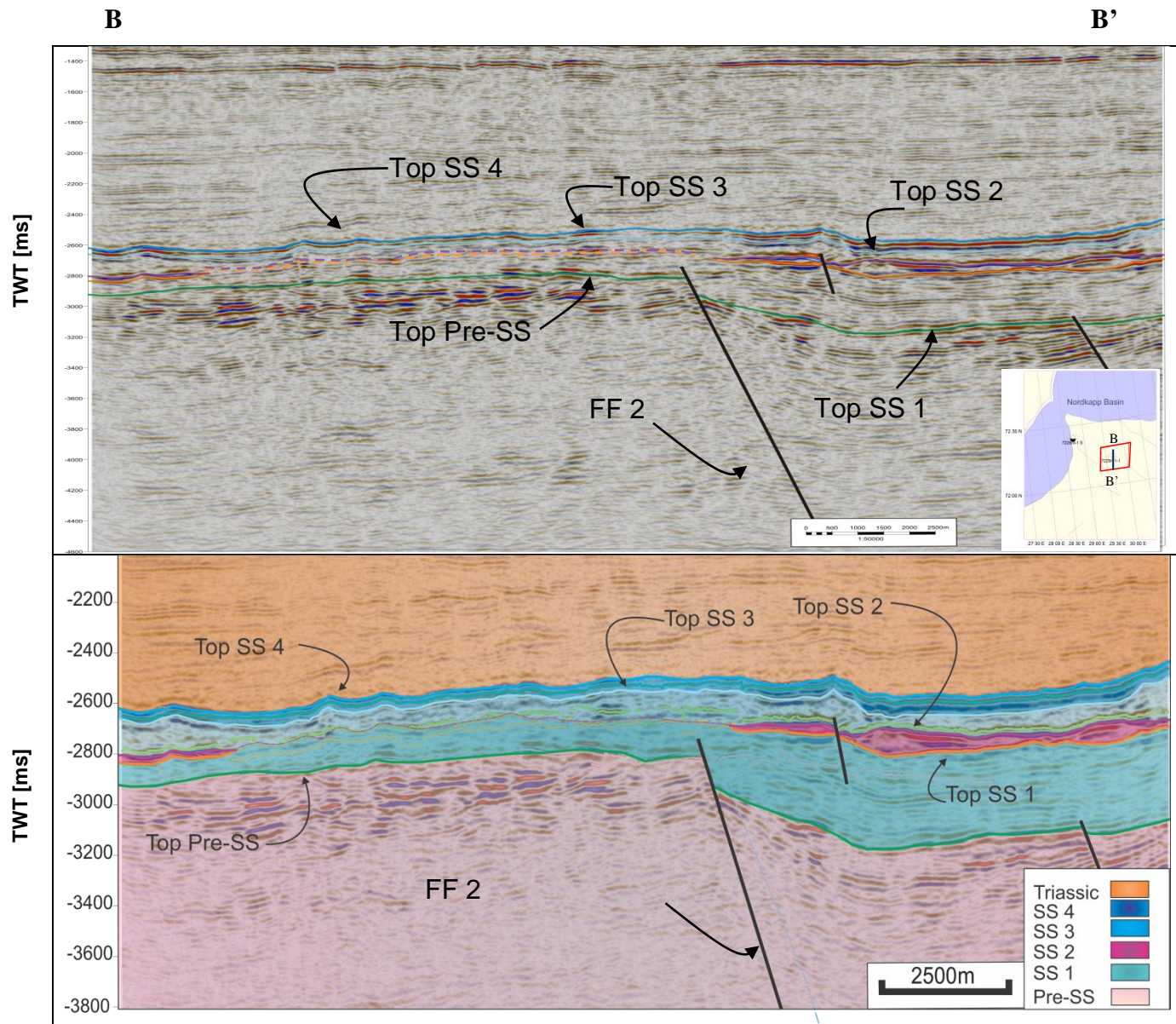


Figure 42 - Seismic sections of Area C on northern Finnmark Platform. A) Seismic x-line 627; B) Geoseismic x-line 627.

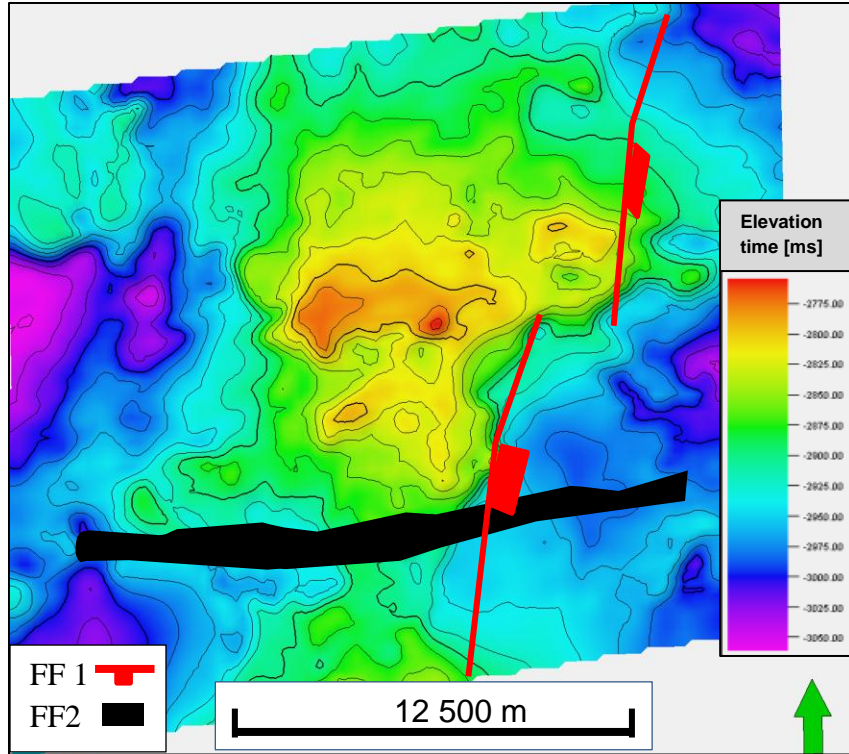


Figure 43 - Time surface map of top Pre-SS displayed with position of deeper seated faults.

Interpretation Pre-Seismic Sequences

The lower part is interpreted as the pre-Devonian basement. The interpretation of the lower part as basement is also supported by the observed in well data results, which encounter Pre-Devonian basement (e.g. Appendix 1.2: Appendix 1.4).

The middle part has been affected by eastern dipping normal faults. These faults are interpreted as crosscutting the lower and middle parts of Pre-SS (Figure 41; Figure 42). The geometry of the unit is interpreted as showing indications of growth strata, which is evidence of syn-tectonic deposition (Figure 41; Figure 42). The sedimentary succession is interpreted as fluvial facies consisting of the Soldogg and Tettegras Formations.

The upper part is interpreted as draping the underlying topography. This succession is interpreted as late syn-tectonic to post-tectonic deposition (Figure 41; Figure 42). The facies is therefore interpreted as consisting of heterolithic sediments composed of shale and sandy facies, equivalent to Blærerot Formation.

The topographic high is interpreted as created by FF 1. FF 1 has been interpreted as being tectonically active during the middle and early part of Pre-SS, interpreted as the middle Tournaisian – early Viséan (Figure 42). FF 2 occurred subsequent to the deposition of top Pre-SS and thus, crosscuts the top Pre-SS surface.

5.2.1.2 Seismic Sequence 1

Description Seismic Sequence 1

The top of the SS 1 is defined by an increase in acoustic impedance giving a red peak in the seismic section (Table 7). The top and base of SS 1 is laterally continuous and define the sequence, which extends throughout the entire seismic area.

The sequence is divided into two different seismic facies units. The first facies unit (SF 3) is identified by parallel reflectors and semi-continuous reflections, with low to medium amplitudes and low frequencies. The bounding relationship of the SF 3 is limited to the flanks of the survey and, absent in the center of the area (Figure 41; Figure 42). The reflectors within SF 3 are dipping away from the center of the area, where the SF 3 is absent (Figure 41). The second seismic facies (SF 5) unit is considered as a chaotic and relatively discontinuous reflection unit. The unit is confined within the center of the seismic area (Figure 41).

Figure 42 shows a normal fault (FF 2) that crosscut the top Pre-SS horizon, and extends further into the SS 2 succession. The orientation of FF 2 is presented on the surface map as an orange line (Figure 44A). FF 2 originated during deposition of SS 1, hence, resulting in a thicker accumulation of SF 3 in the hanging wall succession of the normal fault (Figure 42).

The time thickness map shows the thickness variations in SS 1 (Figure 44B). The isochron map presents a thickness variation directed from north to south of the area. The average thickness in succession on top of the structural high is 75 ms. thick, while the average thickness in the lower elevated areas are approximately 225 ms. thick (Figure 44B). The northern part consists of relatively thin SS 1, with average thickness of 75 to 100 ms. (Figure 44B).

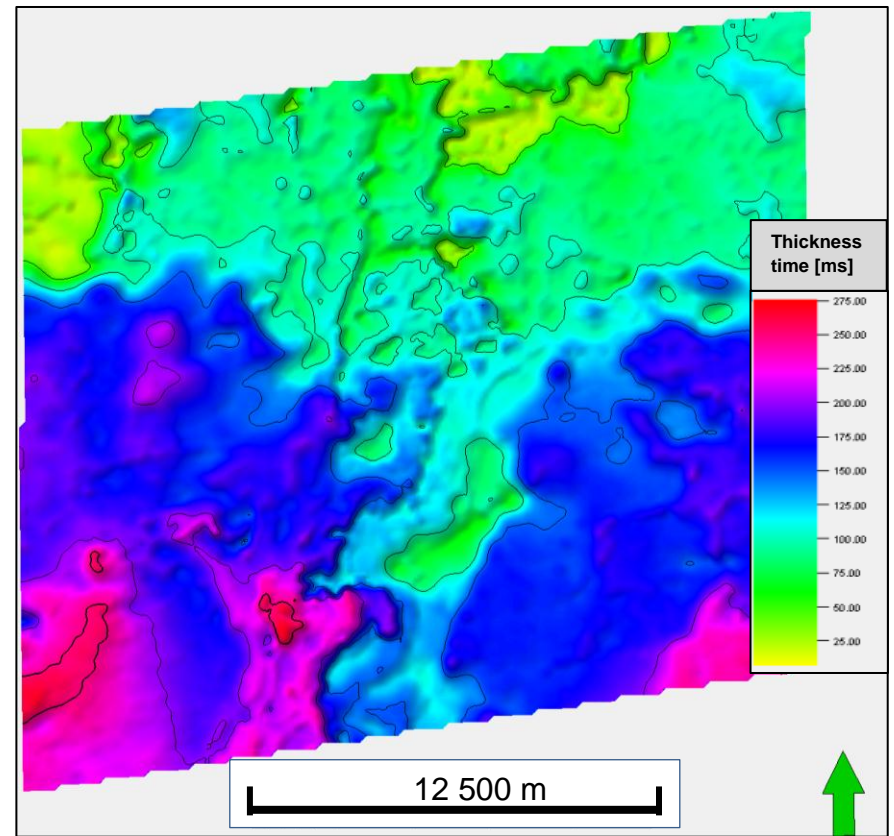
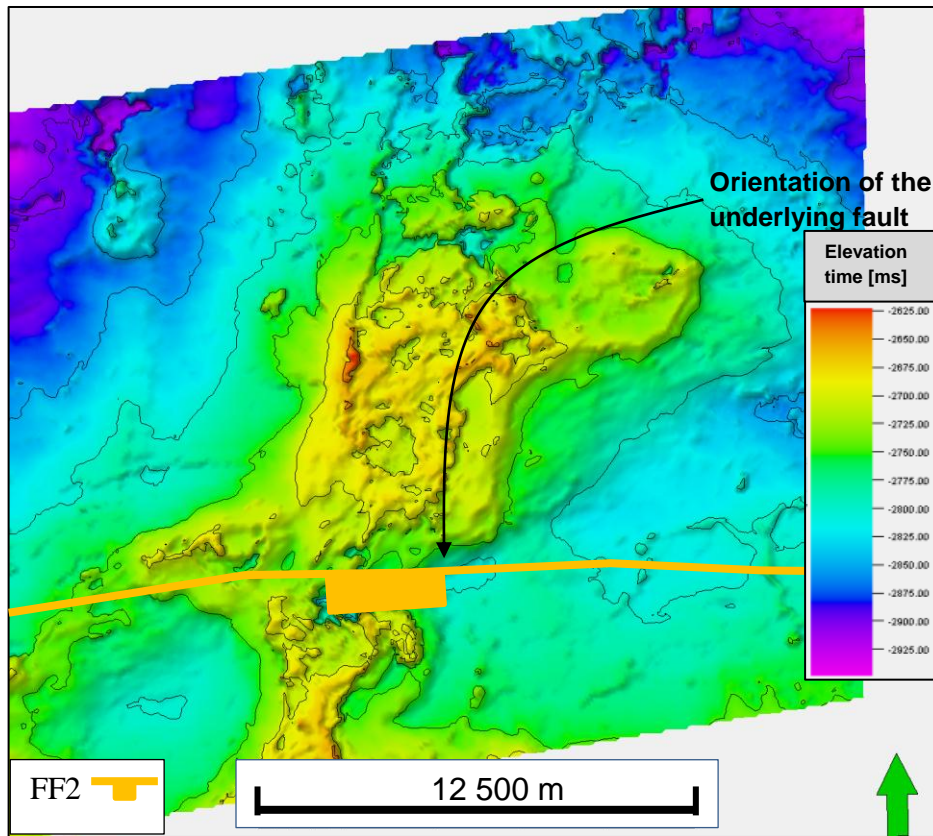


Figure 44 - A) Time surface map of top SS 1; B) Time thickness map of SS 1.

Interpretation Seismic Sequence 1

SS 1 is interpreted as heterolithic sedimentary succession. The lower part of the sequence is interpreted as deposits of alluvial sediments. The upper part is interpreted as deposits of muddy-limestone facies.

SF 3 reflections are dipping away from the center of area, where SF 5 is identified (Figure 41; Figure 42). SF 3 is interpreted as deposited in the lower elevated areas surrounding the structural high, whilst SF 5 is interpreted as deposited along the structural high. SF 3 is interpreted as deposited in a platform interior environment, and composed of limestone-rich facies. SF 5 is interpreted as the lower part of a carbonate build-up complex, with sedimentary composition of protozoan carbonate (Appendix 1.3).

The deposition of the SS 1 succession is interpreted as deposited during a period of active tectonic events, which is evident by the syn-tectonic strata in Figure 42. The seismic character is defined as sub-parallel and, in parts, parallel in the footwall side of the fault (Figure 42), and by a deposition of syn-tectonic succession in the hanging wall (Figure 42). The syn-tectonic succession is interpreted as comprising of sediments equivalent to the Ugle Formation (Figure 6). The timing of FF 2 is interpreted as occurred during the middle Bashkirian (Figure 44A). The tectonic event affecting the deposition of SS 1 is interpreted as the mid-Bashkirian extensional event (Johannesen and Steel et al. 1992). The structural event crosscuts the paleo-high structure in the middle and southern sector of the area (Figure 42). The latest stage of the SS 1 is interpreted as a stable tectonic period resulting in deposition of homogenous muddy-limestone sediments. The isochron map reveals that the paleo-high developed by the faulting event might have impacted the deposition of SS 1. The map indicates that there was very little deposition of SS 1 on top of the paleo-high structure (Figure 44B).

5.2.1.3 Seismic Sequence 2

Description Seismic Sequence 2

The SS 2 is identified by the top reflector being a strong decrease in acoustic impedance seen in the seismic section as a blue trough (Table 7). The top and base of SS 2 are laterally extensive throughout the entire seismic area.

The sequence can be sub-divided into two different seismic facies units. The first seismic facies (SF 4) unit is considered to have a relatively uniform reflection geometry and constant thickness, despite some variations where it thins towards the center of the area (Figure 41). The reflections are considered as sub-parallel and continuous with strong amplitudes and frequencies in the top and base reflectors. Internally, SF 4 is identified by primarily discontinuous and, in places, semi-continuous reflections. The second seismic facies (SF 5) is defined as discontinuous and chaotic reflections. The thickness of the SF 5 is considered as thin, and the unit is confined to the center of the area (Figure 41; Figure 42).

The surface map of top SS 2 is showing the outline of the deposition of the two different seismic facies units. The surface map shows a dipping of SS 2, towards the east, north and west of the area. The morphology of the SF 4 is considered as gentle topography. SF 4 is confined to the deeper parts, of the area, and the unit is laterally absent along the high (Figure 45A). The extent of SS 5 is confined to the center of the area, and is considered to be very thin (Figure 41; Figure 42). The isochron map illustrates the thickness variations in SS2 (Figure 45B). The thicknesses in SS 2 vary between the two seismic facies units. The thickness of SF 4 is considered as generally uniform, apart from a relatively small area in the northern part of the area (Figure 45B). SF 5 are considered as showing thicknesses within meter scale, and thus the uncertainty related to the mapping of SF 5, is considerable due to the seismic resolutions in the area (Table 6).

The areas consisting of medium to high amplitudes in the RMS Amplitude map are interpreted as areas composed of SF 4 (Figure 46A). SF 5 is identified in RMS amplitude map, as areas with low to zero amplitudes (Figure 46A). The RMS Amplitude map is showing a multiple amplitude anomalies with high amplitudes, along the margin of the paleo-high (Figure 46A). The variance map identifies the lateral continuity of the SS 2 (Figure 46B). Figure 46B shows low variance in the section where SF 4 is located, this is exemplified by the areas marked with blue arrow in Figure 46B. The areas consisting of high variance are confined to the locations of SF 5. This is exemplified by the green arrow indicating the high variance zones in Figure 46B.

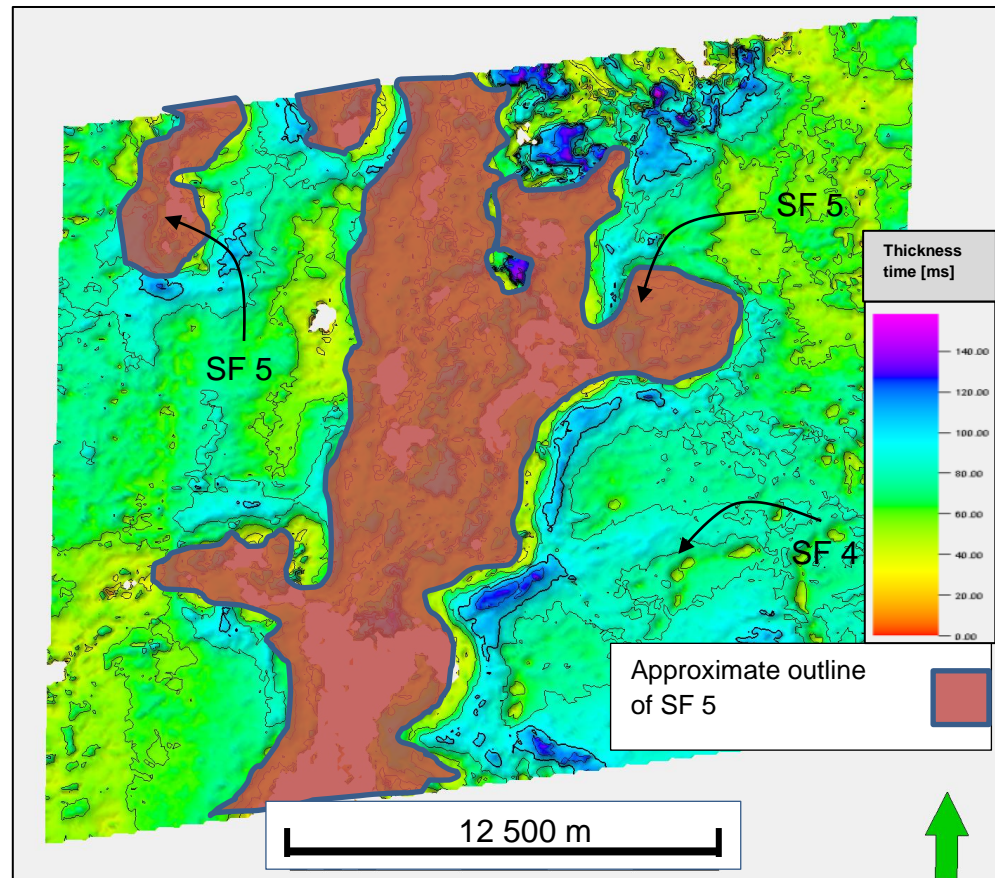
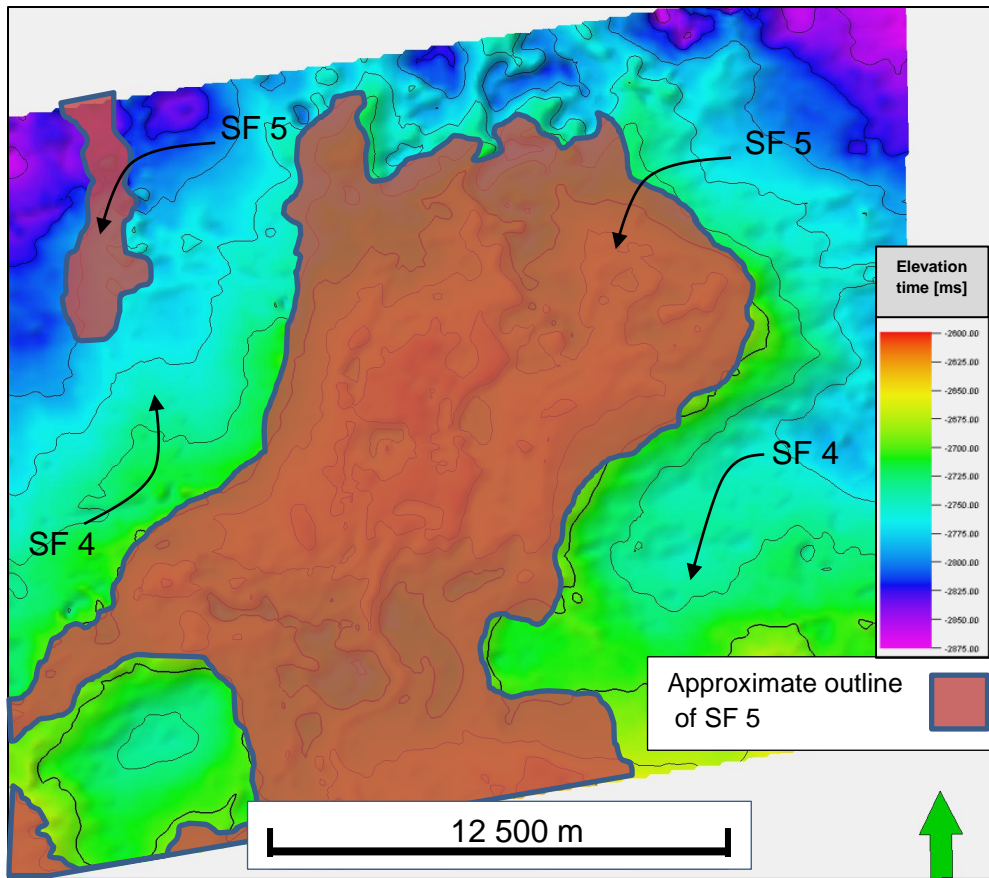


Figure 45 - A) Time surface map of top SS 2; B) Time thickness map of SS 2.

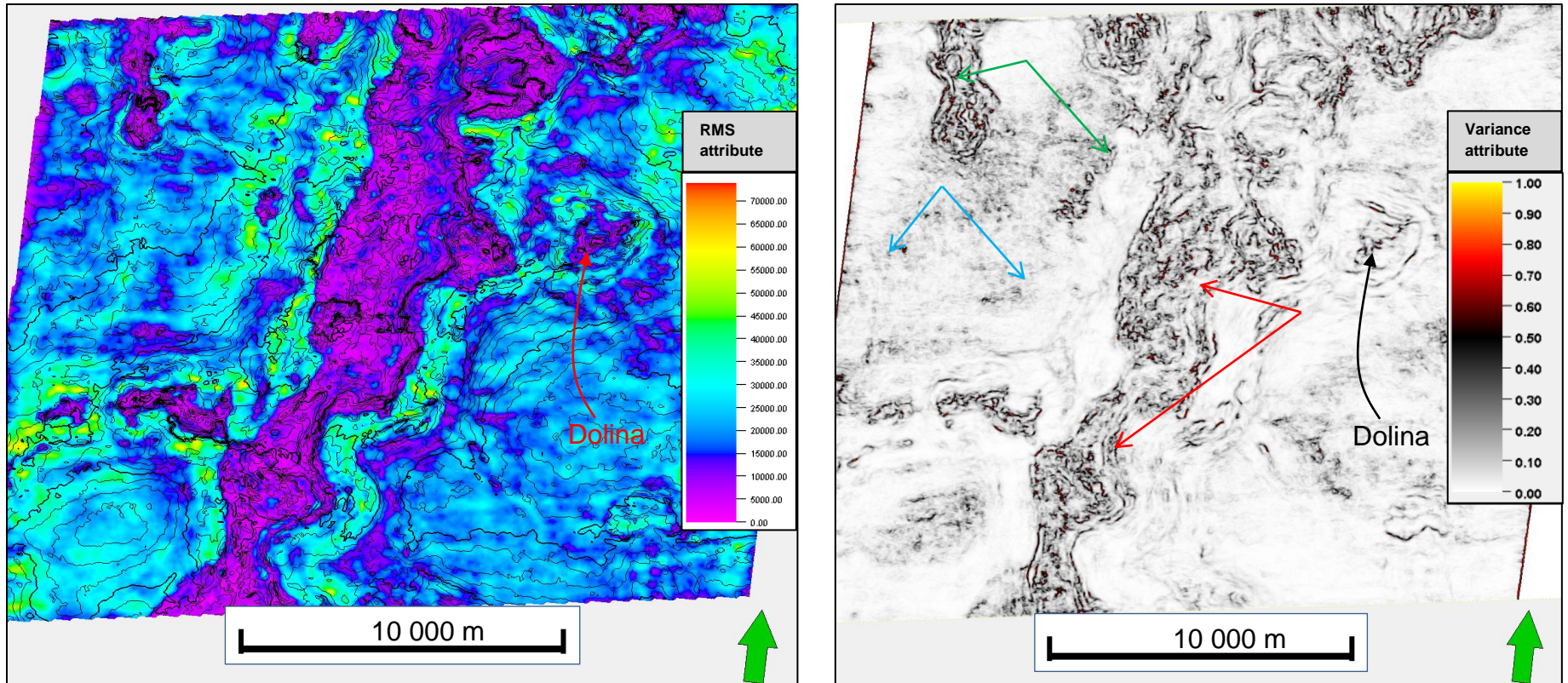


Figure 46 - Seismic attribute maps of SS 2. A) RMS Amplitude map of SS 2. The red arrow indicate interpretation of doline structure; B) Variance map from time-slice $z = -2692$ ms. presenting near top SS 2 (The red and green arrows indicate areas of high variance, the blue arrow indicate low variance zones, and the black arrow show the interpretation of doline structure).

Interpretation Seismic Sequence 2

The sedimentary succession within SS 2 is interpreted as a heterolithic facies consisting of a layered mixture of evaporites, carbonates and dolomites. SF 4 is interpreted as a layered evaporite sequence, deposited during sea-level lowstand. The lowstand sea-level resulted in the precipitation of hypersaline seawater confined to the deeper situated flanks of the area. The internal reflectors within the SS 2 are interpreted as remnant fragments of carbonate, siliciclastic and evaporitic sediments. The remobilization of the evaporite sequence is creating the chaotic internal reflectivity pattern due to the broken and chaotically organized sedimentary fragments (Figure 40; Figure 41). The generally uniform thickness of the sequence is interpreted as constant precipitation of evaporites throughout the entire area, during lowstand sea-level. This resulted in uniformly thick deposition SF 4, in the deeper seated areas.

SF 5 is interpreted as a carbonate build-up succession confined along the topographic high. The SF 5 is interpreted as subjected to subaerial exposure during lowstand sea-level, resulting in development of karst-induced features such as doline structures (Figure 46).

The RMS Amplitude map is interpreted as giving a general outline of the extent of the SS 3 evaporite sequence and the subaerially exposed carbonate surface (Figure 46A). The strong amplitude anomalies on the margin are interpreted as areas where the evaporite sequence is pinch-out along the margin of carbonate succession on the paleo-high (Figure 46A). The high connectivity in SS 2 is showing the main outline of the layered evaporite sequence (Figure 46B). The areas with relatively low variance along the paleo-high structure coincide with the areas that had zero amplitude anomalies in the RMS Amplitude map (red arrow in Figure 46B). This observation supports the interpretation that the RMS and variance maps present the locations where the layered evaporite sequence pitches out toward the subaerially exposed carbonate unit on the structural high (Figure 46B).

5.2.1.4 Seismic Sequence 3

Description Seismic Sequence 3

The top of the SS 3 is defined as an increase in acoustic impedance and a red peak in the seismic section (Table 7). The lateral continuity of the SS 3 is identified throughout the entire seismic area.

The SS 3 is characterized into two different units defined on differences in the seismic facies characteristics. The first unit (SF 6) is identified as by parallel and semi-continuous reflectors, with a uniformly thick geometry of the unit. The second facies (SF 5) is identified by mound shaped geometry located in the center of the area (Figure 41; Figure 47A). SF 5 is defined by contoured-shaped and chaotic reflections with discontinuous continuity.

The time surface map of top SS 3 is illustrate the seismic geomorphology of the sequence (Figure 47A). The map is show a large structural complex, which is directed vertically above the paleo-high, described in the Pre-SS surface (Figure 47A; Figure 43). Figure 47A does not express any structural complexes beyond the antecedent high. The sequence is considered to show a gentle topographic expression in the lower elevated settings (Figure 47A).

The isochron map is visualizing the thickness variations in SS 3 (Figure 47B). The map present the outline of the two different seismic facies units identified in SS 3 (Figure 47B). The thick parts show the mound shaped SF 5 succession, and the thinner parts present the extent of SF 6 (Figure 47B). The RMS Amplitude map illustrates the two different facies units as comprising of differences in amplitude (Figure 48A). The strong amplitude locations located in the western and eastern flanks of the area, associated with the lateral extent of SF 6. Secondly, the lower amplitude areas, which are confined to the center the area, similar to the locations of SF 5 (Figure 48A). The variance map illustrate the outline of the mound-shaped structure as an reticulated feature, which consist of low variance, opposed to the adjacent surroundings shown as high variance (Figure 48B).

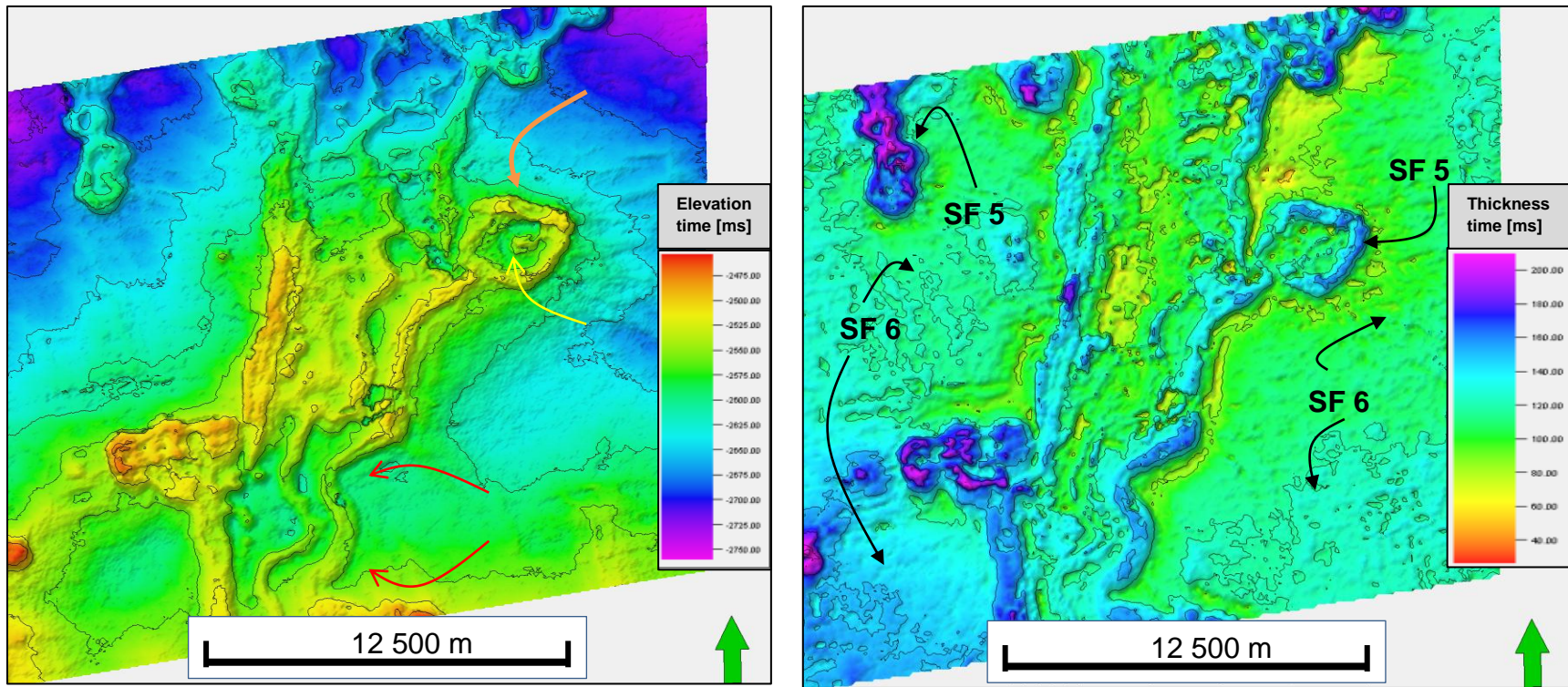


Figure 47 - A) Time surface map of top SS 3 (Yellow arrow = Doughnut structure, Red arrow = Horseshoe structures, Orange = Karst-induced doline structure); B) Time thickness map of SS 3.

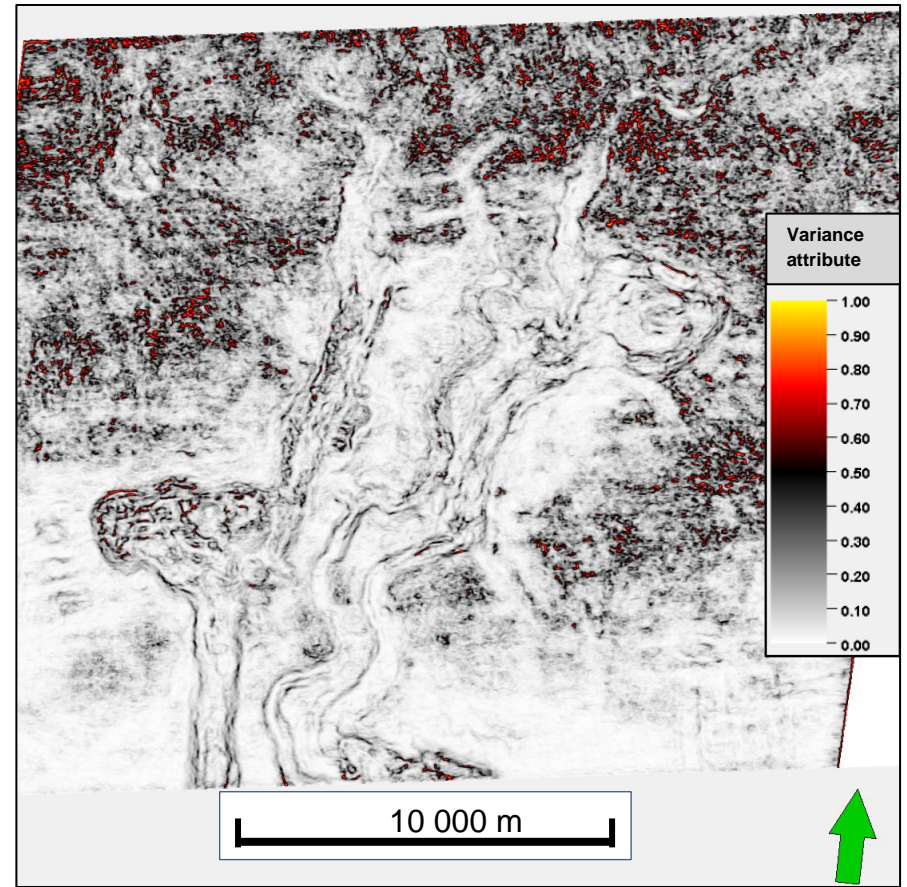
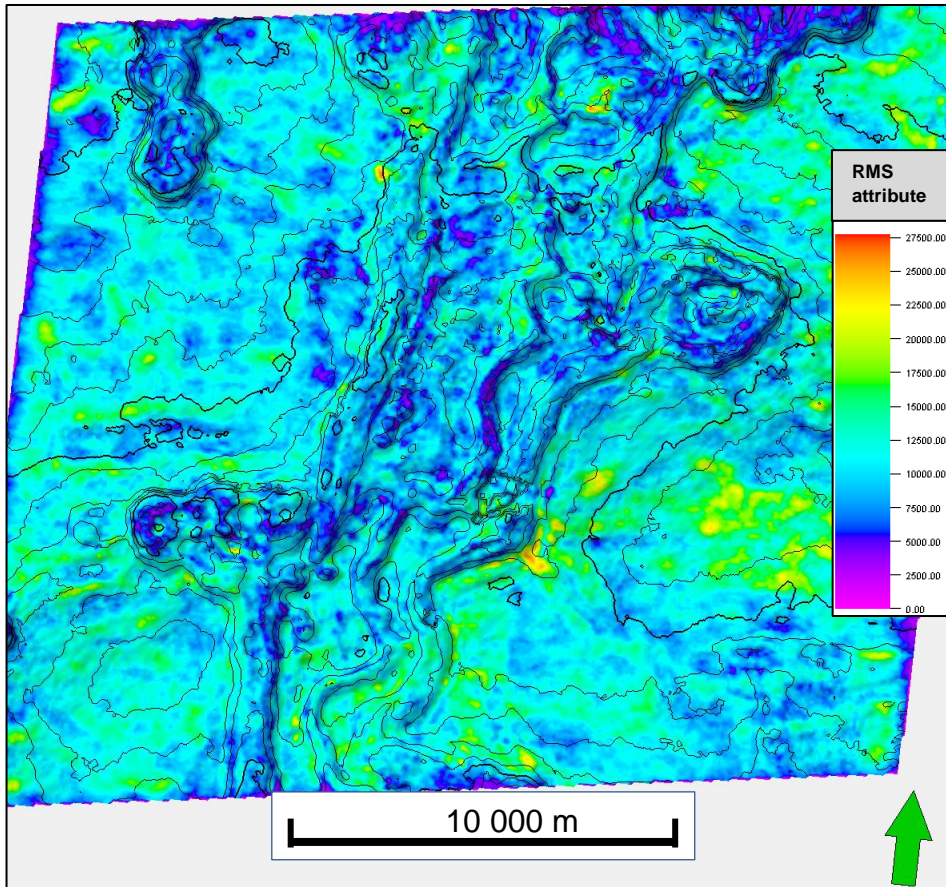


Figure 48 - Seismic attribute maps of SS 3. A) RMS Amplitude map of SS 3; B) Variance map of near top SS 3 taken from time-slice $z = -2544$ ms. presenting near top SS 3.

Interpretation Seismic Sequence 3

SF 5 is interpreted as consisting of heterozoan carbonate build-ups with a biota that consist of bryozoan and crinoids (Appendix 1.3). Internally, the build-up complex consists of facies of protozoan- and heterozoan biota from both Gipsdalen- and Bjarmeland Groups. The growth of the carbonate succession occurred on a paleo-high structure developed by the faulting event that occurred in the Pre-SS period (Figure 41). The carbonate build-up succession has been subaerially exposed multiple occasions during the deposition, due to the glacio-eustatic sea-level fluctuations. The repeated periods of sea-level lowstand has resulted in karst-induced structures. The solution structures formed by karstification processes are interpreted as influencing the growth-form of the carbonates, during transgressed sea-level. Hence, the carbonate build-ups grew on antecedent karstic topography (Figure 47A). The doline structure marked with an orange arrow in Figure 47A is interpreted as supporting evidence, for antecedent karstic influence of the carbonate growth. The succession is developed on antecedent topography of protozoan build-ups consisting of a biota of Palaeoaplysina phylloid-algae build-ups. The well data from well 7229/11-1 support the facies interpretation of the carbonate build-up succession. The well penetrates the respective succession within the area and thus, confirms the carbonate facies.

SF 6 is interpreted as facies consisting of muddy-limestones deposited in a platform interior environment. The karst-induced structures develop a morphology identified on the surface map as doughnut and horseshoe structures (Figure 47A; Chidsey et al., 1997). The horseshoe feature is marked as a red arrow; the doughnut feature is highlighted with a yellow arrow (Figure 47A).

5.2.1.5 Seismic Sequence 4

Description Seismic Sequence 4

The top of SS 4 is identified as an increase in acoustic impedance, displayed in the seismic section as a red peak (Table 7). SS 4 is identified as a reflection unit with uniform thickness. The top of the sequence is presented as an increase in acoustic impedance (Table 7). The sequence is considered having a reflection geometry that is uniformly thick throughout the area.

One distinct seismic facies (SF 7) has been identified within the sequence. Internally, the SS 4 is defined by parallel and continuous reflectors, with strong amplitudes and low frequencies (Figure 41). The uniform thick unit has a thickness of approximately 30 ms (Figure 41; Figure 42). The geometry of the unit is consistent with the undulating topography of the SS 4.

The surface map of the top SS 4 horizon is presents a surface map with similar structural elements as observed by SS 4 (Figure 49A). The top SS 4 horizon imprints the identical morphology as observed in of the top SS 3. The thickness map of the area presents evidence for uniform deposition of SS 4 throughout the seismic area due to the uniform thickness along the entire area (Figure 49B). The average thickness of the SS 4 unit is calculated to be an approximately 15-20 ms. thick succession (Figure 49B).

Interpretation Seismic Sequence 4

The sedimentary facies within SS 4 is interpreted as fine-grained siliciclastic sediments. The depositional environment is interpreted as pelagic. The facies interpretation is supported by the well data results of well 7229/11-1 (Appendix 1.3; Figure 41; Figure 42). The constant thickness shown in the isochron map indicates uniform deposition throughout the entire area (Figure 49B).

The surfaces map of top SS 4 show similar structural signatures as described in SS 3 (Figure 49A; Figure 47A). The surface map is interpreted as imprinting the morphology of the underlying stratigraphy caused by pelagic deposition of SS 4. SS 4 is interpreted as draping the undulating topography of SS 3 (Figure 49A). The interpretation of the depositional system is a deep marine environment (Appendix 1.1; Appendix 1.3). During the Late Permian, the Barents Sea region where located at a wet and cold climatic setting (Figure 6). The climatic setting resulting in massive erosion of the hinterland, which were deposited as fine-grained siliciclastic sediments due to pelagic and hemipelagic deposition (Stemmerik et al., 1999; Appendix 1.3). Figure 49B shows constant thickness of SS 4 throughout the area, interpreted as indications of outer marine deposition.

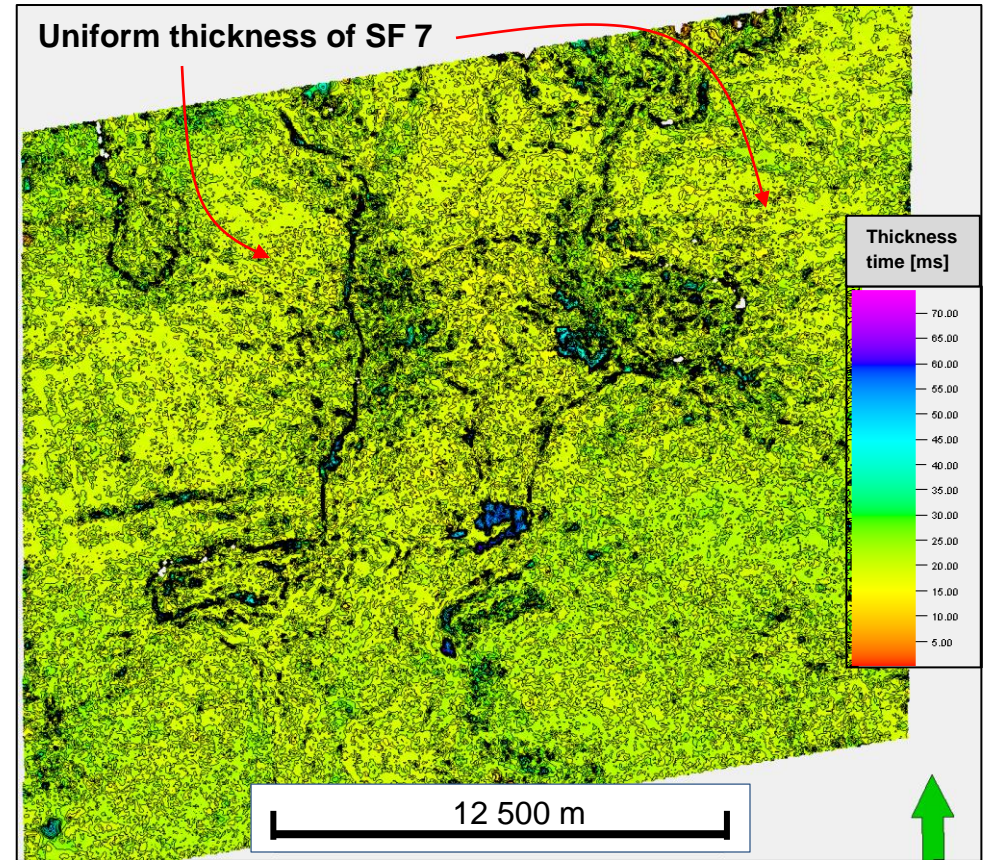
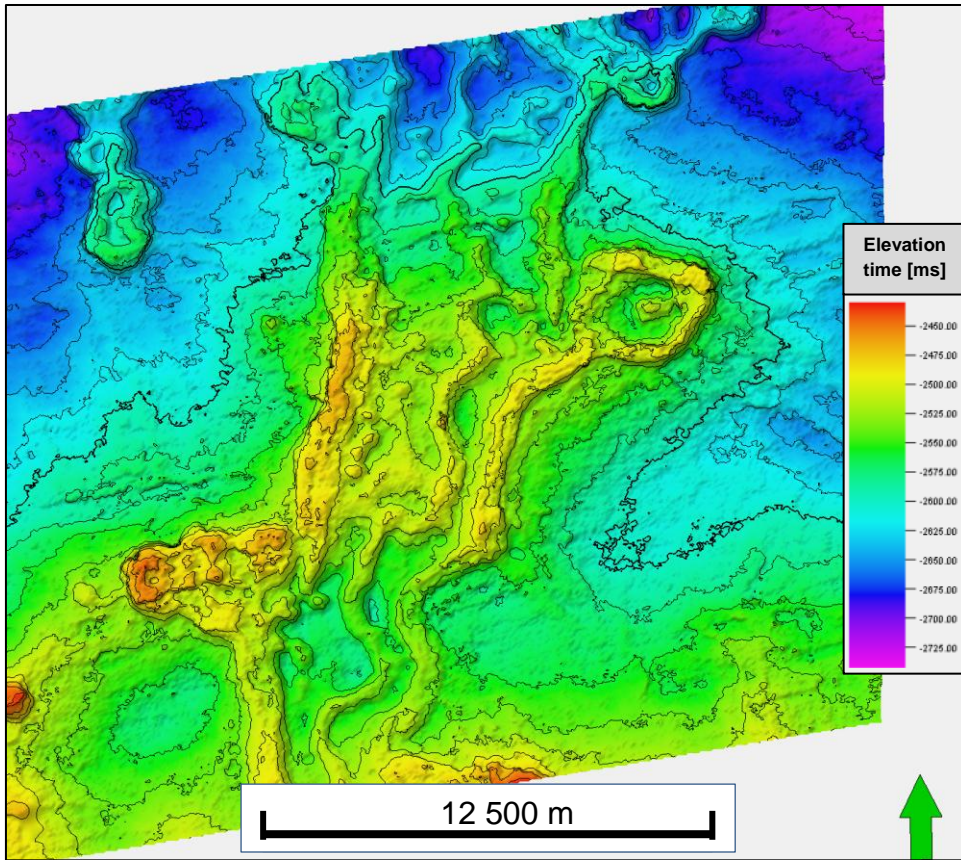


Figure 49 - A) Time surface map of top SS 4; B) Time thickness map of SS 4.

5.2.2 Seismic Area D (ST9802)

The Seismic Area D is situated on the southeastern section of the Finnmark Platform approximately 75 km north of the Norwegian mainland and 80 km south of the Nordkapp Basin (Figure 50). The seismic area is subjected to little tectonic influence, although some normal faulting have occurred overtime, e.g. a northeast dipping normal fault that crosscuts the Carboniferous to Late Jurassic succession (Figure 51). To illustrate the seismic geomorphology of the seismic sequences, to seismic lines has been used, and a 70 km long SW-NE oriented inline and a 27 km long NW-SE oriented x-line (Figure 51; Figure 52). To illustrate the sequences better on the inline, a zoomed inline of the northern section is used; the area where this line is taken from is marked on figure 51 and presented in figure 53.

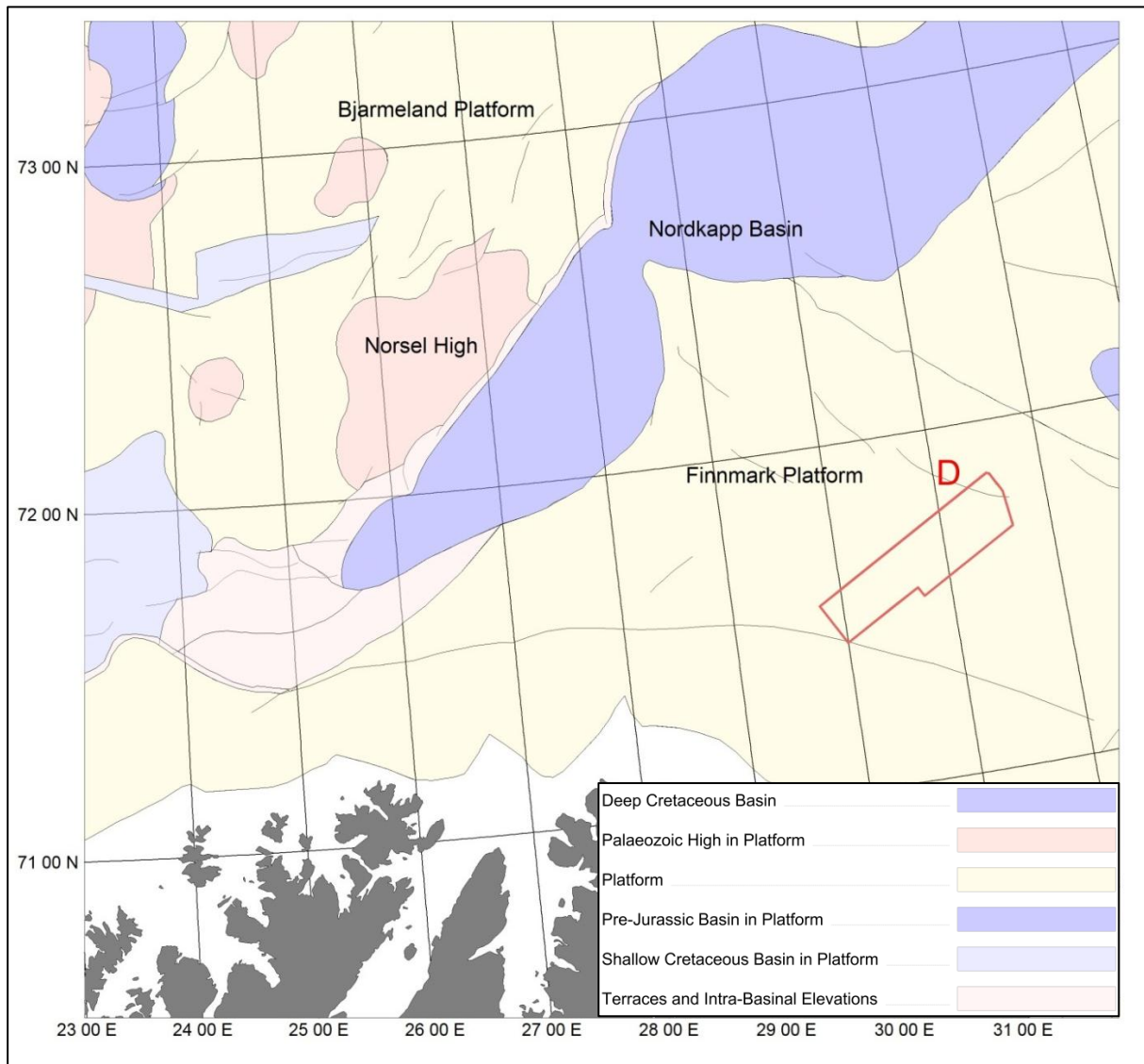


Figure 50 - Regional map of SC Norwegian Barents Sea highlighted with the outline of Seismic Area D on the Finnmark Platform.

5.2.2.1 Pre-Seismic Sequences

Description Pre-Seismic Sequences

The top of Pre-SS is identified as a decrease in acoustic impedance and therefore, results in a blue trough (Table 7). The reflections vary within the succession.

The Pre-SS are divided into two parts, lower and upper. The lower part (SF 1) is identified as chaotic and discontinuous reflectors with low amplitude and frequency. The facies extends throughout the entire seismic cube. SF 1 starting at a depth of 2500 – 3000 ms. in the NE part of the area, and thicken toward the SW, where the unit starts at approximately 2300 ms. (Figure 51).

The upper part (SF 2) consists of sub-parallel and semi-continuous reflections, with strong amplitudes and frequencies. The bounding relationship with the two parts, show that SF 2 drape the topography of SF 1. This is visible by of the strong reflectivity within SF 2 in the north, which has distinctively stronger amplitudes and frequencies, compared with the southern part of the area (Figure 51; Figure F2).

The area has been subjected to major and minor faulting events, the most prominent faulting relates to the large northward dipping normal fault. This fault crosscut the Upper Jurassic down to the Pre-SS, in northern part of the area (Figure 51). There are multiple minor northward dipping faults, which is confined to the upper part of the Pre-SS succession, in the northern part of the area (Figure 52; Figure 53). The surface map present two structural lineaments marked with dotted orange lines (Figure 54). The structural lineaments were developed during the early stages of SF 2. The lineaments are orientated in a NW-SE direction (Figure 54). The surface map identifying the northern part as consisting of reticulated and circular features (Figure 54).

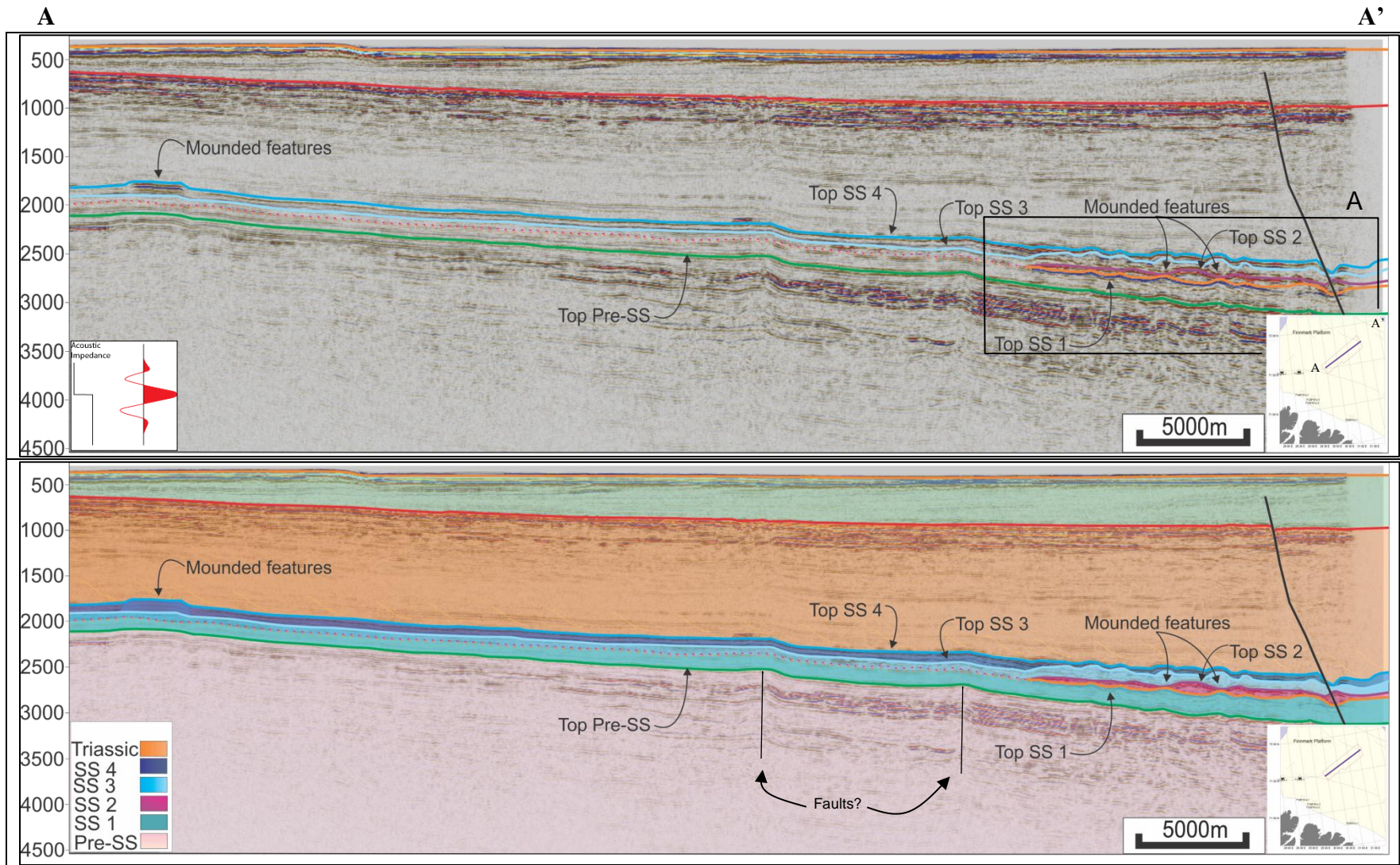


Figure 51 - Seismic sections of Area D on southeastern Finnmark Platform. A: Seismic Inline 1796, B: Geoseismic Inline 1796.

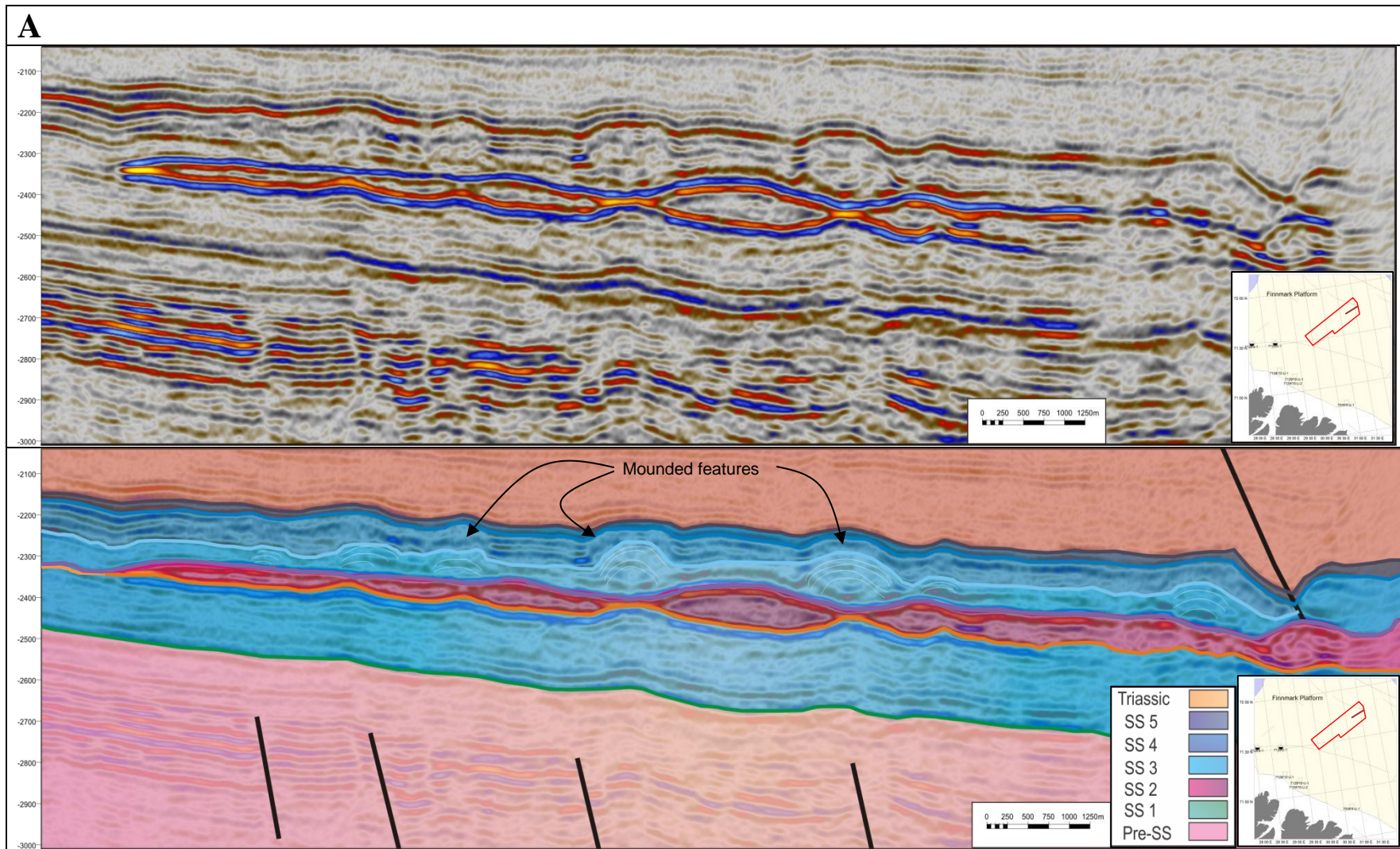


Figure 52 - Zoomed seismic section of Seismic Area D highlighting the carbonate build-up successions on the northeastern flank of the seismic area. A: Seismic Inline 1796, B: Geoseismic Inline 1796.

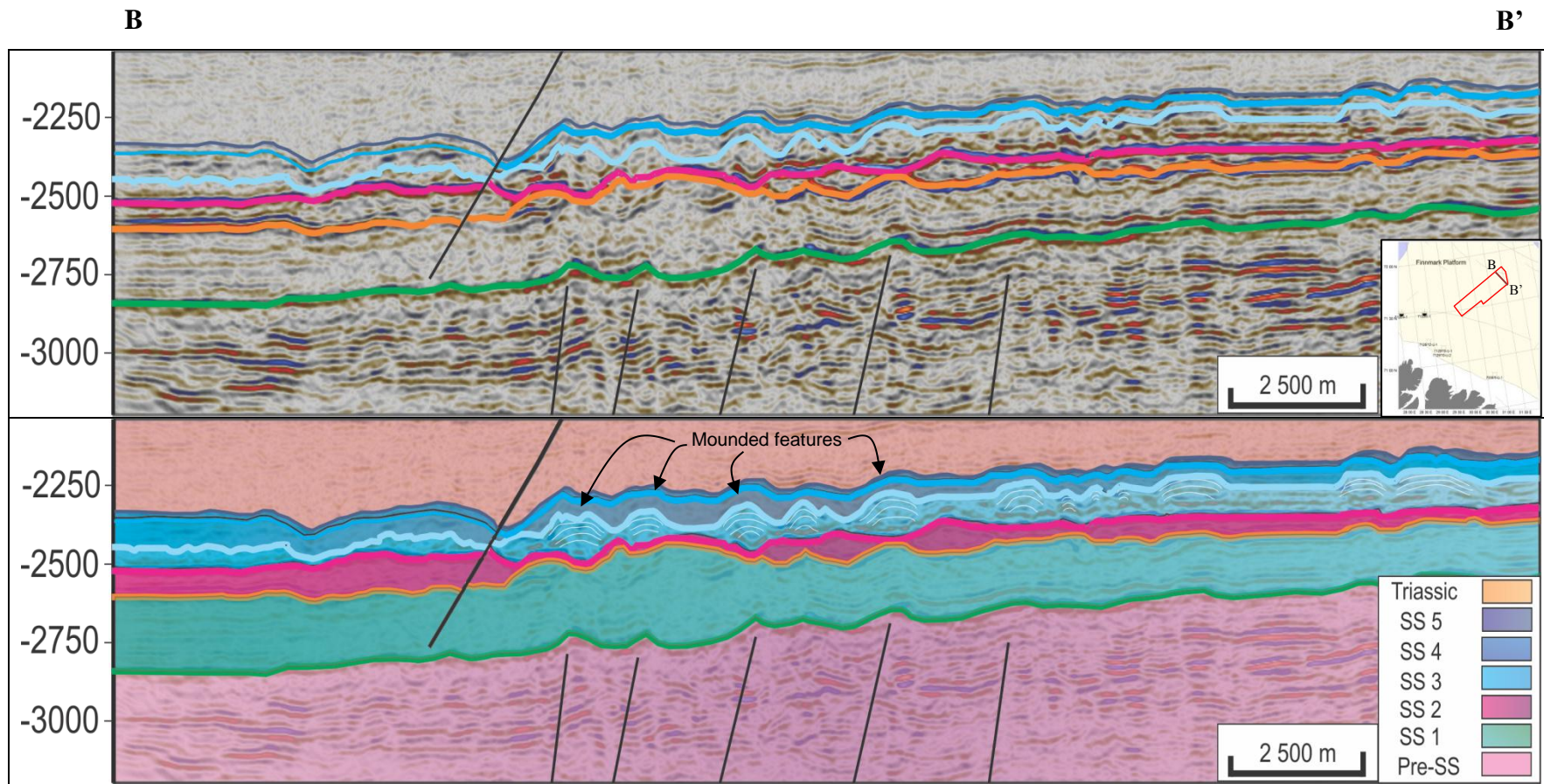


Figure 53 - Seismic section of Area D on southeastern Finnmark Platform. 16A: Seismic Xline 7151, 16B: Geoseismic section of xline 7151.

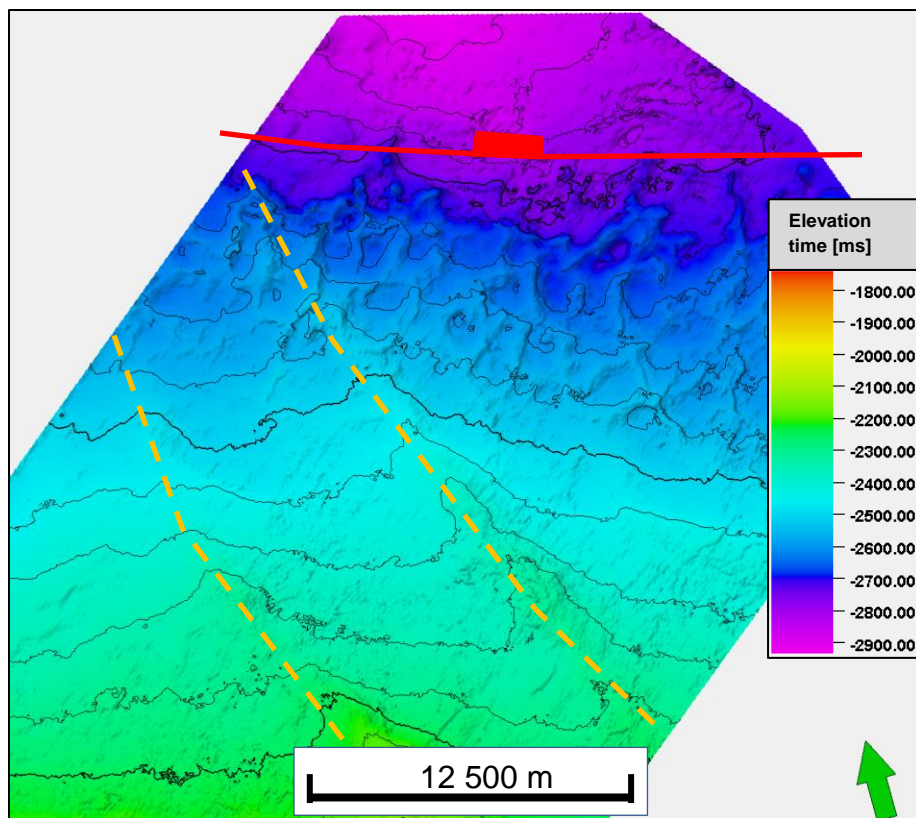


Figure 54 - Time surface map of top Pre-SS. The red line in the north of the area represents a normal fault oriented NNW-SSE, this fault is crosscuts the Carboniferous-Upper Jurassic strata in the area. The two orange dotted lines represent the orientation of the structural lineaments striking NW-SE.

Interpretation Pre-Seismic Sequences

Pre-SS is interpreted as consisting of two different lithological successions. The lower part is interpreted as the basement, and consists of pre-Devonian metamorphic rocks similar to the basement succession identified in well data, e.g. 7226/11-1 and 7128/4-1 (Appendix 1.2; Appendix 1.4).

The upper part is interpreted as the Billefjorden Gp. that is a dominated fluvial facies. The seismic reflection geometry of this respective unit is considered very thin in the SE and thickens significantly in the NE direction (Figure 51). The northern part of the area is interpreted as subjected to higher accommodation space during deposition of the Billefjorden Gp., opposed to the areas towards the center and south (Figure 51). The fluvial dominated succession is interpreted as a northward prograding sequence due to the higher abundance of heterogeneous reflections with strong amplitudes in the northern part of the area (Figure 51; Figure 52).

The area is interpreted as subjected to higher topographic relief, and therefore, results deposition of heterolithic fluvial facies. The surface map shows numbers of polygonal structures located in the north of the area (Figure 54). These features are interpreted as imprints of the overlying stratigraphy due to the pull-up effects caused by the higher velocities in the overburden sediments.

5.2.2.2 Seismic Sequence 1

Description Seismic Sequence 1

The top of SS 1 is identified as an increase in acoustic impedance (Table 7). The top and base of SS 1 is laterally extensive, and identified throughout the entire area. SS 1 is defined to comprise of one seismic facies unit (SF 3). Internally, SS 1 is characterized as a uniform and homogenous succession consisting of parallel to sub-parallel reflectors, with semi-continuous to continuous continuity (Figure 51; Figure 52; Figure 53). The amplitude strength and the frequency content are identified to be low.

The surface of top SS 1 horizon shows the present day geomorphology the sequence (Figure 55A). The surface map illustrates the resemblance with the structural lineaments, which is observed and described in the Pre-SS surface map (Figure 55A; Figure 54). The structural lineaments are identified as oriented in a NW-SE trend. The different lineaments are observed in the southern and northern part of the area (Figure 55A). The seismic geomorphology of the SS 1 succession varies dependent on the different parts of the area, from south towards the north (Figure 55A). The southern part consists of a structural high. The central section is dominated uniform deposition with low relief, followed by the northern segment with structural components consisting of reticulated features encircling cells with lower elevation (Figure 55A). The isochron map shows the thickness variations within SS 1. The thickness map presents a gentle and gradual thickening of the sequence, from southwest towards the northeast, in the direction of the Nordkapp Basin (Figure 55B).

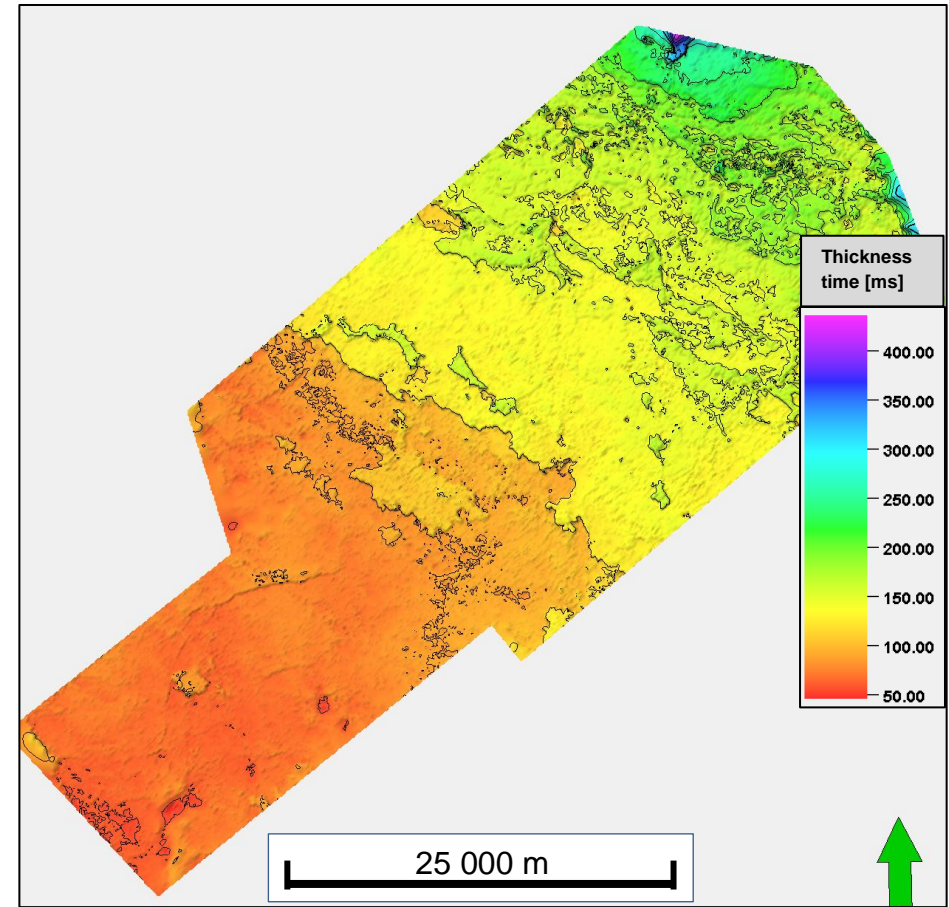
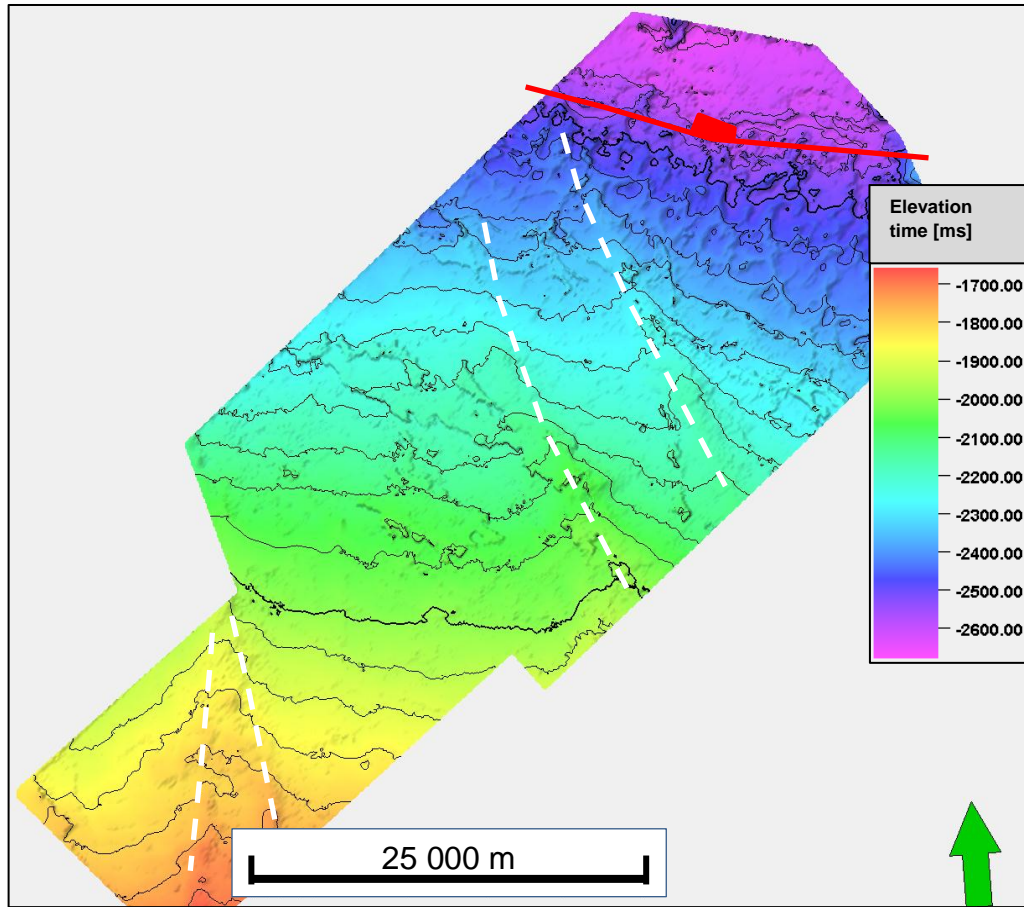


Figure 55 - A) Time surface map of top SS 1. The white dashed lines present the structural lineaments. Red line presents the direction of the major normal fault; B) Time thickness map of SS 1. The isochron map shows a gradual thickening of the sequence towards northeast.

Interpretation Seismic Sequence 1

The sequence is interpreted as a heterolithic facies that consist of carbonate, dolomite and siliciclastic sediments. The dominant facies within the sequence is interpreted to be carbonate. This is also supported by the two closest wells to the area i.e. 7128/4-1 and 7128/6-1 (Appendix 1.4; Appendix 1.5). These wells encounter mostly carbonate units with some siliciclastic shale rich units being the flooding surfaces. The depositional setting of this environment is interpreted to be a shallow marine environment with deposits of fine-grained limestone deposits.

The values used for calculating the slope angle are approximate values taken from the time thickness map. Where *depth* is the depth of the deepest section in the north of the area, *length* is the approximate length from the thinnest to the thickest section of the area (Figure 56). The conceptual calculation is conducted to illustrate the slope angle affecting the platform morphology of the Finnmark Platform:

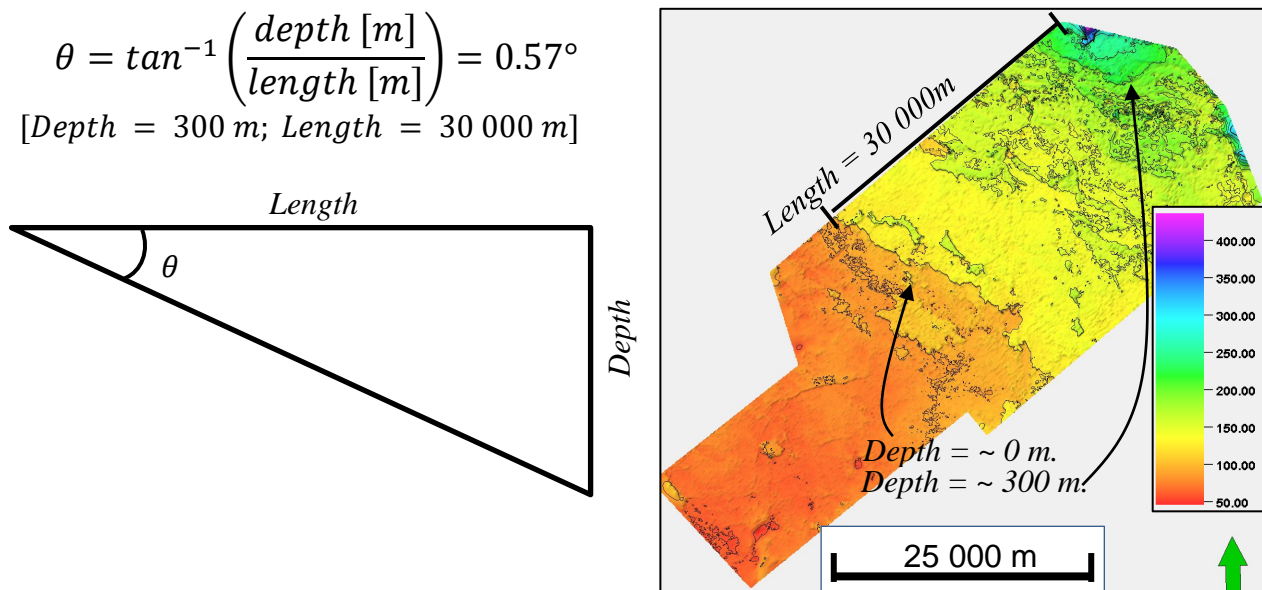


Figure 56 – Conceptual calculation of the slope angle of the Finnmark Platform. The isochron map of SS 1 annotated with length and depths.

The values applied for the calculation of the slope angle are approximate values and has only been applied to illustrate the gentle dip of the seismic area towards the Nordkapp Basin. The calculation is therefore illustrative and variations in depth further towards the basin might significantly affect the slope angle. The based on the illustrative slope angle, the platform morphology of the area is interpreted as being a part of a large epeiric platform ($\theta < 1^\circ$), with the Nordkapp Basin as the major basin for the Finnmark Platform. The interpretation of an epeiric platform is supported by the widespread and lateral extent of the carbonate succession, which is identified from Sverdrup Land the west and Timan-Pechora Basin to the east (Wright & Bruchette 1998; Beuchamp, 1994; Stemmerk et al., 1999).

5.2.2.3 Seismic Sequence 2

Description Seismic Sequence 2

The SS 2 is identified by the top reflector showing strong decrease in acoustic impedance giving a blue trough in the seismic (Table 7). The sequence is sub-divided into two different seismic facies units.

The first seismic facies (SF 4) is confined to the northern part of the area. The facies is characterized by reflections that have a contoured shape, with continuous reflectors in the top and base. The top SS 2 is defined as amplitudes and frequencies with high magnitude. SF 4 is characterized by undulating geometry with thick and thin units (Figure 52; Figure 53). Internally, the reflectivity pattern within SF 4 is considered as discontinuous and chaotic reflectivity, within the thick structures (Figure 53). The second seismic facies (SF 3) is considered as distributed in the central and southern part the entire area. SF 3 is considered to be very thin and, in mostly, below the seismic resolution (Table 6). The reflection character of SS 3 is defined as parallel and semi-continuous reflections (Figure 52).

The surface map is generated of the first seismic facies (SF 4) within the SS 2. The map illustrates the geomorphology of the top of sequence (Figure 57A). The seismic geomorphology of SF 4 is identified in the seismic sections as thin and thick units (Figure 52). The morphology of the surface show a number of cell-shaped features, encircled by attached ridge shaped features, with higher elevation (Figure 57A). The isochron map of SF 4 presents a notable arrangement of structural highs and lows (Figure 57B). The highs are associated with the thick units identified in the seismic section and contrarily, the structural lows are associated with the thin sections (Figure 57B; Figure 52).

The RMS Amplitude map displays areas subjected to high seismic amplitudes confined within the similar areas as the thin units observed in the isochron map (Figure 58A; Figure 57B). The amplitude anomalies with high amplitudes are associated with the reticulated ridges that encircle the circular features (Figure 58A). The RGB color blend map presents the circular shaped structures as features with frequency content of approximately 20 Hz, displayed as green colored circles (Figure 58B). The most prominent reticulated shapes that surround the circular cells have a frequency content of approximately 15 Hz, which is colored as yellow. The areas that are defined by higher frequencies, colored in purple, are areas not affected by the development of thick and thin structures (Figure 58B).

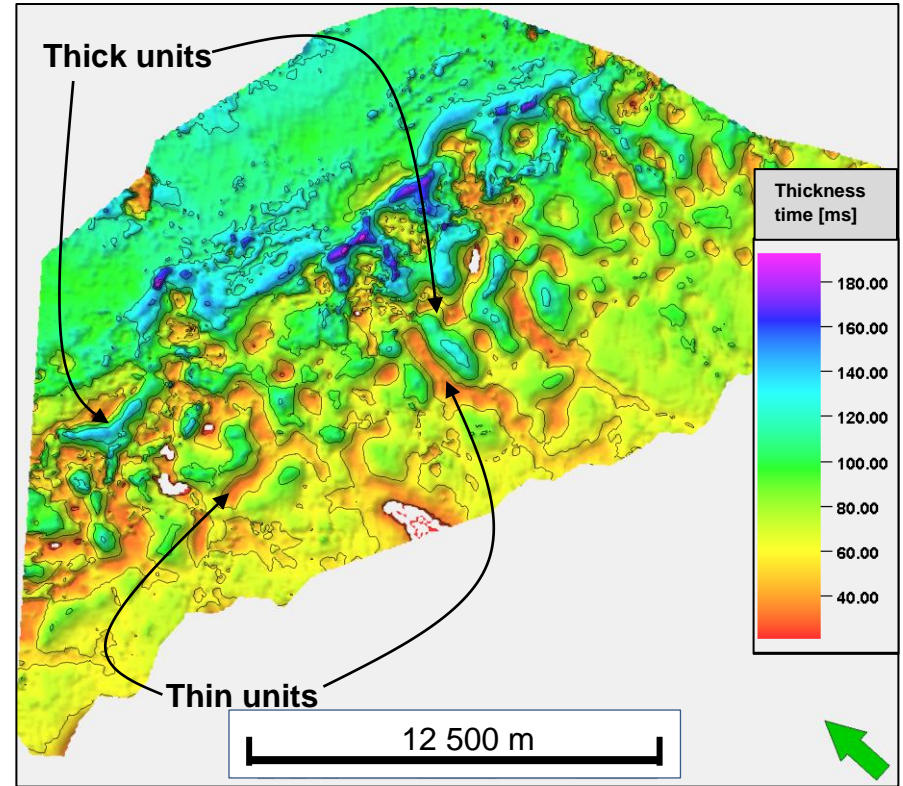
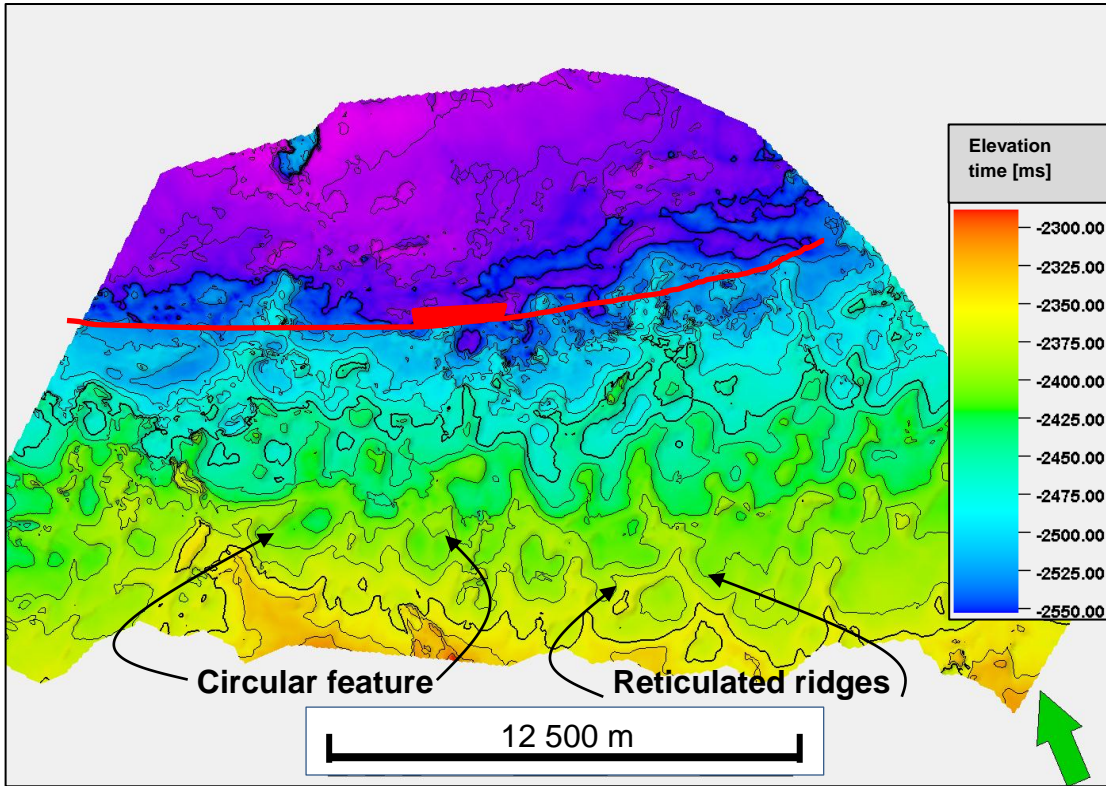


Figure 57 - A) Time surface map of top SS 2; B) Time thickness map of SS 2.

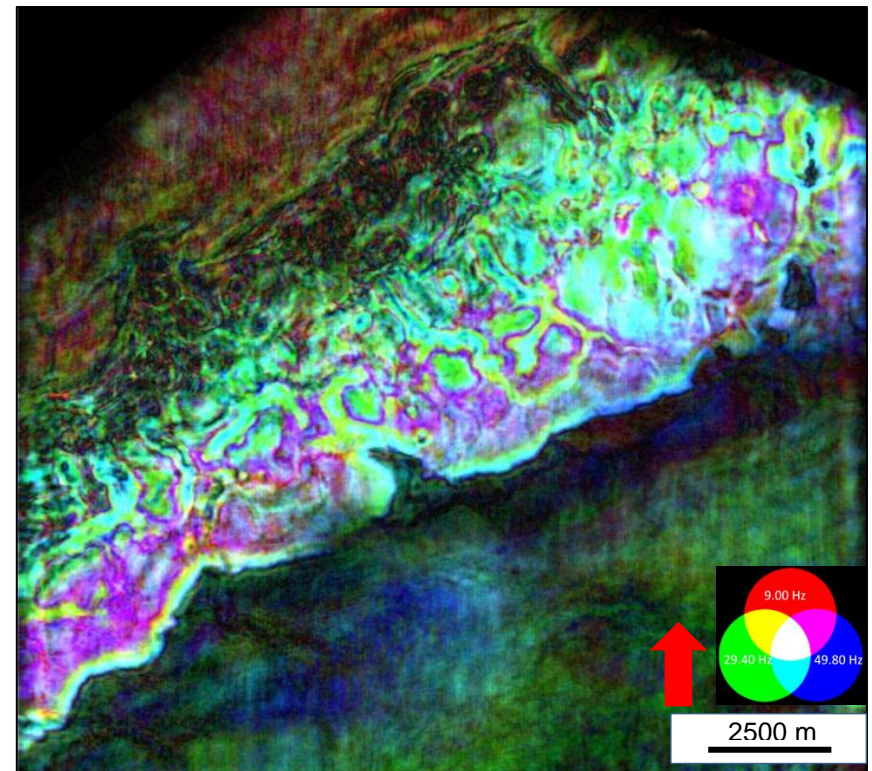
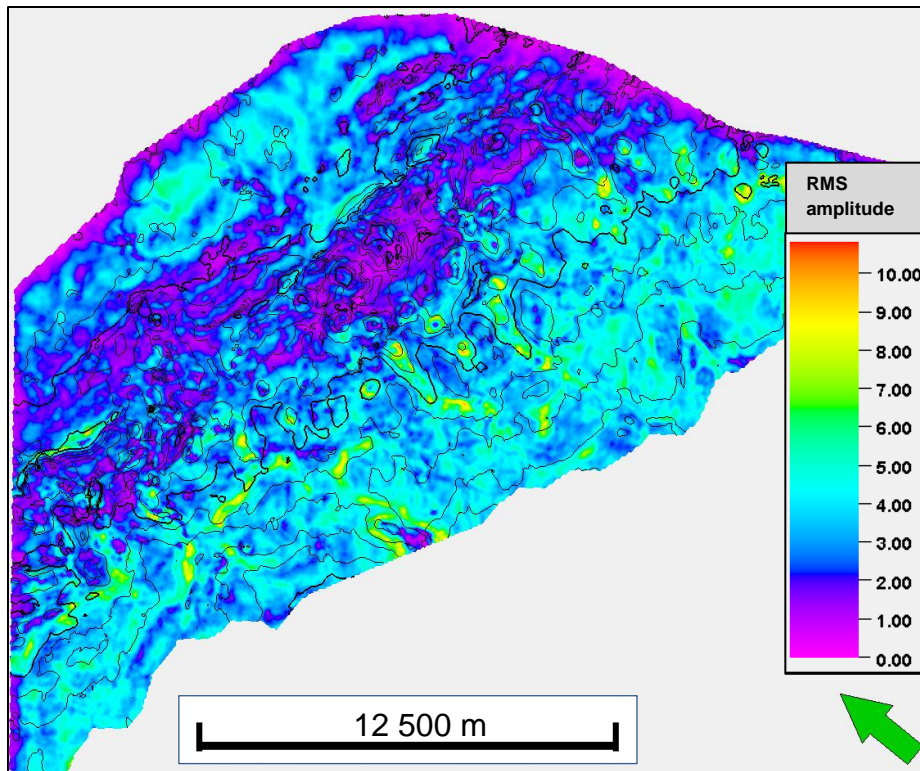


Figure 58 - Seismic attribute maps of SS 2. A) RMS Amplitude map of SS 2; B) RGB Color blend map of near top SS 2 taken from time-slice $z = -2256$ ms. equivalent to near top SS 2. (Red color = 9.00 Hz, Green color = 29.40 Hz, Blue color = 49.80 Hz).

Interpretation Seismic Sequence 2

SF 4 located to the north of the area is interpreted as layered evaporite sequence deposited during sea-level lowstand in Pennsylvanian to Early Permian. The unit is interpreted as layers of autochthonous evaporites, which are affected by later remobilization.

The contoured shaped structures are interpreted as created due to salt withdrawal, from the areas where the evaporite sequence currently is thin. This effectively, results in lateral expulsion of evaporites, creating salt pillow structures. The internal reflectivity within SF 4 is interpreted as lithology fragments, broken-up the evaporite remobilization. SF 3 is interpreted as a depositional environment of inner platform setting. The facies within this sequence is interpreted as fine-grained muddy-limestone.

The relationship with thin- and thick evaporite sequences, is interpreted as caused by lateral variability in effective vertical stress, on the mobile autochthonous evaporite layer. The lateral differences in vertical stress are created by lateral differences in density of the overlying sediments. This means that the areas in the SS 2 where the thin, salt weld-shaped structures are located, has been subjected to a vertical loading effect of the overlying strata that are higher than its lateral loading (Maione, 2001). As a consequence, the present-day morphology of SS 2 is caused by the remobilization of the evaporites. The lateral expulsion of mobile evaporites creates the relationship with thick and thin structures (Figure 52; Ge et al., 1997).

The differences in amplitude variations between the thickening and thinning is interpreted as the higher amplitude anomalies is showing areas subjected to major evacuation of evaporites and creating salt weld structures. The lower RMS amplitudes confined within the cell-shaped structures are interpreted as locations with thicker units of evaporites.

5.2.2.4 Seismic Sequence 3

Description Seismic Sequence 3

The top SS 4 is identified by an increase in acoustic impedance and effectively a seismic signal responding in a red peak (Table 7). SS 4 is defined by two different seismic facies units.

The first facies (SF 5) is identified by a mound shaped feature with chaotic and discontinuous reflection configuration. Within the first unit, the amplitude and frequency content is considered to be low. The average thicknesses of the mounded features are identified to be approximately 150 ms thick (Figure 52). The second facies (SF 6) is located laterally adjacent to the mound shaped features; this sequence has a reflection geometry consisting of parallel and semi-continuous reflectors. The magnitude of the amplitude is low to medium, and low frequencies (Figure 52). The bounding relationship of the second sequence is identified as present in the areas where the mounded shapes are absent. The second facies is laterally extensive throughout the entire seismic area, opposed to the first seismic facies which is locally confined to the NE area, at similar extent as observed by the presence of the underlying of SF 4 that was observed in SS 2 (Figure 51).

The surface map created of the horizon of top SS 4 horizon present the geomorphology of the SS 4. Figure 58A visualize the morphology of the SS 4, which comprises of connected features that surround circular and sub-circular features with lower elevation. The time thickness map presents the thickness variations within the SS 3 (Figure 59B). The isochron map presents three different thickness areas. The first is the reticulated polygonal features; the second is the cell shaped structures encircled by the reticulated structures, and finally the northern area that has a very low thickness (Figure 59B). The isochron map presents reticulated and polygonal structural elements with an average thickness of 80 ms. the thicknesses of the sub-circular depressed features are approximately 50 ms. thick. The northern sector has a uniform thickness of approximately 30 ms. (Figure 59B).

The variance map enlightens the morphology of the sequence. The central part of the map shows the reticulated shaped features with high variance, which encircles the cell-shaped features that has low variance. The second seismic facies is displayed on the variance map as the areas toward the south that is represented by constant low variance (Figure 60A). The RGB color blended map distinguishes the similar morphology within the SS 3 as observed in the variance map. The reticulated shaped features are presented in red and yellow colors, and the cell-shaped features are shown in purple color (Figure 59B). The second seismic facies are identified toward the south as a dark-blue and green color (Figure 60B).

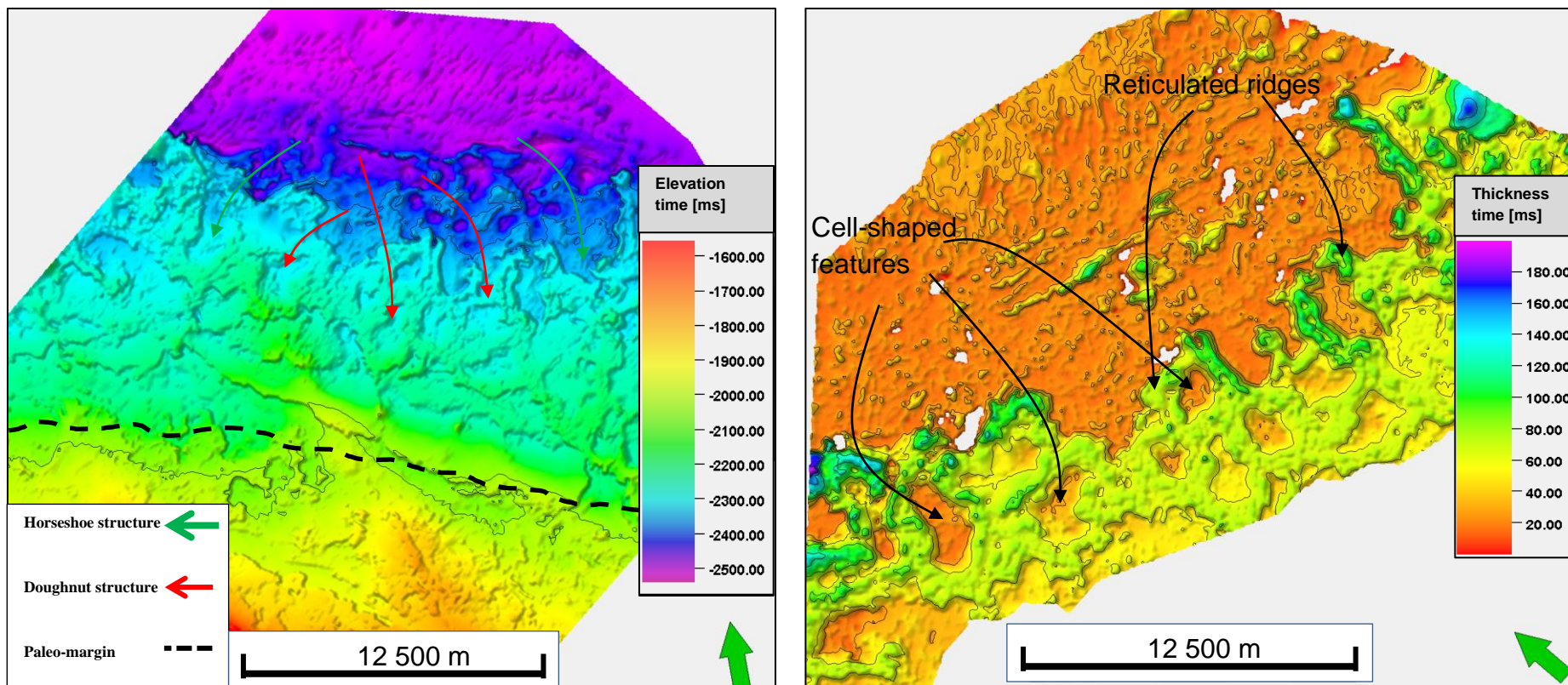


Figure 59 - A) Time surface map of top SS 3; B) Time thickness map of SS 3.

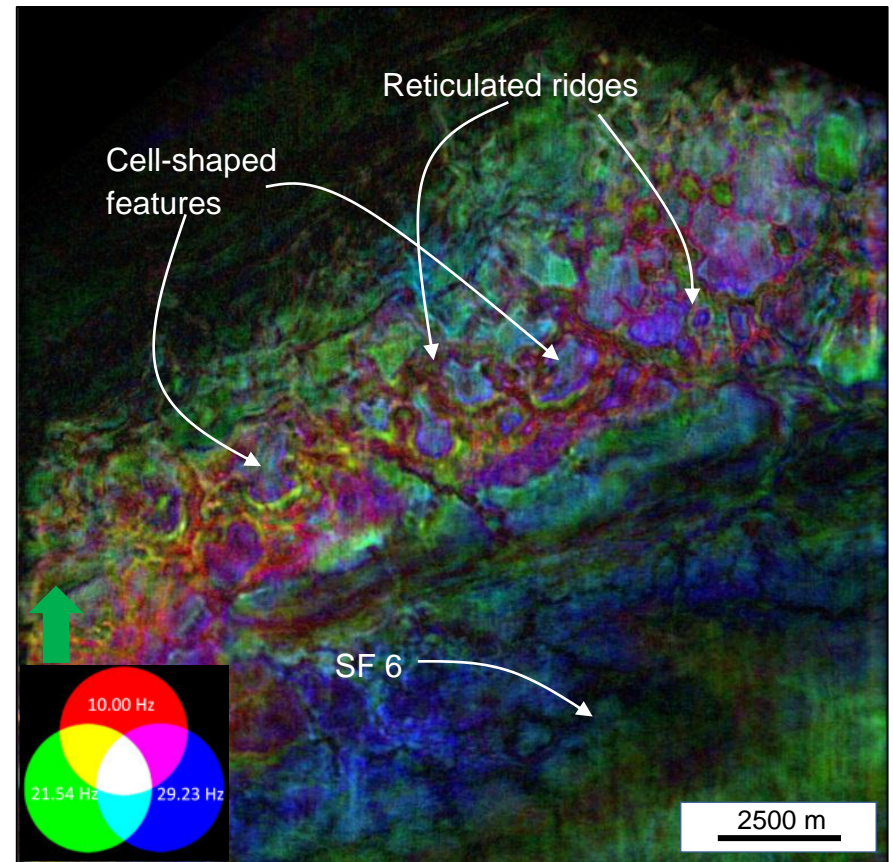
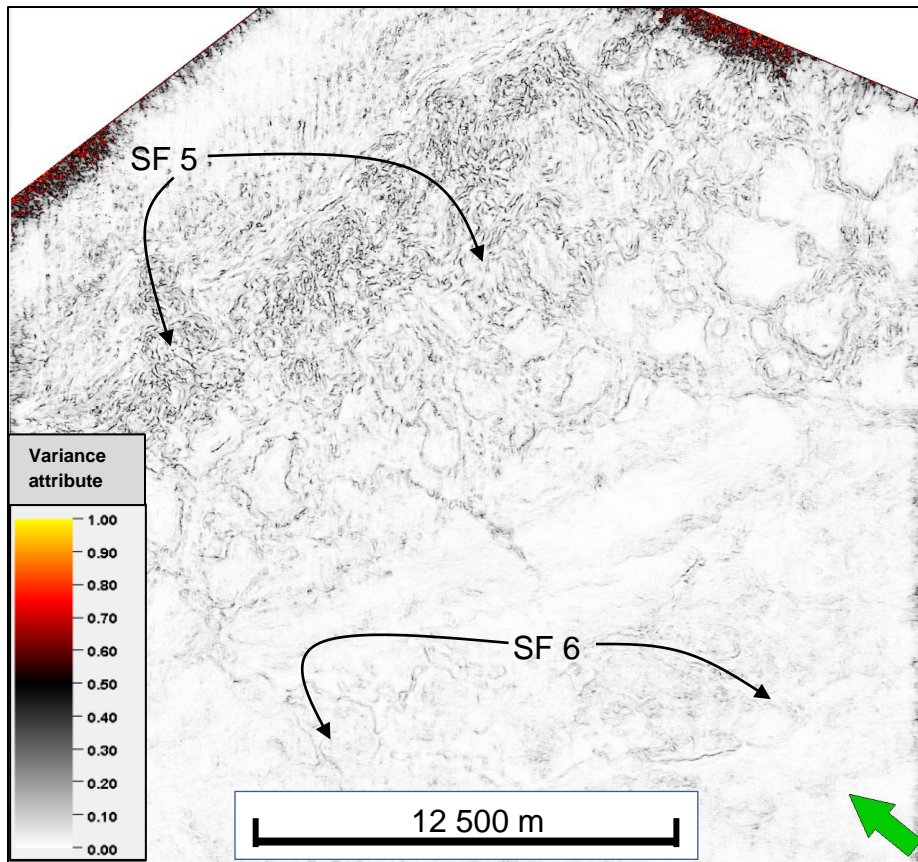


Figure 60 - Seismic attribute maps of SS 3. A) Variance map of near top SS 3 taken from time-slice $z = -2044$ ms.; B) RGB Colorblend map of taken from near top SS 3 from time-slice $z = -2044$ ms. (red color = 10.00 Hz, Green color = 21.54 Hz, Blue color = 29.23 Hz).

Interpretation Seismic Sequence 3

The SS 3 is interpreted to comprising of two different types of sedimentary facies. SF 5 is described as mound shaped features, and has been interpreted as a carbonate build-up succession. The SS 3 is interpreted to consist of both protozoan and heterozoan carbonate biota from the Gipsdalen and Bjarmeland Groups (Figure 52).

SF 6 is interpreted to consist of a sedimentary facies succession dominated by homogenous lithology. The facies is interpreted as a muddy-limestone succession deposited in a low-energy and calm environment. The facies succession is located laterally adjacent to the mound shaped features and the depositional environment is interpreted as interior lagoon setting, whilst the more laterally extensive, continuous and parallel layers the area is interpreted as deposited in a low-energy platform interior environment.

Figure 59A presents structural features that are interpreted as carbonate build-ups that link-up in networks, and build around circular and sub-circular lower elevated features. The circular and sub-circular features are interpreted as interior lagoonal settings (Figure 59A). The geomorphic zonation of the carbonate build-up succession is interpreted to as of doughnut, horseshoe and composite build-up structures (Chidsey et al., 1997). Examples of the different shapes are presented with arrows in the figure; the doughnut shape is identified as a red arrow, the horseshoe as a green, and the overall configuration of the reticulated features is creating composite structures as partly doughnut, and partly horseshoe features (Figure 59A). The trend of the polygonal build-up complex is considered to be relatively confined to an E-W trend (Figure 59A). The NE-SW orientation of the polygonal carbonate complex is interpreted to be governed by the paleo-margin. The direct shut-down of the carbonate build-up succession is defined by the light penetration curve due to the sea-level depth (Eq. 1.3; Figure 4). Figure 59A presents the interpretation of the paleo-margin as a white dashed line.

The variance and RGB color blend maps are interpreted as presenting two different sedimentary settings (Figure 60A; Figure 60B). First, the reticulated structures are interpreted as polygonal carbonate build-up complexes that prograde toward the basin and are restricted east-west setting. The cell-shaped structures with low variability; these features are interpreted as remnants of antecedent karstified structures that has developed solution structures such as doline features. During the transgressed sea-level the structures is drowned and thus, develop interior lagoon setting with facies of muddy limestone and evaporites. The second facies is the low variance area confined towards the southeast sector of the area; this area is interpreted as a platform interior setting with a facies dominated by fine grained limestone.

5.2.2.5 Seismic Sequence 4

Description Seismic Sequence 4

The top of SS 4 is defined as an increase in acoustic impedance and therefore, as a blue trough in the seismic section (Table 7). The top and base of SS 4 is laterally extensive throughout the area.

SS 4 is defined to comprise of two different seismic facies units. The first facies (SF 7) is identified as a uniformly thick unit approximately 30 ms. thick, with a homogenous reflectivity pattern (Figure 51; Figure 53). The internal reflectivity pattern in the succession is characterized as parallel and continuous reflectors, with low to medium amplitudes, and low frequencies. The character of the reflections is continuous throughout the entire seismic volume, except in the SE of the seismic area.

In the southern part of the area, the facies character of SS 3 changes dramatically and, is identified as the second seismic facies (SF 9). The seismic facies is defined as a mound shaped feature with parallel and continuous internal reflectors (Figure 51). The magnitude of the amplitude and frequencies is characterized as high amplitude and high frequency. The thickness of the mounded feature is defined as 100 ms. thick (Figure 51). The bounding relationship of the seismic facies is laterally non-extensive and thus, is only confined within the mound shaped feature.

The surface map of top SS 4 reveals the geomorphology of a large single mound shaped structure (Figure 61A). The mounded feature is located vertically above the structural lineament in the southern sector of the area identified in the top Pre-SS surface (Figure 61A). The geomorphology of the mound shaped features observed in SS 3 differs from the shape and geometry of the mounded feature within SS 4. The mound shaped structure within SS 4 is significantly wider laterally. The large mounded structures does not present any indications of karstification or paleo-karstification affecting its morphology, opposed to the geometric shapes observed in SS 4 that is comprised of a number of cellular depressed features (Figure 61A). The isochron map indicates a relatively uniform planar area surrounding a large mounded feature. The mounded feature has an average thickness of approximately 100 ms. and the uniform thick surface surrounding the mound has a thickness of approximately 70 ms. (Figure 61B).

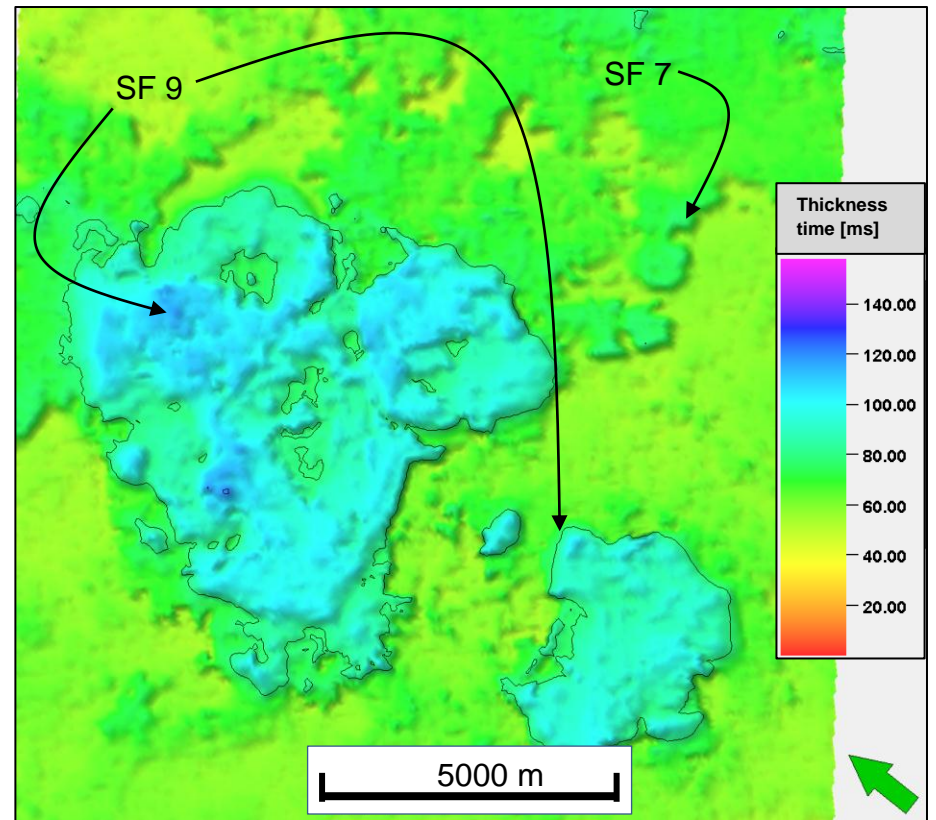
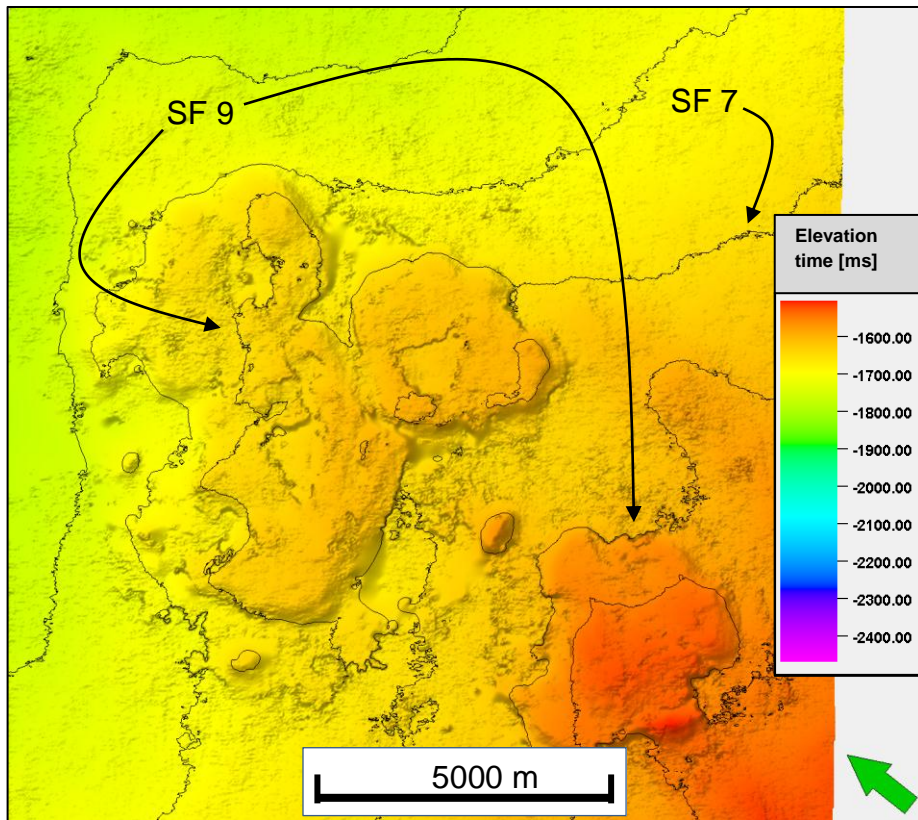


Figure 61 - A) Time surface map of SS 4; B) Time thickness map of SS 4.

Interpretation Seismic Sequence 4

The SS 4 has been interpreted to consist of two different facies units, defined as SF 7 and SF 9. The first facies (SF 7) is interpreted as a pelagic or hemipelagic deposition, with a facies that consist of homogenous limestones. The supporting evidence for the interpretation of SF 7 is the well data results from wells 7226/11-1 and 7229/11-1 (Appendix 1.2; Appendix 1.3), which both penetrate as fine-grained limestone succession within the Røye Formation.

The second facies (SF 9) is defined by its mound shaped structure. The mounded feature is interpreted as calcareous spiculite build-up. The supporting data the spiculite build-up interpretation is the well results from wells 7128/4-1 and 7128/6-1 located on the Finnmark Platform (Appendix 1.4; Appendix; 1.5). These wells penetrate a similar succession with the identical seismic character as seen in Area D (Figure 13A; Ehrenberg et al., 1998a).

The spiculite build-ups grew as isolated build-ups in open marine environment (Larssen et al., 2005). The spiculite build-ups are restricted along the inner margins of the Finnmark Platform. The location of the spiculite mound is interpreted to be confined to the structural high developed by the normal faulting eventing in the Pre-SS, which developed a structural high (Figure 55A). The conformable surface surrounding the spiculite mound is indications that the neighboring area was located in a relative flat surface and thus, generated favorable conditions for deposition of SF 7 (Figure 61A; Figure 61B).

5.2.2.6 Seismic Sequence 5

Description Seismic Sequence 5

The top of SS 5 is identified by a decrease in acoustic impedance and therefore a blue trough in the seismic section (Table 7). The top of the sequence is laterally defined by continuous reflector throughout the entire seismic area. Internally, the sequence is defined as one seismic facies (SF 8), comprised of parallel and continuous reflectors (Figure 51; Figure 52; Figure 53).

The surface map of the top SS 5 horizon is presenting the similar geometry and topographic expression as described in the underlying SS 4 succession (Figure 62A). The surface map of SS 5 presents several structural elements: (1) the mounded feature located in the south that was identified and described in SS 4, (2) the structural lineaments identified in top of Pre-SS, and (3) the geomorphology of the cellular structures described in the SS 3.

The isochron map shows the thickness variations within the sequence (Figure 62B). The time thickness map presents a relatively uniform thick succession from south to north. The average thickness is approximately 70 ms. throughout the area. The variations is high in the northern sector where the variations in thickness is high, ranging up to 120 ms. The isochron map also shows an distinct thickening above the mounded feature in the south (Figure 62B). Nevertheless, the general thickness variations throughout the entire area are relatively low, and only show distinct thickness variations vertically above paleo-features.

Interpretation Seismic Sequence 5

The facies within SS 5 is interpreted as a homogenous siliciclastic succession. The parallel and continuous seismic reflections are interpreted to represent homogenous deposition (Figure 51; Figure 52). The geometry of the seismic reflections within SS 5 is interpreted as draping the underlying paleo-topography.

The depositional environment is interpreted as open marine pelagic or hemipelagic deposition. The surface map interpreted as showing imprints of the underlying topography, and the isochron map which present uniform thickness of SS 5 throughout the area, is interpreted as supporting evidence of pelagic or hemipelagic deposition. The well data results from well 7229/11-1 on the Finnmark Platform support this interpretation (Appendix 1.3). The well 7229/11-1 encounters a relatively thick unit of shale, in the top of Tempelfjorden Group, which is equivalent to the facies interpreted for SF 8.

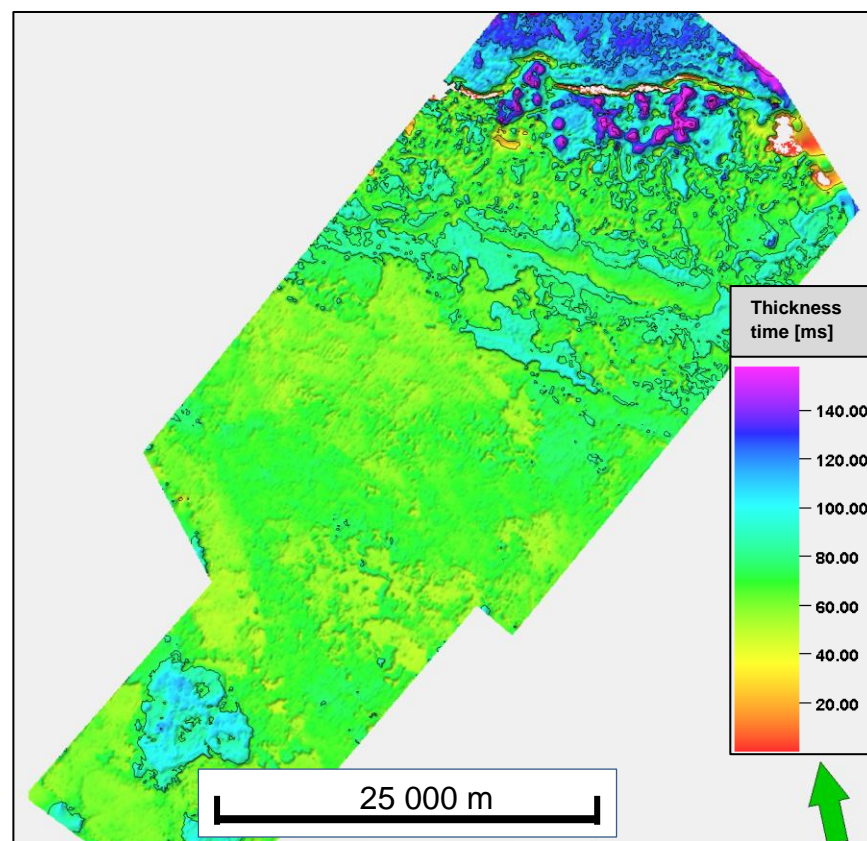
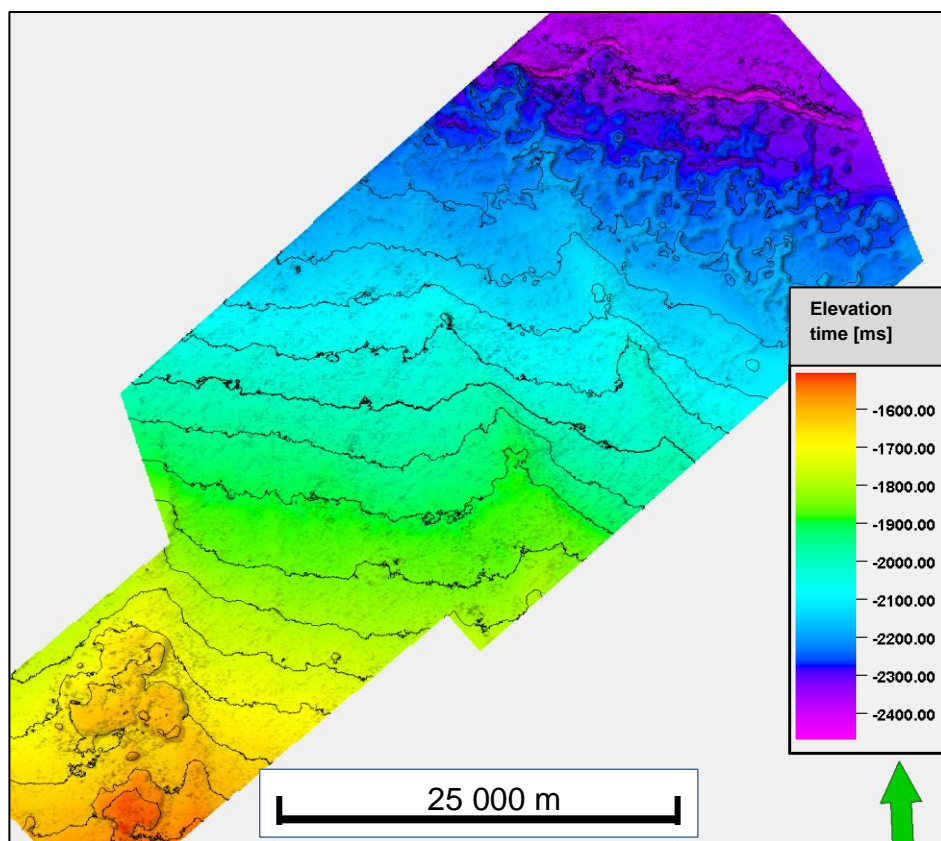


Figure 62 - A) Time surface map of top SS 5; B) Time thickness map of SS 5.

5.3 Summary

5.3.1 Bjarmeland Platform

The two seismic areas A and B have been interpreted and are located on the eastern and western flank of the Bjarmeland Platform. The interpretation of the two different areas has been conducted by distinguishing the different key reflectors into seismic sequences, and then characterizes the seismic facies settings within these sequences. The seismic sequences and its associated seismic facies that are identified on the Bjarmeland Platform have been summarized in Table 15. The different seismic facies units are based on seismic characteristics that differ from the adjacent reflectivity pattern and thus, are interpreted as presenting differences in depositional setting and facies.

The Pre-SS has been separated into different seismic parts (Table 9). The lower part (SF 1) is interpreted as the Pre-Devonian basement and the upper part (SF 2) as the fluvial dominated Billefjorden Group (Table 9). This structural influence on the succession resulted in deposition of syn-tectonic sediments. These sediments are identified as deposited in half graben structures, and as post-tectonic deposition, which drape the underlying topography.

The SS 1 is identified as two distinct seismic facies (SF 3). The main facies unit (SF 3) within the sequence is characterized by homogenous and parallel reflectors (SF 3). SF 3 is interpreted as deposited in a platform interior environment and thus, resulted in uniformly distributed deposits throughout the entire area. The facies within the sequence is interpreted as limestone dominated facies. The second facies unit (SF 5) is confined along the margin of the Nordkapp Basin. SF 5 is defined as a mounded feature that consists of chaotic and contoured reflections. The sedimentary succession within SF 5 is interpreted as a carbonate barrier reef.

SS 2 is identified as consisting of one seismic facies (SS 4). The top of SS 2 is defined by a seismic reflection defined as a strong decrease in acoustic impedance. The base of SS 2 is defined by an increase in acoustic impedance. Internally, the SS 2 has a reflection configuration consisting of chaotic and discontinuous reflectors (Table 9). The SS 2 is interpreted as a layered evaporite sequence that is deposited in restricted platform interior environments during glacio-eustatic sea-level lowstand.

The SS 3 is considered to consist of two different seismic facies configurations (Table 9). The first seismic facies (SF 5) has a reflection configuration consisting of a mound-shaped feature and has a discontinuous to semi-continuous reflectors. The second seismic facies (SF 6) consists of a parallel and continuous reflection configuration. The differences in the seismic facies in SS 3 have been interpreted to present differences in depositional settings in the seismic sequence. The mound-shaped features were interpreted as carbonate build-up complexes, and the parallel continuous reflectors were interpreted as deposited in a calm and stable depositional environment, in platform interior and in open marine settings.

The SS 4 is characterized by a uniform thick sequence in both of the areas. The SS 4 is presented as one distinct seismic facies (Table 9). The reflection configuration of the SS 4 is considered as parallel and continuous. The reflection geometry is considered as draping the SS 3 and thus, deposited in concordance with the paleo-topography. This sequence was interpreted as an outer marine depositional facies consisting of sediments deposited pelagic or hemipelagic. The sequence is interpreted as consisting of a spiculitic limestone facies equivalent to the Røye Fm. (Figure 6).

The SS 5 is defined by a set of reflectors that has a parallel and continuous configuration (SF 8). The top of the unit is identified as a decrease in acoustic impedance with a magnitude of the amplitude identified as low to medium (Table 9). The geometry of the SS 5 is interpreted as deposited in concordance with the bathymetry during deposition and to have a depositional setting being pelagic or hemipelagic. SS 5 is interpreted to consist of a siliciclastic facies equivalent to the Ørret Fm. that was identified in well 7124/3-1 and 7226/11-1 (Appendix 1.1; Appendix 1.2).

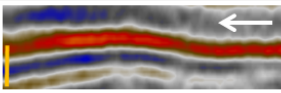
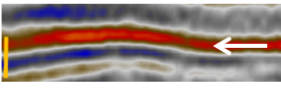
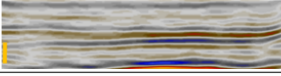
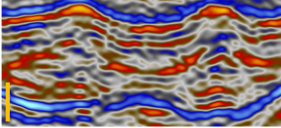
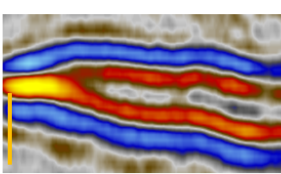
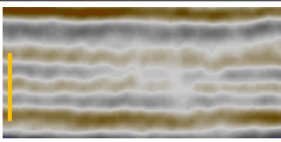
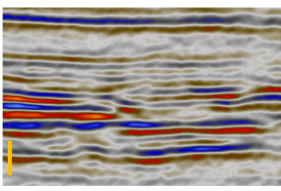
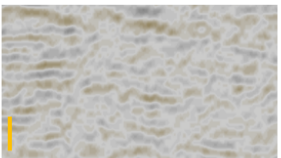
| Bjarmeland Platform | | | | | | | |
|----------------------------|----------------|----------------------------------|----------------------------------|---|---|--|---|
| Seismic Sequence | Seismic Facies | Reflection Configuration | Reflection Continuity | Reflection Amplitude and Frequency | Bounding Relationship | Depositional Environment | Example (vertical bar represents 50 ms.) |
| SS 5 | SF 8 | Parallel | Continuous | Low to medium amplitude and low frequency | Continuous and draping underlying topography | Pelagic or hemipelagic |  |
| SS 4 | SF 7 | Parallel | Continuous | High amplitude and low frequency | Continuous and draping underlying topography | Pelagic or hemipelagic. Chert and spiculitic limestone facies |  |
| SS 3 | SF 6 | Parallel | Continuous | Low to medium amplitude and low frequency | Parallel deposited laterally | Interior-lagoon and platform interior setting |  |
| SS 3 / SS 1 | SF 5 | Mound-shaped, contoured, chaotic | Discontinuous to semi continuous | Low amplitude and high frequency | Restricted to the warm- and cool water carbonate build-up sequence. | Protozoan and heterozoan carbonate build-ups |  |
| SS 2 | SF 4 | Contoured, sub-parallel | Continuous to semi-continuous | High amplitude and low frequency | Restricted to the areas with high abundance of overlying SF 5. Grading laterally to SF 4 and SF 5 | Platform interior, interior lagoon, and sag-basin evaporite deposits |  |
| SS 1 | SF 3 | Parallel | Semi continuous | Low amplitude and low frequency | Semi-continuous reflections grading laterally to facies 3 and 4 | Platform interior Muddy-limestone deposits |  |
| Pre-SS | SF 2 | Sub-parallel | Semi Continuous | Low to high amplitude and low to high frequency | Grading vertically to SF 1 and the unit thickens as syn-depositional half-graben fills. | Lower succession is a syn-depositional siliciclastic facies, the top is a fluvial facies deposited low relief environments |  |
| Pre-SS | SF 1 | Chaotic | Discontinuous | Low amplitude and low frequency | Located non-conformally below SF 2 | Pre-Devonian metamorphic basement |  |

Table 9 - Seismic facies summary table for the Bjarmeland Platform region.

5.3.2 Finnmark Platform

The two areas C and D are located in the northeast and southeast of the Finnmark Platform. The structural setting of the two different areas varies significantly. The structural component controlling the deposition of Area C is considered as a structural high developed by a normal faulting event in the Mississippian. The structural elements identified in the Area D are negligible for the deposition of the carbonate build-up sequence although it controls the deposits of local syn-tectonic sediments deposited in the Mississippian. The seismic interpretation of the area has been conducted by identifying the different seismic sequences in the area and the seismic facies within these different sequences.

The Pre-SS has been defined into two different parts (Table 10). The lower part (SF 1) is defined as metamorphic basement of pre-Devonian origin, and the upper part (SF 2) is interpreted as the Billefjorden Group.

The SS 1 is identified as one seismic facies and, in places, two seismic facies (SF 3 and SF 5). SF 3 is considered as a syn-tectonic sequence in area C, where the SS 1 has the characteristics of a syn-tectonic unit filling a depocenter in a half graben (Table 10). The half graben structure in area C has been interpreted as developed during the mid-Bashkirian rifting event, which occurred in the earliest stages of the deposition of SS 1. Besides filling the half graben structure and effectively being a syn-tectonic sedimentary succession in this part of area C; the SS 1 unit is deposited conformably in both areas with a uniform thick sequence in Area D and on the footwall block of Area C.

The SS 2 are identified in both to the seismic areas, as a sequence that consists of two different seismic facies units (Table 10). SF 4 is characterized by a decrease in acoustic impedance defining the top, and an increase of acoustic impedance as its base. Internally, the reflection configuration is defined as contour-shaped and with sub-parallel reflector configuration. The reflections are considered to be continuous to semi-continuous (Table 10). The primary composition of SS 2 is interpreted a layered evaporite unit, composed of evaporites, carbonate and dolomites.

The SS 3 are represented by two different seismic facies assemblages. The seismic character of the first seismic facies (SF 5) is identified as a mound-shaped geometry, with contoured and chaotic reflectors. The reflection continuity is considered as discontinuous to continuous (Table 10). The second seismic facies (SF 6) unit is characterized by a reflection configuration that consists of parallel reflectors, with a continuous to semi-continuous reflection continuity. The first seismic facies is interpreted as a carbonate build-up succession that builds upon antecedent topography, and the second facies is interpreted as platform interior deposits consisting of a muddy-limestone facies.

The SS 4 is considered to be composed of two different seismic facies (Table 10). The first seismic facies (SF 7) is identified by parallel and continuous reflectors. SS 4 is interpreted as

deposited in concordance with the underlying topography, and deposited as uniformly thick throughout both of the areas. SF 7 is interpreted as deposits deposited in a stable tectonic environment, and by pelagic or hemipelagic deposition that consist of spiculitic and cherty limestone. The second seismic facies (SF 8) is identified as confined to southern part of Area D. SF 8 is defined as a mound-shaped feature consisting of semi-continuous reflectors. SF 8 is interpreted as a spiculite build-up deposited in an open marine environment.

The SS 5 consists of one seismic facies (SF 9) and is characterized by parallel and continuous reflections (Table 10). The lateral extent of SS 5 is confined to Area D. The geometry of the reflector is considered as draping the pale-topography signature of SF 5 and SF 8. The sedimentary facies within SS 5 is interpreted as deep marine pelagic or hemipelagic deposition, consisting of fine-grained siliciclastic sediments (Table 10).

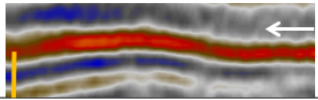
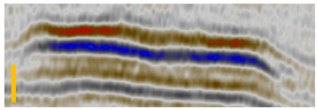
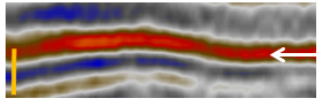
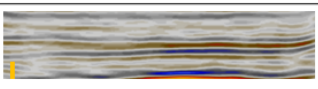
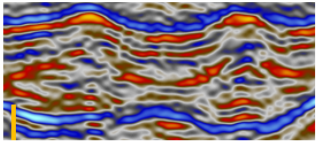
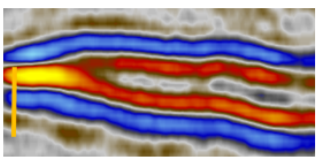
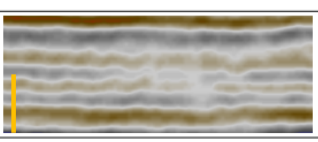
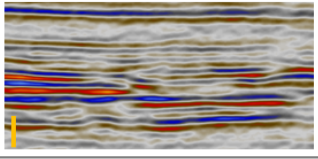
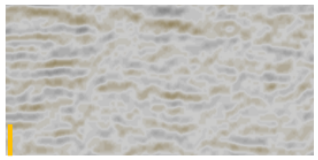
| Finnmark Platform | | | | | | | |
|-------------------|----------------|----------------------------------|----------------------------------|---|---|--|---|
| Seismic Sequence | Seismic Facies | Reflection Configuration | Reflection Continuity | Reflection Amplitude and Frequency | Bounding Relationship | Depositional Environment | Example (vertical bar represents 50 ms.) |
| SS 5 | SF 8 | Parallel | Continuous | Low to medium amplitude and low frequency | Continuous and draping underlying topography | Pelagic or hemipelagic |  |
| SS 4 | SF 9 | Mounded | Semi-continuous | Medium to high amplitude and high frequency | Restricted to the mounded feature | Cherty spiculite mounds |  |
| SS 4 | SF 7 | Parallel | Continuous | High amplitude and low frequency | Continuous and draping underlying topography | Hemipelagic. Chert and spiculitic limestone facies |  |
| SS 3 | SF 6 | Parallel | Continuous to semi-continuous | Low to medium amplitude and low frequency | Parallel deposited laterally | Interior-lagoon and platform interior setting |  |
| SS 3 / SS1 | SF 5 | Mound-shaped, contoured, chaotic | Discontinuous to semi continuous | Low amplitude and high frequency | Restricted to the warm- and cool water carbonate build-up sequence. | Protozoan and heterozoan carbonate build-ups |  |
| SS 2 | SF 4 | Contoured, sub-parallel | Continuous to semi-continuous | High amplitude and low frequency | Restricted to the areas with high abundance of overlying SF 5. Grading laterally to SF 4 and SF 5 | Platform interior, interior lagoon, and sag-basin evaporite deposits |  |
| SS 1 / SS2 | SF 3 | Parallel | Semi-continuous | Low amplitude and low frequency | Semi-continuous reflections grading laterally to facies 3 and 4 | Platform interior Muddy-limestone deposits |  |
| Pre-SS | SF 2 | Sub-parallel | Semi-continuous | Low to high amplitude and low to high frequency | Grading vertically to SF 1 and the unit thickens as syn-depositional half-graben fills. | Lower succession is a syn-depositional siliciclastic facies, the top is a fluvial facies deposited low relief environments |  |
| Pre-SS | SF 1 | Chaotic | Discontinuous | Low amplitude and low frequency | Located non-conformably below SF 2 | Pre-Devonian metamorphic basement |  |

Table 10 - Seismic facies summary table for the Finnmark Platform region.

6. Discussion

6.1 Bathymetric Control on Carbonate Development

6.1.1 Structural Control

The structural control in regards to the distribution of the carbonate reefs are considered prominent on both of the Bjarmeland and Finnmark Platform. The areas mostly affected by tectonic influence are areas A and C. These areas have been highly affected by events of normal faulting prior to the deposition of the carbonate successions (e.g. Figure 21D; Figure 41B; Figure 43). The tectonic events occurred during the period of Pre-SS interpreted as the Early Carboniferous. These events resulted in development of uplifted footwall highs, causing favorable conditions for carbonate growth on the uplifted footwall (Figure 63). The photosynthesis is a considerable factor governing the growth of carbonate systems, the photosynthesis is light dependant, which means that the photosynthetic process decreases with sea-level (Equ. 1.3; Figure 4). The importance of the seafloor bathymetry and the development of structural elements on the seafloor are dominant factors for the controls on the carbonate build-up distribution.

The significance of the glacio-eustatic sea-level fluctuations in conjunction with the structural highs generated ideal conditions for carbonate build-ups on uplifted highs. The principal build-ups processes occurred during highstand sea-level. During highstand, the carbonate complexes grew on the uplifted footwall blocks with high-relief, and muddy-carbonate facies deposited in platform interior environments in the lower elevated areas (Figure 63). In contrast, during sea-level lowstand, precipitation of hypersaline sea-water resulted in deposition of evaporites restricted platform, and in the deeper seated Nordkapp Basin. In addition, karst-induced processes altered the carbonate surface on the subaerially exposed carbonate surfaces.

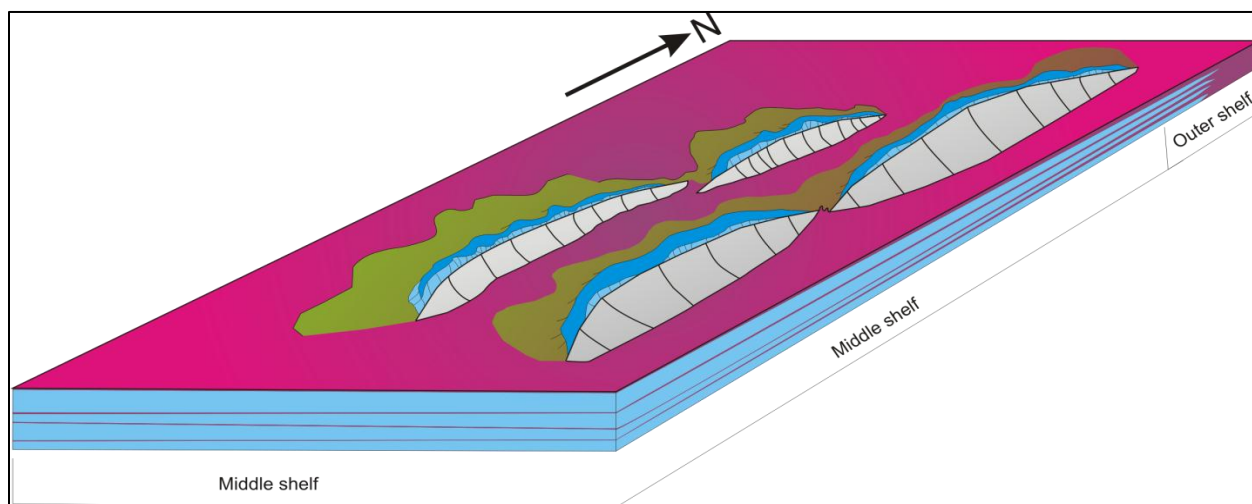


Figure 63 – Geological model of carbonate systems growing on footwall uplifted highs.

6.1.2 Antecedent Karst Topography

The karstification processes affect subaerially exposed carbonate surfaces during sea-level lowstand. The carbonate surface is then subjected to dissolution processes which can be divided into two different karstification processes, epikarst and endokarst. These processes can occur separately or together. Endokarst surface is considered as the process where development of subsurface caves and canyons occurs. This may create structures such as collapse doline structures. Epikarst surfaces, on the other hand, are a solution process affected by the surface environment, e.g. rain in combination with CO₂ creating carbon-acid that further dissolves the carbonate surfaces.

The protozoan carbonate succession in the Norwegian Barents Sea was affected by substantial glacio-eustatic sea-level fluctuations. The number of periods affected by sea-level lowstand resulted in multiple periods of karstification processes, altering the carbonate surface (Stemmerik et al., 1999). During the following period of transgression, the carbonate build-up succession grew on areas subjected to little or no alteration, e.g. on the flanks of doline structures. The impact of antecedent topography is interpreted as the primary triggering factor, for the growth and development of the carbonate systems in the areas located on the Bjarmeland and Finnmark Platforms.

The morphology of the carbonate succession is interpreted as a network of build-up ridges that develops cellular structures (Figure 36A). The geomorphology of the carbonate successions in the four seismic areas, are considered different. However all have a distinct property in common which is interpreted as governed by the underlying, paleo-karstic morphology.

The similarities between the top SS 3 surfaces in all of the four areas are shown as reticulated ridge systems. Nonetheless, their lateral extent and geometry differ (Figure 26A; Figure 36A; Figure 47A; Figure 59A). The geomorphological character of seismic area B and D has distinct similarities. These similarities are related to the growth of reticulated carbonate ridges, encircling deeper elevated cellular structures (Figure 64). These distinct structural features have characteristics shape similar to the classical morphology of karstified doline and collapse karst structures (Ford and Williams, 1989). Similarities are also identified between areas A and B, both of these areas have a developed structural elements defined by Chidsey et al. (1996) as doughnut and horseshoe structures. The development of the doughnut and horseshoe structures are confined to the carbonate build-up structures subjected to highest relief. This is evident by the development of large horseshoe structures in the carbonate build-up succession interpreted as a barrier reef in Area A, and the doughnut structure created in the carbonate build-up on the uplifted footwall block on the Finnmark Platform in Area C (Figure 64B). The development of doline structures locally on the large build-up complex in Area A is interpreted as being developed during period of subaerially exposure and karstification. This is followed by continuous growth of the carbonate system avoiding growth and development in deeper elevated areas (Figure 64A).

There is a considerable resemblance between the doline structure termed ‘The great blue hole’ located off the coast of Belize (Figure 65A), and the circular doughnut structure located on the western flank in Area C (Figure 65B; Figure 64B). The similarities between the two different areas are the development of carbonate build-ups in the rim of the doline structure. The dimension between the two different sinkholes differs significantly. The great blue hole has a diameter of 500 meter opposed to the doughnut structure in Area C, which has a diameter of approximately 2000 meter (Figure 65A; Figure 65B). The development of the karstified systems in Area C and Belize are both endokarst surfaces. On these areas, the solution process has created subsurface caves that cause collapse of the overburden sediments, which results in the doline structures. The noticeable difference in scale between the great blue hole in Belize and Area C is insignificant for the development of carbonate build-ups on the rim of the doline structures. The development of doline structures in meter and kilometer sizes are widely recognized in both the modern and ancient independent of the process generating the structure (White, 2006).

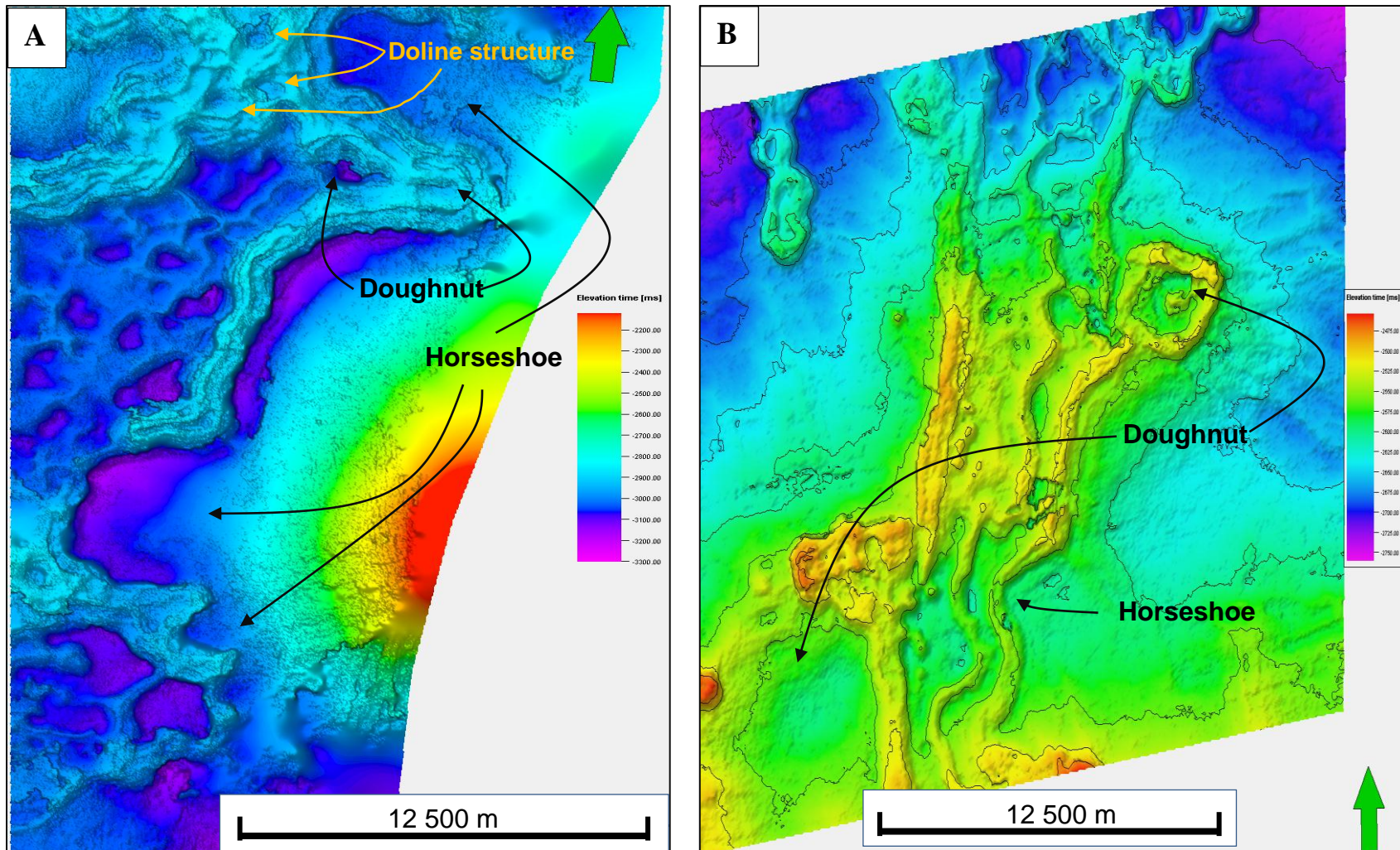


Figure 64 Comparison of surface maps of SS 3 from Area A and Area C, presented with structural features. A) Area A presented with proposed examples of horseshoe and doughnut structures; B) Area C presented with doughnut and horseshoe structures.

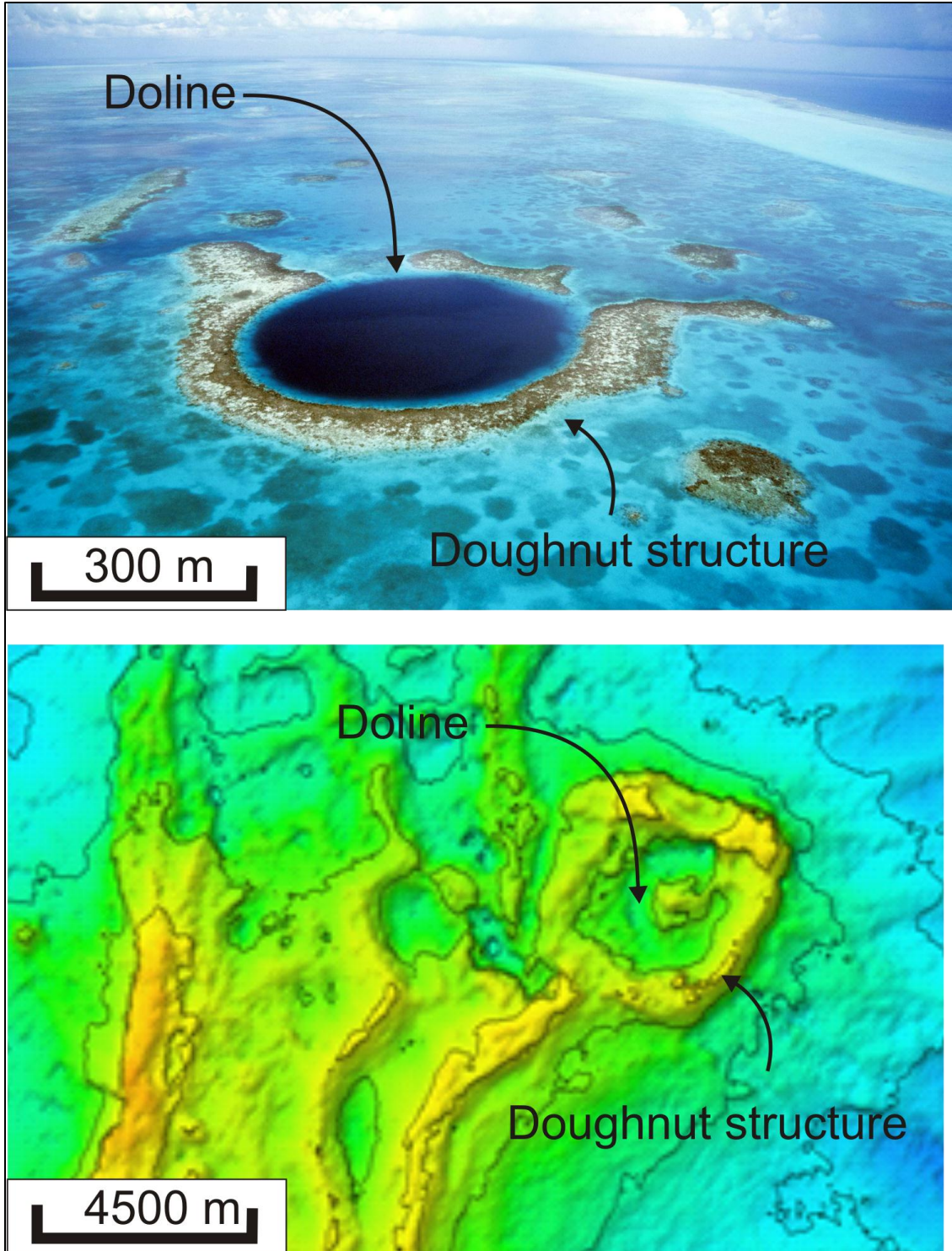


Figure 65 - Comparison of modern and ancient sinkhole and doughnut structure. A) The great blue hole, Belize (Image copyright of José Luis Zapata); B) Doughnut structure in Area C shown on the surface map of SS 3.

Reticulated carbonate ridges located in lagoonal environments has been observed and described in modern day analogues e.g. Kanton Island, Abrolhos Island, Mataiva Island and Isla Pérez (Figure 66). Their origin and controlling factors in regards to their growth-shape and development are discussed (e.g. Schager and Purkis, 2015; Gischler et al., 2014). Hypotheses considering the origin of the reticulated shaped carbonate ridges are identified as (1) biotic self-organizing, (2) fluid dynamic pathways within the lagoon environment, (3) antecedent karst topography (Schlager and Purkis, 2014).

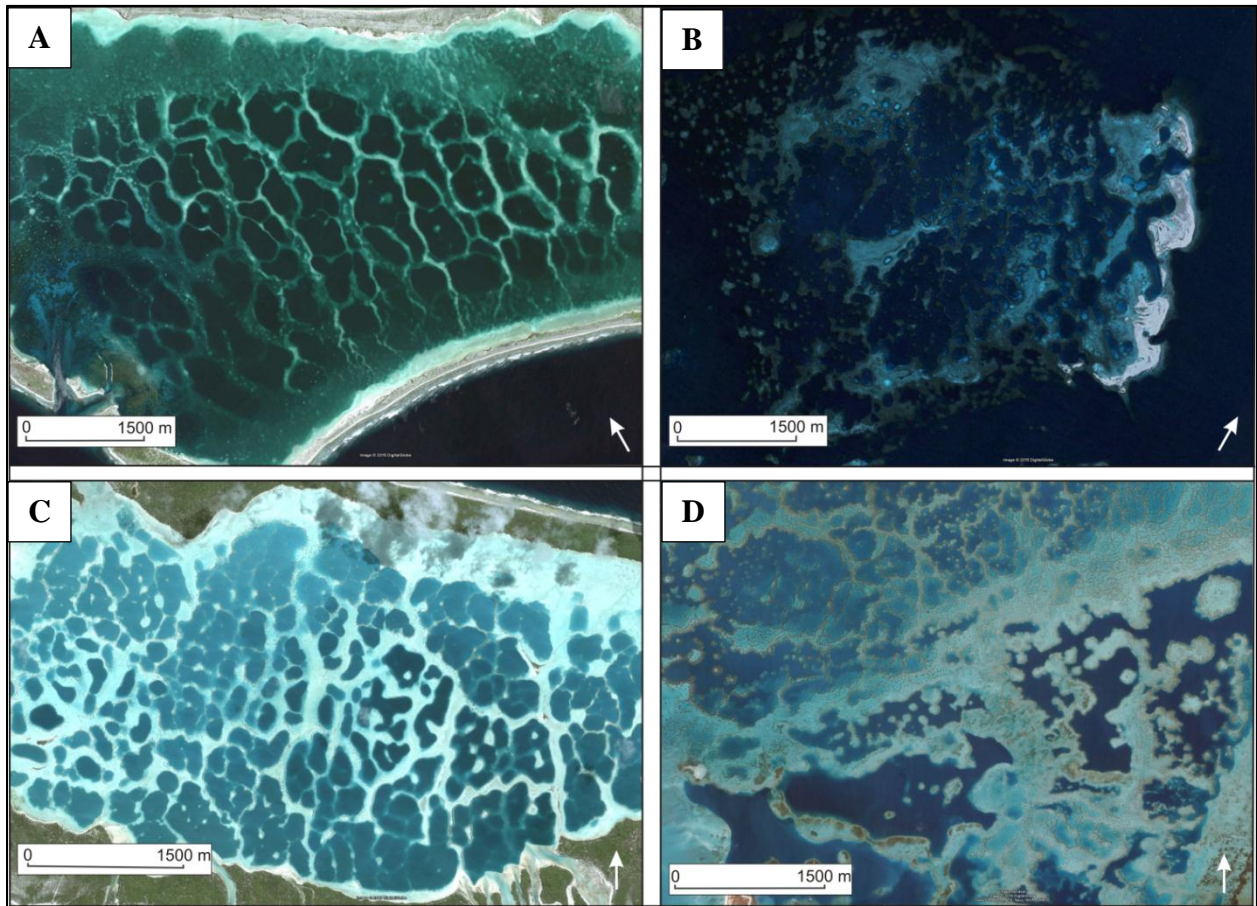


Figure 66 - Analogue compilation of Holocene reefs with attached patch and pinnacle reef architectures. The similarity between the images is the reticulated carbonate network enclosing cells of no reef growth. The dark cells enclosed by reticulate carbonate network. The dark cells are deeper seated structures, and the white ridges are patch reef (<20m relief) and pinnacle reef (>20m relief) ridges. A) Kanton Island, Kiribati, B) Abrolhos Island, Western Australia, C) Mataiva, French Polynesia, D) Isla Pérez, Mexico. Modified from Blanchon (2011); Images copyright of Google Earth and DigitalGlobe, 2015.

The antecedent-karst topography as the principal factor controlling the development and growth of lagoonal patch or pinnacle reef networks, was initially described by Hoffmeister and Ladd (1945), concluding that there is a significant relationship between the morphology of solution structures and the geomorphology of the carbonate reef systems developed in the lagoon setting. This theory has been further strengthened by more recent studies which applies karstified surfaces

as their interpretation for the development of the pinnacle reef networks (e.g. Purdy and Bertram, 1993; Gischler et al., 2014).

The development of the reticulated build-up systems confined to the lagoonal setting overall controlled by the sea-level and the bathymetry expressing the antecedent topography. The initial system grows on higher structures causing favorable conditions for the carbonate build-ups to develop. The multiple number of sea-level fluctuations altered the initial morphology of the carbonate surface by karstification processes occurring during sea-level lowstand. The following carbonate build-up processes creates morphological expressions, which imprints the karst-induced surface.

The areas on the Bjarmeland and Finnmark Platforms has a developed a significant number of thin and thick sequences laterally located to each other (Figure 67A; Figure 67B). The interpreted geological model of the reticulated build-up system, in response to sea-level is illustrated in Figure 67C and Figure 67D, these systems illustrates the impact of glacio-eustatic highstand sea-level on the growth of the carbonate mound and the development of interior lagoon setting in the areas (Figure 67C). During sea-level lowstand the carbonate terrain is subaerially exposed resulting in karstification and further alteration of the morphology of the carbonate surface, and precipitation of evaporitic sediments in the interior lagoonal environment (Figure 67D).

The map view of the structures developed in the area is identifying relatively circular structures that encircle an interior lagoon (Figure 67E). These structural features develop into reticulated build-up systems (Figure 67D). Comparing the geomorphological characteristics of reticulated carbonate patterns from modern day analogues with the reticulated carbonate build-up system observed in Area A the similarities are conspicuous (Figure 68). The analogue models and the area has a distinct similarity in their growth-shape, all of the systems develop in lagoon environments as networks of pinnacle reefs (Blanchon, 2011). The carbonate network ridges observed in the two analogue images from the Mataiva and Abrolhos Islands presents number of ridges interlinked and encircle structural lows; the similarities from the with the analogue systems and the lagoonal environment in Area A is striking. These systems has developed their structural architecture based on the imprints of underlying topography of antecedent karst systems, whereas the structural low features are interpreted as solution structures such as doline structures (Figure 65; Figure 68; Gischler et al., 2014).

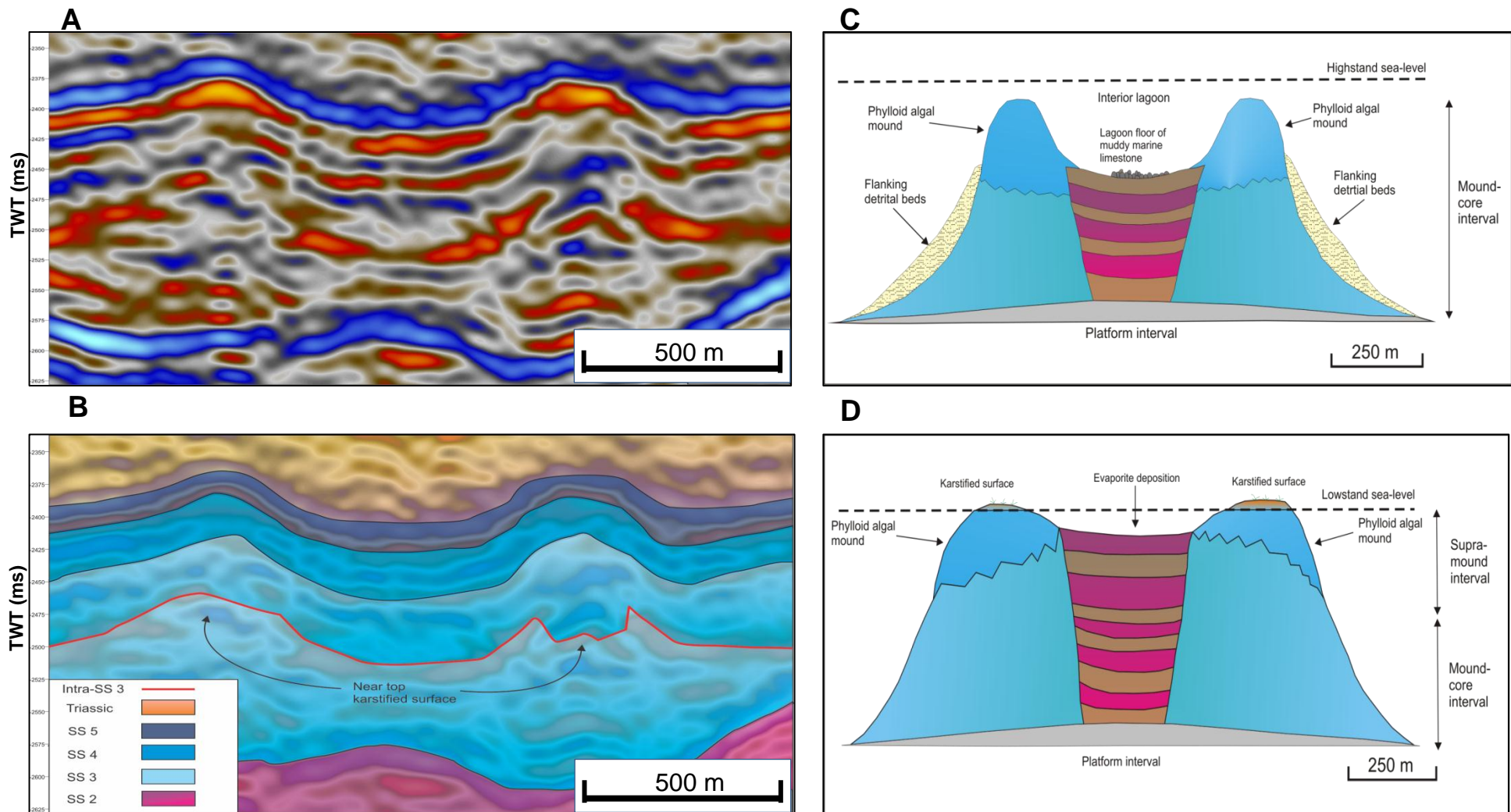


Figure 67 - Geological model of carbonate build-ups developing the seismic geomorphology based on the topography of antecedent karstified surface. A) Seismic section of Area D; B) Geoseismic section of Area D illustrating the karstified protozoan carbonate surface; C) Highstand sea-level model of the build-up development; D) Lowstand sea-level development of the carbonate build-up; E) 2D map view of a build-up mound; F) 3D geological model of the carbonate build-up network developed in the lagoon environment.

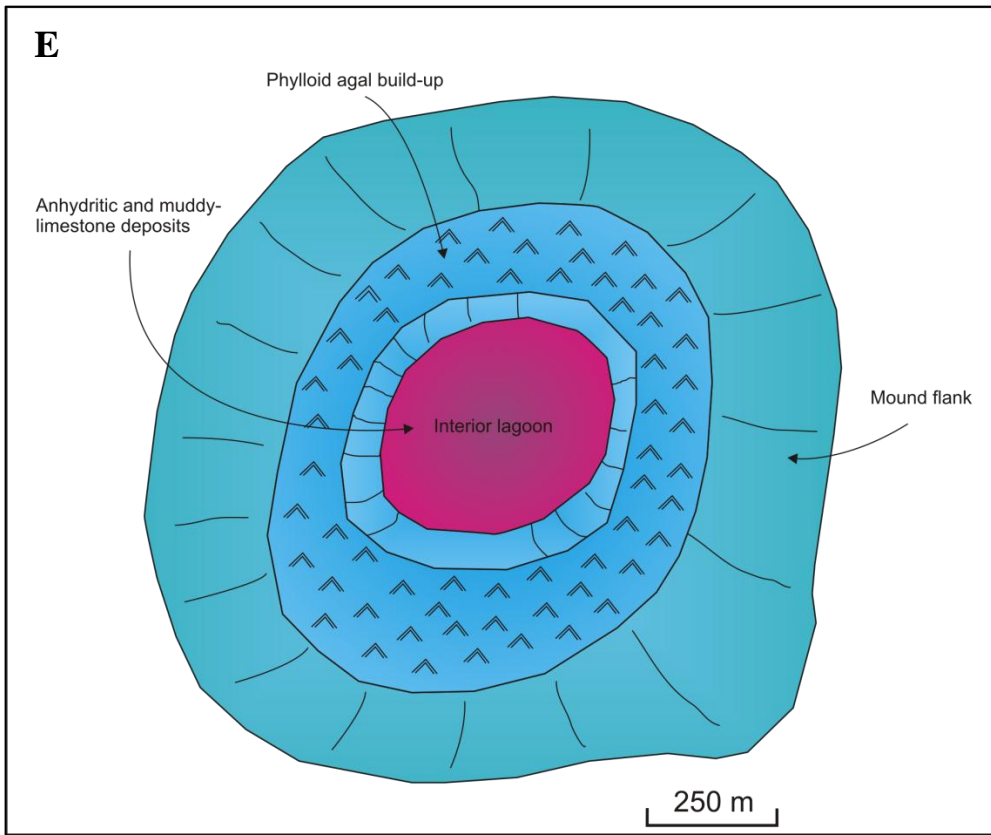


Figure 67E - 2D map view of a carbonate build-up mound (Modified from Chidsey et al. 1996).

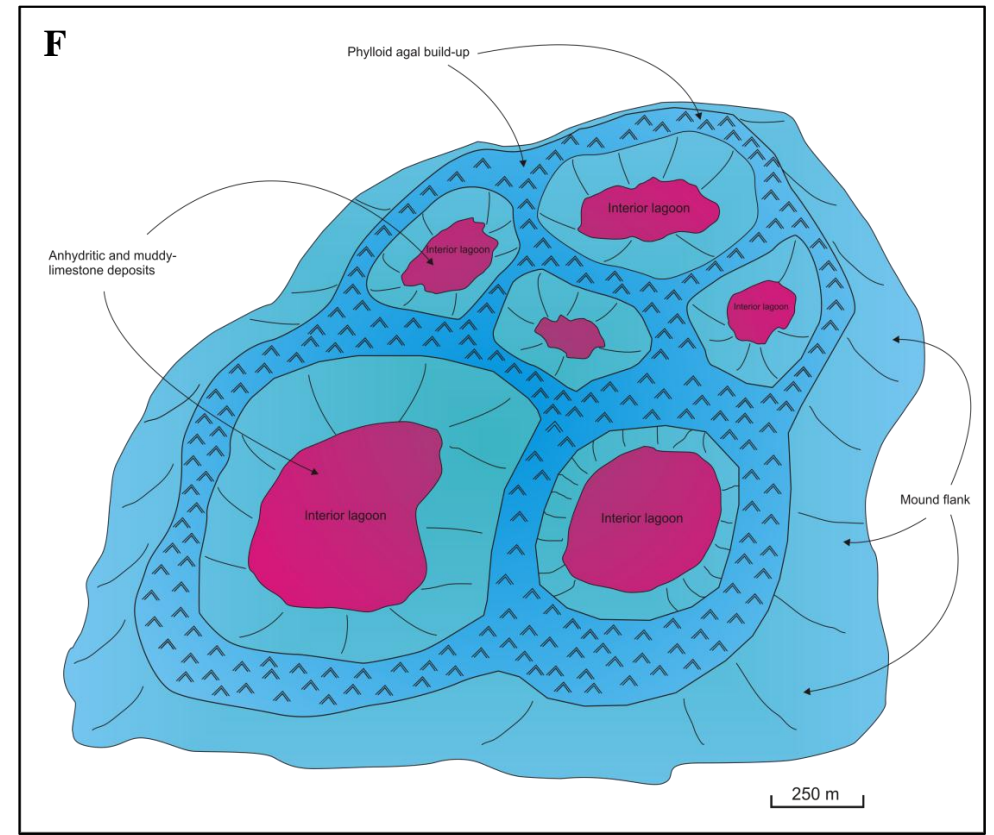


Figure 67F - 3D geological model of reticulated carbonate build-up development in a lagoonal environment.

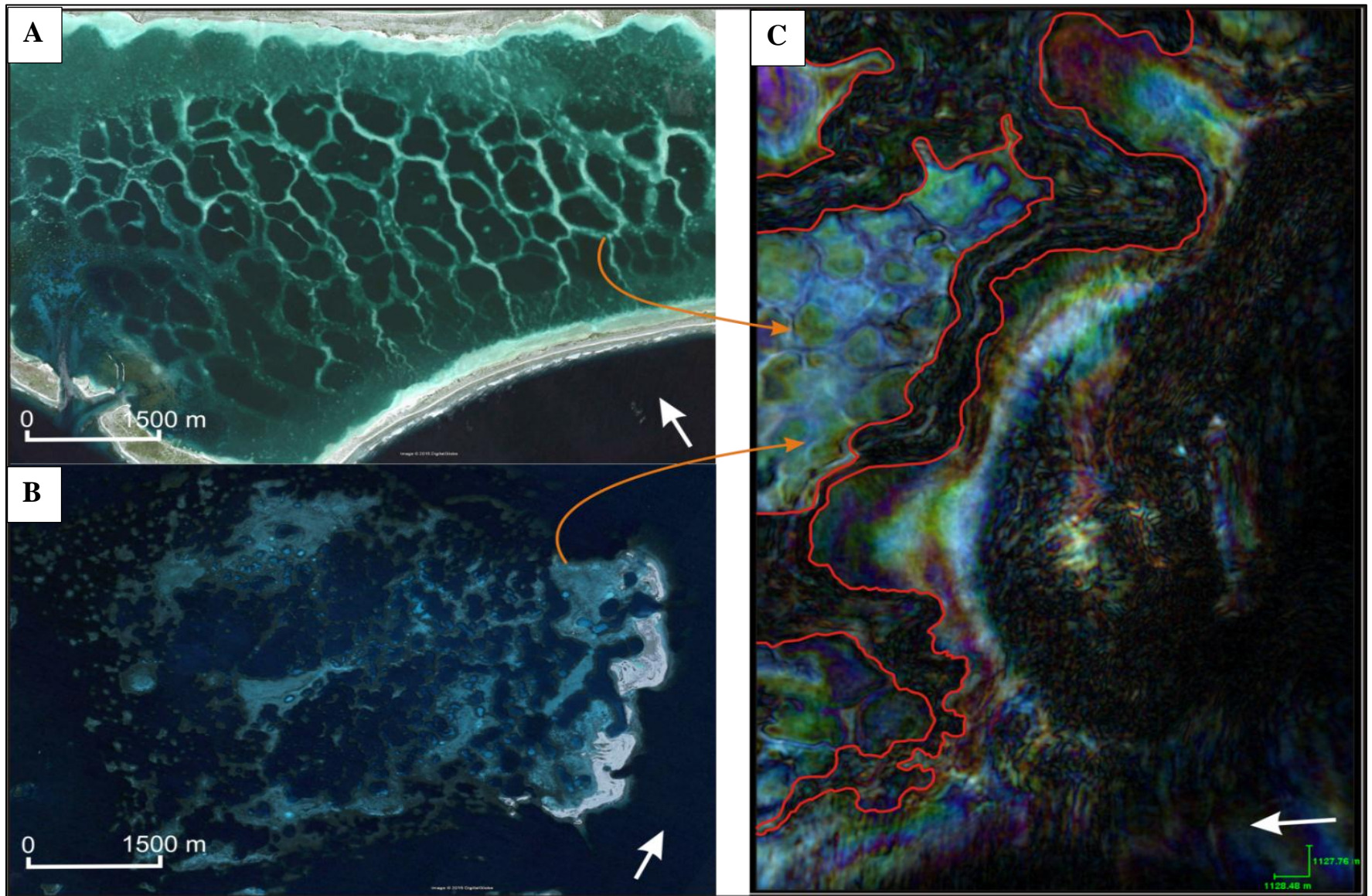


Figure 68 - Comparison of the geomorphological characteristics of reticulated carbonate systems from analogues versus the Top SS 4 surface in seismic Area A. A) Kanton Island, Kiribati; B) Abrolhos Island, Western Australia; C) Seismic Area A, Norwegian Barents Sea. Images copyright of Google Earth and DigitalGlobe, 2015.

6.2 Hydrodynamic Control

The importance of hydrodynamic controls on carbonate systems has been long known since Darwin (1842) revealed the impact of wave, wind and currents on the development of carbonate reefs. The hydrodynamics of carbonate reefs includes a series of controlling factors (Figure 2). The most dominant factor for determining the fluid motion in large scale reefs are often wave-controlled flows (Rogers et al., 2013; Monismith, 2007). The hydrodynamic processes are known to impact and alter the growth shape of the carbonate systems (Rogers et al., 2013; Chappell, 1980). The importance of the wave influx affecting the carbonate build-up complex is determined by three main factors. The first and most prominent factor is the waves that carries and transport sediments out of the carbonate complex. The transportation of sediments away from the system is an important factor to keep the carbonate complex healthy, for it to continue its growth (Rogers et al., 2013). The second factor is the influx of nutrition that is carried with the wave and current motions. The intake of nutrition and photosynthetic production escalate with increase in water motion (Genin et al., 2009; Rogers et al, 2013). The third factor for is considered to be the wave force, which may alter the growth shape, and prevent further expansion of the system by breaking the carbonate reef complex.

6.2.1 Wave Movement Control

The impact of water movement controls on the carbonate systems in the south central Barents Sea is considered as a factor affecting the carbonate system. The Bjarmeland and Finnmark Platforms are interpreted as part an epeiric platform with a very low gradient. The platform configuration is interpreted as controlling the deposition of the sedimentary succession in SS 1.

The seismic facies classification of SS 1 is interpreted as showing a period of overall tectonic quiescence. However, the Finnmark Platform was influenced by active tectonic events in the mid-Bashkirian, affecting the deposition of the lower part of SS 1 (Larssen et al., 2002). The platform morphology of the Bjarmeland Platform is interpreted as a rimmed shelf, orientated towards the Nordkapp Basin. The morphology of the Finnmark Platform is interpreted as a ramp, directed towards the Nordkapp Basin (Figure 56). The low gradients of the two platforms resulted in free circulation and open marine conditions during this period, resulted in deposition of fine grained carbonates (James and Kendall, 1992).

The carbonate build-up succession identified as the mound-shaped structural complexes seen in SS 3, are interpreted as influenced the wave energy. The direction of wind on carbonate systems is defining the systems into two different categories, dependent on differences in geomorphic zonation, which are windward and leeward sides. The largest reef building complexes develop in the windward side, while the more subtle structures develop on the leeward side. The distribution of the leeward and windward effect on the carbonate build-up system in the Barents Sea varies dependant on different areas. The areas are impacted differently based on wind and wave motion current, which influences the growth-form of the carbonate build-up systems.

The most significant differences between leeward and windward systems are a comparison of the surface maps of top SS 3 from seismic area A and B. Both of these systems are located on the Bjarmeland Platform although their position from the Nordkapp Basin varies, and thus their position of wind and wave direction differs significantly. The windward direction is considered as sourced from the Nordkapp Basin. Figure 69A shows a large build-up complex that was developing on the windward margin of the Bjarmeland Platform. The build-up complex interpreted in area A suggests that the windward direction is coming from the Nordkapp Basin, and has therefore, developed as a barrier complex (Figure 69A). The carbonate complex in the western section of the Bjarmeland Platform is located further north from the Nordkapp Basin. The area is interpreted as located on a leeward margin of the Bjarmeland Platform (Figure 69B).

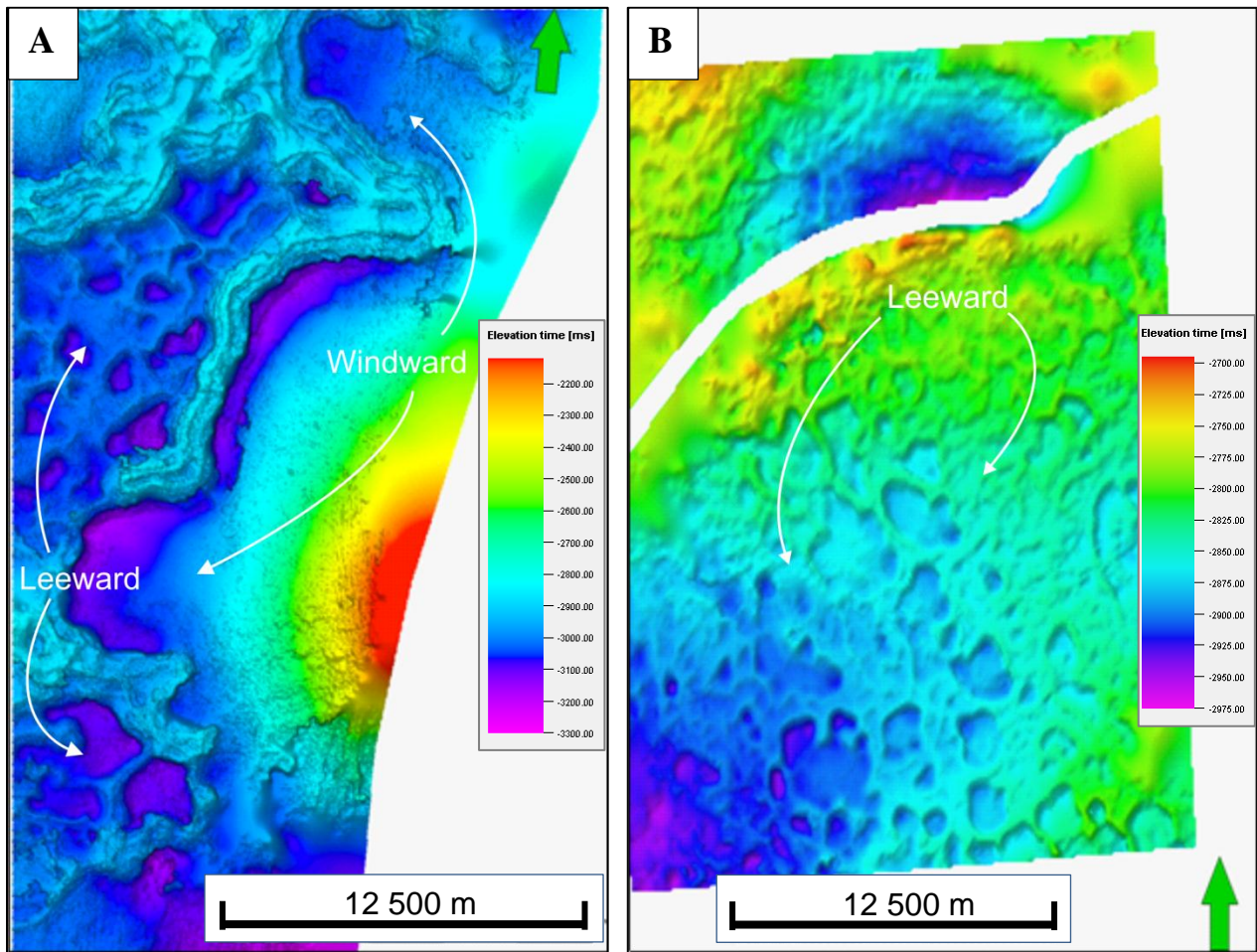


Figure 69 – The windward and leeward directions on the Bjarmeland Platform areas. A) Area A has the windward direction from located from the direction of the Nordkapp Basin to the east and leeward direction to the west. B) Area B is interpreted as located in a platform interior setting and is not subjected to a specific windward direction.

6.2.2 Spur and Groove

Spurs and grooves are reef features common in modern reefs from the Caribbean Sea, Indian Ocean and the Pacific Ocean (Rogers et al., 2013). The spur structure is described as an elevated carbonate complex located in the fore reef zone. The groove is identified as patches or channels situated in a deeper elevated setting, and consist of shoreline sediments (Figure 70). The spurs and grooves structures are found in a variety of carbonate systems, e.g. fringing reefs and barrier reefs. The characteristic morphology of the spurs and groove structures are the perpendicular orientation to the platform margin and water movement direction. The shapes and structure of spurs and grooves are identified as primarily determined by the wave energy. The spurs and groove structures are preserving their thickest succession in areas with high wave energy, in contrast to the little to no presence, in the areas with low wave energy (Rogers et al., 2013). The most common interpretation of the hydrodynamic purpose of the spur and groove systems, are considered as transportation pathways for detrital sediments, out of from carbonate systems (Rogers et al., 2013; Blanchon, 2011). The geometry of the spurs and groove structures are identified as relatively small scaled; the spurs are considered to have an average length perpendicular to the shoreline of 5 – 150 m and a width of less than 10 m. The grooves are defined to have an average width of 1 – 100 m. (Blanchon, 2011; Rogers et al., 2013).



Figure 70 - Spurs and grooves at Sombrero Key Reef in the Florida Keys (Modified from Shinn, 2011; Image copyright of Mike Theiss).

The calculation of the vertical- and horizontal seismic resolution of the four areas exceeds the classical size of the spurs and groove structures. Nonetheless, the isochron maps of the SS 4 from area B presents structures, identified to have characteristic geometric shape of a spur and groove systems (Figure 71). Despite the similarity in the geometry, the scales of the structures on the Bjarmeland Platform are identified as much larger than the generalized spur and groove systems (Figure 71). The approximate size of the spurs structures in Area B, are hundreds of meter wide and kilometers long. The groove structures have a width scale in hundreds of meter and the length of the grooves are kilometers long (Figure 71). The spurs and groove system in the Barents Sea region is considered as unrealistic interpretation, and thus the geometric shape of SS 4 is caused by other processes, than being a spur and groove system. The second argument is the platform location where the system is located. The carbonate build-up system in Area B is interpreted as deposited in platform interior environment, thus, not in a fore reef zone where spur and groove system develop.

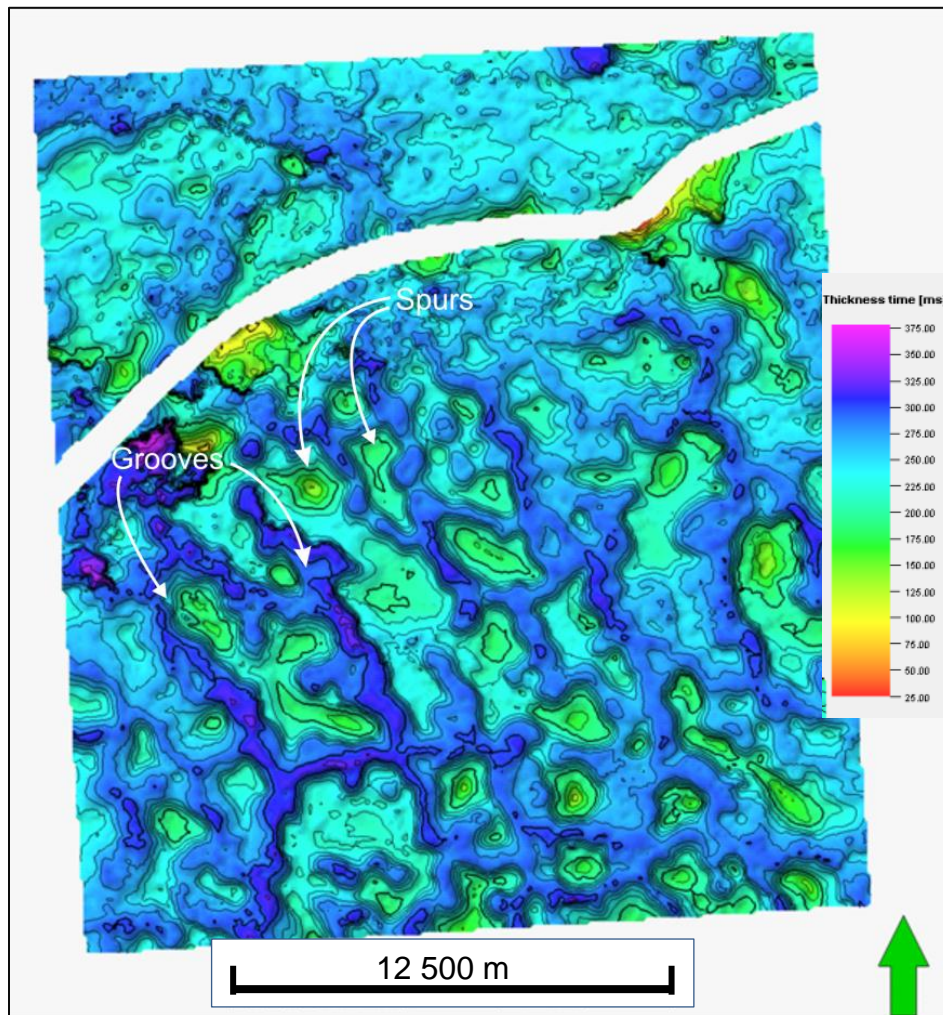


Figure 71 - Example of the possible spur and groove system on the Bjarmeland Platform.

6.2.3 Biotic Self-organization

Biotic self-organization has been considered as one of the possible controlling factors for development of reticulated carbonate build-up systems in Holocene reef systems (Schlager and Purkis, 2014). Ecological studies of several modern treeline systems in peatland, savanna and arid climatic environments, reveals that treeline networks develops due to self-organizing (Rietkerk and Van de Koppel, 2008; Baudena and Rietkerk, 2013). The interconnected tree networks identified from peatlands in Western Siberia reveals a development of cell-shaped structures, which consists of shrubs encircled by reticulated ridges of trees (Rietkerk et al., 2014). The self-organizing of tree systems has been interpreted as governed by limiting influx of nutrition, where the reticulated structures grow perpendicular to the flow direction of the groundwater (Rietkerk et al., 2004). The impact and effect of autocatalysis as an important controlling factor in biotic self-organizing, process of autocatalysis in ecology relates to the configuration of two or more processes where the product itself is the catalyst for the reaction (Ulanowicz, 2008). The result of autocatalyst in ecological systems relates to the development of patterns described as ‘Turing patterns’, which is caused by the relationship between activator-inhibitor systems is caused by the different rates of diffusion (Figure 72A; Turing, 1953). This means that when the inhibitor system diffuses faster than the activator, the system results in development of spatial patterns. Vice versa, when the activator diffuses faster than the inhibitor system, the resulting effect is development of reticulated patterns (Turing, 1953; Siteur et al., 2014). There is therefore a resemblance between development of Turing patterns, and the system dependency on feedback into the system (Figure 72; Siteur et al., 2014). That is, the positive feedback is dominating in the short distances, and negative feedback at longer distances (Figure 72B; Figure 72C).

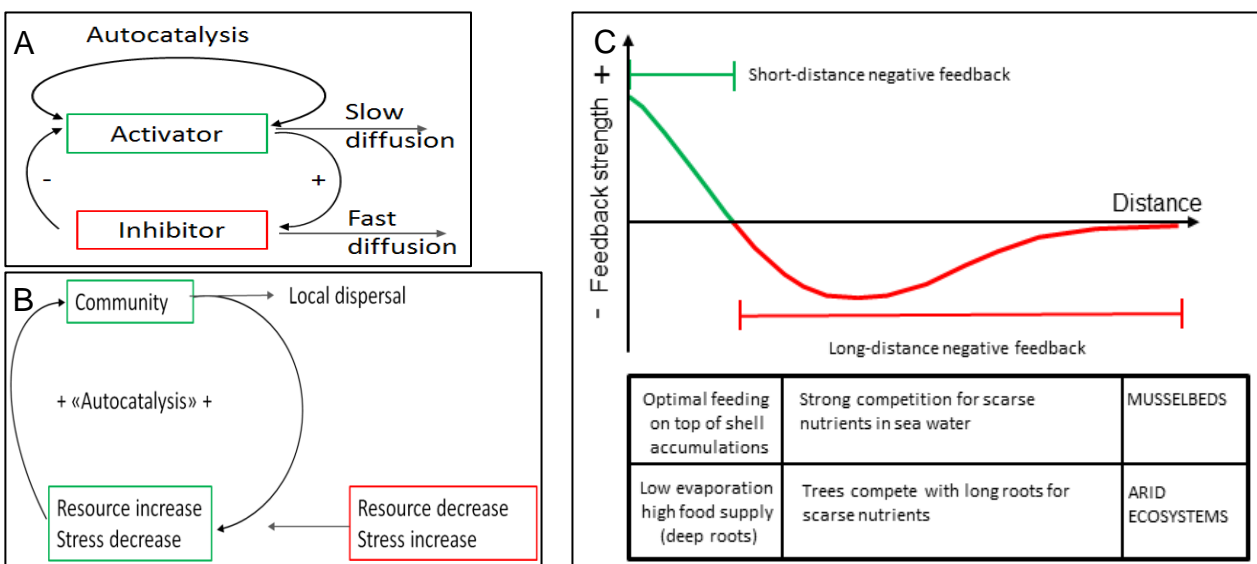


Figure 72 – A) Autocatalysis in activator-inhibitor system; B) Impact of autocatalysis on the scale dependent feedback in ecological systems; C) Biotic self-organization of musselbeds and treeline systems. The red- and green lines represent the model of long- and short-distance facilitation (Modified from Rietkerk and Van de Koppel, 2008; Schlager and Purkis, 2014).

The system-internal feedback resulting in self-organization is a plausible cause for the development of reticulated carbonate build-up ridges in the lagoon environmental setting. The self-organizing pattern is developed to infer nutrition, fresh-oxygen and water into the biota systems. These self-organizing systems are interpreted as presenting significant resemblance with the organization of cell-shaped treeline ridges in Western Siberia, the reticulated pinnacle reefs systems in Mataiva Island, and the carbonate build-up network in the platform interior environment located in Area A, in the Barents Sea (Figure 73; Rietkerk et al., 2004). The dimensions between the treeline systems in Western Siberia and the reticulated carbonate systems in Mataiva Island, and in Area A differ. The Siberian treeline system that is in meter scale has significantly smaller diameter, compared with the two carbonate systems, which both are in kilometer scale (Figure 73). Despite the scale differences between the different systems, the morphology of systems has a remarkable resemblance. The resemblances between the three systems are linked to the development of Turing patterns, caused by distance related feedback in the systems (Figure 73; Figure 72; Turing, 1953).

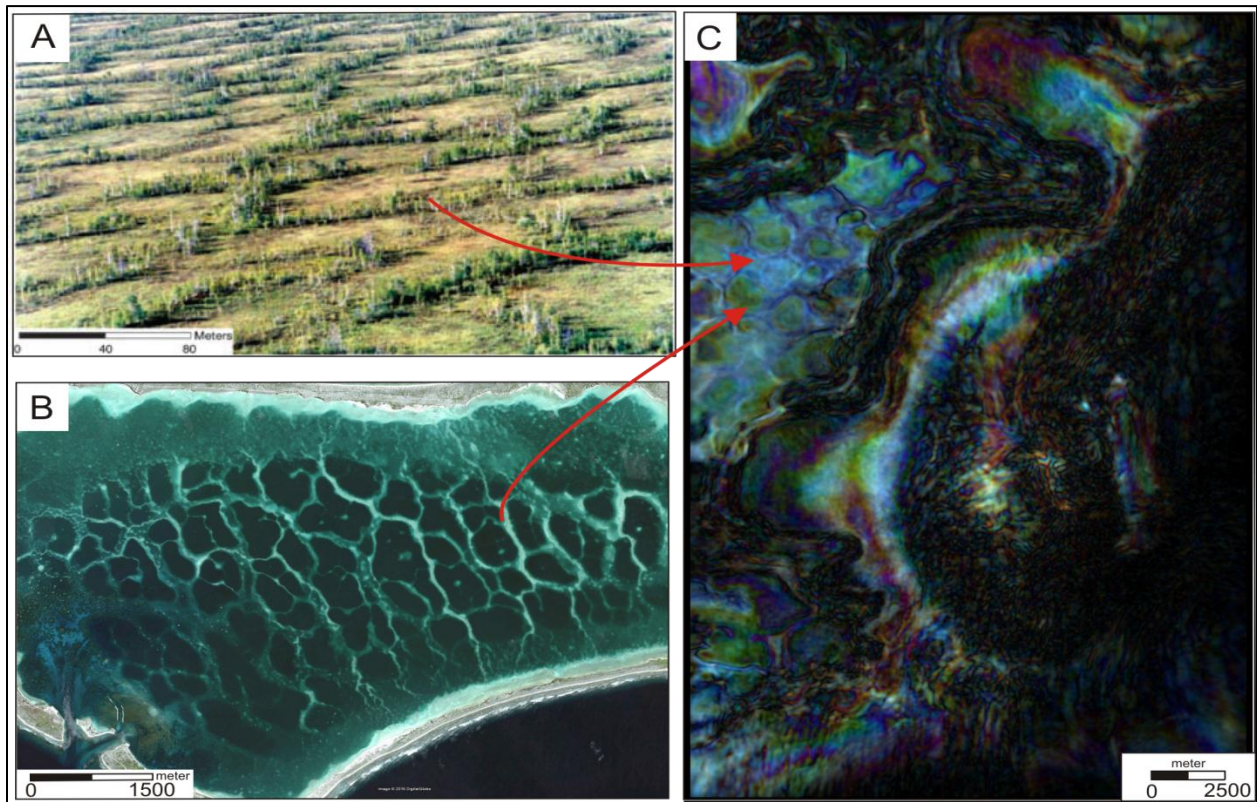


Figure 73 - Comparison of maze pattern networks of trees, and shrubs versus reticulated carbonate build-up systems. A) Tree networks in Western Siberia; B) Reticulated reefs in Mataiva Island, C) Reticulated carbonate build-ups, Bjarmeland Platform. (Figure A is modified from Rietkerk et al., 2014)

6.3 Evaporite as Controlling Factor on Carbonate Build-up Development

Several factors and mechanisms can trigger the mobility of salt. Tectonic impact is acknowledged as the most profound triggering factors for remobilization of evaporites. Regional extension is emphasized as the common tectonic triggering effect. The impact of regional extension has influenced the initiation and growth-shape of the salt structures (Jackson and Vandeville, 1994; Ge et al., 1997). The triggering effect of salt remobilization affected by differential loading are noticed more often, although the impact and of loading has been given less attention compared to the tectonic influence (Ge et al., 1997).

Differential loading are recognized as affected by lateral variations in thickness, and density of the sediments superposed on the evaporite layer. The effect of differential loading causes two different deformation patterns, occurring independently or together (Ge et al., 1997). The first deformation pattern a termed expulsion rollover. These structures are created by differential loading, affected by progradation of terrigenous clastic systems, for example, delta or alluvial fan systems (Ge et al., 1997). The kinematics of a prograding system results in differential loading on the basal salt layer and thus, the progradation of terrigenous sediments trigger the remobilization of evaporite layer (Ge et al., 1997). The second deformation pattern develops where the thickest part of the overlying sedimentary layer, sinks into the basal evaporite unit; therefore results in lateral expulsion of evaporites (Ge et al., 1997). This result in vertical thinning of the evaporite unit subjected to loading effects, developing salt weld structures. The laterally evacuated evaporite succession creates salt tectonic structures (e.g. salt pillow and salt stocks).

The salt tectonic component affecting the Barents Sea region is highly recognized in the Nordkapp Basin that comprises of large salt diapiric structures (e.g. Nilsen et al., 1995). The salt tectonic structures in the Nordkapp Basin with development of salt diapirs are evidences of precipitation of halite within the evaporite succession deposited during this period (Nilsen et al., 1995). The impact of mobile evaporite units within the Gipsdalen Gp., on the Bjarmeland and Finnmark Platforms is, however, hitherto undescribed. The result chapter of this study identify the relationship between the evaporitic sequences, defined in this study as SS 3, and the carbonate build-up succession, defined as SS 4 (e.g. Figure 30; Figure 31; Figure 52). The described layered evaporite sequence is interpreted as deposited on the platform interior and in the Nordkapp Basin, during a multiple periods of glacio-eustatic sea-level lowstand in the Pennsylvanian. The evaporite deposits confined to the platform interior settings has been described as gypsum and anhydrite rich and thus, considered to be immobile (e.g. Samuelsberg et al., 2003).

The Area B and D located on the Bjarmeland and Finnmark Platforms presents the distinctive relationship between the evaporite and carbonate sequences (Figure 8). The coherence between these sequences, are a general thickening and thinning succession (e.g. Figure 52). Figure 52 show the characteristic relationship between SS 2 and SS 3. The SS 3 are presented as thick

mounded feature, opposed to the underlying SS 2 unit, which is thin. In contrary, where the SS 3 succession is thin, underlying evaporitic SS 2 succession is shown as thick pockets (Figure 52). The isochron maps from Area B calculated of the two different sequences illustrates the distinct relationship between the thickening and thinning. Comparison of Figure 74A and Figure 74B, demonstrates the locations where the evaporite succession is thick in the isochron map of SS 2, is resulting in a considerably thin succession of SS 3 in the similar locations. Vice versa, where the isochron map of SS 2 is thin, the isochron map of SS 3 shows a recognizable thickening (Figure 74).

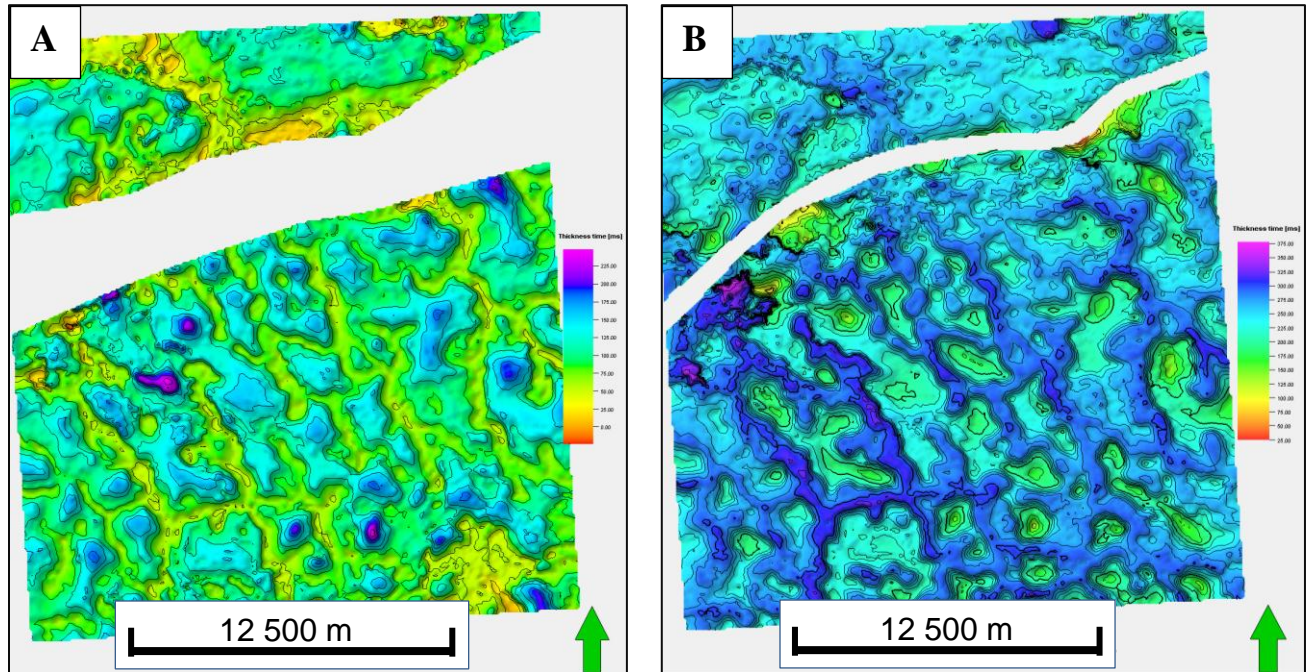


Figure 74 - The thickness variations of evaporite and carbonates. A) The isochron map of Seismic Sequence 2 (adapted from Figure 34); B) The isochron map of Seismic Sequence 3 (taken from Figure 36).

The thickness relationship of the SS 2 and SS 3 successions was initially interpreted as an evaporitic control on the deposition and distribution of carbonate build-ups. This interpretation was strengthening by the observations, show that the carbonate build-ups are thick in the areas where the evaporitic successions are thin. The interpretation of relationship were that the non-evaporitic conditions developed more favorable conditions for the carbonate fauna grow, opposed to the more saline evaporitic conditions.

The favorable interpretation of the carbonate versus evaporite relationship is salt tectonics, and effectively differential loading. The loading effect is interpreted as affecting layered evaporite sequence, resulting in remobilization. The differential loading resulted in evacuation of SS 2, and consequently created of salt weld and salt pillow structures (Figure 75). The continuous growth of the carbonate successions on the topographic highs created by the carbonate build-up complex, resulted in thick accumulation of carbonates build-ups, compared to the lateral side consisting of thinner successions of SS 3.

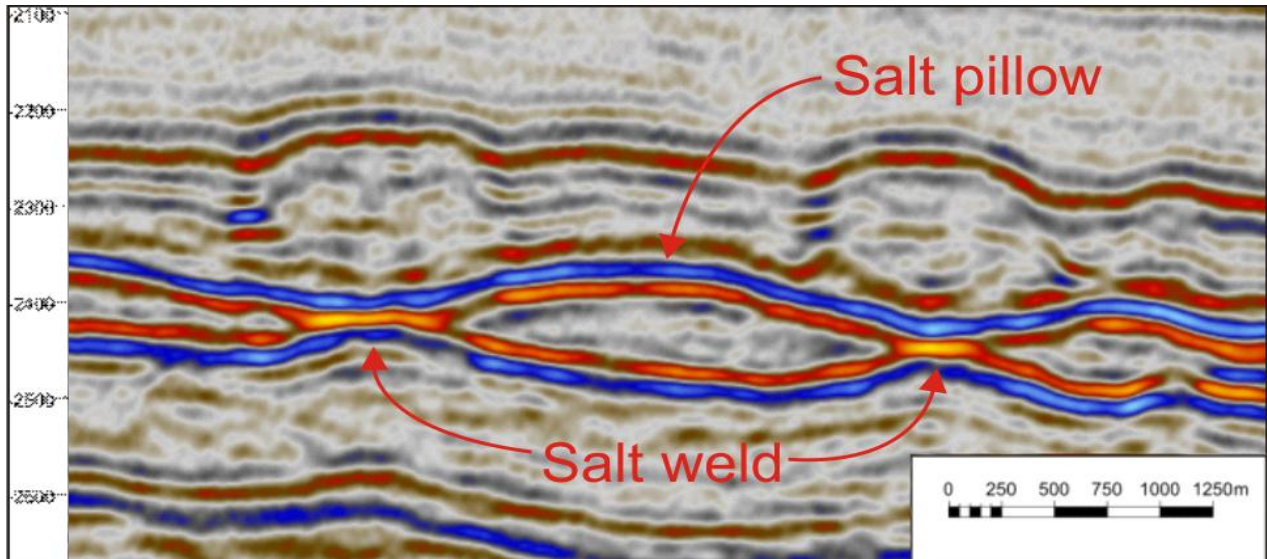


Figure 75 - Development of salt weld and salt pillow structures caused by differential loading effects. The expelled salt migrates into the salt pillow structure, while salt weld structures develop in the areas where the salt discharged.

The enhanced effect of the differential loading was affected by differences in the stress field, which developed on the undulating mobile evaporite surface (Lou et al., 2013). Simultaneously as the salt pillow grew, the overlying SS 3 succession started too convex. Contrarily, vertically above the thinner evaporitic SS 2 succession, the carbonate build-up succession started to concave. The concave and convex development of the carbonate sediments on top of the undulating evaporitic surface resulting in changes in stress field of the SS 3 succession (Lou et al., 2013). The stress field is increased vertically above the salt weld structure, and decreases above the salt pillow. This results in contraction of the carbonate build-up structure vertically above the thin salt succession, and consequently extension vertically above the thick evaporite unit (Figure 76).

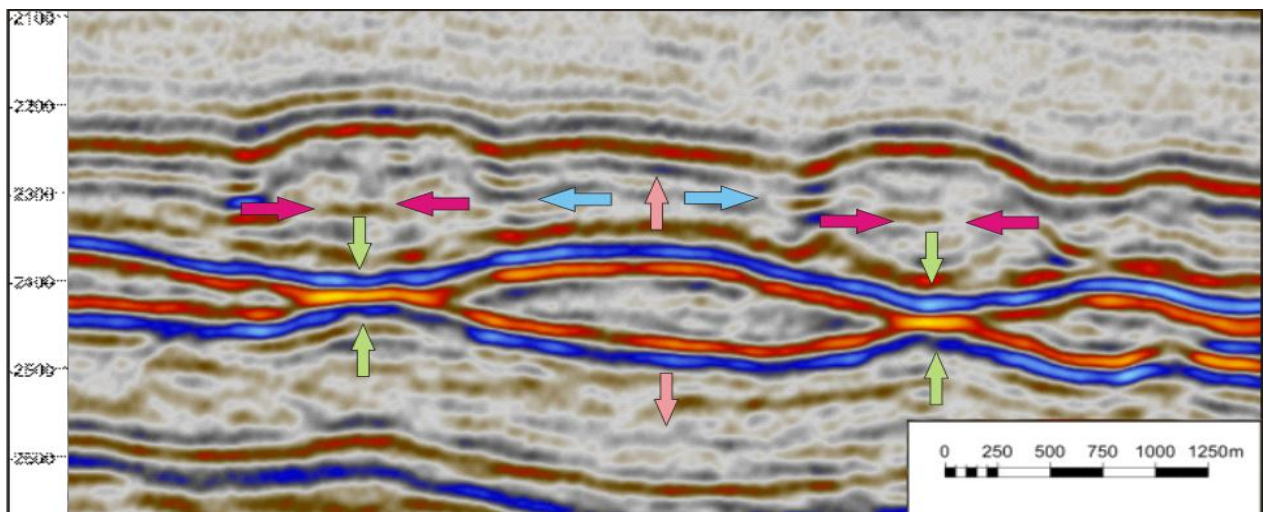


Figure 76 - Differences in stress contraction and extension affecting the differential loading of the mobile evaporite unit (Modified from Lou et al. 2013).

The differences in the salt weld and salt pillow structures are identified by in the RMS amplitude map of SS 2. The RMS amplitude map of the SS 2 define the salt weld structures as areas with high amplitudes, and the salt pillow structures as the adjacent low amplitude zones (Figure 77). The internal reflectivity and low resolutions within salt pillow structures coincide with the observations identified on the seismic section of the salt pillow structures (Figure 76; Figure 77).

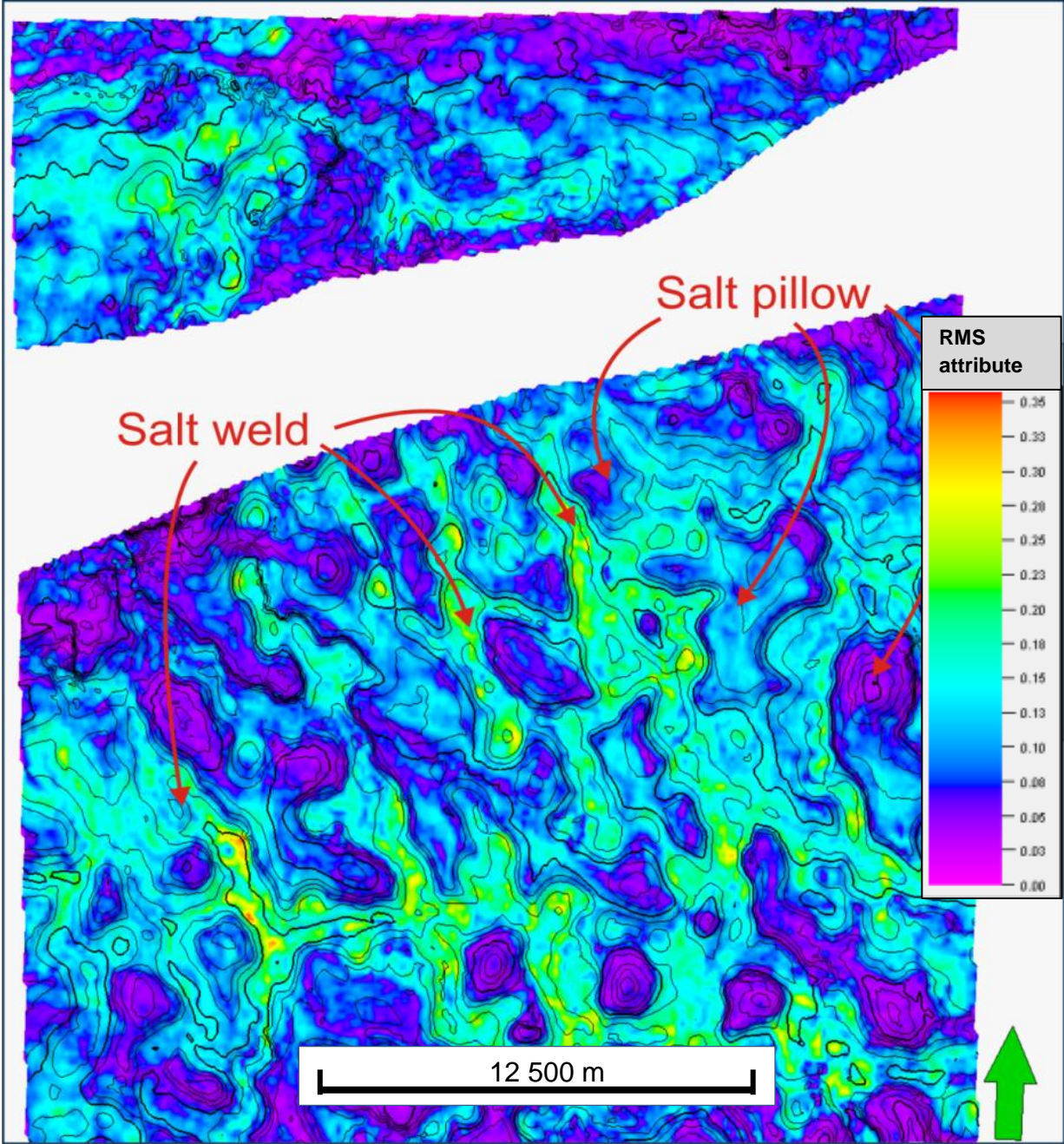


Figure 77 - The RMS Amplitude map of SS 2 presenting the different salt tectonic structures (i.e. salt weld and salt pillows structures).

7. Conclusions

The study was set out to explore the Upper Paleozoic carbonate succession in the south west Barents Sea. The study has identified the differences in carbonate geomorphology and characteristics, as well as characterizing the nature and type of the main controlling factors. The research objectives this thesis were; (1) to determine, compare, and contrast geomorphological and characteristics of the carbonate succession on the Bjarmeland and Finnmark Platforms, (2) to quantify and describe the differences and similarities of the carbonate geomorphology in the units on the Bjarmeland- and Finnmark Platforms (3) determine the physical controlling factors on the distribution of the carbonate build-up development, and lastly (4) examine the impact of evaporite deposits on the development distribution of the carbonate build-up development.

The Bjarmeland Platform environment has been interpreted as a part of a large epeiric platform stretching from Greenland to Timan-Pechora. The Nordkapp Basin situated between the Bjarmeland and Finnmark Platform, and occurs as a basin for the two platforms. Hence the platform morphology of the Bjarmeland Platform is defined as a rimmed shelf oriented towards the basin (Figure 78A). The southern part of the platform consists of a large barrier reef complex. The initial phase of the carbonate build-up system was triggered by growth on paleo-topographic structures developed by normal faulting in the Late Devonian-Mississippian. The carbonate morphology with development of reticulated carbonate build-ups in the lagoonal environment, are interpreted as created by a combination of biotic self-organization and antecedent karst-induced structures. The glacio-eustatic sea-level fluctuation resulted in numerous periods of highstand and lowstand sea-level and thus, resulted numerous periods of karstification and carbonate growth. The carbonate build-up succession on the Finnmark Platform is interpreted as primarily governed by the antecedent topography, developed by the tectonic events in the Mississippian with development of structural highs on footwall uplifted blocks (Figure 78B). The carbonate geomorphology is caused by the influence of topography antecedent-karst systems.

The synchronous geological time period that defines the different seismic sequences develops the framework for the interpretation of the regional depositional model in the south central Barents Sea region (Figure 78). The hinterland is situated in the current location of mainland Norway during the period of SS 2 and SS 3. The depositional map of SS 2 presents a period of overall regional sea-level regression, hence resulting in subaerial exposure and karstification of the carbonate build-ups on both platforms. Lowstand sea-level also resulted in deposition of evaporites along parts of the two platforms, and thick basinal evaporites in the Nordkapp Basin (Figure 78A). The regional depositional map of SS 3 presents an period of regional sea-level transgression and therefore, causing development of carbonate build-ups on the pre-seated karstified carbonate structures located on the structural highs, and development of fine-grained limestone in the open marine and platform interior environments (Figure 78B).

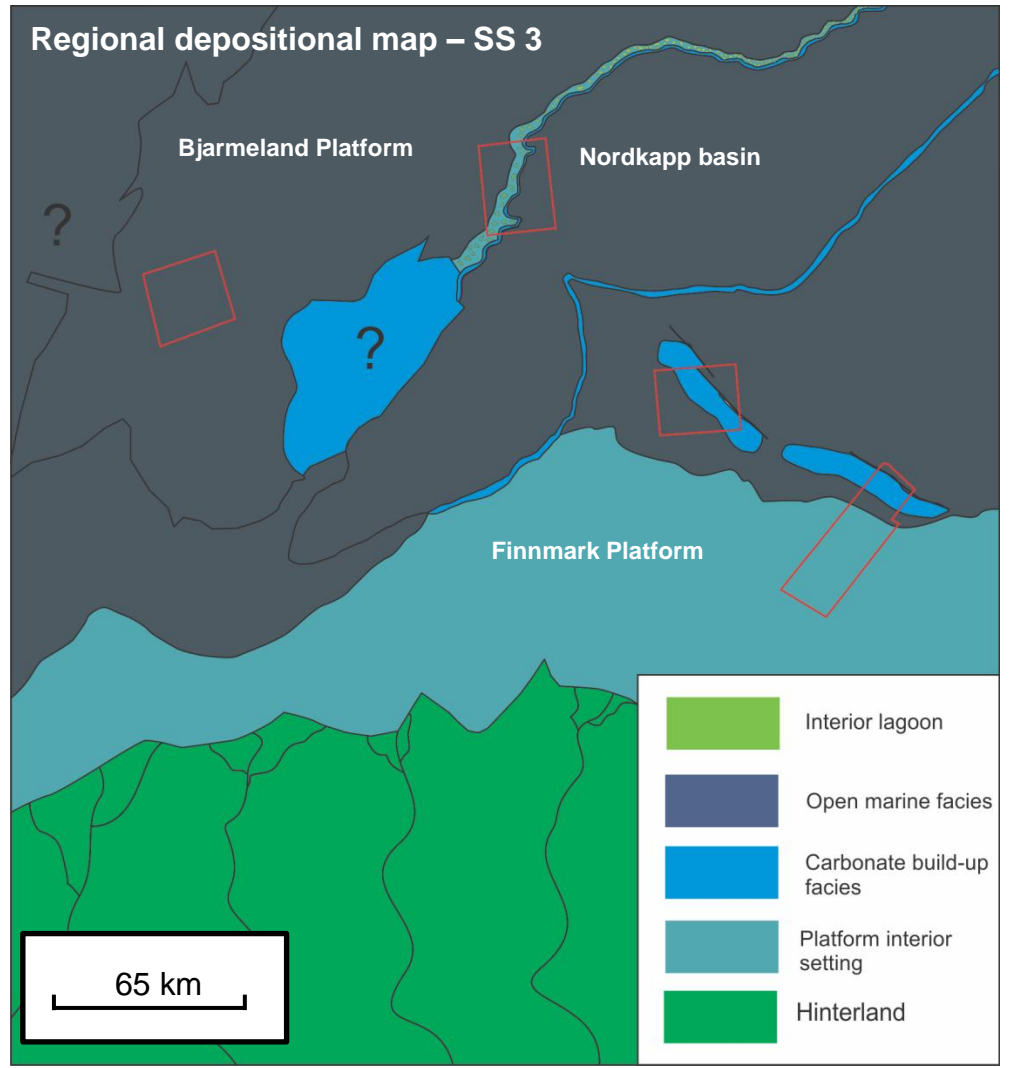
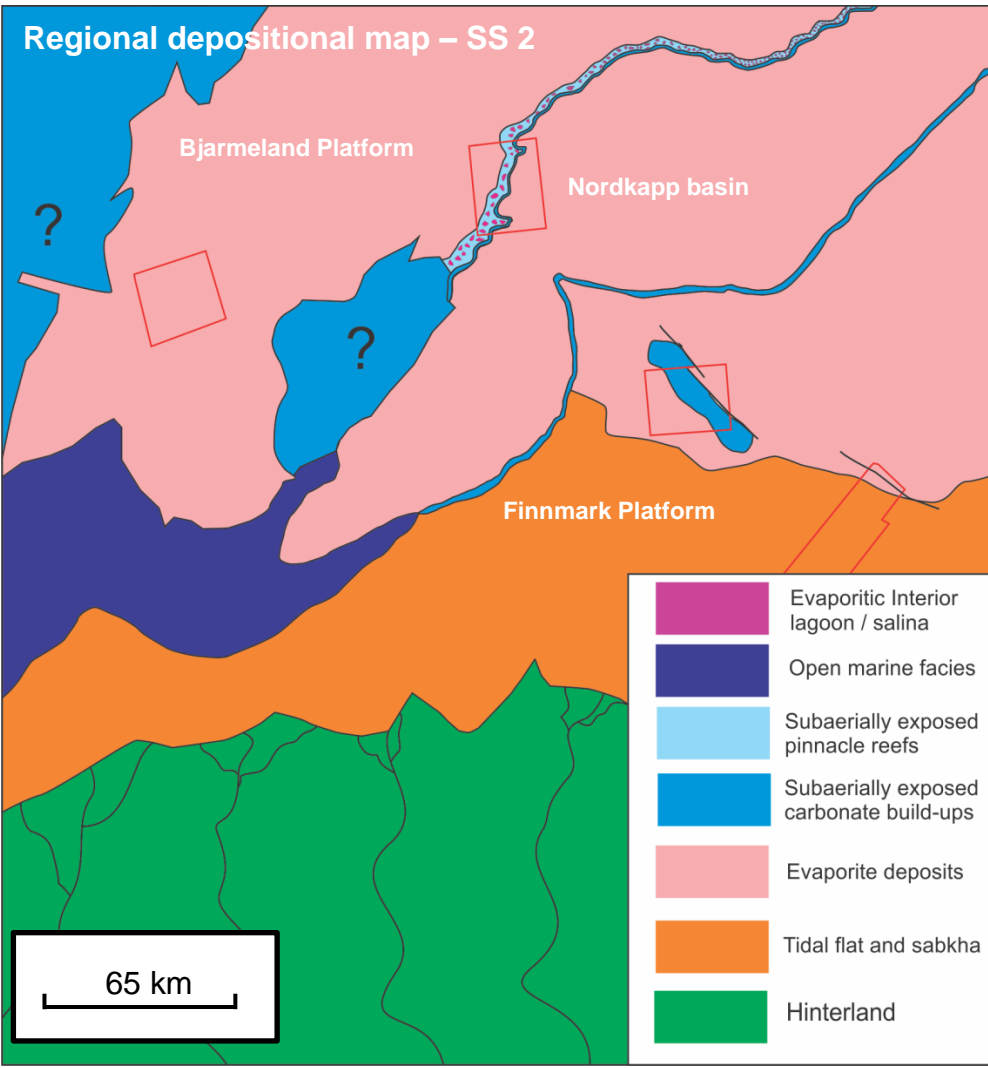


Figure 78 - Regional depositional model of the south central Barents Sea. A) Depositional model of Seismic Sequence 2; B) depositional model created for Seismic Sequence 3.

This section synthesizes the empirical results obtained to address the main research objectives addressed for this thesis project.

1. What is considered as the main controlling factor affecting the carbonate build-up development?

The principal factor for controlling the development of the carbonate build-up succession is considered as antecedent topography. The initial phase of the carbonate succession is an inheritance of topography developed by paleo-highs structures. The following phase presents the development of the carbonate geomorphology. The carbonate morphology is interpreted as primarily controlled by antecedent karst topography, created during the periods of glacio-eustatic sea-level lowstand. The evidences for the antecedent karst topography as the only physical controlling factor for the carbonate geomorphology are circumstantial. On this basis, the impact of biotic self-organizing within the carbonate build-up systems is interpreted as being an important influence contributing to the carbonate build-up development.

The dominant and controlling factor for the development of the carbonate build-ups, on both the Bjarmeland and Finnmark Platforms are considered as a combination of antecedent topographic highs, hydrodynamic controls and seafloor bathymetry.

2. Are there any significant similarities between the carbonate build-up succession on the Bjarmeland Platform and the Finnmark Platform?

The carbonate successions on the Bjarmeland and Finnmark Platforms share the similarities related to the structural elements and the antecedent topographic control. The carbonate build-up successions are most profound in the areas subjected to ancient tectonic events resulting in paleo-high structures present during deposition of the carbonate succession. Because of this, areas not subjected to structural components, demonstrate little to no growth of carbonates build-ups, and rather result in deposition of platform interior facies and evaporite precipitation.

3. Does the layered evaporite sequence control the distribution and development of the carbonate build-up succession?

The impact of the underlying evaporite on the carbonate build-up successions, in regards to the distribution and development, is considered negligible or non-existing. The growth of thick carbonate build-up accumulation, vertically above thin parts of an evaporite sequence, is related to differential loading of the carbonate on the mobile layered evaporite unit. This implies that during the loading of the evaporite unit, and the following subsidence, the carbonate build-ups continued their growth on the paleo-topography, in which resulted in thick successions of carbonate build-ups. The lateral effects of the evaporite expulsion, beneath the carbonate build-up succession, resulted in pillow-shaped structures of mobile evaporite, developed adjacent to the build-up succession.

8. References

- Ahlborn, M., L. Stemmerik, and T.-K. Kalstø, 2014, 3D seismic analysis of karstified interbedded carbonates and evaporites, Lower Permian Gipsdalen Group, Loppa High, southwestern Barents Sea: *Marine and Petroleum Geology*, v. 56, p. 16-33.
- Baudena, M., and M. Rietkerk, 2013, Complexity and coexistence in a simple spatial model for arid savanna ecosystems: *Theoretical Ecology*, v. 6, p. 131-141.
- Beauchamp, B., 1994, Permian climate cooling in the Canadian Arctic: *Geological Society of America, Special Paper*, 288, p. 299-246.
- Beauchamp, B., B. Olchowy, 1994, Early Permian buildups (Tolkien reefs) associated with subaqueous evaporites, Canadian arctic: a record of syn-tectonic to post-tectonic reciprocal uplift and subsidence, *in* Permo-Carboniferous Carbonates Platforms and Reefs. SEPM – Society of Sedimentary Geology, Special Publication, 78, p. 133-153.
- Beauchamp, B. and A. Desrochers, 1997, Permian warm- to very cold-water carbonates and cherts in northwest Pangea, *in* N. P. James and J. A. D. Clarke, eds., *Cool-water carbonates: SEMP - Society for Sedimentary Geology, Special Publication*, 56, p. 327-347.
- Bice, D. M., 1991, Computer simulation of carbonate platform and basin systems: *Kansas Geological Survey, Bulletin* 233, p. 431-447
- Blakey, R., 2011, Paleogeography and geological evolution of the earth, rectangular global maps: Colorado Plateau Geosystems, Inc., <http://cpgeosystems.com/mollglobe.html> (assessed January, 21, 2014).
- Blanchon, P., 2011, Geomorphic Zonation, *in* D. Hopley, ed., *Encyclopedia of Modern Coral Reefs: Encyclopedia of Earth Sciences Series*, Springer Netherlands, p. 469-486.
- Blendinger, W., B. Bowlin, F. R. Zijp, G. Darke and M. Ekroll, 1997, Carbonate buildup flank deposits: an example from the Permian (Barents Sea, northern Norway) challenges classical facies models: *Sedimentary Geology*, 112, p. 89-103.
- Brown, A. R., 2011, *Interpretation of Three-Dimensional Seismic Data, Seventh Edition: AAPG Memoir 42, 7th Edition/SEG Investigation in Geophysics, No. 9*, Published jointly by American Association of Petroleum Geologists and the Society of Exploration Geophysicists.

- Bugge, T., G. Mangerud, G. Elvebakk, A. Mork, I. Nilsson, S. Fanavoll, and J. O. Vigran, 1995, The Upper Palaeozoic succession on the Finnmark Platform, Barents Sea: *Norsk Geologisk Tidsskrift*, v. 75, p. 3-30.
- Carrillat, A., Hunt, D., Randen, T., Sonneland, L., and Elvebakk, G., 2005, Automated mapping of carbonate build-ups and paleokarst from the Norwegian Barents Sea using 3D seismic texture attributes, *in* Doré, A. G., and Vining, B. A., eds., *Petroleum Geology: North-West Europe and Global Perspectives*, Proceedings of the 6th Petroleum Geology Conference: London, Geological Society, p. 1595-1611.
- Chappell, J., 1980, Coral morphology, diversity and reef growth: *Nature*, 286, p. 249 – 252.
- Chidsey, T. C. J., and D. E. Eby, 1996, Geological and reservoir characterization of shallow-shelf carbonate fields, Southern Paradox Basin, Utah, *in* A. C. Huffman, Jr., W. R. Lund, and L. H. Godwin, *Utah Geological Association Guidebook: Utah Geological Association*, p. 39 – 56.
- Chidsey, T. C. J., and D. E. Eby, 2003, Heterogeneous shallow-shelf carbonate buildups in the Paradox basin, Utah and Colorado: Targets for increased oil production and reserves using horizontal drilling techniques: *Utah Geological Survey*, p. 1- 29.
- Colpaert, A., N. Pickard, J. Mienert, L. B. Henriksen, B. Rafaelsen and K. Andreassen, 2007, 3D seismic analysis of an Upper Paleozoic carbonate succession of the Eastern Finnmark Platform area, Norwegian Barents Sea: *Sedimentary Geology*, 197, p. 79-98.
- Darwin, C., 1842, *On the structure and distribution of coral reefs*, Walter Scott, London, p. 214.
- Di Lucia, M., J. Sayago, G. Frijia, M. Mutti, C. Cotti, A. Sitta, 2014, Facies and seismic analysis from the Late Carboniferous-Early Permian Finnmark Carbonate Platform (Southern Norwegian Barents Sea): A assessment of the carbonate factories and depositional geometries: *AAPG Bulletin*, Submitted.
- Dodson, P., 2014, Technology Explained - Completing the Picture: *Geo ExPro*, v. 11, p. 92 - 96.
- Elvebakk, G., D. W. Hunt and L. Stemmerik, 2002, From isolated buildups to buildup mosaics: 3D seismic shed new light on the upper Carboniferous-Permian fault controlled carbonate buildups, Norwegian Barents Sea: *Sedimentary Geology*, 152, p. 7-17.
- Ehrenberg, S. N., E. B. Nielsen, T. A. Svånå, and L. Stemmerik, 1998a, Depositional evolution of the Finnmark carbonate platform, Barents Sea: results from wells 7128/6-1 and 7128/4-1: *Norsk Geologisk Tidsskrift*, v. 78, no. 3, p. 185-224.

- Flügel, E., 2004, *Microfacies of Carbonate rocks, Analysis, Interpretation and Application*: Springer Verlag, Berlin, p. 976.
- Ford, D., and W. Paul, 1989, *Karst Hydrogeology and Geomorphology*: Wiley-Blackwell, 576 p.
- Frakes, L. A., J. E. Francis, J. I., Syktus, 1992, *Climate Models of the Phanerozoic*: Cambridge University Press, Cambridge, pp. 274.
- Gabrielsen, R. H., R. B. Færseth, L. N. Jensen, J. E. Kalheim, and F. Riis, 1990, Structural elements of the Norwegian continental shelf: *NPD Bulletin*, v. 6, p. 1-32.
- Ge, H., M. P. A. Jackson, and B. C. Vendeville, 1997, Kinematics and dynamics of salt tectonics driven by progradation: *AAPG Bulletin*, v. 81, p. 398-423.
- Genin, A., S. G. Monismith, M. A. Ridenbach, G. Yahel, J. R. Koseff, 2009, Intense benthic grazing in a coral reef: *Limnol. Oceanogr.*, v. 54, 3, p. 938 – 951.
- Gischler, E., D. Storz, and D. Schmitt, 2014, Sizes, shapes, and patterns of coral reefs in the Maldives, Indian Ocean: the influence of wind, storms, and precipitation on a major tropical carbonate platform: *Carbonates and Evaporites*, v. 29, p. 73-87.
- Henriksen, E., A. E. Ryseth, G. B. Larssen, et al., 2011, Chapter 10 Tectonostratigraphy of the greater Barents Sea: implications for petroleum systems: *Geological Society, London, Memoirs 2011*, 32, p. 163-195.
- Hoffmeister, J. E., and H. S. Ladd, 1945, Solution Effects on Elevated Limestone Terraces: *Geological Society of America Bulletin*, v. 56, p. 809-818.
- Jackson, M. P. A., and B. C. Vandeville, 1994, Regional extension as a geologic trigger for diapirism: *Geological Society of America Bulletin*, v. 106, p. 57 – 73.
- James, N. P., 1997, The cool-water depositional realm, *in* N. P. James and J. A. D. Clarke, ed., *Cool-water carbonates: SEMP – Society of Sedimentary Geology, Special Publication*, 56, p. 1-20.
- Johannessen, E. P., R. J. Steel, 1992, Mid-Carboniferous extension and rift-infill sequences in the Billefjorden Through, Svalbard: *Norwegian Journal of Geology*, v. 72, p. 35-48.

- Jones, N. P. and A.C. Kendall, 1992, Introduction to carbonate and evaporite facies models. *In* R. G. Walker and N. P. James, *Facies Models – response to sea level change*: Geological Association of Canada, Ontario, p. 265-275.
- Keary, P., M. Brooks and I. Hill, 2002, *An Introduction to Geophysical Exploration – 3rd edition*, Blackwell Science Ltd, Oxford, p. 262.
- Larssen, G. B., G. Elvebakk, L. B. Henriksen, S-E. Kristensen, I. Nilsson, T. J. Samuelsberg, T. A. Svånå, L. Stemmerik and D. Worsley, 2002, Upper Palaeozoic lithostratigraphy of the Southern Norwegian Barents Sea: *NPD Bulletin*, v. 9, p. 76, 63 figs., 1 tbl.
- Larssen, G.B., Elvebakk, G., Henriksen, L.B., Kristensen,, S.-E., Nilsson, I., Samuelsberg, T.J., Svånå, T.A., Stemmerik, L. Og Worsley, D., 2005, Upper Palaeozoic lithostratigraphy of the southern part of the Norwegian Barents Sea: *NGU Bulletin*, v. 444, p. 3-45.
- Lidz, B., E. Shinn, J. H. Hudson, H. G. Multer, R. Halley, and D. Robbin, 2008, Controls on Late Quaternary Coral Reefs of the Florida Keys, *in* B. Riegl, and R. Dodge, eds., *Coral Reefs of the USA: Coral Reefs of the World*, v. 1, Springer Netherlands, p. 9-74.
- Luo, G., M. A. Nikolinakou, P. B. Flemings, and M. R. Hudec, 2012, Geomechanical modeling of stresses adjacent to salt bodies: Part 1—Uncoupled models: *AAPG bulletin*, v. 96, p. 43-64.
- Loucks, R. G., C. Kerans and X. Janson, 2003, Platform-Margin, Slope, and Basinal Carbonate Depositional Environments: Bureau of Economic Geology online learning module, http://www.beg.utexas.edu/lmod/IOL-CM02/old_work/cm02-step01.htm (assessed January, 23, 2014).
- Maione, S. J., 2001, Discovery of ring faults associated with salt withdrawal basins, Early Cretaceous age, in the East Texas Basin: *The Leading Edge*, v. 20, p. 818-829.
- Monismith, S. G., 2007, Hydrodynamics of coral reefs: *Annual Review of Fluid Mechanics*, v. 39, p. 37 – 55.
- Nilsen, K. T., B. C. Vendeville, J.-T. Johansen, 1995, Influence of regional tectonics on halokinesis in the Nordkapp Basin, Barents Sea, *in* M. P. A. Jackson, D. G. Roberts, and S. Snelson, eds., *Salt tectonics: a global perspective*: AAPG Memoir 65, p. 413–436.
- Samuelsberg, T. J., G. Elvebakk, L. Stemmerik, 2003, Late Paleozoic evolution of the Finnmark Platform, southern Norwegian Barents Sea: *Norwegian Journal of Geology*, 83, p. 351-362.

- Sayago, J., M. Di Lucia, M. Mutti, A. Sitta, A. Cotti, G. Frijia, 2014, Late Palaeozoic seismic sequence stratigraphy and palaeogeography of the Loppa High in the Norwegian Barents Sea: *Marine and Petroleum Geology* - submitted.
- Schalger, W., 2005, *Carbonate Sedimentology and Sequence Stratigraphy: SEMP* - Society for Sedimentary Geology, Tulsa, Oklahoma, p. 206.
- Schlager, W., and S. Purkis, 2014, Reticulate reef patterns – antecedent karst versus self-organization: *Sedimentology*, v. 62, p. 501-515.
- Shinn, E., 2011, Spurs and Grooves, *in* D. Hopley, eds., *Encyclopedia of Modern Coral Reefs: Encyclopedia of Earth Sciences Series*, Springer Netherlands, p. 1032-1034.
- Simm, R. and R. White, 2002, Tutorial: Phase, polarity and the interpreter's wavelet: *First Break*, v. 20, p. 277-281.
- Siteur, K., E. Siero, M. B. Eppinga, J. D. Rademacher, A. Doelman, and M. Rietkerk, 2014, Beyond Turing: The response of patterned ecosystems to environmental change: *Ecological Complexity*, v. 20, p. 81-96.
- Stemmerik, L., G. Elvebakk, I. Nilsson, and S. Olausen, 1995, Comparison of upper Bashkirian-upper Moscovian high frequency cycles between Bjornoya and the Loppa High, western Barents Sea: *Sequence stratigraphy - concepts and applications*, p. 215-227.
- Stemmerik, L., G. Elvebakk, and D. Worsley, 1999, Upper Paleozoic carbonate reservoirs on the Norwegian Arctic Shelf: delineation of reservoir models with application to the Loppa High: *Petroleum Geoscience*, v. 5, p. 173-187
- Stemmerik, L., and D. Worsley, 2005, 30 years on; Arctic upper Palaeozoic stratigraphy, depositional evolution and hydrocarbon prospectivity: *Norwegian Journal of Geology*, v. 85, p. 151-168.

- Stemmerik L., 2008, Influence of Late Paleozoic Gondwana glaciations on the depositional evolution of the northern Pangean shelf, North Greenland, Svalbard, and the Barents Sea, *in* C. R. Fielding, T. D. Frank, and J. L. Isbell, eds., *Resolving the Late Paleozoic Ice Age in Time and Space: Geological Society of America Special Publication*, 441, p. 205–217.
- Turing, A. M., 1953, The chemical basis of morphogenesis, *Bulletin of Mathematical Biology*, v. 52, p. 153-197.
- Rey, P., J. P. Burg, and M. Casey, 1997, The Scandinavian Caledonides and their relationship to the Variscan belt: *Geological Society, London, Special Publications*, v. 121, p. 179-200.
- Rafaelsen, B., J. Pajchel, K. Hogstad, H. Robak and T. Randen, 2003, Upper Paleozoic carbonate build-ups in the Norwegian Barents Sea – New insights from 3-D seismic and automated facies mapping: Extended abstract, 65th EAGE conference & exhibition, Stavanger, June 2nd – 5th 2003.
- Rafaelsen, B., G. Elvebakk, K. Andreassen, L. Stemmerik, A. Colpaert and T. Samuelsberg, 2008, From detached to attached carbonate buildup complexes - 3D seismic data from the Upper Palaeozoic, Finnmark Platform, southwestern Barents Sea: *Sedimentary Geology*, 206, p. 17-32.
- Rankey, E. C., S. L. Reeder, and J. R. Garza-Pérez, 2011, Controls On Links Between Geomorphical and Surface Sedimentological Variability: Aitutaki and Maupiti Atolls, South Pacific Ocean: *Journal of Sedimentary Research*, v. 81, p. 885-900.
- Rietkerk, M., S. C. Dekker, P. C. de Ruiter, and J. van de Koppel, 2004, Self-Organized Patchiness and Catastrophic Shifts in Ecosystems: *Science*, v. 305, p. 1926-1929.
- Rietkerk, M., and J. Van de Koppel, 2008, Regular pattern formation in real ecosystems: *Trends in ecology & evolution*, v. 23, p. 169-175.
- Rogers, J. S, S. G., Monismith, F. Feddersen, C.D. Storlazzi, 2013, Hydrodynamics of spur and groove formations on a coral reef: *Journal of Geophysical Research*, v. 118, 6, p. 3059 – 3073.
- Rønnevik, H., B. Beskow, and J. H. P., 1982, Structural and stratigraphic evolution of the Barents Sea: *Canadian Society of Petroleum Geologists*, v. 8, p. 431-440.
- Puchkov, V. N., 2009, The evolution of the Uralian orogen: *Geological Society, London, Special Publications*, v. 327, p. 161-195.

- Purdy, E. G., and G. T. Bertram, 1993, Carbonate concepts from the Maldives, Indian Ocean: AAPG Special Volumes, 34, p. 1-55.
- Purkis, S. J., G. P. Rowlands, B. M. Riegl and P. G. Renaud, 2010, The paradox of tropical karst morphology in the coral reefs of the arid Middle East: *Geology*, v. 38, p. 227-230.
- Ulanowicz, R.E., 2008, Autocatalysis, *in* S. E. Jørgensen and B. D. Fath, eds., *Systems Ecology* Vol. 1 of *Encyclopedia of Ecology*, Oxford: Elsevier, v. 5, p. 288-290.
- Vail, P. R., 1987, Seismic stratigraphy interpretation procedure, *in* Bally, A.W., eds., *Atlas of seismic stratigraphy: AAPG Studies in Geology No. 27*, v. 1, p. 1-10.
- White, W. B., 2006, Groundwater Flow in Karstic Aquifers, *in* J. W. Delleur, eds., *The Handbook of Groundwater Engineering*, Second Edition, CRC Press, p. 21-47.
- Wright, V. P., and T. P. Burchette, 1998, Carbonate ramps: an introduction: Geological Society, London, *Special Publications*, v. 149, p. 1-5.

Appendices

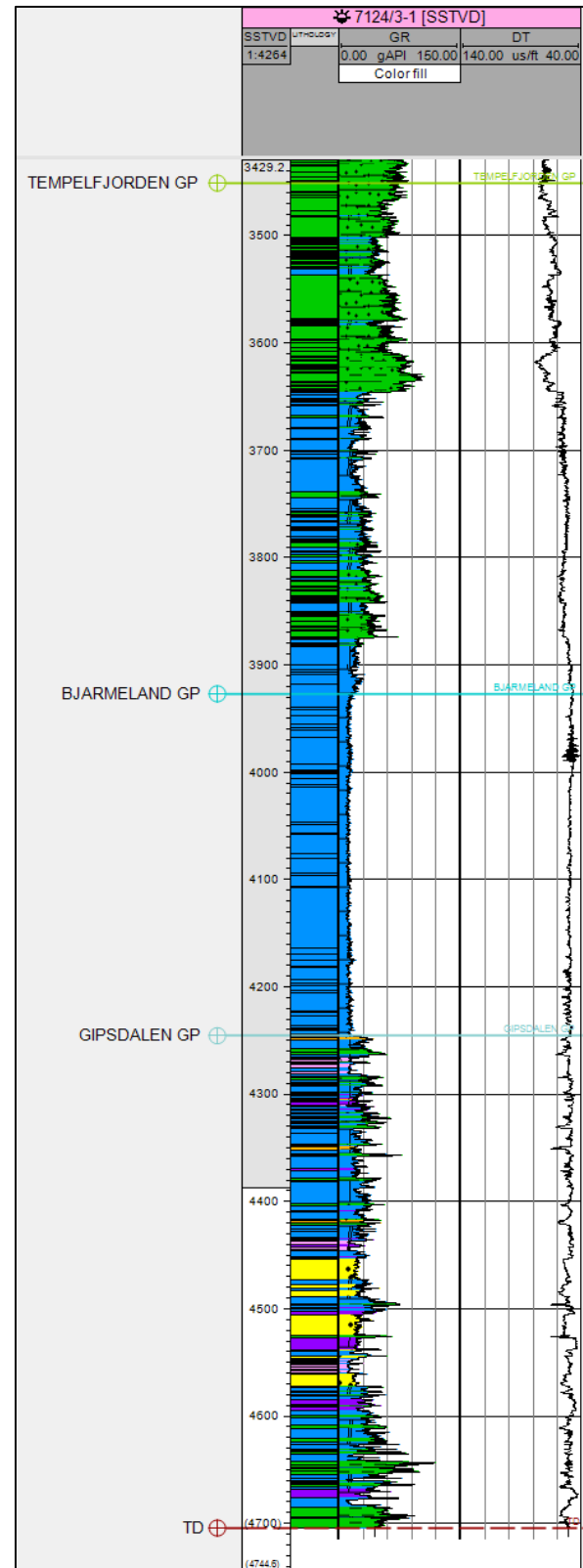
Appendix 1 - Well descriptions

Appendix 1.1 - Well 7124/3-1

The well logged down to a true vertical depth at 4705m and the deepest penetrated group was the Gipsdalen. The Gipsdalen Gp. was encountered at 4248m. The group can be divided in three different sections categorized based on difference in facies distribution. The lower succession (4705 – 4570m) consist of shale, dolomite and carbonate facies dominated facies. The response in the gamma ray shows an upward-decreasing trend toward the middle section (Figure 79). The middle section consists of three distinct sand bodies interbedded with carbonate and dolomite facies. The depositional trend shows a rhythmic pattern in depositional from sand-rich facies transitioning into carbonate and dolomite dominated facies (Figure 79).

The Bjarmeland Gp. is located at a depth of 4245 – 3928m. The carbonate succession in the well is homogenous and with a gamma ray response showing very low activity (Figure 79). The low changes in the gamma ray response feature a thick and continuous succession of carbonate deposits with similar facies characteristics.

The upper part of the Paleozoic succession encountered in the well is the Tempelfjorden Gp. The group is located at a true vertical depth of 3028 – 3451m. The section can be divided into three units. The lower unit (3028 – 3880m) is a carbonate unit with relatively small variations in the gamma ray response. The middle unit (3880 – 3640m) consists of shale and carbonate facies. The base of the unit is a shale unit followed by multiple series of shale and carbonate interlayering. The unit is identified as an overall upward-decrease in gamma ray response (Figure 79). The upper unit (3640 – 3451m) is dominated by siliciclastic shale-rich facies interlayered with some carbonates. The base of the unit is a thick succession of shale followed by an upward-decrease in the gamma ray response until 3535m, then followed by an upward-increase in the gamma ray response toward the top of the Tempelfjorden Gp. located at 3451m (Figure 79).



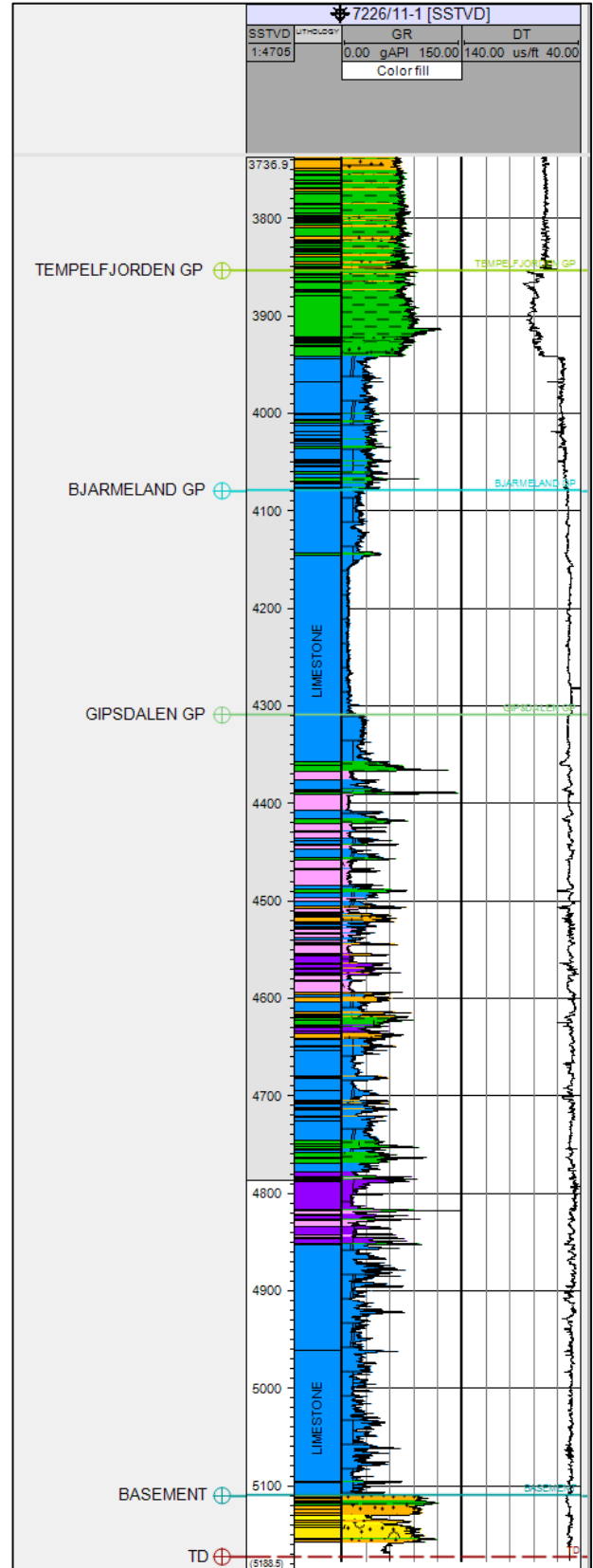
Appendix 1.1: Figure 79 - Well data of the Upper Paleozoic succession in well 7124/3-1.

Appendix 1.2 - Well 7226/11-1

The basement is encountered at a depth of 5104 m and stopped drilling at true-vertical depth of 5188.5m. The basement in the well is metamorphic and consists of schist with amphibolite rich facies. The basement rock is dated to be of pre-Devonian in age, sediments originated from the Caledonian Orogeny (Ehrenberg et al., 1998a).

The deposition of sediments between the pre-Devonian schist and the Pennsylvanian carbonate succession is eroded, and therefore resulted in hiatus of minimum 100 Ma. The carbonate succession is deposited directly overlying the Caledonian basement rock. The Gipsdalen Gp. is located at a depth of 5104 – 4310m. The succession can be divided into four different sections. The first section (5110 – 4780m) consists of an approximately 250m thick succession of shallow-water limestone facies followed by a roughly 40 m succession of dolomite with interlayered anhydrite (Figure 80). The second section (4780 – 4640m) is characterized by a base of siliciclastic shale units followed by a prominent carbonate facies with an upward-decrease in gamma ray response. The third section (4640 – 4370m) is characterized as a section with significant amount of sea-level fluctuations evident by the changes in sediment composition with anhydrite, carbonate, dolomite and shale (Figure 80). The fourth section (4370 – 4310m) is located on top of a major flooding surface with a 10 m shale succession followed by a 50m thick carbonate section with uniform gamma ray response, suggesting similar carbonate facies.

The Bjarmeland Gp. is located at a depth of 4310 – 4080m. The group can be divided into two different sections with different characteristics in the gamma ray response. The lower section (4310 – 4150m) consists of a homogenous carbonate succession evident by the uniform gamma ray response. The



Appendix 1.2: Figure 80 - Well data of the Upper Paleozoic succession in well 7226/11-1.

upper section (4150 – 4080) is identified as a carbonate succession with relatively uniform gamma ray response but with higher values than those observed in the lower section. The base of the section is a shale unit that is representing a flooding surface, the shale unit is also defining a change in facies composition into a carbonate system represented by a higher gamma ray values (Figure 80).

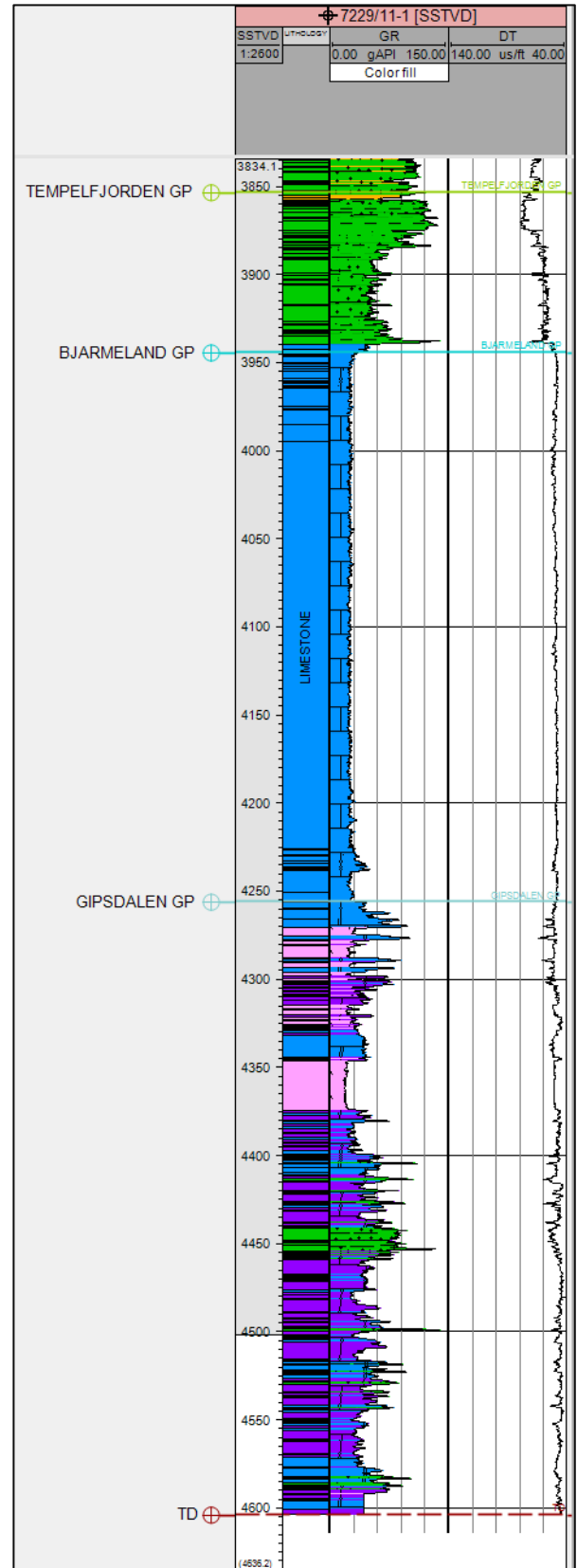
The Tempelfjorden Gp. is located at a depth of (4080 – 3854m). The group is divided into two main sedimentary units; the lower unit is a carbonate facies and the upper unit is shale dominated (Figure 80). The lower unit (4080 – 3940m) consists of a relatively heterogeneous carbonate succession with some thin interlayering of shales. The upper unit is separated from the lower unit by a drowning unconformity defining a facies change into a deeper-marine environment with significantly higher siliciclastic influxes opposed to the lower unit (Figure 80).

Appendix 1.3 - Well 7229/11-1

The well has been drilled to a true vertical depth of 4605m with the deepest penetrated group being the Gipsdalen Gp. The Gipsdalen Gp. is defined into two different units; lower unit from 4605 – 4440m, and upper unit 4440 – 4255m 8 (Figure 81). The lower unit is characterized by carbonate and dolomite facies, with some interlayering of shale. The upper unit can be divided into three different segments. The upper unit differs significantly from the lower by the facies succession that consists of thicker carbonate deposits, dolomites, and significant deposits of anhydrite (Figure 81). The lower segment is identified as an upward-decrease in gamma ray response from a dolomite and shale dominated facies, followed by dolomite facies and ending with a thick accumulation of anhydrite. The base of the middle succession is a 10-15m thick carbonate succession with *Palaeoplysina*-phylloid algae build-ups then transitioning into an upward-decrease in gamma ray to an anhydrite and dolomite dominated facies, with some interlayering of carbonate units (Figure 81). The upper segment is an approximate 20 meter of carbonate sediments of *Palaeoplysina*-phylloid algae build-ups (Figure 81).

The Bjarmeland Gp. is located from 4255 – 3945m. The characteristic of the gamma ray response in the section is identified as a uniform and very low gamma ray activity (Figure 81). The carbonate biota in the well consists of bryozoan dominated build-ups and crinoids (Larssen et al., 2002). The porosity in the well is anhydrite filled due to intrusions after deposition.

The Tempelfjorden Gp. is located at a depth of 3945 – 3853m. The succession consists of thick basinal siliciclastic deposits (Figure 81).



Appendix 1.3: Figure 81 - Well data of the Upper Paleozoic succession in well 7229/11-1.

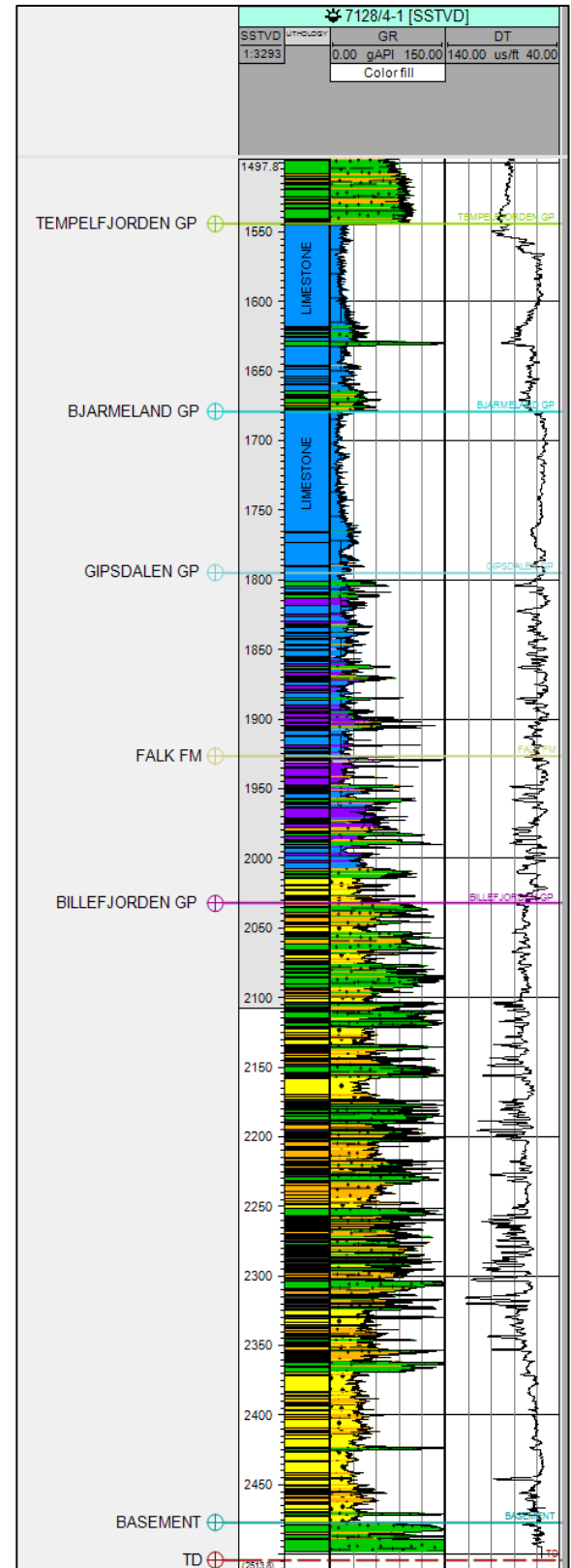
Appendix 1.4 - Well 7128/4-1

The basement in the well is cored, and has been analyzed as low grade metasedimentary basement consisting of shale (Figure 82; Ehrenberg et al., 1998a).

The siliciclastic sedimentary succession in the Billefjorden Gp. can be divided into two different facies units. The lower unit is ranging from 2475 – 2375m and the upper unit from 2375 – 2033m (Figure 82). The lower section is a sand rich unit with occasional infill of silt and shale. The depositional environment in this area is a fluvial depositional environment evident by the two fining upward sequences bounded by shale dominated flooding surface (Ehrenberg et al., 1998a). The upper unit is dominated by a more silt and shale prone succession (Figure 82). The unit consists of numerous coarsening sequences, consistent with a depositional environment of meandering river systems (Figure 82). The numerous series of thin beds consistent with high velocities coincides with coal deposit within the Billefjorden Gp.

The Gipsdalen Gp. can be separated into two primary units; lower and upper (Figure 82). The lower section of consists of a facies composed of alluvial sediments with conglomerate and occasional sandstone units (Figure 82). The alluvial succession was deposited during a tectonically active period, and then followed by distinctive change in facies to carbonate platform (Ehrenberg et al. 1998a). The carbonate facies consists of carbonates, dolomites, evaporites and some siliciclastic deposits. The facies characteristics are consistent with a warm, shallow-marine environment. The upper section consists of carbonates, dolomites and some siliciclastics associated with flooding surfaces (Figure 82). The carbonate compositions are limestone and Palaeoaplysina-phyllloid algae build-ups.

The Bjarmeland Gp. can be separated into two different facies units; the lower unit ranging from 1795 – 1770 m and the upper ranging from 1770 – 1680 m. The lower unit is identified as an increase in gamma ray response this increase is identified as the early Sakmarian (Ehrenberg et al. 1998a). The upper unit is identified by a significant change in facies



Appendix 1.4: Figure 82 - Well data of the Upper Paleozoic succession in well 7128/4-1.

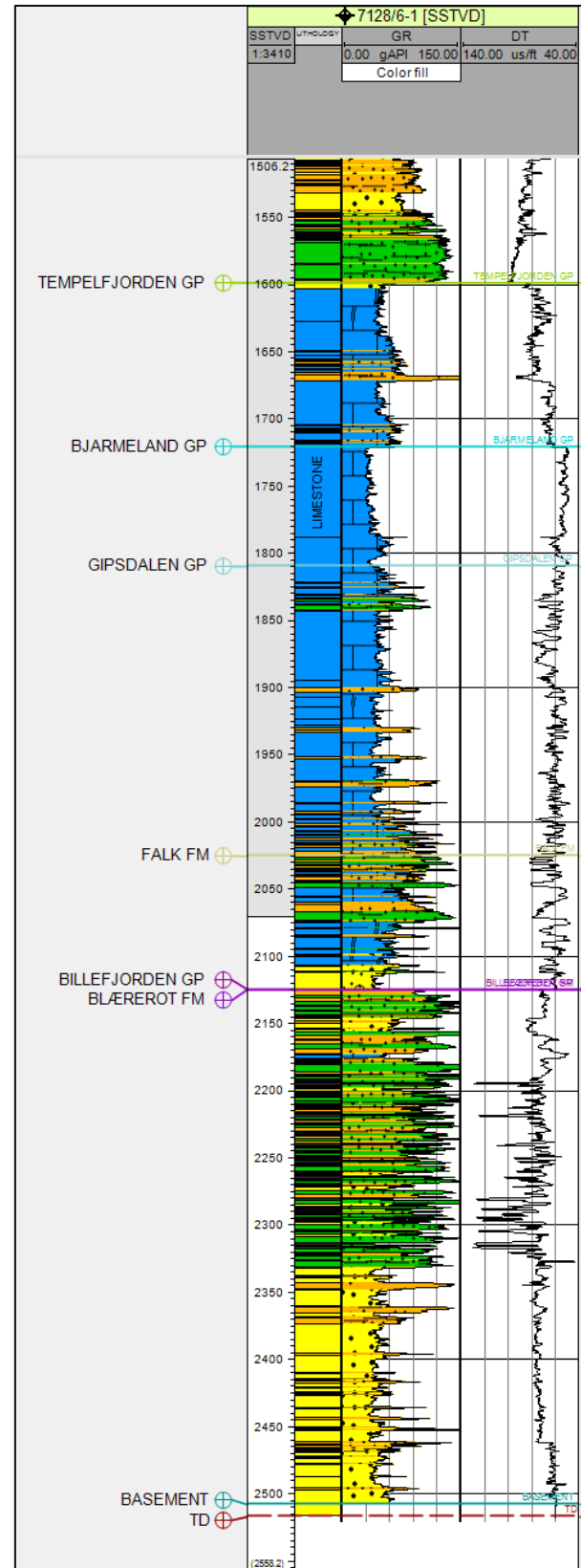
characteristics seen in the well (Figure 82). The unit is characterized by a very low gamma ray activity throughout the entire unit. This unit consists dominantly of bryozoan-echinoderm dominated assemblage, this indicates a significant change in depositional environment to a cooler, and deeper-marine environment (Stemmerik et al. 1999; Ehrenberg et al. 1998a).

The Tempelfjorden Gp. is ranging from the Kungurian to Late Permian in age. The gamma ray response indicates that the succession consists of two periods of upward-decreasing in the gamma ray response, bounded by a distinctive flooding surface. Each of the units have a distinctive pattern where the base of the unit consists of siliciclastic shale and silt deposit, followed by a upward-decrease in gamma ray consistent with increased biological content and decrease in siliciclastic input (Figure 82). The biota in 7128/4-1 consists primary of calcareous spiculite, and spiculitic-limestone (Ehrenberg et al., 1998a).

Appendix 1.5 - Well 7128/6-1

The siliciclastic sedimentary succession in the Billefjorden Gp. can be divided into two different facies units. The lower unit is ranging from 2507 – 2332m and the upper unit from 2332 – 2125m (Figure 83). The lower unit characterized as very sand rich unit with occasional infill of silt and shale. The depositional environment have been identified as fluvial depositional environment, with the lower unit composed of channel fill sediments with the infrequent deposition of silt and shale interpreted as crevasse splay and overbank deposits (Ehrenberg et al., 1998a). The upper unit consists of higher abundance of shale, silt and coal. The high velocity response from the sonic log (> 130.00 us/ft) is evidence of coal accumulations (Figure 83).

The Gipsdalen Gp. can be separated into two primary units; lower and upper (Figure 83). The lower unit ranges from 2125 – 2025m and consist of a facies composed of siliciclastic and carbonate sediments. The lower section of the unit consists of alluvial sediments of conglomerate and occasional sandstone units (Figure 83; Ehrenberg et al., 1998a). The alluvial succession was deposited during a tectonically active period, and then followed by distinctive change in facies to carbonate platform (Ehrenberg et al. 1998a). The carbonate succession consists of carbonates, dolomites, evaporites, and with some siliciclastic deposits consistent with flooding surfaces. The facies characteristics are represents warm, arid, and shallow-marine environment and the carbonate biota is composed of are limestone and Palaeoaplysina-phyllloid algae build-ups. The upper unit ranges from 2025 – 1809m and consists of carbonates, dolomites and series of shale deposits (Figure 83). The series of flooding surfaces is an evidence of the high and frequent fluctuations in the sea-level. The lower part of the section is altered by a high abundance of rapid sea-level fluctuations, the middle section consists longer periods of carbonate deposition bounded by flooding surfaces. The upper section of the unit is identified as a distinct upward-decreasing in gamma ray response from shale to carbonate facies (Figure 83).



Appendix 1.5: Figure 83 - Well data of the Upper Paleozoic succession in well 7128/6-1.

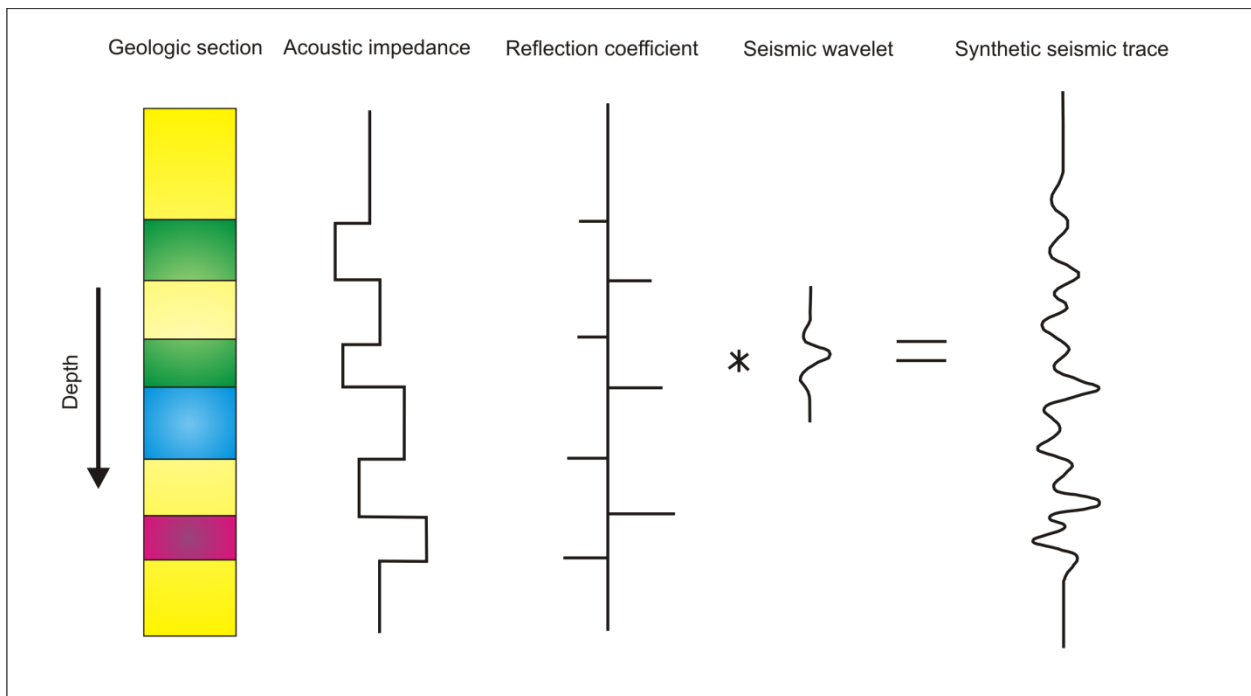
The carbonate facies in well 7128/6-1 share the similar tendency as well 7128/4-1. The Bjarmeland Gp. is divided into two facies units. The lower unit ranging from 1809 – 1790m and it is identified as upward-increase in gamma ray. The upper unit ranges from 1790 – 1720m and it is identified by a significant change in facies characteristics (Figure 83). The unit is characterized by an upward-decrease in gamma ray response, the gamma ray activity throughout the unit is very low (Figure 83). The well consists of the same depositional facies seen in well 7128/4-1, with a biota that is dominated by bryozoan-echinoderm assemblages (Ehrenberg et al. 1998a).

The Tempelfjorden Gp. is ranging from 1720 – 1600m and can be divided into two units. Similar to well 7128/4-1 is it evident that there are two periods of upward-decrease in gamma ray response, bounded by a flooding surface (Figure 83). The upward-decrease may be a response of lower clay content consistent with the increase of productivity of biological content (Ehrenberg et al., 1998a). The biota in biological content in the well consists primary of calcareous spiculite deposits (Ehrenberg et al., 1998a; Beauchamp, 1994). The lower section of the unit is classified as a drowning unconformity evident by the distinctive change in facies from underlying carbonate biota in the Bjarmeland Gp. to a shale-dominated deposition in the base of the Tempelfjorden Gp. The upper unit have the similar upward-decreasing trend as the lower unit (Figure 83). The facies distribution in the unit differ from the lower unit as a result of the higher abundance of spiculitic limestone and spiculites (Ehrenberg et al., 1998a).

Appendix 2 - Seismic interpretation and attribute methods

Appendix 2.1 - Seismic well-tie background

The seismic well-tie procedure is an important step because the purpose is to tie the information obtained in the well data with the seismic section. The procedure consists of two main objectives; the first is to accurately tie the seismic data in time with the well log data given in depth. The second is to identify what causes the reflections observed in the seismic data by analyzing the synthetic seismogram generated from the acoustic impedance contrast in the well (Vail, 1987). The synthetic seismogram is generated a result of forward modeling created to predict the seismic response of the lithologies in the well bore. The synthetic seismogram is a 1-D model of acoustic energy traveling through lithologies. It is generated by convolving the reflectivity derived from the sonic (acoustic) and density logs, combined with a wavelet obtained from the seismic data (Figure 84).



Appendix 2.1: Figure 84 - Synthetic seismogram theory (Modified from Keary et al., 2002).

Appendix 2.2 - Vertical and horizontal resolutions

To calculate the vertical resolution in the seismic data cube, one needs to consider the dominant wavelength (λ). The wavelength is a quotient of the wave velocity (v) divided by the dominant frequency (f):

$$\text{Wavelength:} \quad \lambda = \frac{v}{f} \quad (\text{Equ. A.1})$$

Note that the wave velocities for a given lithology (generally) increase with depth, following that the dominant frequency decrease with depth as a result of the attenuation of high frequencies (Brown, 1999). Consequently, the seismic resolution weakens as the depth increases.

The maximum resolution possible to adapt form a seismic reflection that is represented by a single wavelet is assumed to range between one-quarter and one-eighth of the dominant wavelet (Keary, 2002). The threshold value is assumed in the calculation of the vertical resolution to be one-quarter:

$$\text{Vertical resolution (VR):} \quad VR = \frac{1}{4} * \frac{v}{f} \quad (\text{Equ. A.2})$$

Where the v is the average seismic velocity and f is the dominant frequency.

The seismic wave is traveling in three dimensions after being sent from the source. The horizontal resolution is calculated from the Fresnel zone. The Fresnel zone is known as the interface of the energy of a signal that is returned to the detector within half a wavelength of the initial reflected arrival interferences (Keary, 2002). The horizontal resolution of seismic survey is noted as the minimum lateral distance between to reflecting points that is needed when recognizing two separate reflection points (Brown, 2011). The lateral resolution of the survey is given by calculation of the Fresnel zone after migration:

$$\text{Horizontal resolution (HR):} \quad HR = \frac{\lambda}{4} \quad (\text{Equ. A.3})$$

To calculate the respective wavelengths, VR and HRs from the different seismic cubes, average velocities and frequencies was needed. These values were extracted from the surrounding well data and from the seismic cubes. The frequency variations between the different cubes are not considerable. However, their dominant frequencies range from 17.25 – 27 Hz (Table 7; Table 6). The average velocities were derived from the top Bjarmeland Gp. reflector for all the wells and thus, due to depth variations, among others, there is a large variation in average velocities applied to the equations for the different areas (Table 11). For the two seismic areas located on the Bjarmeland Platform it has been assumed similar average velocities in the top Bjarmeland Gp., as a result of the low well density. The two areas on Finnmark Platform have lower uncertainty in the well control and thus, different well have been used to derive the average acoustic velocity (Table 11).

| Average acoustic velocities for Bjarmeland Group | | | | | |
|---|---------------------------|----------------|---------------------------|----------------|---------------------------|
| Area A and Area B | | Area C | | Area D | |
| Wells | Average velocities | Wells | Average velocities | Wells | Average velocities |
| 7124/3-1 | 6417 m/s | 7229/11-1 | 5088 m/s | 7128/4-1 | 1679 |
| 7226/11-1 | 5965 m/s | | | 7128/6-1 | 1720 |
| 7229/11-1 | 5088 m/s | | | | |
| | | | | | |
| Average | 5823 m/s | Average | 5088 m/s | Average | 4936 m/s |

Appendix 2.2: Table 11 - Acoustic velocities for the Bjarmeland Group

The results of the calculation of the vertical- and horizontal resolutions, and the wavelet are listed in the underlying table (Table 12). From the calculated results it is evident that the two areas on Bjarmeland Platform have obtained relatively similar results in the vertical- and horizontal resolutions. The areas on Finnmark Platform differ from each other in the vertical resolution, whereas Area D has significantly lower resolution than Area C (Table 12); Although, both of the areas on the Finnmark Platform have obtained similar horizontal resolution (Table 12).

| | BG0804 | NH0608 | SH9102 | ST9802 |
|------------------------------|---------------|---------------|---------------|---------------|
| Wavelength | 232.9 m | 215 m | 295 m | 232 m |
| Vertical Resolution | 58.8 m | 59.92 m | 73.7 m | 50.1 m |
| Horizontal Resolution | 58.2 m | 53.75 m | 73.6 m | 73.6 m |

Appendix 2.2: Table 12 - Calculated results of the wavelength, vertical- and horizontal resolution of the four seismic areas.

Appendix 2.3 - Seismic attribute background

9.2.2.1 Spectral Decomposition

The spectral enhanced volume is created by a multiplication of the source volume and the different bandwidth volumes.

Seismic Area A:

$$\text{Spec. Enh. Vol} = \frac{(im1+(im2*0.1)+(im3*0.05)+(im4*0.05)+(im5*0.25))}{1.45} \quad (\text{Equ. A.4})$$

The input parameters applied to the equation are *im1* equals the source input volume, and *im2* to *im5* is the enhanced bandpass volumes (*im2* = bandwidth 14.20 Hz, *im3* = bandwidth 18.30 Hz, *im4* = bandwidth 22.50 Hz, *im5* = bandwidth 35.00 Hz).

Seismic Area B:

$$\text{Spec. Enh. Vol} = \frac{(im1*(im2*0.1)+(im3*0.2)+(im5*0.45)+(im6*0.1))}{2.05} \quad (\text{Equ. A.5})$$

Note that the *im1* equals the source input volume, and *im2* to *im6* is the enhanced bandpass volumes (*im2* = bandwidth 13.85 Hz, *im3* = bandwidth 36.92 Hz, *im5* = bandwidth 44.62 Hz, *im6* = bandwidth 48.46 Hz).

Seismic Area C:

$$\text{Spec. Enh. Vol} = \frac{(im1+(im2*0.05)+(im3*0.05)+(im4*0.05)+(im5*0.20)+(im6*0.20))}{1.55} \quad (\text{Equ. A.6})$$

The input parameters applied to the equation are *im1* equals the source input volume, and *im2* to *im6* is the enhanced bandpass volumes (*im2* = bandwidth 17.70 Hz, *im3* = bandwidth 21.50 Hz, *im4* = bandwidth 25.40 Hz, *im5* = bandwidth 29.20 Hz, and *im6* = bandwidth 33.10 Hz).

Seismic Area D:

$$\text{Spec. Enh. Vol.} = \frac{(im1+(im2*0.1)+(im3*0.05)+(im4*0.1)+(im5*0.1))}{1.35} \quad (\text{Equ. A.7})$$

The input parameters applied to the equation are *im1* equals the source input volume, and *im2* to *im5* is the enhanced bandpass volumes (*im2* = bandwidth 52.30 Hz, *im3* = bandwidth 44.60 Hz, *im4* = bandwidth 40.80 Hz, and *im5* = bandwidth 36.90 Hz).